# MPC base sur des réseaux de neurones pour une autoconsommation optimale d'énergie photovoltaïque

Irati Zapirain

université de BORDEAUX

THÈSE EN COTUTELLE PRÉSENTÉE

POUR OBTENIR LE GRADE DE

# DOCTEURE DE L'UNIVERSITÉ DE BORDEAUX

**ET DE L'UNIVERSITE UPV/EHU**

ÉCOLE DOCTORALE
DES SCIENCES PHYSIQUES ET DE L'INGENIEUR

**ÉCOLE DOCTORALE PARTENAIRE :**
**SYSTEMS ENGINEERING AND AUTOMATION**

Automatique, productique, signal et image,
Ingénierie cognitique

Par Irati ZAPIRAIN

# NEURAL NETWORK BASED MODEL PREDICTIVE CONTROL FOR AN OPTIMAL PHOTOVOLTAIC ENERGY SELF-CONSUMPTION

Sous la direction de :
Octavian CUREA
Haritza CAMBLONG

Soutenue le 16/12/2024

Membres du jury :

| | | |
|---|---|---|
| Mme Matilde SANTOS PEÑA, | Professeure des universités, Universidad Complutense de Madrid, | Présidente |
| Mme Maider SANTOS-MUGICA, | Directrice de recherche, Tecnalia Research & Innovation, | Examinatrice |
| M Aitzol EZEIZA RAMOS, | Professeur associé, Universidad del País Vasco, | Examinateur |
| M Tudor-Bogdan AIRIMITOAIE, | Professeur associé, Université de Bordeaux, | Examinateur |
| Mme Najiba MRABET BELLAAJ, | Professeure des universités, University of Tunis El Manar, | Examinatrice |

Rapporteurs :

| | |
|---|---|
| M Mahamadou ABDOU TANKARI | Professeur associé, Université Paris-Est Créteil |
| M Ramon ZAMORA | Professeur associé, Auckland University of Technology |

*Amama, aitite, amona eta aitonari,*
*por haber sido el ejemplo del trabajo duro y el sacrificio.*
*Os lo debo todo.*

# *ACKNOWLEDGMENTS*

First of all, I would like to thank the UPV/EHU and the Université de Bordeaux for giving me the opportunity to do my Thesis in cotutelle. I have had the opportunity to learn first-hand about the excellent cooperation between the two universities. In this regard, thanks to Euskampus for all the work of organising events and workshops that has helped to materialise this cooperation. I would also like to thank the *ESTIA Recherce* group from ESTIA Institute of Technology for hosting me for long days and for giving me a hand whenever I needed it.

I would like to thank Tavi for having supported me all these years and for having helped me whenever I found myself in dead ends. Zer esanik ez Haritzari, 4 urte hauen ondoren, ez baititut esker onekoak ez diren beste hitzik zuretzat. Eskerrik asko nirekin izandako pazientziagatik eta zure lanerako prestutasunagatik, asko ikasteaz gain, lankide eta bidelagun izateagatik. Millesker tesiaren etapa bakoitzean zehar zuen denbora eskeini didazuen guztioi, Juanjo, Unai, Zina, Tudor…. Eta nola ez eskertu Garaziri, momentu askotan nire penak entzun eta ulertu zezakeen bakarrenetakoari. Eskerrik asko hirugarren urte gogor hortan eguna alaitzen zenidaten laborategiko guztiei, bereziki Juleni, lanean eta kalean beti eguna pixka bat hobea egiteagatik.

Millesker nire lagunei bizitza oso bat nire ondoan egoteagatik, itzultzen naizen bakoitzean etxean sentiarazteagatik. Eskerrak eman nahi dizkiot ere nire familiari, beti babestu eta ni zaintzearren. Bereziki nire ama, aita eta Pauleri, nigan sinesteagatik, beti aurrera begiratzen erakusteagatik eta gauzak zail jartzen direnean nirekin egoteagatik. Zuek gabe ezin izango nuen lan hau inola ere amaitu.

Para terminar, quiero dar las gracias a todos esos leales siempre que me habéis enseñado a no rendirme, a perseverar y no conformarme con migajas. Eskerrik asko, bihotzez.

# *ABSTRACT*

Digitisation and decentralisation are two key concepts guiding and driving the energy transition, a fundamental shift towards decarbonising our energy systems. These trends are encouraging the transformation of energy systems into cleaner, more sustainable and efficient models. Among the various approaches emerging in this context, self-consumption (SC) of photovoltaic (PV) energy has gained significant attention as a viable strategy to enhance decentralised electricity generation and consumption. Self-consumption facilitates the integration of renewable energy sources (RES), contributing to the decarbonisation of the energy mix.

A key enabler in this context are Energy Management Systems (EMS), which provide the necessary technological framework to effectively manage energy flows within a SC scheme. EMS can act on flexible loads (FLs) to adapt the consumption curve, so that it follows the PV production curve as closely as possible.

The objective of this PhD Thesis is to develop a Model Predictive Control (MPC) type EMS applied to a real building within a SC framework. The optimisation-based EMS is designed to control the *heating ventilation and air conditioning* (HVAC) system of a building by adjusting the set point temperature in order to maximise the self-consumption rate (SCR), ensuring occupant thermal comfort and minimising computational cost.

The scientific literature shows that integrating predictions into an EMS can improve its performance. In this work, the EMS forecasts, one day ahead, (1) the building's energy consumption without considering the consumption of the HVAC system, and (2) the PV production of the SC. To make both predictive models computationally less demanding, predictive models based on the *nonlinear autoregressive with exogenous inputs* (NARX) neural network have been proposed, a simple type of machine learning model that has been trained with a reduced dataset.

Additionally, the MPC uses linear models of the building's thermal behaviour and heat pumps. The thermal model represents the building's thermal dynamics. A NARX model trained with excitation tests data has been designed to capture the nonlinearities of the HVAC system. The NARX has been linearised at operation points of interest to minimise the computational cost of the MPC. Finally, the linear NARX models have been compared to a linear model identified with the excitation tests data.

This Thesis concludes by the development of the EMS optimisation problem and the validation of its performance by the increase in SCR achieved.

# *RÉSUMÉ*

La numérisation et la décentralisation sont deux concepts clés qui guident et stimulent la transition énergétique, une transition fondamentale pour atteindre la décarbonation du modèle énergétique. Ces tendances poussent à transformer les systèmes énergétiques vers des modèles moins polluants, plus durables et plus efficaces. Parmi les différentes approches qui émergent dans ce contexte, l'autoconsommation (AC) d'énergie photovoltaïque (PV) a gagné une attention significative comme stratégie viable pour améliorer la génération et la consommation décentralisées d'électricité. L'autoconsommation favorise l'intégration des sources d'énergie renouvelable (ENR), contribuant ainsi à la décarbonation du mix énergétique.

Un élément facilitateur clé dans ce contexte est le Système de Gestion de l'Énergie (SGE), qui fournit le cadre technologique nécessaire pour gérer efficacement les flux d'énergie au sein d'un schéma d'AC. Les SGE peuvent agir sur des charges flexibles (CFs) pour adapter la courbe de consommation, de manière à suivre au mieux la courbe de la production PV.

L'objectif de cette thèse de doctorat consiste à développer un SGE de type MPC (Contrôle Prédictif Basé sur Modèle) appliqué à un bâtiment réel dans le cadre de l'AC. Le SGE basé sur l'optimisation est conçu pour contrôler le système de climatisation d'un bâtiment en ajustant la température de consigne afin de maximiser le taux d'autoconsommation (TAC), en assurant le confort thermique des occupants et en minimisant le coût computationnel.

La littérature scientifique montre que l'intégration de prédictions dans un SGE peut améliorer ses performances. Dans ce travail, le SGE effectue une prévision à un jour de : (1) la consommation énergétique du bâtiment sans prendre en considération la consommation du système de climatisation et (2) la production PV de l'ACC. Afin que les deux modèles prédictifs soient moins exigeants en termes de calcul, des modèles prédictifs basés sur le réseau neuronal *nonlinear autorregressive with exogenous inputs* (NARX) ont été proposés, un type de modèle d'apprentissage automatique simple qui a été entraîné avec un ensemble de données réduit.

De plus, le MPC utilise des modèles linéaires du comportement thermique du bâtiment et des pompes à chaleur. Le modèle thermique représente la dynamique thermique du bâtiment. Un modèle NARX entraîné avec des données de tests d'excitation a été conçu afin de capturer les non-linéarités du système de climatisation. Le NARX a été linéarisé autour de points de fonctionnement pertinentes afin de minimiser le coût computationnel du MPC. Enfin, les modèles linéarisés du NARX ont été comparés à un modèle linéaire identifié avec les données des tests d'excitation.

Cette thèse se conclut avec le développement du problème d'optimisation du SGE et la validation de ses performances avec l'augmentation du TAC obtenue.

# *RESUMEN*

La digitalización y la descentralización son dos conceptos clave que guían e impulsan la transición energética, una transición fundamental para alcanzar la descarbonización del modelo energético. Estas tendencias están impulsando la transformación de los sistemas energéticos hacia modelos menos contaminantes, más sostenibles y más eficientes. Entre los diversos enfoques que surgen en este contexto, el autoconsumo (AC) de energía fotovoltaica (FV) ha ganado una atención significativa como una estrategia viable para mejorar la generación y el consumo descentralizados de electricidad. El autoconsumo ayuda a la integración de fuentes de energía renovable (FER), contribuyendo a la descarbonización del mix energético.

Un facilitador clave en este contexto es el Sistemas de Gestión de la Energía (SGE), que proporciona el marco tecnológico necesario para gestionar eficazmente los flujos de energía dentro de un esquema de AC. Los SGE pueden actuar sobre cargas flexibles (CFs) para adaptar la curva de consumo, de manera que siga lo mejor posible la curva de la producción FV.

El objetivo de esta tesis doctoral consiste en el desarrollo de un SGE de tipo MPC (Control Predictivo Basado en Modelo) aplicado a un edificio real en el marco del AC. El SGE basado en la optimización está diseñado para controlar el sistema de climatización de un edificio mediante el ajuste de la temperatura de consigna con el fin de maximizar la tasa de autoconsumo (TAC), asegurando el confort térmico de los ocupantes y minimizando el coste computacional.

La literatura científica muestra que la integración de predicciones en un SGE puede mejorar su rendimiento. En este trabajo, el SGE realiza la previsión a un día de: (1) el consumo energético del edificio sin tomar en consideración el consumo del sistema de climatización y (2) la producción FV del AC. Con el objetivo de que ambos modelos predictivos sean computacionalmente menos exigentes, se han propuesto modelos predictivos basados en la red neuronal *nonlinear autorregresive with expogenous inputs* (NARX), un tipo de modelo de aprendizaje automático simple y que ha sido entrenado con un conjunto de datos reducido.

Además, el MPC utiliza modelos lineales del comportamiento térmico del edificio y las bombas de calor. El modelo térmico representa la dinámica térmica del edificio. Se ha diseñado un modelo NARX entrenado con datos de tests de excitación con el objetivo de captar las no linealidades del sistema de climatización. El NARX ha sido linealizado en puntos de operación de interés con el objetivo de minimizar el coste computacional del MPC. Por último, los modelos lineales del NARX han sido comparados con un modelo lineal identificado con los datos de los tests de excitación.

Esta Tesis concluye con el desarrollo del problema de optimización del SGE y la validación de su rendimiento mediante el aumento de la TAC logrado.

# *LABURPENA*

Digitalizazioa eta deszentralizazioa energia-trantsizioa gidatzen eta bultzatzen duten funtsezko bi kontzeptu dira, energia-ereduaren deskarbonizazioa lortzeko funtsezko trantsizioa. Joera horiek energia-sistemak gutxiago kutsatzen duten, iraunkorragoak diren eta eraginkorragoak diren ereduetara eraldatzea bultzatzen ari dira. Testuinguru horretan sortzen diren hainbat ikuspegiren artean, energia fotovoltaikoaren (FV) autokontsumoak arreta handia lortu du elektrizitatearen sorkuntza eta kontsumo deszentralizatua hobetzeko estrategia bideragarri gisa. Autokontsumoak energia-iturri berriztagarriak integratzen laguntzen du, mix energetikoa deskarbonizatzen lagunduz.

Testuinguru horretan, Energia Kudeatzeko Sistema (EKS) funtsezko bideratzailea da, autokontsumo kolektiboko eskema baten baitan energia-fluxuak eraginkortasunez kudeatzeko behar den esparru teknologikoa ematen baitu. EKSek karga malguetan eragin dezakete kontsumo-kurba egokitzeko, FV ekoizpenaren kurbari ahalik eta ondoen jarraitzeko.

Doktore-tesi honen helburua MPC (Ereduan Oinarritutako Kontrol Prediktibo) motako EKS bat garatzea da, autokontsumoaren esparruan, benetako eraikin bati aplikatuta. Optimizazioan oinarritutako EKSa eraikin baten klimatizazio-sistema kontrolatzeko diseinatuta dago, kontsigna-tenperatura doituz, autokontsumo-tasa maximizatzeko, okupatzaileen erosotasun termikoa ziurtatuz eta kostu konputazionala minimizatuz.

Literatura zientifikoak erakusten du iragarpenak EKS batean integratzeak errendimendua hobetu dezakeela. Lan horretan, EKSak egun baterako aurreikuspena egiten du: (1) eraikinaren energia-kontsumoa klimatizazio-sistemaren kontsumoa kontuan hartu gabe, eta (2) Autokontsumoren FV ekoizpena. Bi eredu prediktiboak konputazionalki ez hain pisutsuak izateko helburuarekin, neurona-sarean oinarritutako eredu prediktiboak proposatu dira, *nonlinear autoregresive with expogenous inputs* (NARX) motakoak. Ikasketa automatiko eredu sinple bat da eta datu-multzo txiki batekin trebatua izan da.

Gainera, MPCak eraikinaren joera termikoaren eta bero-ponpen eredu linealak erabiltzen ditu. Eredu termikoak eraikinaren dinamika termikoa adierazten du. Kitzikapen-testen datuekin entrenatutako NARX eredu bat diseinatu da, klimatizazio-sistemaren ez-linealtasunak atzemateko. NARXa intereseko funtzionamendu puntuen inguruan linealizatu da, MPCren kostu konputazionala minimizatzeko helburuarekin. Azkenik, NARXen eredu linealak eszitazio-testen datuekin identifikatutako eredu lineal batekin alderatu dira.

Tesi honen amaieran, EKSren optimizazio-arazoa garatzen da eta haren errendimendua baliozkotzen da, lortutako autkontsumo tasaren gehikuntzaren bidez.

# *TABLE OF CONTENTS*

# *LIST OF FIGURES*

# *LIST OF TABLES*

# *ACRONYMS*

| | |
|---|---|
| **AnM** | Analytical model |
| **ANN** | Artificial Neural Network |
| **AR** | Autoregression |
| **ARIMA** | Autoregressive integrated moving average |
| **ARMA** | Autoregressive moving average |
| **ARMAX** | Autoregressive moving average with exogenous input |
| **ASI** | All-Sky Imagers |
| **BESS** | Battery Energy Storage System |
| **BiLSTM** | Bidirectional LSTM |
| **BJ** | Box-Jenkins |
| **BPNN** | Backpropagation NN |
| **CC** | Cloud cover |
| **CL** | Controllable load |
| **CNN** | Convolutional neural network |
| **COP** | Coefficient of performance |
| **CSC** | Collective self-consumption |
| **CV** | Coefficient of variation |
| **DG** | Distributed generation |
| **DHW** | Domestic Hot Water |
| **DL** | Deep Learning |
| **DMS** | Demand Side Management |
| **DR** | Demand Response |
| **DSO** | Distribution System Operator |
| **EC** | Energy Community |
| **ECMWF** | European Centre for Medium-Range Weather Forecasts |
| **EMS** | Energy Management System |
| **ENN** | Elman neural network |
| **EPBD** | Energy Performance of Buildings Directive |
| **ESS** | Energy Storage Systems |
| **EU** | European Union |
| **EV** | Electric Vehicle |
| **EWH** | Electric water heater |
| **FFNN** | Feedforward neural network |
| **FL** | Flexible load |
| **GA** | Genetic Algorithm |
| **GD** | Gradient Descent |
| **GP** | Gaussian Process |
| **GRU** | Gate recurrent unit |
| **GSG** | Greenhouse gas |
| **HCEMS** | Hierarchical Centralized Energy Management System |
| **HTA** | Medium voltage overhead lines |
| **HVAC** | Heat, Ventilation and Air Condition |
| **IDEA** | Instituto para la Diversificación y Ahorro de la Energía |
| **IEA** | International Energy Agency |
| **IoT** | Internet of Things |
| **lmNARX** | Linearised model of NARX |
| **LPV** | Linear parameter varying |
| **LR** | Linear regression |
| **LSTM** | Long-short-term memory |
| **LTLF** | Long-term load forecasting |
| **MAE** | Mean absolute error |
| **MAPE** | Mean absolute percentage error |
| **MF** | Meteo France |
| **MG** | Meteo Galicia |
| **MILP** | Mixed-integer linear programming |
| **MINLP** | Mixed-integer nonlinear programming |
| **ML** | Machine Learning |

| | |
|---|---|
| **MLP** | Multilayer perceptron |
| **MPC** | Model Predictive Control |
| **MSE** | Mean square error |
| **MTLF** | Medium-term load forecasting |
| **NCL** | Uncontrollable load |
| **NIOP** | Nonlinear input-output model |
| **NLP** | Nonlinear programming |
| **NMI** | Normalised Mutual Information |
| **NMPC** | nonlinear MPC |
| **NN** | Neural Network |
| **nRMSE** | normalised RMSE |
| **NWP** | Numerical Weather Prediction |
| **nZEB** | nearly Zero Energy Buildings |
| **OP** | Operating point |
| **PCA** | Principal Component Analysis |
| **PH** | Prediction horizon |
| **PMO** | Personne Moral Organisatrice |
| **PRBS** | Pseudorandom binary sequence signal |
| **PSO** | Particle Swarm Optimisation |
| **PV** | Photovoltaic |
| **QP (IP)** | Quadratic Programming interior-point method |
| **RA** | Regression analysis |
| **RB-EMS** | Rule-based EMS |
| **RC** | Resistor-capacitor |
| **RES** | Renewable Energy Sources |
| **RF** | Random Forest |
| **RL** | Reinforcement Learning |
| **RMSE** | Root mean square error |
| **RNN** | Recurrent Neural Network |
| **SA** | Statistical Analysis |
| **SARIMA** | Seasonal autoregressive integrated moving average |
| **SB** | Smart Buildings |
| **SB-MPC** | Sampling-based MPC |
| **SC** | Self-consumption |
| **SCR** | Self-consumption rate |
| **SDG** | Sustainable Development Goal |
| **SGA** | Sequential-grid-approach |
| **SISO-MPC** | Single-Input Single-Output MPC |
| **SQP** | Sequential Quadratic Programming |
| **STLF** | Short-term load forecasting |
| **SVM** | Support vector machine |
| **SVR** | Support vector regression |
| **TSO** | Transmission System Operator |
| **TW** | Time window |
| **UKGBC** | UK Green Building Council |
| **VSTLF** | Very short-term load forecasting |
| **WT** | Wavelet transform |
| **zoh** | Zero-order hold |

## *ABBREVIATION LIST*

| | |
|---|---|
| $T_{in}$ | Indoor temperature |
| $Energy_{consum}$ | Total energy consumed by all consumers |
| $Energy_{prod}$ | Total energy produced by the generating installation |
| $INE_{h,i}$ | Individualised net energy calculated each hour for each consumer. |
| $Q_{hp}$ | Heat pump consumption |
| $Q_b$ | Building consumption |
| $T_{ext}$ | External temperature |
| $T_s$ | Sampling time |
| $T_{sp}$ | Set point temperature |
| $t_R$ | Rise time |
| $t_{im}$ | Maximum pulse duration |
| $\beta_{h,i}$ | Distribution coefficient of each hour associated to each consumer. |
| $\Delta T_{hyst}$ | Hysteresis value |
| ε | Margin of the bounding decision |
| $R^2$ | Coefficient of determination |
| tansig | Hyperbolic tangent |
| TRANSYS | Transient System Simulation program |
| $Wind_{speed,\ dq}$ | Weighted wind seed array considering wind direction |
| $C$ | Regularization parameter |
| $Hyst$ | Hysteresis signal |
| $N$ | Number of cells in the shift register |
| $OCC$ | Building occupancy |
| $Var$ | Variance |
| $n$ | Total number of measured data |
| $r$ | Pearson correlation coefficient |
| $\gamma$ | Influence of a single training example |
| $J$ | Cost function |
| $G_{PV}$ | PV gain |
| $Q_{pv}$ | Predicted PV production in kWh |
| $Q_{cons}$ | Predicted building consumption without HVAC system consumption in kWh |
| $T_{comf}$ | Comfort temperature |
| $T_{ext,mean}$ | Previous day average external temperature |
| $T_{in,80\%}, T_{in,90\%}$ | Indoor comfort temperature of 80% and 90% of acceptability |
| $P_{PV_{M1}}$ | *E*lectricity produced by the actual PV panels |
| $P_{PV_{M1,\mathrm{MAX}}}$ | Maximum power of actual PV panels |
| $P_{PV_{SYST_{MAX}}}$ | Maximum power of new PV panels |

# CHAPTER 1

# INTRODUCTION

This first chapter serves as an introduction to the work carried out and presented in the following pages. The problem has been introduced, first contextualising it in general terms and then presenting the possible proposed solutions.

This chapter is divided into six parts. First, the problem statement is addressed, attempting to reflect on the reasons that have given rise to this Doctoral Thesis.

Secondly, a general introduction of Energy Management Systems (EMSs) has been carried out in order to give context to the work developed in this first chapter.

Thirdly, the most general aspects of the case study and the EMS proposal have been introduced.

Finally, general objectives of the Thesis are provided together with a brief description of the chapters that form the entirety of the Thesis manuscript.

## 1.1 PROBLEM STATEMENT

The energy model of a country is one of the most important pillars for its independence and stability. For some years now, the debate has transcended the political sphere to enter the social scope, largely due to the undeniable rise in social awareness regarding environmental issue, which has led to debates such as dependency on fossil energy sources or issues related to the need to reduce energy consumption and the emission of harmful gases. Alongside this, the unprecedented rise in electricity prices has had a strong influence on the social debate where the current energy model has been questioned.

In this context, an energy transition is being promoted that leads on the gradual abandonment of fossil sources and is therefore going towards the decarbonisation of the energy model.

Decarbonisation of the energy model involves starting to promote a hybrid model (better known as an energy mix) based on the combination of fossil and renewable sources, which will tend to dispense with fossil sources in favour of renewables and thus reduce greenhouse gas (GHG) emissions. The integration of Renewable Energies Sources (RES) into the grid is one of the key issues for this transition, as well as one of the greatest challenges we face as society.

European institutions have established a strong legal framework for more ambitious renewable energy targets. Currently, the European Union (EU) is a leader in renewable energy in terms of its development and implementation. Nonetheless, to accelerate the transition to clean energy, it was decided to review the Renewable Energy Directive EU/2018/2001 [1] in 2023. The review (Directive (EU) 2023/2413 [2]) sets the target of a minimum 42.5% share of renewable energy at the EU level before 2030, with the possibility of extending to 45% aiming the total independence before the mentioned year to the Russian fossil fuels. Moreover, a robust political framework is established that promotes the electrification of certain sectors, setting new, more ambitious renewable targets for transport, heating and cooling, industry, and buildings.

Furthermore, a higher share of renewables in the grid leads to changes in the traditional electricity grid. The need for a more flexible, intelligent, and efficient electrical grid makes it essential to carry out a transformation.

The traditional centralised grid approach consists mainly of three elements: (a) large power generation plants from various sources (natural gas, nuclear, coal, oil, etc.), (b) transmission lines whose purpose is to transport electrical energy from the generating plants to the point of demand, and (c) points of consumption. In centralised grids, the energy flow is unidirectional, from generation to demand and transmission lines represent a significant point of energy loss.

The energy loss in transmission lines is proportional to their length, providing another reason to promote distributed generation (DG) or small-scale generation. There is generally a clear trend towards a less centralised and more distributed grid, where both the production and consumption of electrical energy occur in a more localised area (see Figure 1.1).

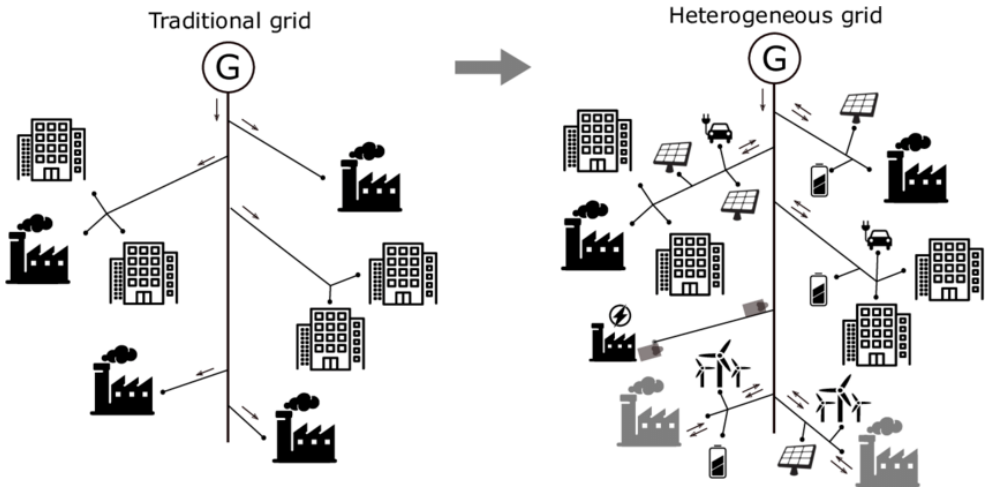


***Figure 1.1***. *Comparative diagram of the traditional network vs the network with distributed generation [3].*

This trend has promoted, among other things, the emergence of elements such as Microgrids and Smart Buildings (SBs) that are perfectly adapted to this type of more decentralised grid. Both facilitate the integration of RES, and more specifically photovoltaic (PV) installations, mainly due to the possibility of installing them on building rooftops [4], thus increasing the injection ratio of energy from renewable sources into the grid.

### 1.1.1 Microgrids

Microgrid concept consists of a group of loads and power sources that operate as a single controllable system supplying both power and heat to their local area. This concept provides a new paradigm for defining the operation of distributed generation [5].

The remarkable advances in control strategies and the technological maturity that exists [6], make Microgrids a reality. However, there are several important aspects to highlight when implementing a Microgrid in a real application.

Microgrid must be technically prepared so that at any given moment can be disconnected from the grid and operate isolated perfectly. From the point of view of the consumer who participates in the Microgrid, its ability to isolate itself is a clear advantage, since it will hardly see any consequences in the event of a failure or black out of the electricity grid. However, in order to be able to isolate itself, the Microgrid must be equipped with Energy Storage Systems (ESS), which require a higher economic investment, as well as making energy management tasks more difficult.

This is why Microgrids are nowadays justifiable and are mainly developed in areas where the electricity grid does not reach or does not work as it should. In places where the electricity grid reaches and operates normally, it is more common to find self-consumption (SC) or collective self-consumption (CSC), which do not require the need for isolation and can provide a high degree of independence from the electricity grid as well as facilitate the integration of RES.

### 1.1.2 Smart Buildings (SBs)

Buildings are among the main energy consumers, accounting for 43% of total consumption in the EU alone [7]. Additionally, the concept of energy efficiency within the building sector was introduced few years ago, more specifically in 1970 with the oil crisis [8]. For instance, in Spain, 58% of buildings were constructed before the first regulation introducing minimum energy efficiency criteria [9]. In addition to the fact that energy efficiency has come to play a key role in the building construction process (thermal insulation of walls, new materials...), it has also led to a massive installation of smart meters in public, commercial, residential and industrial buildings [10]. Smart meters have significantly increased the understanding of the electrical and thermal behaviour of buildings. Since the adoption of Directive 2006/32/EC on energy services, which urged that customers be provided with meters that accurately reflect actual energy consumption and real-time usage information [11], Internet of Things (IoT) technology, along with the concept of Demand Response (DR) and Energy Management System (EMS), has been promoted by institutions [12].

In 2023, the new European Energy Efficiency Directive (Energy Efficiency Directive (EU) 2023/1791 [13]) came into force, aiming to achieve the legislative proposals adopted by the European Commission in July 2021, which are part of the "Fit for 55" package and its complement, the REPowerEU plan in 2022. This new directive leads on more ambitious targets. Particularly regarding the cumulative final energy use savings and increased requirements for energy certificates for buildings. Both new and existing buildings will now need to achieve a better energy rating, needing massive renovations of low-efficiency buildings and the construction of new buildings where energy efficiency becomes an essential aspect. Furthermore, there is a clear promotion to transform buildings into nearly Zero Energy Buildings (nZEB), with a specific package of measures already underway to convert public buildings into nZEBs [14].

The concept of the Smart Building is promoted within this context. A SB is defined in various ways in the literature, one of which is: "buildings whose installations and systems (for example Heat, Ventilation and Air Condition (HVAC), lighting, electricity, security, telecommunications, multimedia, IT, access control, etc.) enable integrated and automated management and control, aimed at increasing energy efficiency, security, usability, and accessibility of the building" [15].

One of the strengths of SBs is the ability to detect, interpret, communicate and respond efficiently to changing conditions [16].

The EU, always aiming to improve energy efficiency, reduce GHG emissions, and create more sustainable urban environments, has been promoting the SBs in recent years, providing both legal and technical frameworks for it. An example of EU policies related to the Smart Building concept includes the "Energy Efficiency Directive". This Directive addresses the importance of installing smart technologies to improve the efficiency of integrated energy systems [13]. Also "Energy Performance of Buildings Directive (EPBD)", which establishes the framework for building performance [17] along with "The revised Energy Efficiency Directive"[13]; and finally, the "Action plan to digitalize the energy system", which highlights the important role of integrating renewable energy into the traditional grid [18].

The ultimate goal is to achieve nZEB. As defined by the UK Green Building Council (UKGBC) in the Net Zero Carbon Buildings Framework [19], these are "buildings that are highly energy-efficient and powered by on-site and/or off-site renewable energy sources, compensating for any remaining carbon balance". The International Energy Agency (IEA) report [20] outlines the timeline to achieve the goals set by the Paris Agreement. Among them, the IEA sets 2030 as the deadline for new buildings to be prepared to produce zero carbon emissions. Similarly, by 2040, 50% of existing buildings should be adapted to be zero-energy emission buildings, with 2050 set as the deadline for 85% of buildings to be prepared to zero carbon emissions.

### 1.1.3 Self-Consumption (SC)

SC refers to the practice of using energy that is produced locally, often from renewable sources [21]. SC can be remarkable solutions for consumers in the face of more decentralised grid models. In fact, they are a more than appropriate systems to favour the integration of RES. In a SC, the aim is to adapt consumption to the generation of RES by, for example, acting on the flexible loads (FLs) of a building. FLs refer to electricity consuming elements, such as household appliances, heating and cooling systems, etc. that in order to shift the timing of electricity demand, their use is strategically modified.

Concerning the advantages provided by SC to consumers, unlike in Microgrids, large ESS are not necessary, significantly reducing the value of the investment. Likewise, this approach reduces the dependence of consumers on the electrical grid, decreasing the energy exchanged with the grid [22], and potentially lowering the cost of electricity. This will be guaranteed as long as a high self-consumption rate (SCR) is achieved, calculated by Equation (1.1).

$$\text{SCR} = \frac{\sum Energy_{consum}}{\sum Energy_{prod}} \quad (1.1)$$

where $Energy_{consum}$ is the energy consumed by all consumers and $Energy_{prod}$ is the total energy produced by the generating installation(s).

Furthermore, consumers can remain connected to the public distribution network, so no additional equipment is required to adopt this model.

#### 1.1.3.1 Collective self-consumption (CSC)

The concept of CSC is a modality of SC gaining popularity. As explained by EDF, "CSC allows locally produced electricity to be shared between producers and consumers connected to the public distribution network within the same geographical area" [23]. Considering the application of an EMS, in either SC or CSC context, there would be no difference. The EMS in a CSC can perform energy management, for example, between the consumption of several buildings and the production of one or several PV plants. In a SC framework, the EMS manages the building's consumption where it is applied to be supplied by the energy produced.

The participants of CSC define the rules for distributing the produced electricity among themselves, and consumers benefit from the locally assigned production (*see* Figure 1.2*)*. This makes CSC an ideal model applicable to Energy Communities (ECs). Moreover, the additional energy supply needed to meet their requirements, together with the use of the distribution grid, is billed by their electricity provider [23].

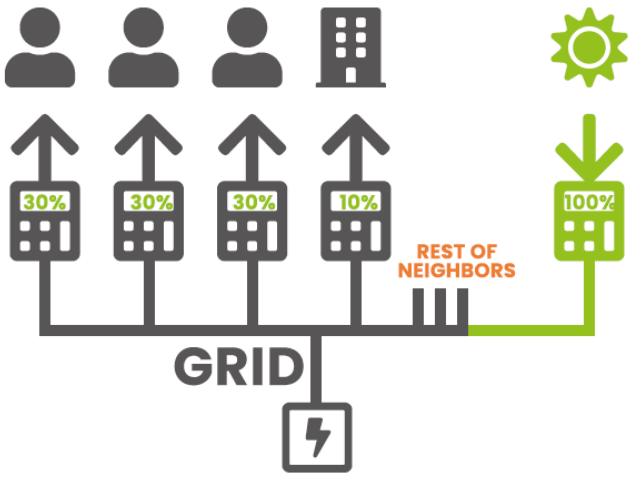


***Figure 1.2**. Simplified scheme of a collective self-consumption* [24].

As stated in [25], SC has limitations, especially regarding the potential investment that must be made in, for instance the installation of a PV production plant. If a group of consumers is

organised, for example in an EC, the amount invested in a PV installation could be in absolute terms higher, thus increasing the amount of energy produced and collectively self-consumed. Achieving a high SCR would translate into greater energy savings and a potentially significant reduction in the electricity bill for associated consumers.

Regarding existing legislation in France and Spain on CSC, in France, the term CSC was introduced into legislation in 2016. CSC is defined in article L.315-2 of the Energy Code. It was in 2018 when Royal Decree 15/2018 recognised the right to CSC in Spain. In the same Royal Decree the right to be able to self-consume electricity without charges being applied was also introduced [26].

Concerning the differences between French and Spanish legislation, one major distinction is the type of generated energy distribution considered by the law. Today, in France, there are different distribution modalities: (a) fixed distribution, (b) predetermined dynamic distribution, and (c) personalised dynamic distribution.

As the name suggests, fixed distribution means that the proportion of produced energy assigned to each consumer is fixed and does not change. Predetermined or default dynamic distribution is done in proportion to the actual consumption of each consumer. Personalised dynamic distribution is based on a formula where the user can customise the distribution. From the perspective of optimising energy distribution in a CSC, dynamic distribution offers greater advantages than fixed distribution. The distribution is calculated a posteriori every 30 minutes in France and every hour and a priori in Spain.

However, in the Spanish case there was only a fixed distribution modality until 2023, so that the distribution among the participants was rigid. For the first time, the amendment to Annex I of Royal Decree 244/2019, through order TED/1247/2021 [27], includes a variable modality. This modality introduces the possibility of changing the value of the distribution coefficients several times a year, at intervals of no less than four months. This allows better use to be made of CSC initiatives.

As noted by *Instituto para la Diversificación y Ahorro de la Energía* (IDAE) in the Self-Consumption Guide published in June 2023 [28] which refers to the distribution coefficient corresponding to each associated consumer as β, the individualised net energy calculated hourly ($INE_{h,i}$) is established by Equation (1.2).

$$INE_{h,i} = \beta_{h,i} * INE_h \tag{1.2}$$

being $INE_{h,i}$ the individualised net hourly energy generated for the hour *h* corresponding to consumer *i*. $\beta_{h,i}$ is the distribution coefficient in the hour *h* for consumer *i* and $INE_h$ the total net hourly energy produced by the generator(s).

Currently, Enedis, the French energy distributor [29], also offers the possibility of a new distribution modality: a *full* personalised dynamic distribution, i.e., ungrouped [30]. This new modality aims to improve the simple personalised dynamic distribution (the third modality mentioned). Before the introduction of this new modality, dynamic distribution was defined by considering all PV generation involved in CSC as if it were from a single entity. With this fourth modality, it is possible to apply personalised dynamic distribution to each of the production installations within the CSC, regardless of whether the installations belong to one or more entities [31]. This will allow for even more precise optimisation of the distribution.

Table 1.1 provides a summary of the advantages and disadvantages of the distribution modalities mentioned above.

***Table 1.1***. *Summary of the characteristics, advantages and disadvantages of the distribution methods established in France.*

| Type | Description | Strengths | Drawbacks |
|---|---|---|---|
| **Static** | Constant allocation coefficients at each 30-minute time step, defined in advance by the PMO*. | Ease use for PMOs*. | ▪ Non-optimal distribution of production.<br>▪ High risk of surplus production. |
| **Dynamic by default** | Variable allocation coefficients at each 30-minute time step, automatically calculated by Enedis in proportion to de consumption of each participant. | ▪ Automatic optimisation of maximum production allocation.<br>▪ No values to communicate to Enedis. | ▪ Benefits large consumers and disadvantages of small consumers.<br>▪ Not customizable. |
| **Dynamic customised** | Variable distribution coefficients at each 30-minute time step defined by the PMO* a posteriori and sent to Enedis. | ▪ Optimisation possible with maximum production allocation.<br>▪ Production allocation can be prioritised. | Every month Enedis must be informed of the values of the distribution coefficients to be applied every 30-minutes. |

*Personne Moral Organisatrice (PMO)

Another advantage of the French framework is related to the perimeter of CSC. In France, CSC can be implemented within a 2 km diameter circumference, whereas in Spain it is limited to 500 m.

Furthermore, within the context of CSC and concerning economic efficiency, one of the most critical aspects is related to electricity consumption tariffs. In France, there are at least 4 or 5 different tariffs throughout the year for connections with medium voltage overhead lines (HTA): tariffs for off-peak and peak hours in winter and summer, and another tariff for peak hours (HTA connection). Additionally, the legislation allows the utilisation of some daily tariff intervals provided by *Linky* smart meter. These bands are designed to enable the Distribution System Operator (DSO) and Transmission System Operator (TSO) to influence user consumption. This allows, depending on the supplier, each consumer to select different tariffs for various time periods and seasons of the year.

Analysing the literature, numerous case studies demonstrate the application of CSC in individual SBs [32], in apartment blocks [33], [34], [35], in several single-family residences [36], in cases where apartment blocks and commercial activity consumption points are combined [37] or even applied in simulation based Microgrids created for industrial parks and university campuses [38]. It has been proven that CSC is applicable and effective in different scenarios despite having various types of consumers and considering different optimisation strategies.

It is worth mentioning that in the Spanish context, given the substantial rise in energy prices, CSC becomes a cost-effective solution. This is demonstrated in [39], where a CSC model applied in Spain is proposed, analysing three different aspects: the sizing of the CSC installation, the use of smart appliances to shift consumption to more profitable times and the distribution of the renewable energy generated by the installation among the consumers participating in CSC. All this is analysed through two models and evaluated in terms of profitability. In this paper, two conclusions should be emphasised. On the one hand, a SC system with surpluses is much more profitable than a self-consumption system without surpluses. On the other hand, it is concluded that a collective installation is more profitable than an individual one.

Due to the significant push CSC have received throughout Europe, grid-connected PV systems have undergone a remarkable transformation, which have evolved from occupying a small market niche to being in several countries one of the primary annual additions in generation capacity [40]. Furthermore, as legislation in various European countries has either reduced or eliminated feed-in tariffs for PV, SC has gained interest to maximise the profitability of the energy generated by PV installations.

## 1.2 ENERGY MANAGEMENT SYSTEM (EMS)

Self-consumption will always be of particular interest if an acceptable SCR can be achieved. EMSs play a key role in saving and managing energy in the systems they operate in. Over the years, extensive research has been conducted on these systems and the enhancement functions they can perform.

The review conducted in [41] showcases works focused on EMS aimed at monitoring and analysing building energy consumption using data processing technology. One notable example is the work in [42], which proposes an energy usage monitoring method, aiming for energy and cost reduction for building occupants. Thanks to the proposed method for monitoring a group of equipment in a commercial building, the proper use of the equipment can be predicted in order to achieve the above-mentioned objectives.

Recent articles primarily focus on increasing energy savings, especially due to the latest EU requirements demanding greater efficiency and energy savings in the building sector. An example of the increasing number of works in the literature focused in this direction is the review in [43], where articles solely focused on reinforcement learning of EMS applied to buildings are analysed to ensure increased energy savings ratios. Likewise, [44] presents an EMS approach seeking to outline a savings plan based on predictions. The EMS is applied to a university campus within a simulation-based Microgrid, and this proposal is seen as highly beneficial in a campus with multiple buildings, to manage energy use and optimize both daily operations and scheduling energy use for an entire semester.

One of the objectives of many EMS is to promote SC in buildings. There are numerous articles seeking to reduce the amount of electricity purchased from the distribution grid by optimizing the use of PV production [45], [46]. The work developed in [47] is a good example of how greater profitability and efficiency are achieved thanks to an EMS that not only seeks maximum utilization of PV production but also manages the heat pump operation to minimize costs while respecting the thermal comfort of the building users. [45] adds another element to the equation, which is shared ESS that will also be used to increase SC based on PV generation, concluding that integrating the designed storage system increases the SCR by 11%. There are also numerous articles integrating Electric Vehicles (EVs) as FLs where EMS acts aiming the increase of SCR [48], [49]. It is interesting to see the conclusions drawn in [50], where the impact of EVs on the SC levels of a home integrating a PV generation facility is analysed. It is concluded that using EVs to store PV energy achieves the self-consumption levels that would be achieved by integrating a battery-based storage system.

Although analysing the literature reveals that the majority of cases where an EMS is proposed are in buildings [51], [52], [53], [54], it is very common to see EMS applied to the e-mobility sector [55], [56], [57] or applied to Microgrids [58], [59], [60], [61]. Also to ECs, which are currently in vogue [62], [22].

Furthermore, it is interesting to analyse the types of EMSs being used for energy management in buildings. Despite having stated that there are countless cases of EMS applied to buildings, few works can be found in the literature where EMS is implemented and validated in a real building.

Demand or load flexibility refers to the practice of adjusting energy using appliances to try to match the electricity supply [63]. Therefore, it is worth noting the importance of identifying potential FLs in buildings beforehand since the energy management strategy will be different. EVs or batteries are a possible FL that have demonstrated to provide a high degree of flexibility to energy optimisation in buildings [64].

One of the main FLs used in Demand Side Management (DSM) or DR is the HVAC system. Associated with the HVAC system, the thermal capacity of the building itself is also an important FL to consider because the thermal inertia of the building will affect HVAC-related consumption. In some cases, Domestic Hot Water (DHW) and its associated tank, which constitute a significant source of consumption in a residential building, are also considered FLs. The mentioned FLs have the advantage over ESSs in that they are already installed in most buildings, while batteries need to be purchased and installed.

Regarding the type of EMS, the most basic EMS are rule-based EMS (RB-EMS) [65]. As RB-EMS is a simple control method, numerous works can be seen where this type of EMS is used to manage systems of not too much complexity. However, for scenarios where control may entail some complexity in terms of the function to be optimised and variables to be controlled, there are other types of EMS such as optimisation-based EMS.

### 1.2.1 Rule-based EMS (RB-EMS)

Starting with RB-EMS, there is a wide selection of papers in the literature employing this type of EMSs to increase the SCR. For example, in [66] an EMS is proposed which combines fuzzy logic with a rule-based algorithm aiming to maximise SC and minimize energy exchange with the grid. Similarly, [67] demonstrates a RB-EMS applied to CSC where the rules are individually defined. In each time step, the building's production is self-consumed as a priority. Then, any surplus is used to charge the battery, and finally, it is exported to the grid if the storage system is full.

As said, in terms of defining the FLs of the building, the HVAC system in relation to the associated thermal capacity should be highlighted. The authors of [68] demonstrate the

advantages of optimizing the operating costs of heat pumps, achieving a cumulative cost savings of 18% at the end of the test period (2 weeks). [69] compares two control strategies applied solely to the optimisation of the air conditioning system in an office building. It is concluded that a basic control strategy such as the on/off strategy of the HVAC system can achieve a consumption reduction of 24.56%. The building's flexibility could even be increased by using heat pumps to heat water at convenient times, so that DHW can be available, avoiding peak load hours.

Regarding the thermal capacity of the building itself, numerous papers go into detail on building thermal models to characterize its thermal behaviour and use it as a FL in a RB-EMS. In [70], a model based on building energy simulation software EnergyPlus is used to simulate the energy and thermal behaviour of the building and use it in a proposed EMS strategy to optimize energy cost and thermal comfort.

Similarly, numerous papers include battery systems as FLs in which an RB-EMS operates. The authors of [71] propose an RB-EMS that aims to maximise net benefit and minimize incurred energy cost by controlling the power used from the Battery Energy Storage System (BESS) to regulate energy consumption from the grid. In [72], a RB-EMS is proposed that considers, in addition to a battery system, a PV energy generation system and prioritizes the consumption of PV energy as well as optimize battery charging scheduling to extend its lifespan.

Unlike HVAC systems or the building's own thermal inertia, BESSs have to be purchased and installed. This has a huge impact on the initial capital investment, as well as the environmental and, in some countries, social implications of lithium mining, among other issues.

### 1.2.2 Optimisation-based EMS

The complexity of the management to be performed by the EMS, as well as the processing time, are two very important factors for choosing the type of EMS to implement. Although it is true that in general optimisation-based EMS require more processing time than RB-EMS [73] in order to effectively carry out energy management in certain scenarios, optimisation is necessary and more than compensates for the fact that it takes more computational time.

Model Predictive Control (MPC) is one of the most common control methods used in optimisation-based EMS. MPC can handle more than efficiently the dynamics of nonlinear systems and strict input constraints. As well, it is able to take into account performance criteria [74]. In [75] a single input single output-(SISO) MPC is implemented in the context of a smart grid, which encompasses energy management along with real-time electricity price optimisation. The SISO-MPC allows controlling electricity usage in commercial buildings while saving energy and managing the energy demand.

MPC can also be applied to energy management in an EC. This is the case in [76] where a Hierarchical Centralized Energy Management System (HCEMS), based on an MPC, is proposed to facilitate energy buying/selling between producers and consumers associated with a community. One of the most important contributions of this work is the demonstration that a greater reduction in the annual energy costs of each dwelling is achieved compared to individual operation. Given the high electricity prices today, the proposal of association in an EC becomes a viable and economical alternative.

Likewise, [77] proposes a MPC-based strategy with the dual objective of minimizing operating costs and maximizing the use of renewable energy in the context of a single building. To reduce the complexity of the building model, it proposes replacing the building with a Microgrid connected to the electrical grid composed of PV panels, BESS and controllable and critical loads. Three types of strategies are compared of which two of them use predictions, while the last one, and used as a benchmark, not. It has been shown that the proposed strategy which includes forecasts can reduce the operating costs of the Microgrid as well as maximise the use of renewables compared to the strategy which does not include forecasts.

Although many of the works found in the literature develop MPCs with the aim of minimizing operational costs, this goal is often combined with a second objective. For example, the work [78], seeks through predictive models and a Sampling-based MPC (SB-MPC) to minimize the total operation cost as well as minimizing harmful gas emissions. They also develop a MPC implemented in a single building that takes into consideration, in addition to cost savings, various environmental aspects and DR. Similarly, in [79] an MPC is employed that includes optimal energy scheduling and predictive models of PV production and building thermal model, aiming to minimize the electricity bill along with ensuring occupants' thermal comfort. The authors of article [80], propose as well, a predictive control strategy based on Artificial Neural Networks (ANNs) for managing electrical consumption and two comfort criteria in an intelligent building. This learning-based MPC, specifically based on ANN models, is compared with conventional MPC, yielding better results with the "intelligent" model.

In cases where SC or CSC is considered, it is more common to design an optimisation-based EMS with the main objective of increasing SCR. This is the case in [81], where the MPC seeks to maximise SCR along with minimizing battery system degradation and grid congestion. As another example, [82] analyses an EC composed of uncontrollable loads (NCLs) and controllable loads (CLs), a community BESS, and shared RES. A MPC is proposed and compared with a standard deterministic optimal control approach. Both have a dual objective, on the one hand, cost minimization and on the other hand, SCR maximisation. The MPC achieves better performance in cost reduction and SCR maximisation.

In summary, it could be stated that it is usually very helpful to implement an EMS in the framework of a SC, because an EMS will ensure a high ratio of SC, which is essential to ensure savings for the CSC participants. Although it may be feasible to propose a simpler RB-EMS, most papers in the literature stand for EMS that include optimisation algorithms because of its better performance when performing more complex systems.

It is important to highlight the significance of identifying the FLs on which the EMS acts, in order to provide a margin of flexibility to, for example increase de SCR of the building. Associated to the building thermal inertia, HVAC has proven to be one of the most interesting FL on which EMS can act because it represents the system with the highest consumption typically found in residential and commercial buildings.

Finally, it is increasingly common to find optimisation-based EMS proposals that include predictive modelling. Forecasts of consumption and production for the next day can be decisive for making decisions and managing energy as efficiently as possible.

## 1.3 CASE STUDY

The case study on which the Thesis work is based falls within a project called EKATE, which consist on "Photovoltaic Electric Energy Management and Shared Self-Consumption in the France-Spain border area, using Blockchain technology and Internet of Things (IoT)." EKATE has been funded under the 3rd call of the INTERREG V-A Spain-France-Andorra Program (POCTEFA 2014-2020).

The specific objective of EKATE is to promote the development of innovative technologies in natural resources through cooperation, in this case within the POCTEFA territory [83]. A consortium that brings together partners from both sides of the Pyrenees, forming a multidisciplinary group, has carried out EKATE. The consortium includes ESTIA (Nouvelle-Aquitaine), UPV/EHU (Basque Country), Enercluster (Navarre), Centre Internacional de Mètodes Numèrics a l'Enginyeria - CIMNE (Catalonia), Développement des Energies Renouvelables dans le Bâtiment et l'Industrie – DERBI (Perpignan), and TECSOL (Perpignan).

Within the framework of EKATE, UPV/EHU research team has developed a pilot action. This pilot project has been used as the case study of the Thesis.

The Izarbel pilot action located in Bidart (France) includes buildings that are part of École Supérieure des Technologies Industrielles Avancées (ESTIA) (see Figure 1.3).


***Figure 1.3.*** *Image of the buildings involved in the Izarbel SC.*

The demonstrator aims to implement an innovative EMS in buildings, in a CSC operation. Initially, newly constructed ESTIA 3 building wanted to be considered. However, since this building is already involved in an individual SC project funded by the Nouvelle Aquitaine region, it could not be included in the CSC perimeter. Therefore, instead of implementing the EMS in a CSC operation, the demonstrator consisted of implementing an EMS in a SC scenario in which the buildings of ESTIA 1 (yellow square) and ESTIA 2 (green square) are included. However, the proposed EMS approach is also valid for implementation in a CSC operation.

There is a PV installation (see Figure 1.4) located on the roof of ESTIA 1. This area is oriented to the southeast and has a slope of 20%.

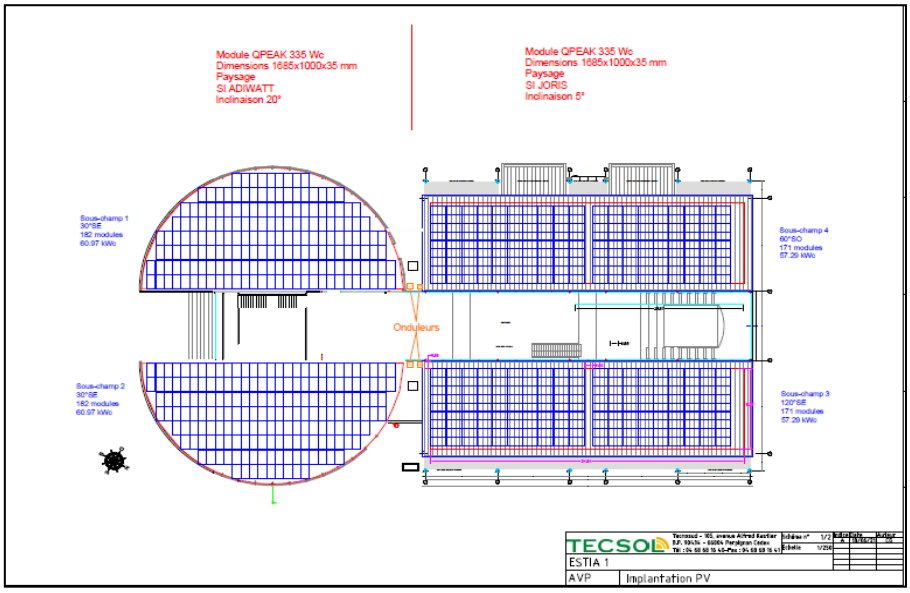


***Figure 1.4.*** *Drawing of the 5,6 kWp PV installation in the ESTIA 1 building.*

Within the EKATE project, it has been intended to enable the buildings that are part of the engineering school to be equipped with 286 kWp of PV installation. Thanks to the project, the necessary funds were raised to carry out the installation. Initially it was expected to increase the existing installation in ESTIA 1 to 117.17 kWp, and the rest were planned to be installed in ESTIA 2 and ESTIA 4 buildings. However, due to delays in the installation, the data of the current installation from 2004 with an installed power of 5.6 kWp was used. However, when validating the EMS through a case study (Chapter 5), the optimisation problem considered the total PV power to be installed in ESTIA 2 building in the short term, i.e. 117.17kWp. Therefore, the measurement of the electricity produced by the existing panels in ESTIA 1, $P_{PV_{M1}}$, has been multiplied by a gain, $G_{PV}$. The gain has been calculated by dividing $P_{PV_{SYST_{MAX}}}$, the maximum power that the new panels would produce according to the PV Syst software [84], i.e. 93.2 kW, by the maximum power produced in 2021 by the current panels, $P_{PV_{M1_{MAX}}}$, i.e. 4.65 kW.

$$G_{PV} = \frac{P_{PV_{SYST_{MAX}}}(W)}{P_{PV_{M1_{MAX}}}(W)} = \frac{93200}{4650} \approx 20 \quad (1.3)$$

The resulting photovoltaic gain was approximately 20 so it has been decided to multiply by 20 times the PV production to show a more realistic scenario.

There will be an organising entity assigned by all the CSC partners, which will be responsible for allocating the production to the different consumption points and for sending the selected distribution coefficients to Enedis, the French distribution grid operator.

The distribution of PV production between the ESTIA buildings is carried out using a personalised dynamic allocation key, i.e. the modality based on a formula where the user can customise the distribution. The distribution coefficients are going to be sent to Enedis and accounted for with a time step of 30 minutes.

During the following section, the intelligent EMS proposal adopted for implementation in the presented case study has been developed.

## 1.4 EMS PROPOSAL

As said, the proposed EMS model is applied to a SC framework where there can be different approaches to energy management for improving the SCR. On the one hand, the sharing of PV production between one or, in case of CSC operation, several buildings can be managed according to some chosen criteria. On the other hand, it is possible to implement an EMS that acts on the building FLs and optimises their operation according to some criteria that could be different from those considered for the PV energy distribution operation. This second approach is the one developed in this Thesis.

The EMS proposed is a MPC type EMS. It is intended to control the heat consumption of the ESTIA 2 building to maximise the SCR by means of the control variable that is the set point temperature (output of the optimisation module). Therefore, by optimally generating the set point temperature, the operation of HVAC system is optimised in order to maximise the SCR of the building.

The optimisation module therefore seeks to increase the SCR to the maximum, but it has always to ensure thermal comfort of ESTIA 2 users. In order to determine what temperature range should be covered by thermal comfort, the adaptive thermal comfort model proposed by Dear and Brager [85] has been used as a reference. This model was developed as a basis for the standards of the American Society of Heating, Refrigerating and Air-Conditioning Engineers (ASHRAE). More details have been given in Chapter 5.

As depicted in Figure 1.5, the EMS employs the predictions of the ESTIA 2 building consumption without considering HVAC system consumption and the PV production. As demonstrated in [77], EMS integrating predictions could improve the optimisation results compared to an EMS that operates without predictions. The predictive model in charge of performing the building energy consumption forecasting is presented in Chapter 2. The PV production forecasting is introduced in Chapter 3.

The control model of the MPC is the model of the FL in which the EMS acts. The FL considered is the HVAC system associated with the thermal capacity of the building, i.e. building thermal model. The modelling of HAVC system and building thermal capacity is depicted in Chapter 4.

The prediction models are updated when the season change, that is to say, even if the models are daily trained, the model hyperpareameters adjustment is done when the season changes. In addition, the building thermal model is updated daily.

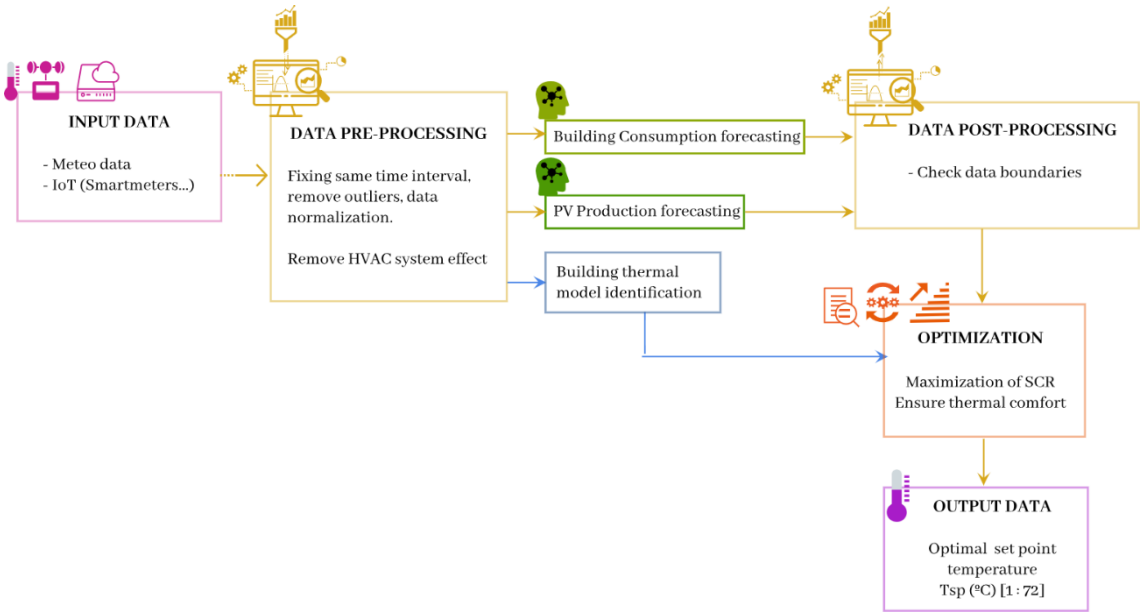


***Figure 1.5**. Flowchart of the proposed optimisation-based EMS.*

The forecasting of consumption and PV generation, as well as the thermal modelling of the building and the modelling of HAVC system have been carried out by means of data-driven models. The data used as inputs to the models have required a pre-processing stage prior to their construction, where modifications have been applied to data to meet the requirements of each model. In this process, missing data or measurement errors have been identified and corrected by interpolation. Then, as not all raw data have the sampling time required by the model, the sampling time has been adjusted, if necessary by averaging or interpolating the original data. The data has been then normalised.

Likewise, as the MPC has to control the consumption of the HVAC system, the prediction of the building's electricity consumption should not include the effect of the HVAC system. Therefore, in the pre-processing stage, the consumption corresponding to the HVAC system has been removed from the total consumption curve of the building.

The aim of the PhD Thesis has been to develop a MPC based on simple models that require a low computational cost. This is why, with regards to the optimisation phase, it has been decided, on the one hand, to use linear models to thermally characterise the building and, on the other hand, to work with predictive models that do not require large amount of data to conduct predictions.

## 1.5 DEFINITION OF GENERAL OBJECTIVES

The objectives of the Thesis have been framed within an innovative scheme for the use of locally produced energy, namely SC.

The general approach of the Thesis aims primarily to develop an intelligent EMS based on forecasting models and implemented in a single building. The EMS must supply the consumption demand of ESTIA 2 building through the PV installation located in ESTIA 1 in order to maximise the SCR of the SC.

Under this general approach, the secondary objectives are described below:

- The design of data-driven predictive models to carry out day-ahead predictions of the consumption of ESTIA 2 building and the production of the PV installation located in ESTIA 1.
- The identification and subsequent modelling of the FL of ESTIA 2 building, on which the optimisation-based EMS will act.
- The design of an optimisation problem in order to maximise the SCR by controlling the set point temperature.
- Ensure at all times that the thermal comfort of ESTIA 2 users is respected.
- The development of prediction and optimisation techniques that have low computational cost.

## 1.6 STRUCTURE OF THE THESIS

The present Thesis consists of five chapters in addition to this introductory chapter.

Each chapter documents the research conducted during each phase of the Thesis, all of which are complementary and essential for the development of the fifth chapter, where the MPC has been developed.

Chapter 2 analyses a predictive model based on an ANN, which forecasts the energy consumption for the next 24 hours of ESTIA 2 building. Chapter 3 introduces an ANN model too but in this third chapter the purpose of the model has been the day-ahead forecasting of the production of the PV installation of ESTIA 1 building. Chapter 4 is dedicated to the design of the thermal model for the building under analysis. The Chapter 5 presents the optimisation problem developed for the purpose of completing the design of the proposed EMS. The last Chapter 6 is dedicated to underline the most important conclusions that have been drawn during the work and the future research lines are enlisted.

Finally, the annexes provide supplementary material, offering a more detailed development of the complementary models studied throughout the Thesis, like statistical analysis models or recurrent neural networks (RNNs) in general, and nonlinear autoregressive with exogenous input (NARX) in particular.

# CHAPTER 2

# BUILDING ENERGY CONSUMPTION FORECASTING

In this second chapter, a data driven predictive model is presented, in particular a nonlinear autoregressive with exogenous input (NARX) type NN. The NARX model aims to perform an hourly day-ahead consumption forecasting of a single building.

Initially, this chapter presents the results of an extensive literature review, justifying the proposed model and methodology. Following the literature study, the chapter outlines the objectives and contributions.

After presenting more in detail the case study the methodology has been introduced. As shown in the methodology section, the work has been carried out in two phases. In the first phase, consumption has been predicted taking into account the effect of the HVAC system and using measured data as inputs to the model. In the second phase, the research has been extended by removing the effect of the heating and cooling system from the consumption curve and using predicted data as inputs. Both phases lead to an analysis of the results obtained under both phases. The performance of the proposed NARX model is compared with other ML models. The chapter concludes with a summary of the conclusions.

## 2.1 PROBLEM STATEMENT

Nowadays our society is facing an unprecedented energy transition process where decarbonisation and digitalisation form two fundamental axes of change.

Energy conservation in building is one of the major topics in Sustainable Development Goals (SDGs). Integration of RES has also been a key issue in the legislation framed within the energy transition. In this context, there is a growing interest in SC and CSC, which makes it possible to integrate RES in a local way and to use the renewable energy produced to supply the demand of, for example, surrounding buildings.

Buildings are responsible for a significant portion of total energy consumption [86]. As of today, 75% of buildings in Europe remain inefficient [87]. In Spain, 30% of the total energy consumed is associated with the building sector, which despite being 10 points lower than in the EU, this percentage is increasing year by year. According to the report of the French Ministry of Energy Transition [88], as in Spain, buildings account for 30% of total consumption in France, and this percentage is rising, although at a slower pace (see Figure 2.1).

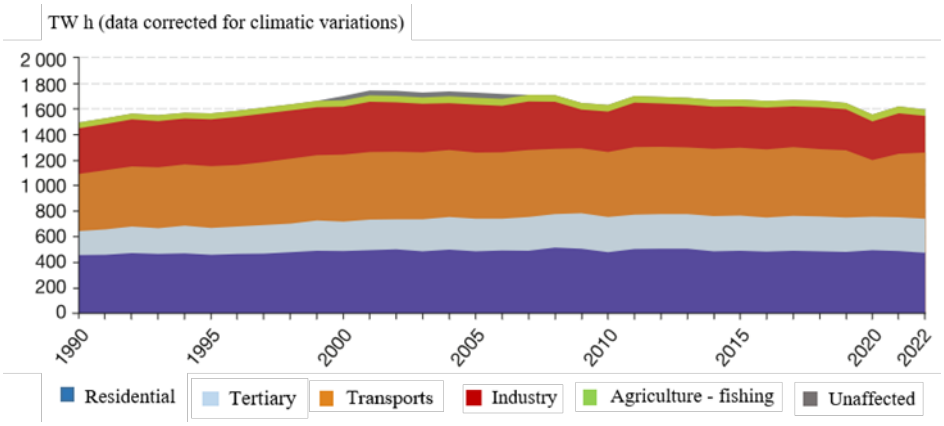


***Figure 2.1**. France final energy consumption by sector [88].*

This makes building sector a key element in contributing to the reduction of energy consumption. Furthermore, buildings offer the possibility of installing PV systems, allowing for the integration of RES and thereby reducing GHG emissions generated by the combustion of fossil energy sources.

To achieve these objectives, energy consumption forecasting might be helpful, not only in the building sector but also in the electrical system. The electrical system hosts many participants who can be affected by inaccurate predictions of the energy that will be consumed next day. Contingency plans, management strategies, and marketing strategies directly depend on consumption forecasts, and prediction errors translate into increased operational costs [89].

Focusing on buildings, it is important to highlight the significance for, for example, an EMS, of including the building's consumption forecast to make optimal decisions regarding energy management. In addition, data used as predictor for performing the forecasting needs to be reliable. Until a few years ago, the meters installed in buildings were far from providing high-quality data. Today, thanks to efforts to equip buildings with IoT technology, data availability is much greater, facilitating modelling tasks and resulting in more reliable and robust models.

However, consumption forecasting is often not an easy task and requires knowledge not only of the modelling process, but also of the characteristics of the data to be used.

The consumption profile generally follows a cyclical and seasonal pattern due to its high dependence on meteorology and users activity and can be represented by a time series of real values [90].

Time series always arise from something observed over time [91] and can be seen in numerous contexts including the measurement of temperature at a meteorological station, the amount of imports or exports of a country, the stock price of any product, annual electricity generation of a PV plant, and so on.

A time series curve can show upward or downward trends, as well as patterns that repeat (seasonal variation) which can be used to predict future values. To take advantage of these patterns and trends for forecasting tasks, numerous prediction methods and models have been proposed.

### 2.1.1 Classification of forecasting models

One of the characteristics that influences the selection of the model is the **prediction horizon (PH) time**. Electric load forecasting has been categorised into four types related to the temporal domain of the forecast: long-term load forecasting (LTLF), medium-term load forecasting (MTLF), short-term load forecasting (STLF), and very short-term load forecasting (VSTLF) [92].

LTLF focuses on the demand forecast horizon of more than one year, including the planning of demand for various electrical systems. MTLF deals with forecast horizons ranging from one month to one year and typically covers network maintenance analysis, electricity price variability, or the organisation of energy distribution on a larger scale [93]. STLF operates within periods ranging from a few minutes to hours or days. It is a factor to consider for daily planning, especially for an electricity company. It is also a critical factor to consider for the implementation of an EMS in a building [93]. Lastly, VSTLF, with a prediction range of between a few minutes and an hour, can be of particular interest for use in Smart Grids and DR applications where real-time electricity deployment is required [94].

However, in most cases found in the literature, PH used for consumption forecasting usually exceeds 15 minutes, sometimes extending to days or weeks. Hence, studies in the literature generally propose STLF instead of VSTLF.

Nevertheless, the most common classification that can be seen in the literature is the one presented in the Figure 2.2. This classification is carried out according to the type of model and are distinguish mainly three major groups: white-box or physical models, grey-box, and finally, black-box or data-driven models [95].

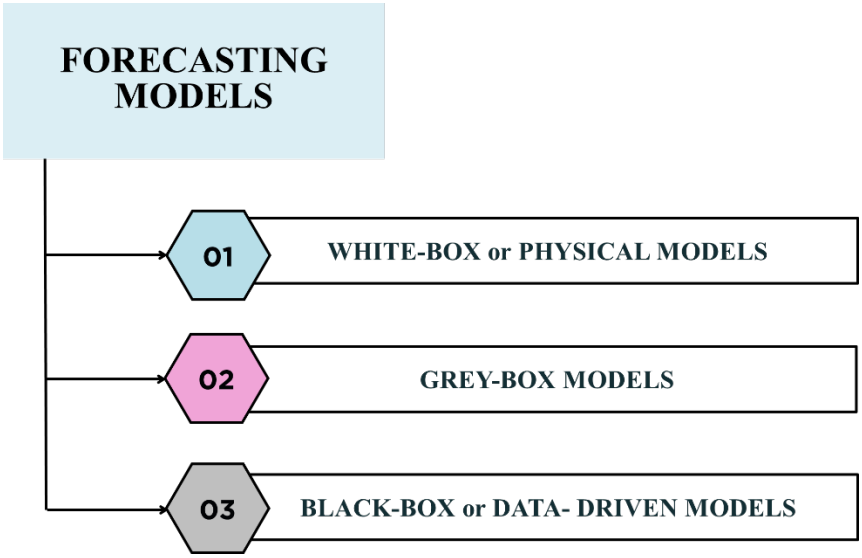


***Figure 2.2**. General classification of forecasting models.*

**Physical models** are those based on mathematical equations that describe physical principles used to calculate energy consumption, for example of a building. As these are complex mathematical models where numerous parameters and formulas must be included, it is common to use specific software to calculate the consumption. The most common softwares used for calculating the energy consumption of a building are EnergyPlus and TRANSYS (Transient System Simulation program). These software are applicable to various scenarios where building consumption needs to be estimated. In [96], for example, TRANSYS software is used to predict the energy demand of a building, evaluating how different parameter values adjustment affect the final result. It is concluded that in general the proposed models achieve a coefficient of variation (CV) of root mean square error (RMSE) less than 10%. EnergyPlus software has also been used in cases where the consumption behaviour of a building under different climatic conditions has been simulated [97].

**Grey-box** are based on the combination of physical models and data-driven models. They are primarily created to simplify the design process of physical models used to predict building consumption [95]. An example of a grey-box model is one that uses data-driven models to

optimise specific parameters of a physical model [98]. There are also numerous studies where, due to insufficient data to feed a black-box model, EnergyPlus or other softwares are used to generate the necessary input data to fed the black-box model which will predict the building's energy consumption [99].

The last category comprises **data-driven models**, also known as black-box models. They are called black box models because they do not establish the relationship between the inputs and outputs of the model; that is, they do not describe the physical principles underlying the system. This characteristic can also be an advantage, as detailed information about the building's physical characteristics and detailed knowledge of the physical phenomena affecting the building's electricity consumption are not required.

These models typically use historical data, in this case for example the electricity consumption of a building, along with external variables (weather data, occupancy data, etc.), to predict the building's consumption.

Several classifications can be find in literature based on model type, but the classification proposed in [98] has been followed.

Data-driven models are divided in three groups (see Figure 2.3):

(a) Statistical Analysis (SA): This is based on the use of statistics to represent some data and study the relationship between variables in the form of time series. The most popular SA methods used for prediction purposes have been regression analysis (RA) and autoregression (AR).

(b) Machine Learning (ML): Machine learning is a method of approximating a function that maps input space to output space by extracting information from data samplings [100]. Supervised and unsupervised learning are two types of ML. In supervised learning, the training of the model is carried out with labelled data, which means that the input data is paired with the desired output data. By contrast, unsupervised learning is based on models that use unlabelled input data for training. Supervised learning is often used for classification or regression while unsupervised learning is used for clustering or anomaly detection tasks in addition to classification [101].

(c) Deep Learning (DL): DL is a subset of ML that uses interconnected neural networks to extract patterns from processed or unprocessed data. It is distinguished from ML models because ML requires expert knowledge to convert raw data into data appropriate for the internal representation of the specific model. In contrast, most of DL models can use raw data. DLs are particularly useful for analysing complex, rich and multidimensional data [102].

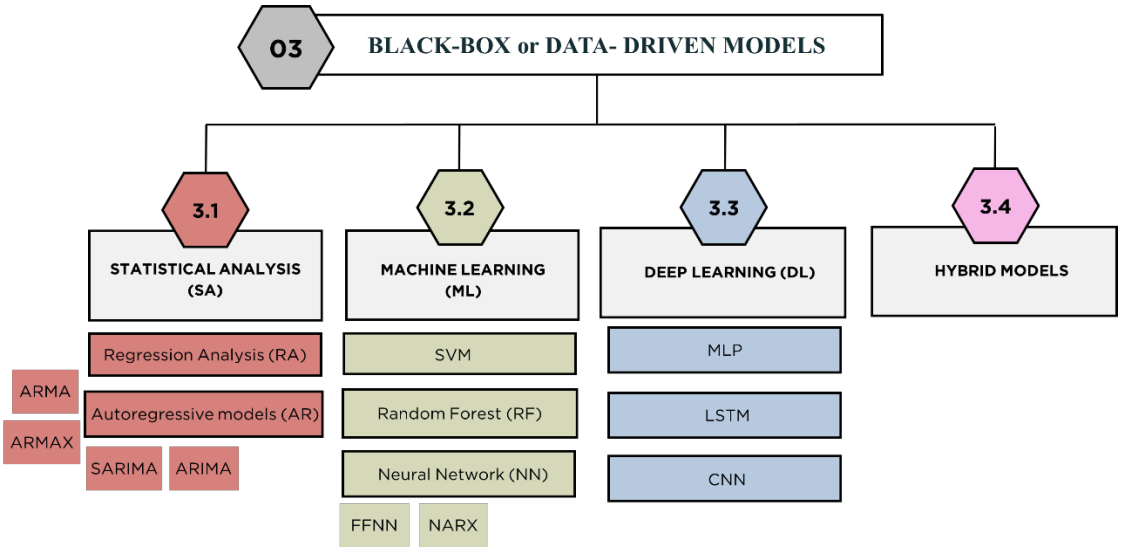


***Figure 2.3**. Classification of data-driven models including some examples.*

Due to their significant impact on the field of energy consumption prediction for buildings, it is important to highlight, on one hand, statistical analysis-based models, more specifically, autoregressive models, and on the other hand, ML models such as ANN or support vector regression (SVR), or neural networks like long-short-term memory (LSTM), typically classified as DL.

The hybrid models have gain significant presence in the literature. These models are those that combine different types of models aiming to improve the performance of the models taken individually. This approach aims to compensate the weaknesses of one model with the advantages of the other.

### 2.1.2 Statistical Analysis (SA): Autoregressive models (AR)

**Autoregressive models**, along with exponential smoothing models, have long been the reference for predicting time series [91]. Autoregressive models have been widely used for many years due to their simplicity in practical implementation for making predictions [90].

Statistical models as a whole have been evaluated by many researchers over the years and in various applications for predictive purposes, yielding more than satisfactory results. Notably, autoregressive integrated moving average (ARIMA) models are an extended version of the autoregressive moving average (ARMA) model. ARIMA models are among the most popular types for time series prediction due to their standard level of short-term accuracy [103]. Moreover, thanks to the Box-Jenkins method, which identifies, estimates and diagnoses mainly ARIMA type models, which allows to increase the accuracy of the predictions. An example can be seen in the work done in [104] where the price of electricity for next 24 hours is predicted using data from the previous three days through the Box-Jenkins method. Using a simple ARIMA model adjusted

with the SPSS program, the electricity price is predicted with a mean absolute percentage error (MAPE) of 3.55%.

More specifically, researchers have also extensively studied the prediction of building electricity consumption based on statistical models for many years. In [105], for example, a seasonal autoregressive integrated moving average (SARIMA) model is used, identified through the Box-Jenkins method, to perform STLF for one of the buildings at Chulalongkorn University (Thailand). The SARIMA model is able to predict weekdays with an average MAPE of 18.82%.

There are even current studies using statistical analysis not only to predict the total consumption of a building but also to predict consumption by zones or rooms of individual buildings. This is the case in the work developed in [106]. Here an ARIMA model is used to predict the consumption of each of the five laboratories analysed. The ARIMA model for one of the laboratories in the building is able to predict its consumption with a RMSE of 0.004247, a more than satisfactory result for an ARIMA model.

The main disadvantage of autoregressive models is that their use is limited to systems that don't present nonlinearities. When the case study involves a nonlinear system the application of this type of model becomes difficult.

Moreover, these models require the identification of the correct model order. Therefore, it is not easy to construct an autoregressive model without training in statistical analysis and a good understanding of the methodology.

Considering all this, and having examined various literature reviews related to the prediction of building electricity consumption, it is clear that there is a rising trend in the use of ML techniques over more classical techniques such as autoregressive methods.

### 2.1.3 Machine Learning (ML)

The increase in literature of ML models for prediction purposes is due to several factors, such as the increasingly easy access to building consumption data and the significant advantage that ML models offer in capturing nonlinearities. In addition, the advanced learning algorithms of ML models and their capability of capturing stationarity of time series are other mayor advantages that present ML models against physical or statistical analysis models.

Several reviews evidence the rising trend of ML models for predicting building electricity consumption. Notably [95] highlights the predominant methods in the literature, focusing on and classifying them according to various characteristics such as input data and data pre-processing methods, building typologies, final energy uses, and forecasting horizons, as well as the evaluation of accuracy. It particularly emphasises the types of models used for this purpose, which

from more than 80 articles analysed, ranging from 2007 to 2019, the vast majority propose ML models to solve the prediction problem.

A more recent paper published in 2023 [107] compiles over 60 articles and reviews data-driven models for predicting building energy consumption. In this case, it includes ARIMA and linear regression (LR) models within the study and compares the number of papers proposing both of them against those proposing ANN, support vector machine (SVM), and Random Forest (RF) models. Although the conclusion is that no single type of model consistently performs better under all conditions, it is stated that ML models produce better results in more studies than statistical tools.

One of the most interesting contributions of this review is its proposal of guidelines for selecting the type of model to use for prediction. These guidelines are designed after analysing the results obtained by each type of model under different situations (data properties, type of energy considered, and type of building explored) and deducing in which conditions each is most appropriate to use, depending on the accuracy of the results obtained. Regarding statistical models, some considerable disadvantages are mentioned, such as ARIMA model's inability to handle independent and correlated inputs, as they can tend towards overfitting and unstable estimates. Similarly, the inability of LR to manage the temporal dependency of the data is highlighted, an important issue when predicting the electricity consumption of a building, as it is a time series.

That said, and in order to see how ML models operate compared to more classical models like AR, dozens of articles can be found in the literature that make the comparison in specific case studies.

### 2.1.4 Comparison between SA and ML models

Before comparing both models, an important aspect that reviews touch on is the metrics used to compare the various types of models presented. Evaluation metrics provide objective criteria for measuring predictive capability, generalisation ability, or overall model quality. Notably [95] breaks down a total of nine different evaluation metrics used in the reviewed papers. Two in particular stand out: MAPE and coefficient of determination ($R^2$).

The former is represented by Equation (2.1) and evaluates the uniform forecast error in percentage terms [103].

$$MAPE = \frac{1}{n}\sum_{i=1}^{N}\frac{|y_j - \hat{y}_j|}{y_j} \times 100[\%] \tag{2.1}$$

where $y_j$ and $\widehat{y_j}$ are the measured and corresponding predicted values. $n$ is the total number of data in the data set considered for performance evaluation.

Equation (2.2) calculates the coefficient of determination.

$$R^2 = 1 - \frac{MSE\ (y_j, \widehat{y_j})}{Var(y_j)} = 1 - \frac{\sum(y_j - \widehat{y_j})^2}{\sum(y_j - mean(y_j))^2} \quad (2.2)$$

being $MSE\ (y_j, \widehat{y_j})$ mean square error between measured and predicted values and $Var(y_j)$ the variance value of the measured data set.

A value for $R^2$ of 1 means a perfect fit between measured and predicted values. A $R^2$ of zero means that there is not relationship between the dependant (output) and independents (input) values, or in other words, the regression line between both is completely horizontal [108] (see Equation (2.3)).

$$0 \leq R^2 \leq 1 \quad (2.3)$$

Comparing SA and ML models, the work introduced in [109] has carried out building consumption predictions of three types of building using an ARIMA model and a SVR model. The most accurate prediction among the two types of models is made by the SVR, with an $R^2$ between 0.07 and 0.1 higher than that of the designed ARIMA models.

In [110] the comparison is extended, and models based on ANN, SVM, and finally, an ARIMA model are designed. Three summer months are used to train the models, and predictions are validated in an office building. It is concluded that the ANN best predicts consumption, achieving a MAPE of 0.1710. The SVM follows with quite similar, though not better, results. The ARIMA model, despite obtaining results very similar to the SVM in predicting weekday consumption, shows a significant increase in error during holidays when consumption remains in standby mode.

More specifically, ANNs have become widely used in recent years for all types of predictions, as evidenced by numerous papers in the literature that position this model type as superior to more classical models. For example, the performance comparison of a traditional autoregressive moving average with exogenous input (ARMAX) model and a NARX neural network, along with a state-space model and a simple FFNN, has been carried out in [89]. Despite all four models obtaining very satisfactory results for predicting the next 24 hours of electricity consumption, the NARX achieves the best MAPE, 0.85%. Similarly, in [111] a comparison is made but this time using, besides the NARX, an Elman neural network (ENN), and an ARMA model to perform a STLF of Jordan's electrical system. The prediction is made using one year of training data (2018 data), and it is concluded that although three types of models are capable of predicting with a

MAPE range between 3.42% and 5.53%, the two types of NN surpass the ARMA. The ARMA presents considerable deviations in its prediction from the consumption curve. From the results, it is derived that the ENN most closely matches the consumption curve and therefore provides the best prediction.

In order to improve the errors that models like ARIMA or ARMA typically produce when predicting time series with seasonal variation, some studies propose a SARIMA model, which includes a term to capture the seasonality of the time series. This is the case in [112], where predictions are made for both one month ahead and the next day for a six-story building using two models: a SARIMA model and a feedforward NN (FFNN) model. Despite having proposed a SARIMA model to capture the seasonality of the consumption data, the ANN predicts with greater accuracy and consistency for both one month and one day ahead.

There is no doubt that, in general, ML models often far exceed the predictive capacity of statistical models.

### 2.1.5 STLF using ML models

STLF can be carried out at different scales, from predicting the consumption of entire regions to predicting the electricity consumption of a single building. In [113], STLF is conducted in two real case studies, predicting the total consumption of Jiangxi Province (China) and the state of California. The authors use an improved SVR model through the sequential-grid-approach (SGA) technique. The results demonstrate that the SGA-SVR significantly improves the prediction accuracy of a standard SVR, particularly for STLF. In the case introduced in [114], the employed prediction model, a hybrid PSO-FFNN model, is validated using consumption data from the New England grid. Here, an hourly prediction is made for different seasons, achieving an extraordinarily high $R^2$ coefficient of 0.9923.

Predicting at Microgrid scale, numerous articles predict short-term industrial load consumption using ML techniques [93]. For example, in [115] an hourly prediction is made one month in advance using a model combining a NARX NN and a more refined model based on LSTM NN. This new combined method is compared with the independent NARX and LSTM models, concluding that the proposed combined method can predict the month with an RMSE 16 times lower (0.0244) than the best LSTM model, which achieves an RMSE of 0.4103.

If the literature search on STLF cases is narrowed down further, a considerable number focus on predicting the load of residential and commercial buildings. In [116], predictions are made one hour and one day ahead for a district comprising residential, commercial, and educational buildings. An ANN based on MLP is employed, comparing its performance with different

numbers of layers, neurons, and learning algorithms. Better MAPEs are achieved when forecasting the individual loads of buildings instead of predicting the entire district's load directly.

When predicting residential buildings, it's worth noting the strong dependence of the consumption curve on human activity within the building under study. This volatility in the consumption curve can pose challenges for accurate STLF. However, it has been demonstrated that this issue can be overcome using NN-based models. An example is [117], where with the aim to mitigate residential building consumption volatility, LSTM and FFNN are proposed, with inputs including consumption curves of household appliances. It has concluded that prediction accuracy can be improved by incorporating the consumption sequences of the building's most energy-intensive household appliances, with LSTM achieving the best prediction with a MAPE of 21.99%.

Commercial buildings have also been studied for STLF. The work introduced in [118] presents a hybrid convolutional neural network (CNN) and LSTM model proposal that predicts consumption curves for two types of buildings—residential and commercial—in Korea. CNN is used to extract input features, feeding into a first LSTM encoder that generates encoded sequences. These sequences then feed into a second LSTM decoder. Results show that the proposed model achieves a MAPE of 0.76%, outperforming other ML models such as SVR with 1.29% MAPE or Gaussian Process (GP) with 0.82% MAPE.

### 2.1.6 Conclusions

It can be observed that the proposals in the vast majority of papers predicting short-term electrical load for both multiple buildings and individual buildings involve designing **highly complex NNs**. The complexity is especially evident in the network structure itself; for example, in the aforementioned paper [116] multiple layer perceptron (MLP)-type networks are proposed with 12 inputs, adjusted between 24 and 48 neurons, and 2 or 3 hidden layers. This complex structure results in the network predicting with a MAPE of 1.71%, requiring 14 hours of training. The same complexity is seen in the previously introduced work where an LSTM with 512 neurons achieves a far from excellent MAPE of 21.99%. Alternatively in [118], where a CNN combined with a double LSTM comprises a staggering 10 layers and over 33,000 parameters. While the MAPE obtained is excellent, the training time is extremely high.

Furthermore, although there are case studies focusing on STLF using NN models for single buildings, the majority in the literature **aggregate consumption curves** from groups of buildings or even entire cities, regions, or countries. In these cases, the consumption curve appears much flatter and less variable, which simplifies the prediction process.

There are works such as the one introduced in [119] where an ANN-based model is trained with a TW of only 3 days and, in addition, the prediction of the small-scale loads of a building is carried

out instead of the entire building consumption forecast. In this way a MAPE of 7.0527% has been obtained. In spite of this, in general, ML models and specifically NNs, when used for predictions, are trained on **large amounts of data**. Most of the literature reviewed utilizes a minimum of 1 year of data to train NN-based models. Moreover, the data used are typically historical measured data, that is, real data. However, in a real scenario the predictive model should not use historical measured data, but predicted data.

Many case studies often involve newly constructed buildings, which, despite having smart meters, may lack sufficient long-term data for model training. Initially it might seem worthwhile in such cases to rely on physical models rather than data-driven models for consumption forecasting because more physical data of new construction buildings might be available. Anyway, it should be considered that physical models may become, over the long term, invalid due to, for example, multiple changes such as the installation of high consuming system occurring in the building [120].

## 2.2 OBJECTIVES AND CONTRIBUTIONS

After analysing the literature and identifying the current trends in using models to predict short-term building consumption, several gaps have been highlighted within the literature.

In this regard, the main objective pursued in this chapter has been to predict the hourly electricity consumption for the next 24 hours of a single building using a NARX-type neural network trained on a small data set.

There are two reasons why the available dataset is limited and therefore the training must be carried out with a small data set:

- The smart meter of ESTIA 2 was activated at the end of 2019. Moreover, due to the pandemic situation, the building's electricity consumption is not representative during certain periods.
- Using a small dataset for training prediction models allows for frequent updates due to low computational demand. Unlike models trained once with several years of data, NARX can account for changes in consumption due to unexpected modifications, such as the introduction of new high-consumption appliances.

The secondary objective has been to perform the predictions as they would be performed in a real system. Thus, predicted data have been used as inputs to the predictive models. In addition, the consumption of the HVAC system has been removed from the overall building consumption. The reason for this removal is that the proposed EMS aims to control the heat from the HVAC system and therefore, the total building consumption cannot include the consumption associated with the HVAC system (see Chapter 5).

In this context, the contributions of the research developed in this chapter need to be noted.

As reflected in the literature analysis, most studies proposing different types of NNs use large data sets for training models which are often quite complex predictive models. In this chapter, a **simply structured** NARX-type NN has been designed and trained on a **small data set**, which allows the possibility of using NNs without the need for extensive data availability.

Furthermore, the performance of NARX is compared with the performance of a LSTM NN, a more complex NN, and with a SVR. The designed models have forecasted electricity consumption for a single building during two different seasons: winter and summer.

In this chapter, has also included the comparison between using an approximate **occupancy** signal and a workday/weekend signal. This latter signal is frequently used in the scientific literature due to a lack of occupancy data.

## 2.3 CASE STUDY

### 2.3.1 ESTIA 2 building description

The electricity consumption prediction has been conducted in the ESTIA 2 building (see Figure 2.4), located in Izarbel Technology Park in Bidart, France. The building comprises four floors: basement, ground floor, first floor, and second floor. It is one of the three current buildings on the ESTIA Institute of Technology campus, where the SC must be implemented (section 1.3 of Chapter I).

***Figure 2.4**. ESTIA 2 building.*

As said, the building is part of the Engineering School and hosts various activities, accommodating different types of users. It includes areas for research teams, university classrooms for student lectures, and spaces for small start-ups with several employees. Considering the diverse schedules and usage patterns of the users, the consumption curve is expected to vary significantly throughout the year.

The building features several sources of electricity consumption, including computers, various laboratory machines (not high-consumption), lighting, and most notably, the HVAC system. This system provides both heating and cooling for the entire building, consisting of 10 external heat pumps connected to 73 internal units. Each external unit supplies heating or cooling to multiple rooms via a heat transfer fluid and fans.

This detailed description sets the context for understanding the varied consumption patterns and the significant role of the HVAC system in the ESTIA 2 building, crucial for developing accurate electricity consumption predictions.

### 2.3.2 Used data analysis

The proposed prediction model for this case study is a NARX model, which is a data-driven type model. The quantity and quality of the input data is crucial for achieving high prediction accuracy. Therefore, data processing, which involves preparing the data to meet the model's requirements, is a fundamental step before starting the model design process.

An initial analysis must be conducted to determine the type and quantity of available data. At this stage, it has been observed that three types of data are available: historical measured consumption data, measured weather data, and building use related data.

#### 2.3.2.1 Consumption data

Building's consumption data has been used to train the prediction model. These data have been provided by the PME/PMI smart meter installed in ESTIA 2 building and has been registered with a time step of 10 minutes.

##### a. First phase

In a first phase, only data from late 2019 (smart meter installation date) until December 2020 has been available (see Figure 2.5).

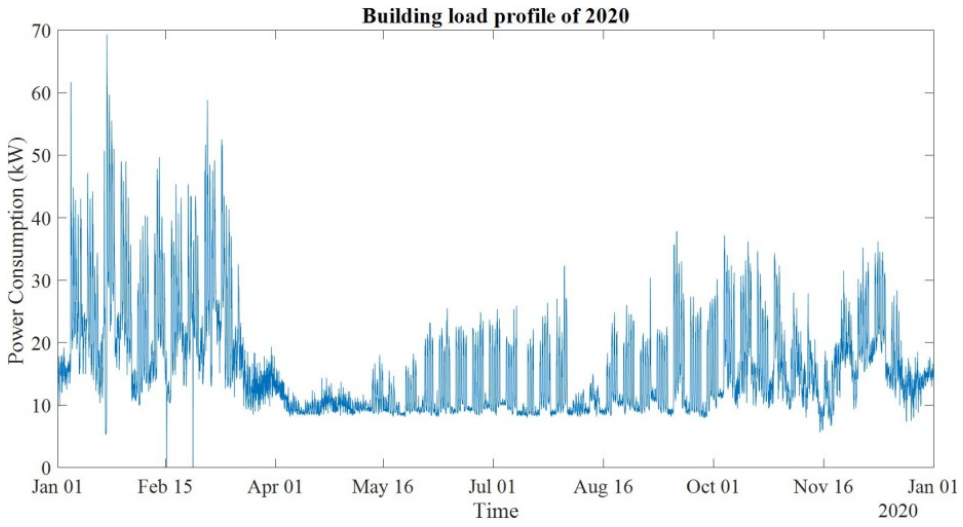


***Figure 2.5**. ESTIA 2 building consumption curve of 2020 without pre-processing.*

An important factor affecting the quality and reliability of this data is the COVID-19 pandemic lockdowns. Specifically, from mid-March to late May 2020 and again from late October to late December of the same year, most individuals who regularly work at ESTIA 2 had to work remotely. This has resulted in a significant amount of data not accurately representing the building's actual operations.

As previously mentioned, two representative months of the year, one from the winter period and one from the end of summer period, have been selected. September and not another summer month has been chosen because of two reasons. On the one hand, there is no normal activity in the months of July and August due to the summer holidays of students and workers. On the other hand, the meteorological data of those months was full of lack of registrations and outliers.

The consumption used in this first phase is the electric consumption with the effect of the HVAC system. It should be mentioned that in the ESTIA 2 building, the users have the possibility to change the set point temperature ( $T_{sp}$) freely in each office or room of the building and thus leading to chaotic operation of the heat pumps. At first glance, several issues can be observed in Figure 2.6. During February, the peaks reach considerably higher consumption values compared to September. Although the week of 14th September sees consumption slightly exceeding 40kW, the average consumption for the entire month remains around 14kW, whereas in winter it rises to 22kW.

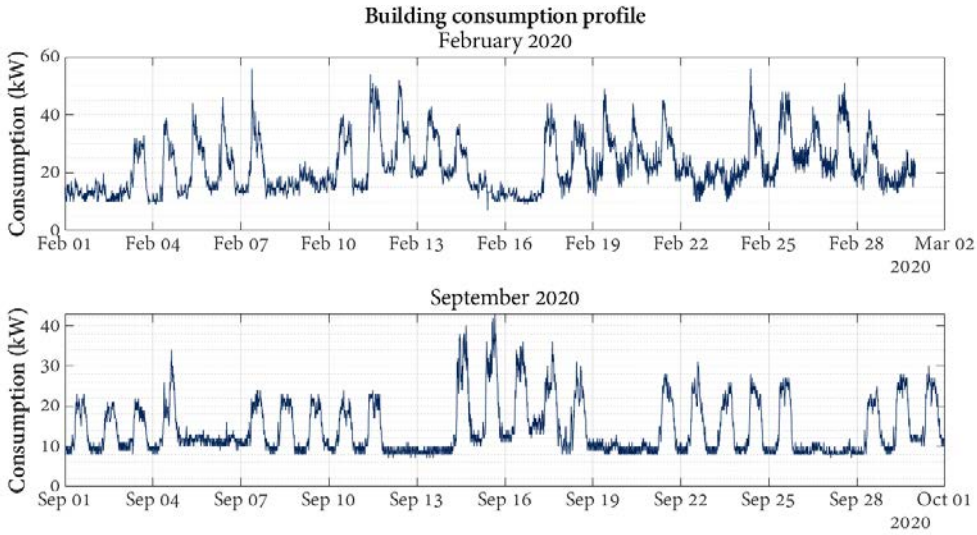


***Figure 2.6.*** *2020 February and September consumption data without normalisation.*

It is also worth highlighting the difference in night-time consumption between the two months analysed. In winter, due to lower temperatures, night-time consumption remains between 15kW and 20kW. In contrast, during the summer, consumption stays around 10kW.

Both the night-time period and weekends in February indicate the significant influence of the HVAC system on the building's overall consumption. Despite the building being unoccupied during the night and weekends, the consumption shows peaks and variations that might initially be attributed to the heating system being activated to face low temperatures.

#### b. Second phase

In the second phase, one of the members of the research team has developed a programme to pre-process the data automatically. The consumption related to the HVAC system has been removed from the overall consumption curve and the sampling time has been fixed in 1 hour (see Figure 2.7).

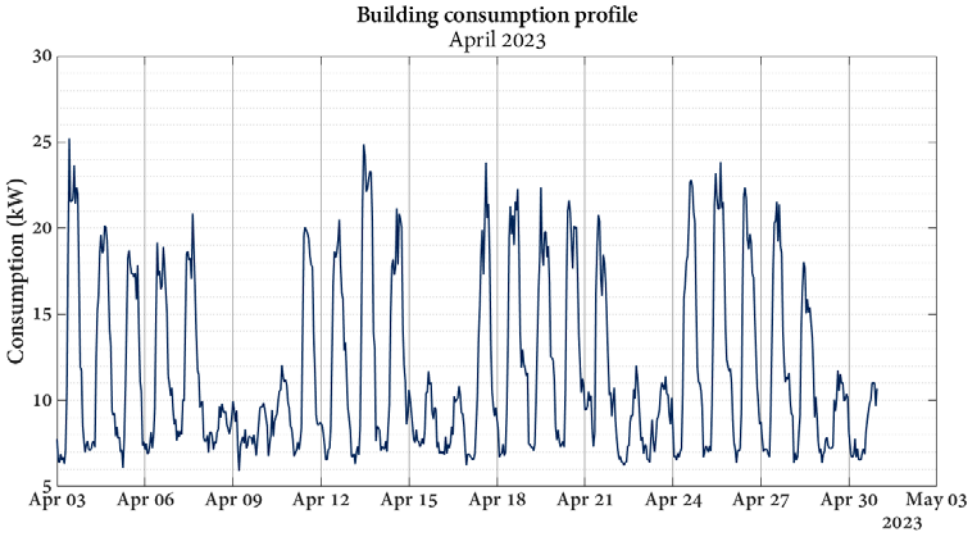


***Figure 2.7****. 2023 April consumption without HVAC system effect and without normalisation.*

The reduction in consumption that can be seen in Figure 2.7 compared to the September graph in Figure 2.6 is remarkable. Both, the consumption peaks and the 'base' consumption that can be seen during the nights demonstrate this. This proves the importance of the HVAC system in the overall ESTIA 2 consumption.

### 2.3.2.2 Meteorological data

#### a. First phase

Due to the influence of meteorological conditions on the consumption, possible weather variables have been considered as inputs to the model.

Meteorological data has been obtained from Meteo France (MF), which stores measured data from the weather station located at Biarritz Airport, approximately 3 km far from ESTIA 2. The downloaded data corresponds to the external temperature ($T_{ext}$) readings from the year 2020, sampled at hourly intervals.

Figure 2.8 shows the $T_{ext}$ data to be considered for the daily consumption prediction during both winter and summer periods.

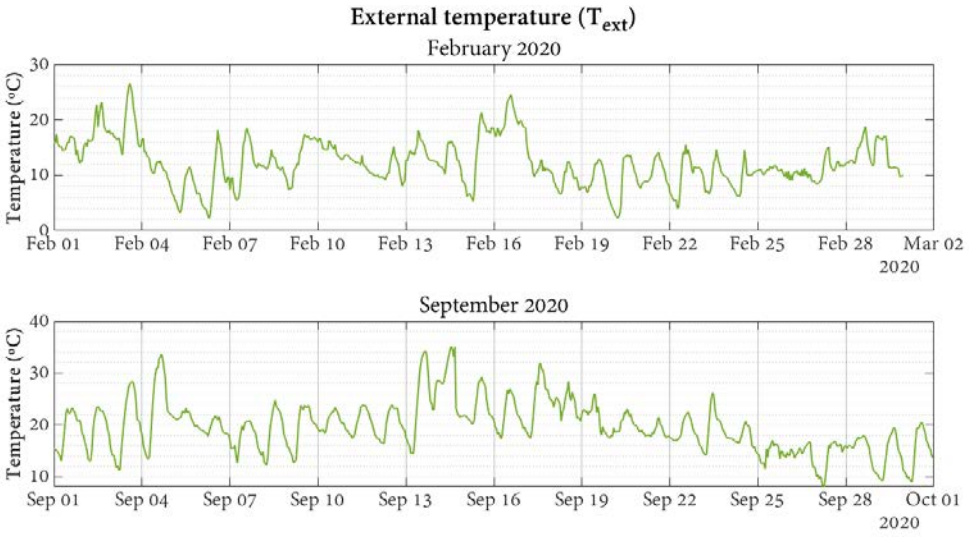


***Figure 2.8**. February and September $T_{ext}$ data without normalisation.*

Looking at Figure 2.8, the difference between summer and winter temperatures is clear. September temperatures are rather warm and probably the use of air conditioning will be lower than in February, in order to maintain thermal comfort in the building. This would explain the flatter curves seen in the September consumption profile (see Figure 2.6). In the same way, bigger consumption peaks when the temperature increases above 30ºC can be observed, more specifically, the 13th or 14th of September.

### b. Second phase

The meteorological data used in the second phase has been predicted temperature obtained from Meteo Galicia (MG). The acquisition and pre-processing of the predicted data has been carried out in order to be able to work on a real system. Figure 2.9 shows the predicted $T_{ext}$ during the month of April.

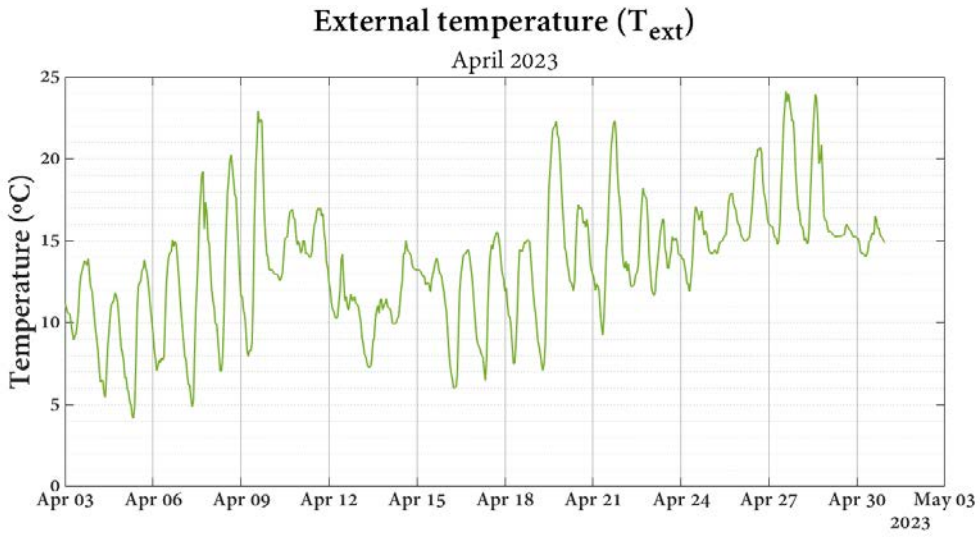


***Figure 2.9**. 2023 April $T_{ext}$ obtained from MG.*

It might be mentioned that being temperatures from the first half of April similar to temperatures in February, the consumption registered on February 2020 is significantly higher than the consumption measured on the first half of April, proving again the significance of the HVAC system in the global consumption.

#### 2.3.2.3 Building use related data

Possible inputs related to building use have also been considered. On one hand, an array has been created to differentiate between workdays ('1') and weekends or holidays ('0') named workday/weekend signal.

On the other hand, using information regarding the schedules of ESTIA 2 users provide by ESTIA Institute of Technology, a daily curve of average building occupancy during workdays ($OCC$) has been designed. Same signal has been used in first and second phases of the work.

The occupancy data reflect two peaks which represent the occupancy of the building at ratio 1 (see Figure 2.10). The decrease around midday corresponds to most users leaving the building for lunch.

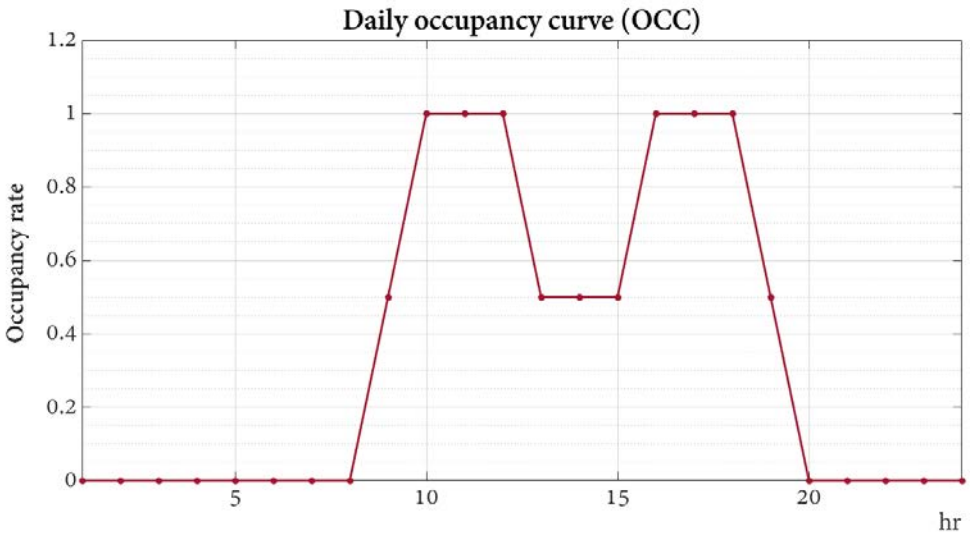


***Figure 2.10**. Occupancy curve of a single day of ESTIA 2 building.*

During weekends and holidays, the occupancy curve has a value of zero. Despite the possibility of specific days, such as Saturdays or certain holidays, when some workers, especially those from start-ups, come to work, the occupancy rate hardly changes.

## 2.4 METHODOLOGY

### 2.4.1 Methodology description

In this subsection, a description of the methodology followed during the research work is provided. In accordance to the objectives depicted in section 2.2, two phases have been divided.

#### 2.4.1.1 First phase

With a time step of 1 hour, the prediction for the following 24 hours has been conducted over a one-month of the end of summer (September) and one month in winter (February). More specifically, the prediction of the average hourly power has been carried out. Both seasons have been considered because consumption patterns vary significantly due to differences in weather. The aim has been to validate the NARX model and to evaluate and compare the accuracy with which NARX, and two more ML models (LSTM and SVR) are able to forecast summer and winter months. The performance of the three models has been assessed and compared based on the minimisation of the mean absolute percentage error (MAPE).

The steps that have been followed in the first phase are illustrated in Figure 2.11.

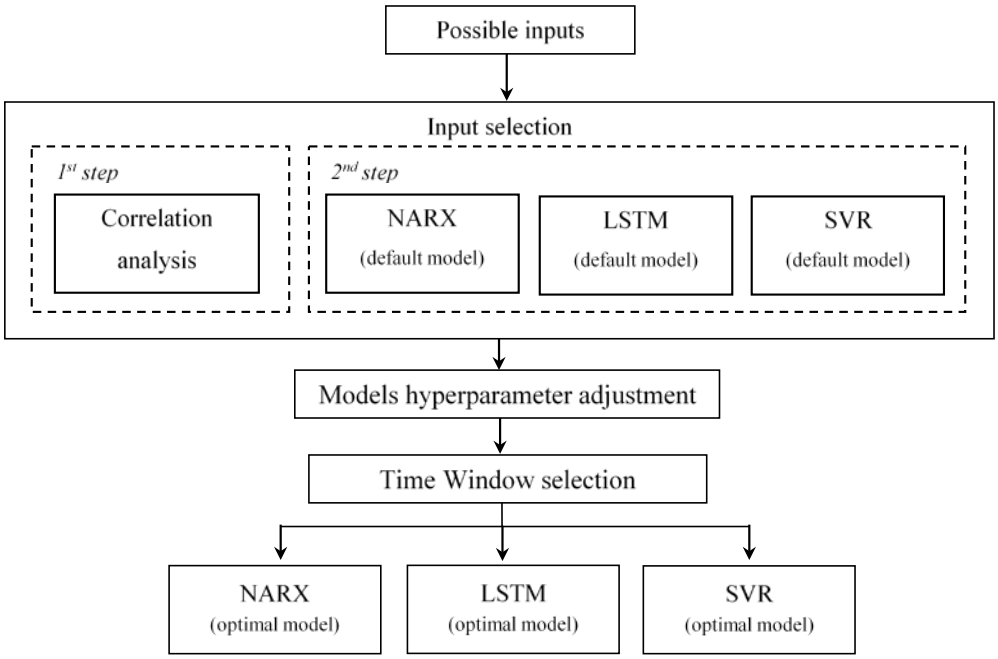


***Figure 2.11**. Flowchart of followed methodology in first phase.*

First, inputs for the models have been selected by carrying out a correlation analysis and then, by making predictions with all possible input combinations.

Regarding the training of the models, a certain Time Window (TW) has been selected. This TW defines the number of days selected to perform the model training. The ML models have been trained with a defined TW on a daily basis to predict the day-ahead consumption. After predicting, for example, the consumption on the 1st day of September, the initial TW is shifted by one day and trained again to predict the 2nd day of September. And so on and so forth until the prediction period is completed.

Taking into account that when training a NN-type model, the initialisation of the weights is executed randomly, we wanted to establish a criterion for the selection of the hyperparameters. As said, the NARX forecasts the entire month, so the NARX predicts three times the entire month on daily training basis. The month average MAPE is calculated each of those three times. This process is repeated for each combination of hyperparameter values i.e. for each model constructed, and the model that the lowest MAPE obtains is selected.

For the design of SVR, Bayesian optimisation has been used to find the optimal hyperparameter values.

#### 2.4.1.2 Second phase

The second phase can be seen as an extension of the first phase. In this second phase, a day-ahead forecasting of ESTIA 2 average hourly power has been performed with a NARX model. With the sampling time of 1 hour, the prediction of the following 24h is carried out during one week of April.

In this case, the HVAC system effect has been removed from the global consumption curve. Furthermore, in the second phase the data used as predictors of the model have been predicted and not measured. Additionally, data acquisition and pre-processing have been performed automatically, as would be done in a real-time scenario. Together with the NARX model, the SVR model is designed and both have been evaluated and compared based on the minimisation of MAPE.

Therefore in this second phase, the acquisition and pre-processing of data has been automated so that these steps can be executed in real time. With regard to the selection of inputs and the TW, i.e. the structure of the model, it has been decided to use the analysis carried out in first phase as a reference. However, this time a time vector has been included as input to the SVR model. In addition, LSTM model is not included between the predictive models analysed.

Same criterion as in the first phase has been followed in order to adjust the hyperparamenters of the NARX model. For the design of SVR, Bayesian optimisation has also been employed for optimizing SVR hyperparameters.

### 2.4.2 Application of methodology

#### 2.4.2.1 First phase

##### a. Data pre-processing

The consumption data from 2020 underwent several processing steps. Initially, deficiencies in the consumption records were identified. Several instances were observed where consumption suddenly dropped to very low levels, such as on the afternoons and evenings of February 20$^{th}$, as well as the 15$^{th}$ and 26$^{th}$ of that month. Linear interpolation has been used to address these outliers.

As mentioned earlier, consumption is recorded at 10-minute intervals, while predictions have been made for each hour of the following day. Therefore, as next step in data pre-processing, the hourly mean value of the load has been calculated.

The final step is the normalisation step. The data has been normalised to the range [0, 1] ([0W, 100kW]). There are several normalisation techniques that are implemented to normalise the input and target data of NNs, such as min-max Normalisation, Z-Score normalisation or Decimal Scaling Normalisation [121]. It is the min-max Normalisation that is most commonly used in the literature (see Equation (2.4)) [122].

$$x^n = \frac{x - \min(x)}{\max(x) - \min(x)} \tag{2.4}$$

Regarding $T_{ext}$, no outliers were detected. The data has been directly normalised ([0, 1]), taking into account historical minimum and maximum values in the studied location ([-10ºC, 40ºC]). Neither the signal differentiating workdays and weekends nor the occupancy curve needed pre-processing.

##### b. Input selection

The input combination selection that best characterise the building's consumption behaviour has been carried out in two steps.

First, a linear correlation analysis has been conducted to determine which variables among external temperature, workday/weekend array and occupancy are most correlated with the building's consumption. Pearson's correlation coefficient has been used for this purpose (see Equation (2.5)).

$$r = \frac{\sum(x - \bar{x})(y - \bar{y})}{\sqrt{\sum(x - \bar{x})^2 (y - \bar{y})^2}} \tag{2.5}$$

where $x$ and $y$ are two different variables and $\bar{x}$ and $\bar{y}$ are the mean values of both.

The Pearson correlation coefficient, *r*, is a measure of the linear correlation between two data sets, ranging from -1 to 1. A positive correlation means that as one variable increases, the other also tends to increase, whereas a negative or inverse correlation indicates that as one variable increases, the other tends to decrease. A correlation is considered strong when the absolute value of the Pearson coefficient is close to ±1.

The correlation analysis has been conducted separately for winter and summer months. Figure 2.12 displays the scatter plot of the calculated coefficients for each season and variable. Additionally, weekends were not considered due to their limited relevance in understanding how potential input variables affect the building's electricity consumption.

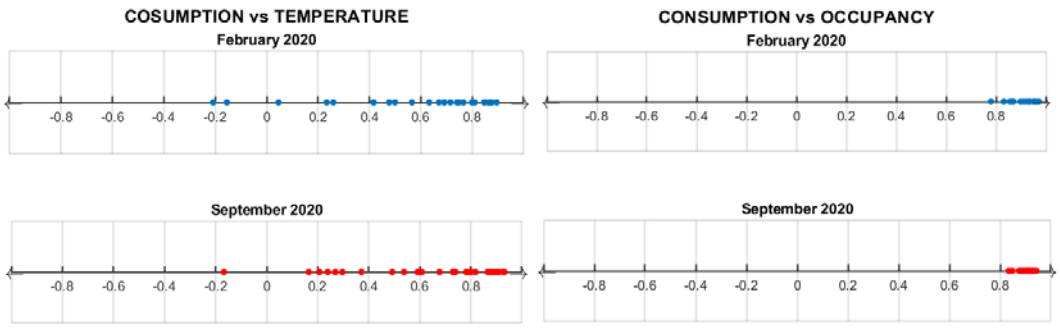


***Figure 2.12**. Daily lineal correlation analysis of possible inputs and consumption curve in different seasons.*

First of all, analysing the scatter plot that corresponds to the correlation coefficients between consumption and $T_{ext}$, it can be observed that on most days there is a significant correlation, where a Pearson coefficient between 0.6 and 0.9 is obtained. It is also noteworthy linear correlation between consumption and building occupancy, with a coefficient greater than 0.8 being obtained practically every day, both in winter and summer.

In the case of winter, it can be strange not to see negative values of the coefficient, i.e. not to see an inverse correlation, in case of consumption and $T_{ext}$. In winter, by basic logic, as external temperatures fall, consumption increases. What happens is that having analysed the correlation on a daily basis, temperatures during the day increase during the morning and start to fall during the evening hours, as does the consumption curve according to the use of the building. This makes the daily correlation between the two variables positive.

Anyway, to corroborate this, a second correlation study has been performed during the entire month of February, taking into account the maximum daily value of $T_{ext}$, and the average

consumption. The correlation coefficient obtained is $r = -0.609$, concluding that there is indeed a global and inverse correlation between both variables when analysed more broadly.

Although the correlation study gives us a preliminary idea of the potential that both $T_{ext}$ and $OCC$ may have as predictors of consumption, a second study has been carried out where we predict with different combinations of inputs with the aim of minimising the MAPE.

Among the different combinations of inputs, the main interest has been to compare the accuracy of the forecasts obtained with, on the one hand, the workday/weekend array and, on the other hand, the $OCC$ curve. The results of this study are given in Table 2.1.

***Table 2.1.*** *Comparison between input combinations with three prediction models (default hyperparameters).*

| Input combinations | Time Window | MAPE Winter | | | MAPE Summer | | |
|---|---|---|---|---|---|---|---|
| | | **NARX** | **LSTM** | **SVR** | **NARX** | **LSTM** | **SVR** |
| Temperature + workday/weekend array | 14 days | 25.6 | 31.4 | 20.08 | 21.7 | 25.84 | 17.19 |
| Temperature + Occupancy | | **18.3** | **19.58** | **20.00** | **13.9** | **13.58** | **15.19** |

The forecasting accuracy achieved with $OCC$ data is much better than the one obtained with workday/weekend array, regardless of the type of model used. Therefore, $OCC$ and $T_{ext}$ have been considered as inputs of the designed forecasting models.

### c. Model hyperparameter adjustment

The process of adjusting the hyperparameters of the three ML models has been carried out similarly for both seasons, summer and winter. Particular attention has been given to the design process of the NARX model, as the LSTM and SVR models have been developed by other members of the research team.

For the NARX model, three different hyperparameters have been adjusted to achieve the lowest MAPE: i) input and feedback delays, ii) number of neurons in the single hidden layer, and iii) activation function for the hidden and output layers. A simulation plan has been designed accordingly.

All possible values for each of the hyperparameters gathered in Table 2.2 have been combined with four TWs that can capture the weekly consumption trend. Each of the possible combinations of the hyperparameter values defined in Table 2.2 constitutes a NARX model.

***Table 2.2**. Simulation plan for NARX model design for first phase.*

| | Training characteristics | Model structure | | Model hyperparameters | | |
|---|---|---|---|---|---|---|
| | | Input combination | Time Window (TW) | Activation function | neurons | input & feedback delays |
| NARX | Learning algorithm: *Levenberg-Marquardt* | Optimal input combination | 7 | Hidden = { sigmoid, tansig}<br>Output = { sigmoid, tansig, linear} | [2, 3, 4, 5, 10] | [2, 5, 10] |
| | Error = MSE | | 14 | Hidden = { sigmoid, tansig}<br>Output = { sigmoid, tansig, linear} | [2, 3, 4, 5, 10] | [2, 5, 10] |
| | Daily NARX training = 3 times | | 21 | Hidden = { sigmoid, tansig}<br>Output = { sigmoid, tansig, linear} | [2, 3, 4, 5, 10] | [2, 5, 10] |
| | | | 28 | Hidden = { sigmoid, tansig}<br>Output = { sigmoid, tansig, linear} | [2, 3, 4, 5, 10] | [2, 5, 10] |

Regarding the selection of the learning algorithm in order to prioritise fast training and low computational time, the *Levenberg-Madquart* algorithm has been used.

Regarding the tune of the delays it has been observed that increasing the delay value does not affect the MAPE result. Therefore, a delay of 2 steps has been set for both, input and feedback.

A general conclusion can be underlined regarding NARX model results gathered in Table 2.3: regardless of the used TW, the best results have been obtained with 5 neurons. As for the activation functions, the hyperbolic tangent (*tansig)* function has been set in the hidden layer and linear function in the output layer.

***Table 2.3.** MAPE results obtained with NARX combining different TW and number of neurons in the hidden layer.*

| Input combinations | Time Window | Nº Neurons | LSTM MAPE | |
|---|---|---|---|---|
| | | | Winter | Summer |
| **Temperature + Occupancy** | 7 days | 2 | 21,3 | 17,6 |
| | 7 days | 3 | 19,65 | 16,4 |
| | 7 days | 4 | 23,1 | 16,75 |
| | 7 days | 5 | **19,4** | **14,3** |
| | 7 days | 10 | 19,86 | 42,45 |
| | 14 days | 2 | 18,25 | 14,6 |
| | 14 days | 3 | 21,5 | **14,3** |

| | | | |
|---|---|---|---|
| 14 days | 4 | 18,9 | 15,15 |
| 14 days | 5 | **14,0** | 14,7 |
| 14 days | 10 | 16,60 | 14,71 |
| 21 days | 2 | 18,55 | 15,2 |
| 21 days | 3 | 16,0 | **12,3** |
| 21 days | 4 | 15,2 | 15,35 |
| 21 days | 5 | **14,9** | 13,0 |
| 21 days | 10 | 15,69 | 15,52 |
| 28 days | 2 | 17,0 | 12,4 |
| 28 days | 3 | 15,4 | 14,5 |
| 28 days | 4 | 15,3 | 14,9 |
| 28 days | 5 | 14,7 | **14,2** |
| 28 days | 10 | **14,59** | 14,97 |

Finally, the selected model characteristics are described in Table 2.4.

***Table 2.4**. NARX proposed model hyperparameter values for energy consumption forecasting of first phase.*

| **Hyperparameters of NARX** | |
|---|---|
| **Hidden layers** | nº of hidden layers = 1 |
| | number of neurons = 5 |
| **Delay vectors** | Input = 2 |
| | Feedback = 2 |
| **Activation function** | Hidden layer = Hyperbolic tangent |
| | Output layer = Linear function |
| **Training parameters** | Learning algorithm: *Levenberg-Marquardt* |

Same procedure has been carried out when designing LSTM neural network. First, the learning rate parameter has been adjusted. Different values ranges (1, 0.1, 0.01, 0.001, 0.0001 and 0.00001) have been considered in order to achieve the lowest MAPE. The lowest value has been obtained with a learning rate of 0.1. Therefore, the adjustment of the number of neurons has been performed with this value. The MAPE values obtained with different TWs and number of neurons have been gathered in Table C.2 of Annex C. Winter results show that the most appropriate number of

neurons is 15, as the lowest MAPE (around 19%) is obtained for the three largest TW ranges. Regarding the summer season, the values remain fairly constant for the range of the analysed neurons number (MAPE around 14%). Summarising, a learning rate of 0.1 and 15 neurons have been selected to perform the forecast of the consumption with LSTM model.

The design process for the SVR model differs from the previous two models. This type of model has three hyperparameters: $C$ is the regularization parameter, ε determines the margin of the bounding decision, and $\gamma$ determines so far, the influence of a single training example reaches. Each combination of these hyperparameters constitutes a SVR model configuration. The hyperparameters have been tuned using Bayesian optimisation [123] and time-sensitive cross-validation. Similar to the NARX and LSTM models, model selection is based on estimating the performance of different configurations to choose the best one. Table C.3 of Annex C reflects the values of C and γ that achieve the most accurate prediction model for the four TW selected.

### d. TW Selection

For the selection of the TW, the MAPE of each model has been analysed with TW values of 7, 14, 21, and 28 days in the months of September and February.

Having a look to Figure 2.13, can be concluded that in almost all cases, there is a significant improvement when moving from a TW of 7 days to a TW of 14 days. Similarly, better MAPE values have been obtained in five out of six cases when moving from a 14-day TW to a 21-day TW. This is not the case when increasing the TW to 28 days, as despite achieving a reduction in MAPE with the SVR and LSTM in summer, in most cases no further reduction in MAPE can be seen than with 21-days TW. Therefore, a TW of 21 days has been selected.

Consequently, 504 data points have been introduced to the models for training in order to forecast next 24 values. Of these 504 data points, 80% have been employed for training the model and 20% for validation.

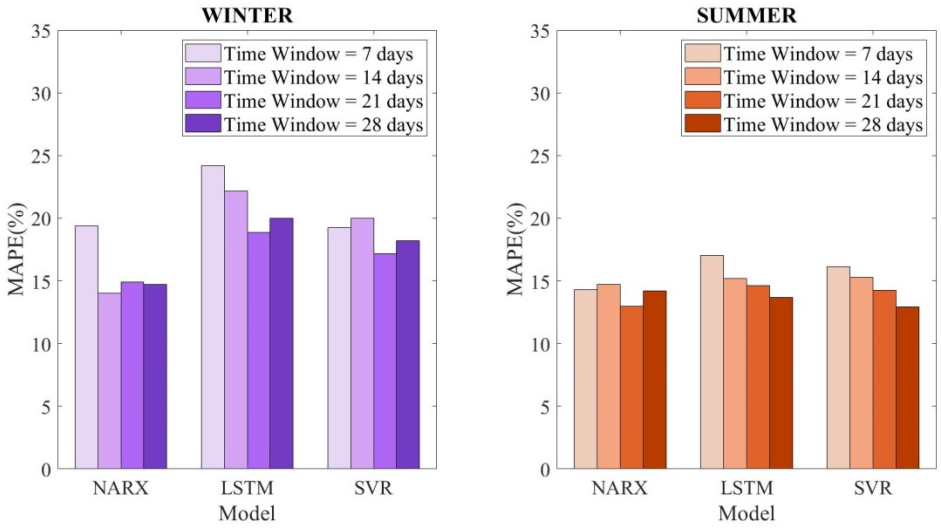


***Figure 2.13**. MAPE values of the three models for different TWs in February and September.*

To summarize, Table 2.5 captures the structure and optimal hyperparameter values selected for each model.

***Table 2.5.** Final structure and optimal hyperparameter values of forecasting models.*

| Inputs | TW | NARX | | LSTM | | SVR | | | |
|---|---|---|---|---|---|---|---|---|---|
| | | delays | neurons | learning rate | neurons | Summer | | Winter | |
| | | | | | | C | γ | C | γ |
| Temperature + Occupancy | 21 | 2 | 5 | 0.1 | 15 | 3.9961 | 2.0133 | 14.4654 | 0.0600 |

### 2.4.2.2 Second phase

The second phase has started by acquiring data from MG and pre-processing it. As said, another PhD student has been in charge of developing a programme to pre-process the data automatically.

The inputs chosen in the first phase have been taken as reference adding the time vector that has been included to the SVR model Furthermore, the selection of TW has also been done based on the first phase, so 21 days have been employed for training the models. Therefore, 504 data points have been introduced to the models for training in order to forecast next 24 values. Of these 504 data points, 80% have been employed for training the model and 20% for validation.

### a. Model hyperparameter adjustment

In this section, particular attention is given to the design process of the NARX model as SVR model has been developed by another member of the research team.

Same NARX hyperparameters as defined in the first phase have been adjusted in this case. The simulation plan described in Table 2.6 has been designed accordingly.

***Table 2.6**. Simulation plan for NARX model design for second phase.*

| | ***Training characteristics*** | ***Model structure*** | | ***Model hyperparameters*** | | |
|---|---|---|---|---|---|---|
| | | ***Input combination*** | ***Time Window (TW)*** | ***Activation function*** | ***neurons*** | ***input and feedback delays*** |
| ***NARX*** | Learning algorithm: *Levenberg-Marquardt*<br>Error = MSE<br>Daily NARX training = 3 times | Temperature + Occupancy | 21 | Hidden = { sigmoid, tansig}<br>Output = { sigmoid, tansig, linear} | [2, 3, 4, 5, 10, 15] | [2, 4, 6, 8, 10] |

The criterion in order to adjust the hyperparameters of NARX has been the same to phase one: minimisation of mean MAPE of the entire predicted period, in this case an entire week. The selected model characteristics are described in Table 2.7.

***Table 2.7**. NARX model hyperparameter values for energy consumption forecasting of second phase.*

| **Hyperparameters of NARX** | |
|---|---|
| **Hidden layers** | nº of hidden layers = 1 |
| | number of neurons = 4 |
| **Delay vectors** | Input = 5 |
| | Feedback = 5 |
| **Activation function** | Hidden layer = Hyperbolic tangent |
| | Output layer = Linear function |

| | |
|---|---|
| **Training parameters** | Learning algorithm: *Levenberg-Marquardt* |

Regarding SVR, the optimal hyperparameters values have been gathered in Table 2.8.

***Table 2.8**. SVR model hyperparameters values for energy consumption forecasting of second phase.*

| **Input combinations** | **TW** | $C$ | $\varepsilon$ | $\gamma$ |
|---|---|---|---|---|
| Temperature + Occupancy + Hour vector | 21 | $10^{-0.93}$ | $10^{-3}$ | $10^{0.36}$ |

## 2.5 RESULTS AND DISCUSSION

The forecasting results are presented in the following subsection. The subsection has been divided into two parts corresponding to the first and second phases respectively.

### 2.5.1 First phase

#### 2.5.1.1 Winter results

MAPE has been calculated for each predicted day. In order to simplify the interpretation of results, it has been decided to calculate the average MAPE for each day of the week that is obtained during the month of February. The MAPE values are presented in Table 2.9.

***Table 2.9**. MAPE mean values of each day of the week in winter season.*

| WINTER | MAPE | | |
|---|---|---|---|
| | **NARX** | **LSTM** | **SVR** |
| **Monday** | **13.52** | 18.12 | 15.30 |
| **Tuesday** | **14.76** | 24.37 | 19.03 |
| **Wednesday** | **14.21** | 22.25 | 17.64 |
| **Thursday** | **15.45** | 23.37 | 16.30 |
| **Friday** | **13.08** | 19.64 | 14.65 |
| **Saturday** | **15.63** | 18.25 | 23.77 |
| **Sunday** | 12.32 | 13.43 | **11.98** |

Results show how NARX model performs better than LSTM and SVR models. Average MAPE obtained in February by each forecasters is 13.98% with NARX, 18.31% with LSTM and 16.96% with SVR.

On the one hand, LSTM clearly predict with lower accuracy. The MAPEs obtained with the LSTM may be derived from the fact that it is not a NN used for cases where a small amount of data is available, but is more suitable for large training data sets.

As for the SVR model, the MAPEs obtained are closer to those obtained with NARX but still do not exceed them. This may be due to the absence of a recurrent term in the SVR model, which is

important when making a short-term prediction such as this one, since the 24-hour consumption ultimately depends on the previous values entered into the model.

It is also interesting to observe the difference in MAPE according to the day of the week, and in particular, the values obtained in the case of the three models for the average of Sunday days. The models are able to follow the consumption curve more precisely on Sundays because there is a high probability on these days that the HVAC system is not in operation and, therefore, the stochastic effect that this system introduces can be eliminated from the equation.

Regarding February week plotted on Figure 2.14, it can be observed that all the forecasting models are able to detect both the trend over a full day and the difference between workdays and weekends.

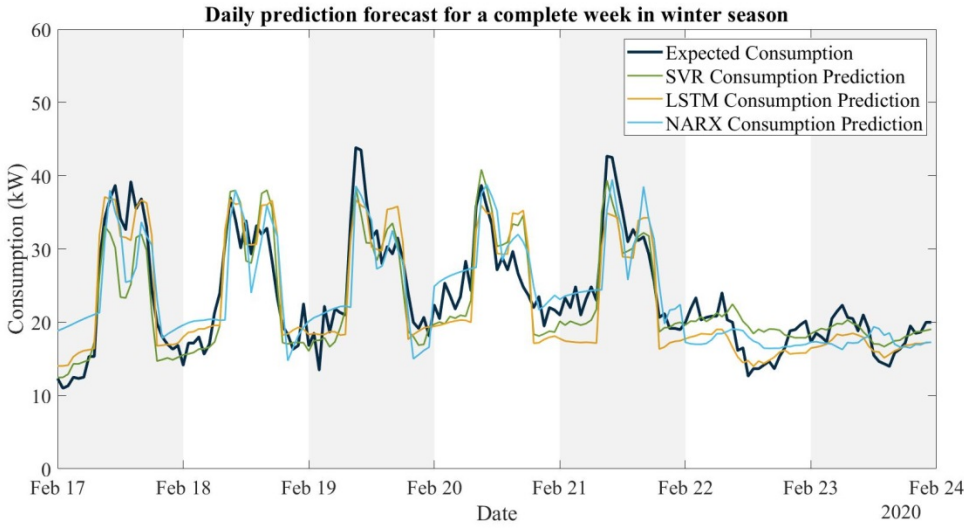


***Figure 2.14**. First phase: prediction of one week's energy consumption of winter season.*

The average MAPE value for Saturdays in February deserves special attention. It is notably worse than that obtained on Sundays, even though the prediction curve is very similar. Looking at Figure 2.14, it can be concluded that this may be due to the fact that the models are not able to follow the variation that exists on Saturday. This variation may be due to the HVAC system, since, due to the low temperatures, the heating may have been activated to maintain a minimum temperature. Anyway, the best prediction results with NARX model have been obtained during workdays, being this important because it will be the workday prediction that will be taken into account in the EMS.

The prediction of the three models differ in particular when consecutive abrupt changes in power consumption occur, especially during the night. These sudden night-time variations could be explained by the on/off behaviour of HVAC units in operation with constant set points but large hysteresis.

#### 2.5.1.2 Summer results

The summer month consumption curve does not show as much variability during the day as the winter consumption curve, and the consumption peaks are not as pronounced. Therefore, it is interesting to see if the models are able to follow it more precisely and improve the error obtained in the prediction of the winter month.

Table 2.10 presents the MAPE calculated by averaging for each day of the week in September.

***Table 2.10**. MAPE mean values of each day of the week of summer season.*

| SUMMER | MAPE | | |
|---|---|---|---|
| | **NARX** | **LSTM** | **SVR** |
| **Monday** | **15.36** | 16.27 | 17.81 |
| **Tuesday** | 17.92 | **13.25** | 13.34 |
| **Wednesday** | 16.38 | 13.94 | **9.76** |
| **Thursday** | **9.54** | 10.82 | 12.01 |
| **Friday** | 10.54 | **9.70** | 11.82 |
| **Saturday** | **8.62** | 12.51 | 15.15 |
| **Sunday** | **5.67** | 16.40 | 21.14 |

As before, NARX model performs the best prediction, with an average MAPE of 12.08%, while the average MAPE of the LSTM model is 14.49% and that of the SVR model is 14.43%.

The three models agree on the quite high error values in the prediction of the first day of the week. This is because in September, when the external temperatures are somewhat high, the building overheats and on Mondays a large part of the consumption is related to the switching on of the HVAC system, which, as has already been pointed out, has a stochastic behaviour that makes it difficult to predict.

Even so, compared to the MAPE values obtained in winter, the improved results during September can be explained by the reduced use of the HVAC system. Indeed, in September, external temperatures are more moderate and there is less need to cool the building. This fact is very interesting, since the summer season is when there is usually more PV production, and therefore, the EMS will be more efficient in increasing the ratio of self-consumed energy.

Regarding Figure 2.15, it can be concluded that the predictive models are capable of capturing the two types of daily trends that occur during the week: workdays and weekends.

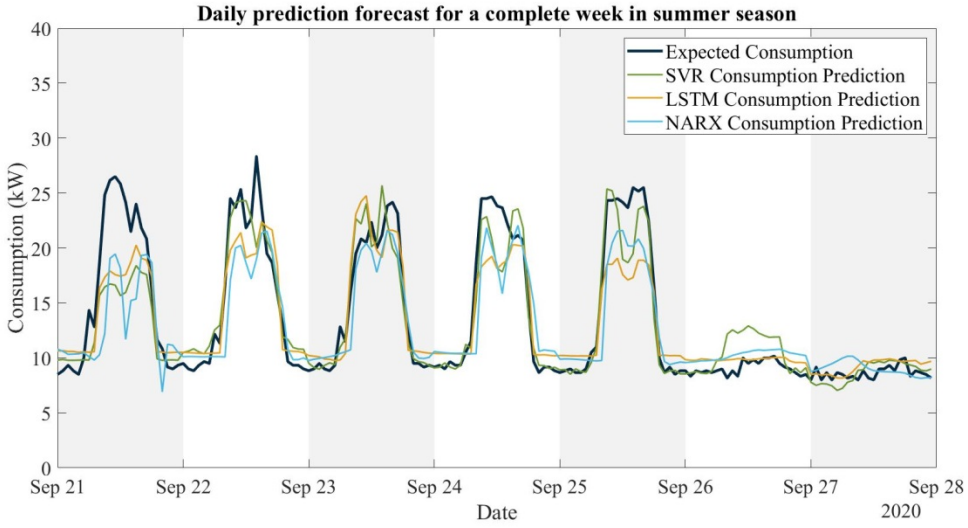


***Figure 2.15**. First phase: prediction of one week's energy consumption of summer season.*

The measured consumption curve in this case shows much less variation than in the case of the winter month. Night-time consumption does not have the sharp shape it did in the winter months. The reduced use of the HVAC system mentioned above clearly influences the consumption curve, leading to a decrease in the amplitude of the saw-tooth behaviour.

The models still do not respond perfectly when there are abrupt changes in consumption, for example, during the first hours of the morning, where none of the models is able to foresee the first increase in consumption that occurs between 08:00 and 09:00 am.

Finally, in most days the three models have problems to reach the consumption peaks and predict the midday drop in consumption associated with lunchtime, which clearly does not occur with such abruptness in the month analysed.

### 2.5.2 Second phase

In order to be able to compare both NARX and SVR models performance, Table 2.11 records the MAPE values that have obtained the models each predicted day.

***Table 2.11**. Second phase: MAPE values of each day of the week.*

| | MAPE | |
|---|---|---|
| | **NARX** | **SVR** |
| **Day 1: 24/04/2023** | 12.85 | **11.30** |
| **Day 2: 25/04/2023** | 12.39 | **11.41** |
| **Day 3: 26/04/2023** | 14.08 | **8.14** |
| **Day 4: 27/04/2023** | 10.78 | **8.62** |
| **Day 5: 28/04/2023** | **13.00** | 13.92 |
| **Day 6: 29/04/2023** | 20.16 | **8.23** |
| **Day 7: 30/04/2023** | 14.51 | **13.49** |

MAPE results clearly show how SVR outperforms NARX model on most days. Considering the mean MAPE obtained by both models during the week, SVR performs 3.62% better than NARX. Despite not being a huge accuracy difference, SVR is clearly better following the curve of consumption can be seen in Figure 2.16.

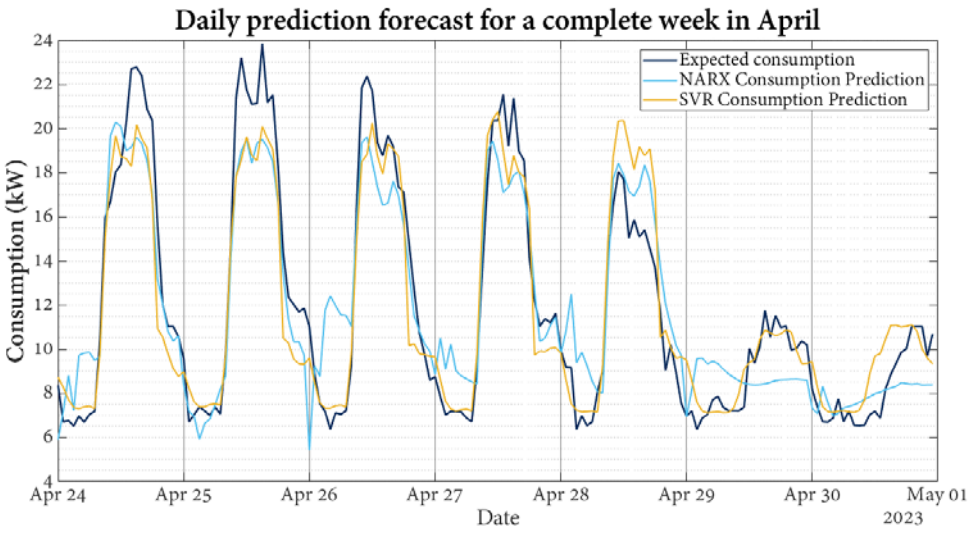


***Figure 2.16**. Second phase: prediction of one week's energy consumption.*

The NARX model clearly has difficulties in correctly predicting the consumption curve at night. Moreover, it is not able to see the small peaks of 2kW of the weekend. It can be seen how the SVR predicts more accurately the weekend peaks, and its prediction does not differ so much from the actual curve during the night.

## 2.6 CONCLUSIONS

In the first phase of this work, NARX, LSTM and SVR machine learning techniques have been used to predict the ESTIA 2 building hourly power consumption for the next 24 hours with a small set of data. For that, external temperature and occupancy of the building have been used as inputs to the model.

The first conclusion that can be drawn is that, in the first phase, the highest accuracy is obtained with the NARX model in both, winter and summer seasons, obtaining a MAPE of 13.98% and 12.08% respectively. The global average MAPE for the NARX model is therefore, 13.03%. Thus, in first phase, the NARX model performs 26% better than the LSTM model and 21% better than the SVR model.

Regardless of the used type of model, the prediction of consumption in the summer month is achieved with a higher accuracy. In the case of LSTM model for example, the MAPE in winter is more than 5% higher than in summer. The better results obtained during the summer month are directly related to the use of the HVAC system. This system has a stochastic behaviour, which makes the prediction of consumption a more complicated task. As the use of the HVAC system is higher in winter months, the prediction is less accurate than in summer. The curves of Figure 2.6 gave from the beginning an idea of the difference in the prediction results between the two periods.

As the EMS requires the HVAC effect to be removed from the overall building consumption, a second phase has been carried out where the data pre-processing stage has been automated and the HVAC related consumption has been removed from the building's electricity consumption curve. In addition, predicted external temperature data has been used as input to the model, as it should be done in a real scenario.

Comparing the NARX results with those of the first phase, it can be seen that the results have not worsened substantially despite the use of predicted temperature data as input. The new curves having less variability, may have helped the model to predict better.

As for the SVR model, there is a clear improvement in the MAPE values compared to those obtained in the first phase. This improvement might be related to the introduction of an hourly vector in the second phase. This input has been able to give the recurrence it lacked in the first phase, which is essential for time series predictions. The SVR is able to predict April week 3.62% better than the NARX.

To sum up, a NARX-based model has been developed. It is not only able to predict a high variability curve with nonlinear characteristics, but also uses a small data set for training and

obtains satisfactory results. Likewise, it is worth highlighting the importance of the input choice and their combination for acceptable prediction. A very substantial improvement has been achieved by introducing, together with the temperature, the occupancy rate of the building instead of the binary array that distinguished only workdays and weekends/holidays.

# CHAPTER 3

# PV PRODUCTION FORECASTING

The third chapter discusses the development of a second model based on a NARX-type NN, designed for performing day-ahead forecasting of PV production.

The chapter begins with a comprehensive literature review of modelling techniques used for the purpose of short-term PV production forecasting, aiming the identification of best-suited model to the specific case study. The literature review has followed by the definition of the objectives of this chapter.

The case study is detailed in a subsequent section, followed by a presentation of the methodology used for designing the predictive model. This section presents two subsections corresponding to the two phases in which the work has been developed. In the first phase, the NARX model has been trained using measured data as inputs. NARX model has been compared with other two ML models and an analytical model (AnM). The second phase is an extension of the first phase, which consisted of developing same models as in first phase to predict the next day's PV production, but in this case, training the models with predicted data from two meteorological agencies. The chapter continues with the presentation of the results and the corresponding discussion followed by a summary of the main conclusions.

## 3.1 PROBLEM STATEMENT

Due to, among other things, the electrification of various sectors such as transport and building, global electricity consumption is increasing year by year [124]. Until not so long ago, coal, oil or natural gas were used to generate electricity, i.e. energy from fossil fuels. However, this practice has been called into question due to two problems; firstly, the massive use of fossil fuels has led to their progressive depletion, and secondly, the major environmental problem caused by the GHGs emitted [125].

RES are presented as an alternative due to their inexhaustible and environmentally friendly nature [126], [127]. Although there are numerous types of systems based on renewable energies, PV energy source has attracted most attention. Proof of this is the high penetration rate of PV systems in national electricity markets (see Figure 3.1) and the more than significant increase in installed capacity year after year (see Figure 3.2).

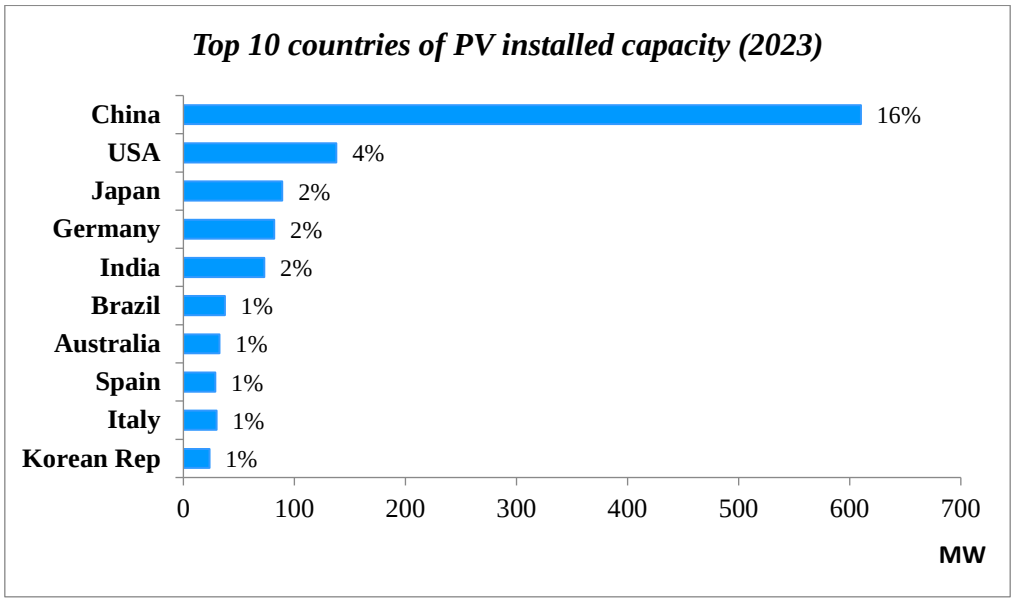


***Figure 3.1**. Total top 10 countries in 2023 based on total PV installed [128].*

According to IRENA report "Renewable Energy Statistics 2024" [128], the global installed capacity of PV power in 2023 reached 1411 GW, seeing an increase of 24.73% compared to 2022. Several studies indicate an exponential growth of installed capacity by 2030 [129].

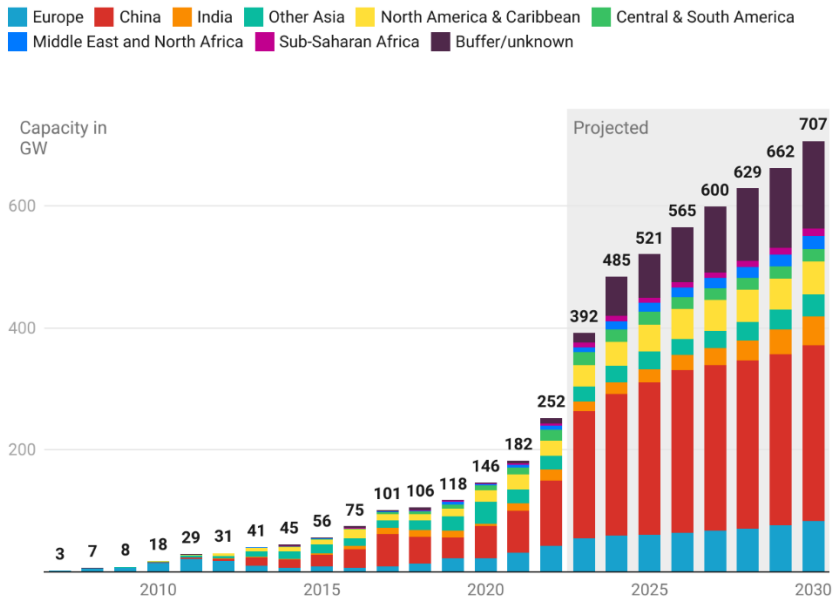


***Figure 3.2**. Global growth and projection of solar installations by country (2022) [129].*

PV energy has a huge potential in both rural and urban environments due to the possibility of installing smaller PV systems in roofs or gardens [130], [131]. However, the high presence of renewable energy installations in the electricity system also has disadvantages. The power output of a PV system changes over time due to the variability of several environmental factors such as solar irradiance, external and PV module temperature, wind speed and direction, etc. The stochastic and unpredictable nature of solar energy can cause problems such as voltage and frequency fluctuations or even system outages [132], ultimately making difficult to manage energy, and more specifically to balance consumption and production [133]. For example, on cloudy days the solar irradiance that the PV system receives fluctuates depending on cloud cover (CC), or rather cloud movements. These random fluctuations have a noticeable effect on the electricity production.

Several measures have been taken to avoid this problem, such as the integration of battery energy storage systems (BESSs) or the development of DR [134], but there are limitations to both. The high cost of batteries makes large-scale battery installation unfeasible in many cases, and the frequent lack of consumer behaviour data makes the application of DR difficult.

It is in this context that the forecasting of PV production gains the attention of the research community. Accurate prediction of PV production can be vital for grid energy planning, as well as to improve system reliability and greatly reduce the effect of uncertainty introduced by the intermittent nature of PV systems [135].

The prediction of PV production has driven a large number of studies where prediction models have been developed for all kind of contexts. Even more with the increasing presence of grid-

connected Microgrids or SBs, which have led to the need to foresee the power generated by PV systems at smaller scales.

Many reviews can be found by analysing the literature in this direction. Among the most interesting is [136] that points out the advantages and disadvantages of the different types of models used for forecasting PV production. As well as the work done in [137], where in addition to briefly highlighting the classification of the type of predictive models, it points out strategies and indicators for the choice of one type of model or another. This last point can be of great interest especially for taking the first steps in the study and design of predictive models.

In order to be able to make an accurate prediction, special attention must be paid to the data that is used as inputs, i.e. the predictors. Generally, inappropriate inputs can cause forecasting errors in a system, such as time delay or cost and computational complexity [138]. The correlation between model inputs and outputs can also affect the performance of the prediction model, so it is useful to analyse the correlation between PV production and different meteorological factors [138]. Nevertheless, the variable that has the greatest influence on PV production is undoubtedly solar irradiance [139].

The scientific community has paid special attention to the forecasting of solar irradiance. The study of solar irradiance spans several disciplines and different fields of knowledge such as atmospheric science, climatology, statistics or data science must be combined [140]. The large effect of solar irradiance on PV production means that the accuracy with which the former is predicted greatly affects the accuracy with which the latter can be predicted. There are different ways of obtaining the data necessary for the determination of solar irradiance.

(a) Satellite Images: High altitude geostationary satellite images are taken and combined with physical models to determine solar irradiance [141].

(b) All-Sky Imagers (ASI): Cameras capable of photographing the sky with a 180° field of view are used to detect cloud motion and altitude. The aim is to determine the future position of clouds in order to predict solar irradiance [142].

(c) Sensor Networks: It consists of creating networks of illuminance meter-type sensors capable of detecting the movement of cloud shadows, thus being able to create models for the prediction of solar irradiance [143].

(d) Numerical Weather Prediction (NWP): They are physical models made up of differential equations that represent physical and thermodynamic phenomena and serve to model conditions over large areas. The generated data can be used both to predict solar irradiance [144], or solar irradiance data can even be generated directly to, for example, feed into a model for predicting PV production [145].

Independently of these physical techniques for obtaining predicted solar irradiance data, there are many papers in the literature that encourage the use of ML models to predict solar irradiance [146], [147], [148], [149].

The effect of other meteorological variables in addition to solar irradiance can also be significant. When constructing a forecasting model for solar power, numerous predictors have been used, such as external temperature in conjunction with solar irradiance [150], as well as wind speed [151]. The latter variable has sometimes been used together with wind direction, as both are related to the variation of module temperature [152]. Module temperature has also been used directly as a predictor, sometimes in combination with wind speed [153]. There are also papers using data such as CC [154] which is often used due to the lack of irradiance data: solar irradiance data can be generated by applying CC to a Clear Sky model. Finally, other predictors such as relative humidity or irradiance intensity, which depend on the time of year or CC, have also been taken into account to predict PV production [155], [156].

An important aspect to take into consideration when analysing predictors is the quality and quantity of data. Many models need inputs that meet certain requirements, which sometimes the available raw data do not. In these cases pre-processing techniques are applied to the data. Among the best known and employed in the literature is Principal Component Analysis (PCA), a method used to reduce the spatial dimension of the inputs [157]. The reduction is achieved by transforming the current data into a new set of variables, which will be called principal components. Other techniques that can be seen in the literature are the wavelet transform (WT) [158], [159] or normalisation [121]. As for normalisation, it is widely used especially in NN based models, to improve convergence during NN training and to avoid the large impact of some inputs due to their high values [160] (see Equation (2.4) of Chapter 2).

It needs to be noted that when pre-processing is applied, sometimes the data needs to be post-processed. As a clearer example, when normalising the data, these data needs to be denormalised after prediction [161].

### 3.1.1 Classification of forecasting models

The models used to forecast PV production could be classified on the basis of various criteria. The first classification can be placed on the difference between models that make deterministic or probabilistic predictions. The probabilistic approach approximates all possible outcomes of PV energy prediction [162]. In contrast, models that predict from the deterministic approach do so without taking into account the uncertainties of the predicted points. Similarly, the evaluation metrics used to determine the performance of models predicting with a deterministic or probabilistic approach are different. Metrics such as MAE, RMSE, MAPE, Pearson correlation

coefficient ($r$) or $R^2$ among others are used for deterministic predictions, as well as, distribution evaluation, quantile evaluation or interval evaluation are used for cases where probabilistic prediction is carried out [163].

Evaluation metrics play an important role in determining the validity of a model to perform a prediction task. Among the most commonly used metrics in papers dealing with PV generation predictions are mean absolute error (MAE), root mean square error (RMSE) and $R^2$.

MAE provides the average in absolute terms of the prediction errors following Equation (3.1) [103].

$$MAE = \frac{1}{n}\sum_{j=1}^{N}\left|y_j - \hat{y}_j\right| \tag{3.1}$$

where $y_j$ and $\hat{y}_j$ are the measured value and its corresponding prediction. $n$ is the total number of data in the data set used for the evaluation of model performance.

RMSE is represented by Equation (3.2) and can be a useful metric when there is interest in identifying huge outliers of the model output, as the square helps to highlight them.

$$RMSE = \sqrt{\frac{1}{n}\sum_{j=1}^{N}(y_j - \hat{y}_j)^2} \tag{3.2}$$

Finally, $R^2$ is represented by Equation (2.2) included in section 2.1.4 of Chapter 2.

Another criterion for classifying the various models that exist for predicting PV production is the prediction horizon (PH). The forecasting horizon can be considered as the period of time in the future in which the forecast should be made [164].

Four categories can be distinguished according to the length of the PH: (a) very short term, (b) short term, (c) medium term and (d) long term. The characteristics of each of the PH are specified in section 2.1.1 of Chapter 2. However, there are works that prefer to use another classification according to the prediction horizon that overlaps the aforementioned classification and which consists of dividing the predictive models into (a) between hours, (b) between days and (c) next day [126].

There is a third classification of models, which is the most widely adopted classification in reviews dealing with PV production [138], [161], [165], [126]. The classification consists of differentiating the models according to their typology. In this regard, the classification of three types of predictive models represented in Figure 2.2 of Chapter 2 is respected: (a) physical models, (b) grey-box models and (c) black-box or data-driven models.

Physical or analytical models (AnM) are based on mathematical equations that relate meteorological variables and PV production. Many of the papers reviewed make use of NWP models. In [166], for example, an extended study is made of multiple physical models that calculate PV production using data obtained from a NWP model. The models are tested for 16 different PV plants with intra-day and day-ahead prediction. It is concluded that the average range of the best and the worst models predict with a nRMSE of 46.1% and 52.1%, being of 12% the relative difference between both.

The accuracy with which AnM predict varies not only by the type of model used, but also to a large extent by the quality of the meteorological data used. The paper [151] introduces a comparison of three physical models which predict PV generation with very good results (< 2% error). Date time array to determine sun position, external temperature, wind speed and solar irradiance, together with the PV cell characteristics obtained from measurements or datasheet have been used as inputs to the model. It is concluded that, although these models do not need a training period and the coefficients could be recalibrated every year, they are highly dependent on the data used in the calibration of the coefficients and the type of approach adopted to calculate the cell temperature. The inability of these models to predict the drop in production due to CC is also discussed, which is a very important issue especially when predicting in short and very short-terms.

Grey-box models are built with a combination of physical and data-driven models. It is therefore not uncommon to see papers where ML models are fed with meteorological data obtained, for example, from a physical model such as NWP or Satellite Imagery [167].

Finally, black-box or data-driven models are of particular interest in research community. As explained in section 2.1.1 of Chapter 2, they do not consider the underlying physical relationships of the system, so their interpretability might be difficult. Furthermore, they are based on training using historical data. Within this type of models, a classification is made as shown in Figure 2.3 of Chapter 2: (a) Statistical Analysis (SA), (b) Machine Learning (ML), (c) Deep Learning (DL) and (d) Hybrid models.

Also noteworthy are the benchmark models used in many papers. These models are used as a reference to compare more complex models. Normally if a type of model, e.g. a ML model, is not able to improve the prediction made by a benchmark model, it is discarded. The persistence model is used as one of a standard model to test any type of prediction model and therefore acts as a benchmark model [126]. In a persistence model, the future value of a time series is calculated under the assumption that nothing changes between the current time and the forecast time [168], therefore, the future PV power will be the same as the current time. This technique is mostly used in short-term forecasting because as the PH increases, so does the output error of the persistence

model [169]. Random model is also used as a reference model. The random model chooses values from the past at random from the time to be predicted. Therefore, in the case of wanting to predict the PV production at 08am of the next day, the model randomly chooses a value of any day from the database recorded at 08am. The random model can present problems during the year, as sunrise and sunset vary.

### 3.1.2 Statistical Analysis (SA): Autorregressive models (AR)

Statistical models are based on the concept of stochastic time series and that is why they have been widely used for time series forecasting in recent years. Among these models, the most widely used are AR models, which are characterised by a regressive term that makes it possible, for example, to take into account the seasonality of the data. Even so, these models are not able to deal with time series involving nonlinearities. This makes the use of statistical models limited for predicting PV production, due to their nonlinearity introduced by the uncertainty of climatic conditions [135].

Models such as ARIMA, which thanks to its integrated term/part (I) able to erase any form of non-stationarity from the time series [170], has proven to be a more than valid model for forecasting PV generation [171]. The seasonal ARIMA model (SARIMA) has shown to be a very interesting variant of the ARIMA model for predicting PV production, proving that in some cases it can even forecast more accurately than an ANN. This is the case in [172], where a SARIMA model that includes external solar irradiance data outperforms current SARIMA model and also two ANN that also have been proposed, succeeding to perform day-ahead forecasting with a nRMSE of 11.12%.

### 3.1.3 Machine Learning (ML)

Although initially physical and statistical models started to be used to predict PV production, ML models are gaining more and more prominence in scientific literature mainly due to their ability to deal with nonlinear behaviours.

Reviewing the literature, the most popular type of ML models for predicting PV generation are both ANN and SVR models.

Starting with SVR models, thanks to the fact that its algorithm works by mapping nonlinear inputs, it is an interesting model to solve the problem of predicting PV generation. In [173], a SVR model is used to predict PV generation with a prediction horizon of 30 days. Two SVR models are proposed for sunny and cloudy days and although the models and parameters vary for each available data set (6 data sets), the overall performance remains in the same range of accuracy MSE below 0.000587.

Furthermore, this model is governed by a principle called structure risk, which consists of balancing the fit of the training data with the complexity of the model to avoid overfitting [173]. Due to this advantage, it has been widely compared to various ANN structures, a type of model susceptible to the problem of overfitting.

As exemplified in [174], it is important to analyse the performance of predictive models not with measured data, but to employ predicted data to train them. In [150], using a SVR model, the energy production of a PV plant in Italy is predicted. Measures and predictions of irradiance and external temperature data are used to predict PV production. It is concluded that the results are highly dependent on the errors of the input data. If the prediction errors of the meteorological data are large, the prediction of solar power generation will not be accurate. In spite of this, not many papers can be found in the literature that make use of predicted meteorological data.

Regarding ANN models, one of the simplest NN models adopted for PV generation prediction is the feedforward neural network (FFNN). This type of NN does not have a feedback loop [175], it is not recurrent. Nevertheless, it can be interesting for the prediction of PV generation by incorporating an input containing temporal information. This is the example of [176], where a comparison is made between an Elman Neural Network (ENN) model and a FFNN to predict PV generation. Four different models have been created for each NN describing four different cases that differ from each other by the selected TW. It is observed that the FFNN is able to predict with a very low MSE of even 0.00097 using only one day of TW and including a time vector. Although the use of simple FFNN for the purpose of solar power prediction can be feasible and interesting results can be obtained, many works propose hybrid models, where not only a FFNN is used but it is combined with other models in order to take advantage of the benefits of both models [177].

NARX models, which do have a recurrent term that allows for better handling of system dynamics, have also been applied to predict PV generation. In [178] a nonlinear autoregressive model (NAR), a nonlinear input-output model (NIOP) and a NARX are compared to predict a full year of PV production of a 78MWp installation. It is found that the NARX with the Bayesian Regularization training algorithm is indeed able to predict with a $R^2$ of 0.748 and a nRMSE of 15.5%. The comparison of NARX with more basic models such as NAR, can show that sometimes a more complex model, where it has to make use of external variables, is necessary to be implemented in certain situations.

Despite this, there are works such as [179] where the NARX is compared with a more complex models classified as DL like LSTM NN. After comparing NARX and LSTM for performing forecasting 1.5 hours-ahead, it is concluded that NARX gives the best results, being both trained with three month data set. The LSTM with three hidden layers and a total of 85 neurons predicts

with a MSE of 0.0279063, compared to the NARX with one hidden layer and 7 neurons which achieves a MSE of $6.52316e^{-4}$. It can be seen that the NARX with a simpler structure predicts more accurately.

### 3.1.4 Deep Learning (DL)

However, DNNs can be a possible solution for PV output prediction problems. An example of this is the work introduced in [180] where CNN, LSTM and a Bidirectional LSTM (biLSTM) models are proposed to predict PV output with a not very common input used for prediction: the level of dust accumulation. It is concluded that either without dust accumulation or with high dust levels, it is the BiLSTM that outperforms both, with an $R^2$ of 0.94 and 0.919 respectively. It is in [181] where DNN models are also used to predict PV production including a PV installation ageing model that provides valuable information on the deterioration of production accuracy in the long term. In this case, in addition to proposing a LSTM and CNN model, the authors propose an Autoencoder and gate recurrent unit (GRU) NN. It is concluded that in general, it is the LSTM and GRU models that most effectively capture long-run dependencies. They predict with a RMSE of 0.1025 and 0.1159 respectively. The CNN presents problems in capturing long-term time series dependencies despite being a powerful model both for spatial data analysis and for extracting features from the input data [182].

DNN models have one thing in common; they need large data sets for training. Proposals can be seen in literature such as [183], where models that can solve lack of data problem in large data sets are proposed. However, there are not many works that propose models able to predict without having large data sets.

### 3.1.5 Conclusions

In summary, after having analysed the available literature on the prediction of PV generation, some aspects stand out. On the one hand, given the large effect of solar irradiance on PV production, it is necessary for solar irradiance forecasting to be as accurate as possible. Thus, it is difficult to find references in the literature comparing different sources of predicted meteorological data, to see which ones provide reliable and accurate data.

As has been proven in [166] the selection of a good prediction model can overcome the errors that can be found in the solar irradiance prediction data. Therefore, it is important to compare different types of predictive models, as well as to contrast these models with simple and well-known benchmark models. Since more complex models such as ML models will only be justified if they are able to improve the operation of the reference models.

In the literature, it has been found that there are repeated cases of ML being used for the prediction of PV generation trained with large data sets. This contrasts with many of the real cases where the accessibility or quality of the data is limited. So it might be of interest to see if the use of ML models can be interesting also in the cases of limited data availability.

## 3.2 OBJETIVES

Starting with the immediate general objective, this Chapter is related to the development of day-ahead forecasting of PV production using a NARX-type NN model trained with small data set. The designed predictive model is then integrated into the optimisation-based EMS developed in Chapter 5 (as explained in section 1.4 of Chapter 1).

In this context, three secondary objectives have been set:

- The identification of the model capable of predicting PV generation with the highest accuracy. Three type of ML models and one analytical model (AnM) have been proposed. The aim has also been to analyse whether the proposed models can outperform benchmark models.

- The proposed models have been trained not only with measured data but also with predicted data from two different meteorological agencies. The objective consists of analysing which meteorological agency provides the best predicted solar irradiance data for day-ahead forecasting of PV generation.

- The analysis of whether the ML models are able to compensate the errors of solar irradiance predictions obtained from the two meteorological agencies. This should be seen by comparing the results of the ML models trained on predicted data with the results of the analytical model built on the same data.

The selection of a good prediction model can overcome the errors of predicted meteorological data. Therefore, ML and in particular NARX models have been proposed as they are models that are able to model nonlinear systems without prior knowledge of the system operation. Moreover, the aim has been to design simple structure ML models trained with small data sets appropriate for the low-computational cost of the MPC that need to be designed.

The accuracy with which the models predict has been shown to be highly dependent on the quality of the predicted input data. Unlike analytical models, ML models may be able to predict PV prediction by taking into consideration the error embedded in the predicted solar irradiance data.

## 3.3 CASE STUDY

Within the EKATE project, a SC applied to ESTIA Institute of Technology has been proposed (see section 1.3 of Chapter I). As mentioned in the same section, the PV installation, which is intended to supply the consumption demand of ESTIA 2 building, is located on the roof of the ESTIA 1 building (see Figure 3.3).

***Figure 3.3**. ESTIA 1 building.*

### 3.3.1 Used data analysis

Two type of data has been used, the PV production data and the meteorological data, more specifically solar irradiance, external temperature and wind speed and direction data.

#### 3.3.1.1 PV production data

PV production data started to be recorded in April 2021 via *Linky* smart meter. Data is recorded every 10 minutes and stored in a local database.

For the first phase, the forecasting of July 2021 month has been performed, being the PV production curve the one plotted in Figure 3.4.

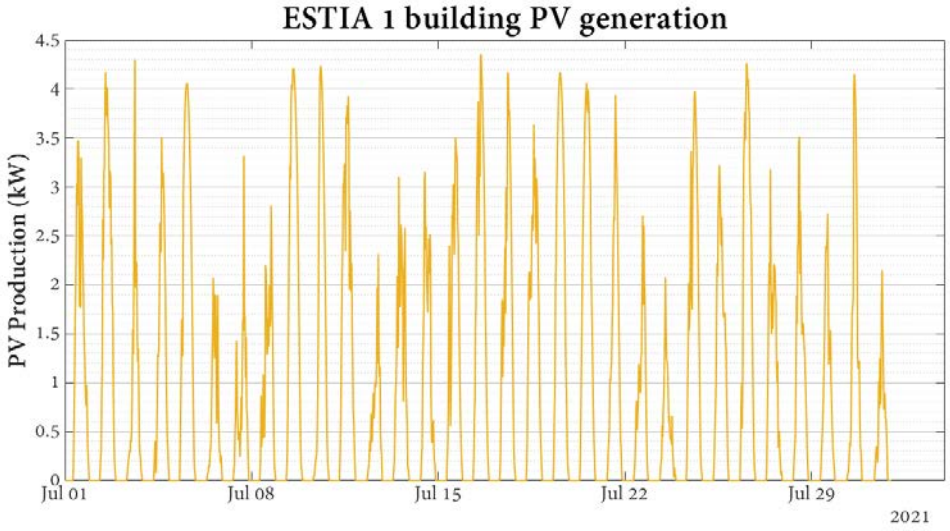


***Figure 3.4.*** *PV production curve of July 2021.*

Regarding second phase, Figure 3.5 shows two different graphs from August and November months in which forecasting has been performed. The yellow curve shows the PV production curve recorded by *Linky* meter from 16$^{th}$ to 30 of August. In this period, peak production exceeds 4kW, a high value considering the installed power (5.6kWp) and the age of the installation (20 years). In contrast, the red curve shows the PV production in the second half of November. It can be seen that in this period the highest peak recorded is 3kW, but with a big difference compared to other days when it barely reaches 400W.

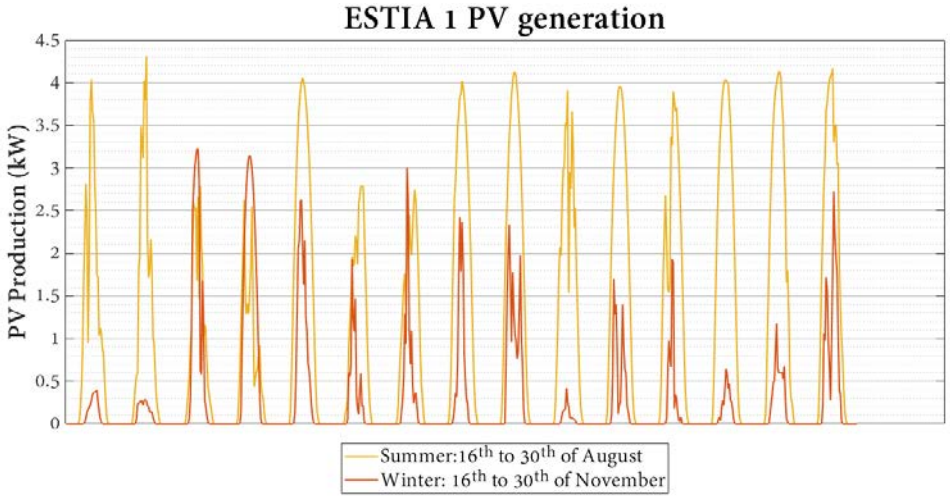


***Figure 3.5****. PV production curves of 15 days of August and November months.*

### 3.3.1.2 Meteorological data

The recording was carried out at the meteorological station located at Biarritz airport (Bidart, France) which is only 3.5km far from ESTIA 1 PV installation. This distance of more than 3km

means that the irradiance recorded at the airport and the irradiance perceived by the PV installation will differ due in particular to the difference in CC of the two locations. This can lead to an error when predicting PV production.

Meteorological variables have been obtained from Meteo France (MF) with one hour of sampling time. These data is measured, i.e. real data.

### a. Temperature, wind speed and direction data

The external temperature ($T_{ext}$) can directly affect the PV module temperature and if the latter is too high it can considerably reduce the efficiency of the PV array.

The wind speed can also be a possible input for the models, as it can vary the temperature of the PV modules and, therefore, buffer the efficiency reduction in periods of high temperatures.

In addition, to the wind speed another vector has been propose as the wind speed goes hand in hand with the wind direction. Only the wind coming from the direct direction of the PV panels has been considered. Taking into account that the panels are at a 20% inclination and oriented towards the southwest 150º with respect to the north, only the wind entering between 60º and 240º with respect to the north has been considered (see Figure 3.6). Thus, the vector takes on a value of 1 when the wind comes from the aforementioned range and zero when it comes from outside the range.

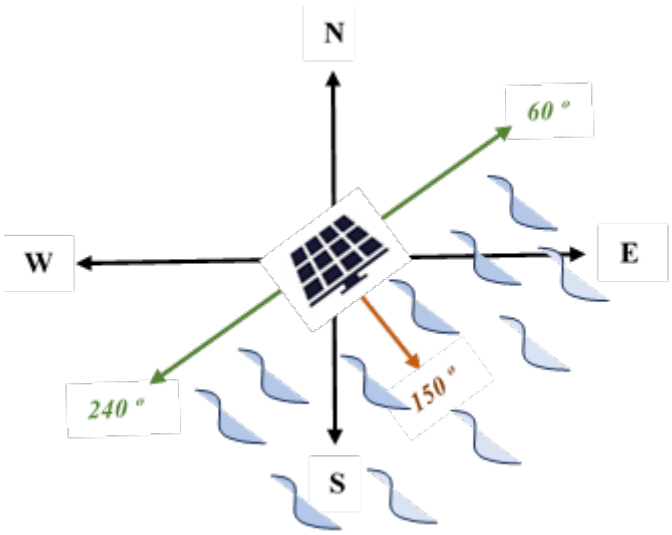


***Figure 3.6**. PV panels orientation and wind direction considered.*

### b. Solar irradiance data

Solar irradiance is considered to be the variable that most affects solar PV production, so the quality of solar irradiance data can be the key to obtaining accurate predictions. In this regard, in

a first phase measured irradiance data from MF has been considered, in concrete, data of July 2021 (see Figure 3.7).

Certainly having collected data from the airport of Biarritz, light pollution can affect the measured values of irradiance, especially at night when the high intensity lights must be switched on. This means that, during night-time periods, the measured irradiance curves show positive values. To overcome this problem, the sunrise and sunset times in both November and August have been checked to determine a night time window (Table C.4 and Table C.5 of Annex C). A filter has been applied to this time band to keep the solar irradiance values at 0. The same filter is applied to the predicted PV power curves, i.e. the PV production data is post-processed.

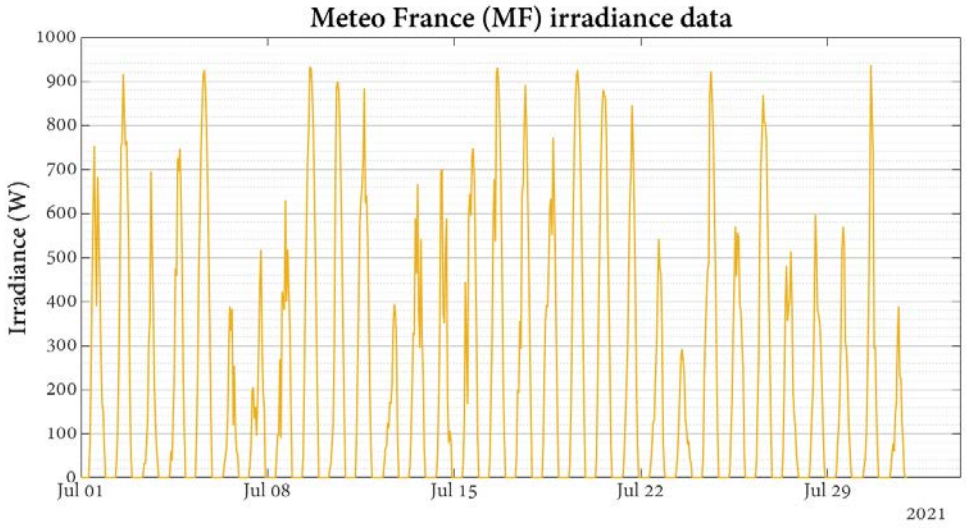


***Figure 3.7**. Meteo France measured irradiance curves of July 2021.*

In a second phase, data from three different meteorological agencies has been obtained. They have all their own data handling processes and models for predicting solar irradiance.

Figure 3.8 shows the solar irradiance curve measured by MF over a short period of 15 days of August and November days. More specifically, it shows the solar irradiance from 16$^{th}$ to 30 August and from 16$^{th}$ to 30 November 2021. There is indeed a strong correlation between production and solar irradiance. Regarding the analysed periods, the measured irradiance is significantly different. While in August (yellow curve) the irradiance curves exceed 800W on many days, in November the solar irradiance reaches a maximum of 440W and on only two days. In most days, the irradiance in August is almost an ideal bell-shaped curve. This explains the production curves analysed in Figure 3.5.

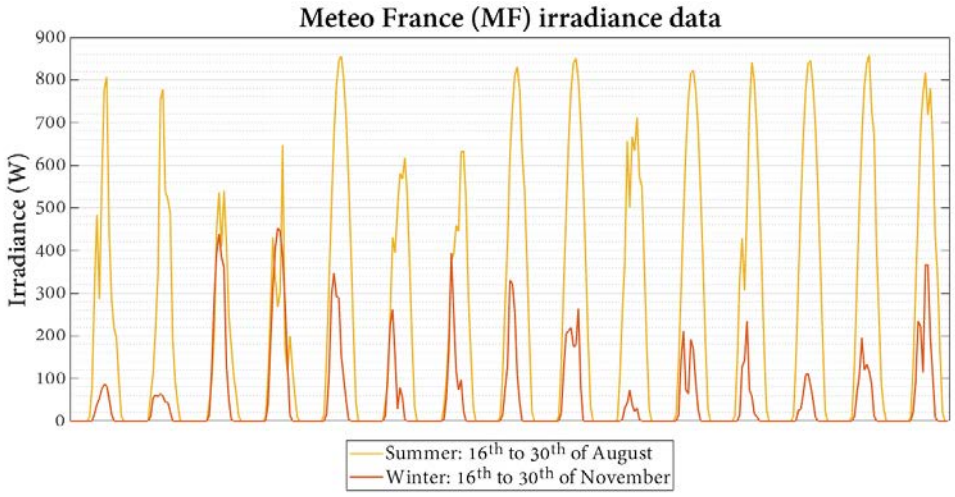


***Figure 3.8.*** *Meteo France measured irradiance curves of 15 days of both August and November months.*

Figure 3.9 and Figure 3.10 show the MG and ECMWF solar irradiance prediction data respectively for the same August and November months.

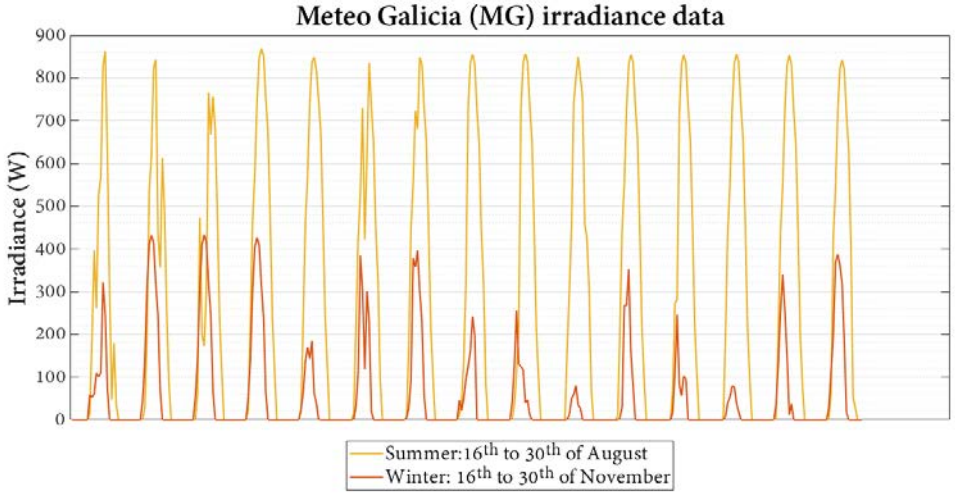


***Figure 3.9****. Meteo Galicia predicted irradiance curves of 15 days of both August and November months.*

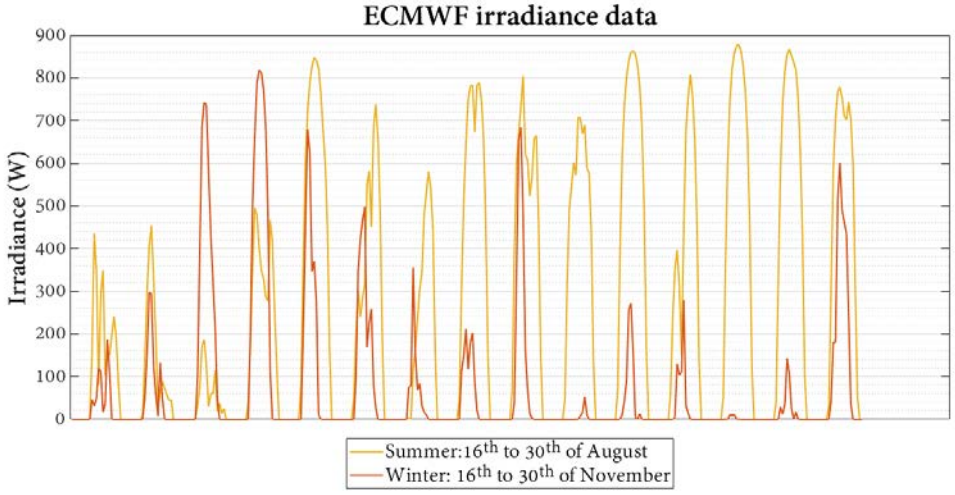


***Figure 3.10**. ECMWF predicted irradiance curves of 15 days of both August and November months.*

A priori, it can be seen that the data from each meteorological service differs notably. The irradiance predicted by ECMWF shows, especially in November, very irregular curves, and in many cases almost zero values. As it is evident, the measured MF irradiance data is the closest to the PV production of both months.

## 3.4 METHODOLOGY

### 3.4.1 Methodology description

The methodology followed to carry out the PV production forecasting has been designed in accordance with the objectives set out in section 3.2. As said, two phases have been differentiated according to the different objectives pursued.

#### 3.4.1.1 First phase

The first phase consists on performing a day-ahead prediction of solar PV generation with a NARX model using measured data of MF. The objective has been to validate the NARX model and to evaluate and compare the accuracy with which this model, two more ML models (FFNN and SVR) and an AnM are able to predict a summer month, namely the month of July 2021. Special attention has been paid to the design process of the NARX model, as the FFNN, SVR and analytical models have been developed by other PhD students of the research team.

A description of the methodology followed is shown in Figure 3.11.

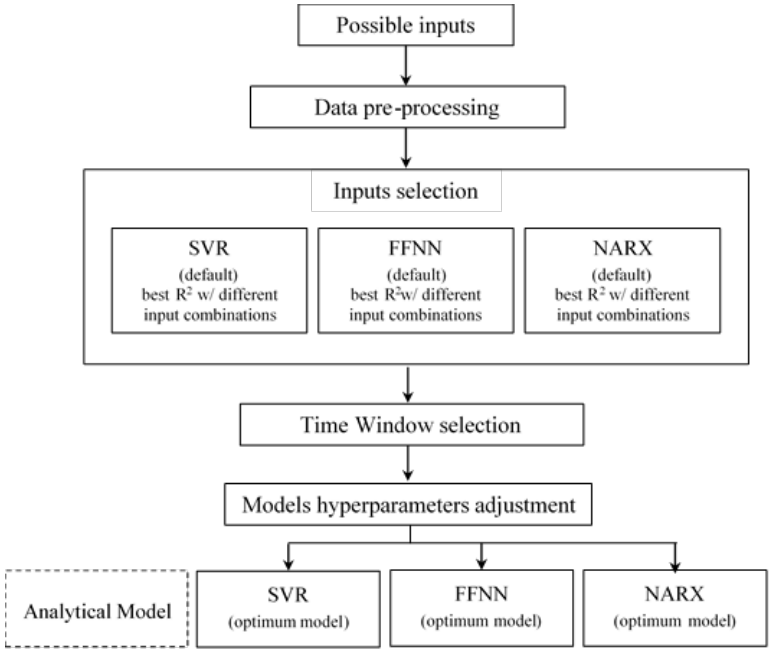


***Figure 3.11.*** *Flowchart of followed methodology in the first phase.*

Solar irradiance, temperature and the vectors that consider wind speed and direction have been included as possible inputs for the predictive models. In order to see which of these variables provide the most information for predicting PV generation, the predictions have been made with each combination of inputs and the accuracy with which the three proposed ML models predict

has been calculated. In this first phase, the inputs have been introduced with a sampling time of 30 minutes, so that the model predicts 48 solar generation samples of the next day.

After the inputs, the optimal TW has been selected for the three ML models to see if the number of days introduced to train the model contributes to improve the accuracy of the prediction.

Finally, the hyperparameters of each model have been adjusted obtaining the best model of NARX, SVR and FFNN. The selection of inputs, the choice of the TW and the search for the best values for the hyperparameters of both NN models have been carried out following the same criterion as in Chapter 2 when designing the models to predict the ESTIA 2 building energy consumption: the model is trained daily and performs day-ahead forecasts. Each time it is trained, the weights of the NN are randomly initialised. As mentioned above, the network predicts the entire month of July, therefore, the network has predicted the entire month three consecutive times in a daily training basis. The average monthly $R^2$ obtained each of the three times is calculated. The process is repeated for each combination of hyperparameter values, i.e. for each model constructed. The model with the lowest average $R^2$ is selected.

Due to the characteristics of the AnM, the design process is completely different. It is based on known mathematical equations. Therefore, the correctness of its design is based on the accuracy of the knowledge-based model parameters.

#### 3.4.1.2 Second phase

In the second phase, day-ahead prediction of solar PV generation has been carried out again with a NARX model, as well as with SVR, FFNN and an analytical model. However, in this phase, the prediction has not only been based on measured inputs obtained from MF, but also on predicted input data obtained from other two meteorological agencies: MG and ECMWF. In addition, the study has been extended by carrying out the prediction in August and November months. In this case too, special attention has been paid to the design process of the NARX model. The rest of the models have been developed by other PhD students of the research team.

Figure 3.12 shows the methodology followed in this second phase.

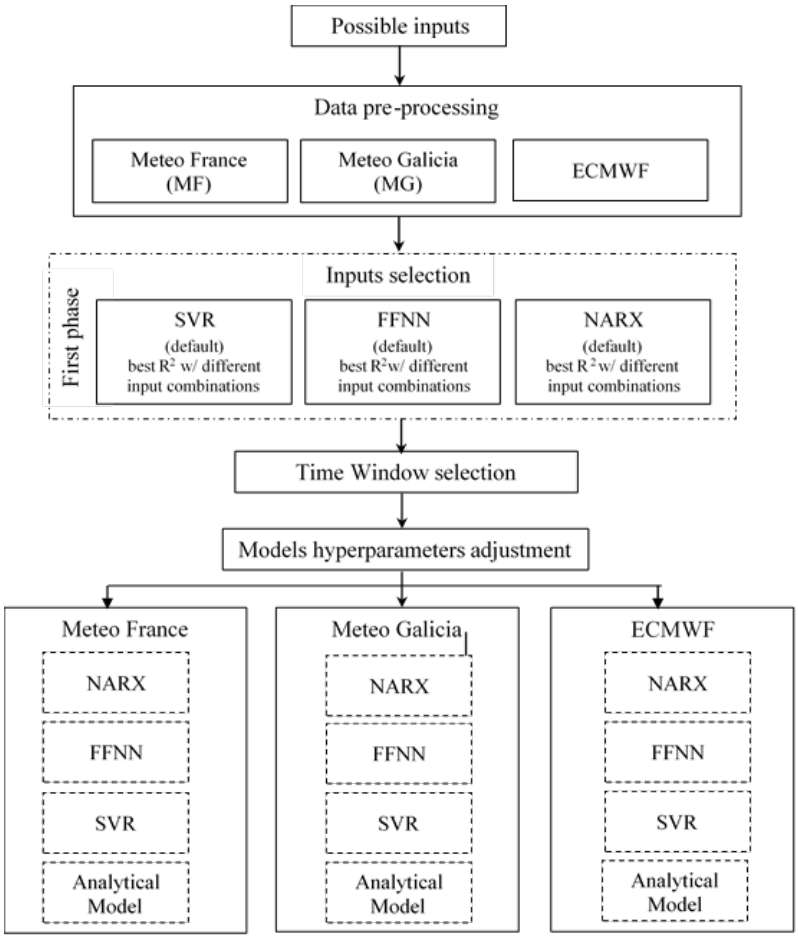


***Figure 3.12**. Flowchart of followed methodology in the second phase.*

As described in Figure 3.12, the analysis started by looking at the possible inputs for the predictive models and proceeding to pre-process the data from the three meteorological agencies. Then, the structure of the three ML models have been defined, by choosing the combination of inputs to be introduced and the TW for training. The last step has consisted of adjusting the hyperparameters of the models. The criterion used for the construction of the predictive models has been the same as in first phase.

In this second phase, the sampling time has been of 1 hour instead of 30 minutes because predicted meteorological data is available with a sampling time of 1 hour. Therefore, the model predicts 24 data points of the following day.

### 3.4.2 Developed models: ML and AnM

The NARX model, due to its ability to model nonlinear systems and to handle time series thanks to its recurrent term, has been one of the ML models to be modelled to forecast PV generation. Both the design and operation of NARX have been detailed in Annex A.

Another ML model proposed is the SVR. The SVR, as explained in Annex A, is also made up of hyperparameters and their adjustment is performed by means of Bayesian Optimisation, an automatic search algorithm based on the Gaussian process [184].

The performance and characteristics of the AnM as well as the FFNN can be consulted in [184].

### 3.4.3 Application of methodology

#### 3.4.3.1 Data pre-processing

Data pre-processing has involved reviewing the data provided by the meteorological agencies and, according to the requirements of the models, preparing them to meet these requirements.

First, both PV production and meteorological data have been analysed to detect and repair possible outliers by linear interpolation. Repeated data has been removed and missing data has been added by linear interpolation.

In the first phase, it has been decided to use a sampling time of 30 minutes, so being PV production data registered every 10 minutes, mean value every 30 minutes has been calculated. In the second phase, a sampling time of 1 hour has been fixed, therefore, production data has been modified by calculating mean hour values.

Finally, the data has been normalised between the range [0, 1] in order to use it in ML models. The data from the three meteorological agencies has been normalised using the ranges of Table 3.1.

***Table 3.1***. Normalisation ranges for all possible inputs.

| **Normalisation** | **MF** | **MG** | **ECMWF** |
|---|---|---|---|
| | **[min, max]** | **[min, max]** | **[min, max]** |
| $\boldsymbol{Production}$ | [0, 4430](W) | [0, 4430](W) | [0, 4430](W) |
| $\boldsymbol{Solar\ irradiance}$ | [0, 984](W) | [0, 950](W) | [0, 935](W) |
| $\boldsymbol{T_{ext}}$ | [-4, 43](ºC) | [-3, 38](ºC) | [-1, 34](ºC) |
| $\boldsymbol{Wind\ speed}$ | [0, 20.5](m/s) | [0, 22](m/s) | [0, 18](m/s) |

#### 3.4.3.2 Input selection

After pre-processing the data, inputs for the ML-based predictive models have been selected. The objective has been to select the inputs that best predicts PV production with the three ML models. The $R^2$ values obtained by each model when using different inputs are gathered in Table 3.2.

***Table 3.2.*** *$R^2$ results of the input combinations tested in the first phase*

| Input combinations | $R^2$ | | |
|---|---|---|---|
| | **FFNN** | **NARX** | **SVR** |
| $\boldsymbol{Solar\ irradiance}$ | **0.893** | **0.828** | **0.913** |
| $\boldsymbol{Solar\ irradiance}$ + $\boldsymbol{T_{ext}}$ | 0.881 | 0.789 | 0.904 |
| $\boldsymbol{Solar\ irradiance}$ + $\boldsymbol{Wind\ speed}$ | 0.879 | 0.794 | 0.906 |
| $\boldsymbol{Solar\ irradiance}$ + $\boldsymbol{Wind\ speed}$**_dq** | 0.870 | 0.776 | 0.905 |

It can be clearly noticed that with solar irradiance alone all three models predict with higher accuracy. Therefore, in first and second phases, solar irradiance has been the single input selected.

#### 3.4.3.3 First phase

##### a. Time Window Selection

After selecting the model entries, the TW has been chosen. For that, a comparison has been made between the use of a TW of 5 days or 10 days analysing in which case the PV production is more accurately predicted. Finally, a TW of 10 days has been selected [185].

Therefore, 480 data samples have been introduced to the model during the training phase, in order to predict 48 values of the next day's PV production. Of these 480 data points, 70% has been used for training and 30% for model validation.

##### b. Model hyperparameters adjustment

Regarding NARX model, the hyperparameters that have been adjusted to improve the accuracy of the predictions for the month of July are the following: (a) the number of neurons in the hidden layer, (b) input and feedback delays and (c) the activation function in the hidden and output layers. It is also possible to add more than one hidden layer to the network. However, as it is considered a simple prediction problem, only one hidden layer has been used.

Each of the possible combinations of the hyperparameters values defined in Table 3.3 constitutes a NARX model.

***Table 3.3.*** *Simulation planning for NARX model design in first phase.*

| | | ***Model structure*** | | ***Model hyperparameteres*** | | |
|---|---|---|---|---|---|---|
| | ***Training characteristics*** | ***Input combination*** | ***Time Window (TW)*** | ***Activation function*** | ***neurons*** | ***input and feedback delays*** |
| ***NARX*** | Learning algorithm: *Levenberg-Marquardt* | Solar irradiance (W) | 10 days | Hidden = {linear, tansig}<br>Output = {linear, tansig} | [1, 2, 3, 4, 5, 10] | [0, 1] and [1,2,3.4] |
| | Error = MSE | | | Hidden = {linear, tansig}<br>Output = {linear, tansig} | [1, 2, 3, 4, 5, 10] | [0, 1] and [1,2,3.4] |
| | Daily NARX training = 3 times | | | Hidden = { linear, tansig}<br>Output = { linear, tansig} | [1, 2, 3, 4, 5, 10] | [0, 1] and [1,2,3.4] |
| | | | | Hidden = { linear, tansig}<br>Output = { linear, tansig} | [1, 2, 3, 4, 5, 10] | [0, 1] and [1,2,3.4] |

For the selection of the number of neurons in the hidden layer, it has been found that the best results were acquired with 1 and 3 neurons, obtaining a significant improvement in the $R^2$ metric (see Table 3.4).

As for the activation function, the default *tansig* function has been set in the hidden layer and the linear function in the output layer. The sigmoid activation function is problematic in case of PV production forecasting due to its codomain being ]0, 1[ , it tends to give problems of stability in the output during the night when having to predict null values.

In the adjustment of both delays, the predictions have been made with different combinations of input and feedback delays.

***Table 3.4.*** *Results obtained with NARX model combining different number of neurons and delays.*

| Nº of Neurons | Input delay | Feedback delay | MAE | RMSE | $R^2$ |
|---|---|---|---|---|---|
| 1 | 0 | 1 | 186.253 | 306.610 | 0.850 |
| | 0 | 2 | 178.890 | 300.114 | 0.850 |
| | 0 | 3 | 170.447 | 285.746 | 0.863 |
| | 0 | 4 | 175.752 | 296.368 | 0.848 |
| | 1 | 1 | 178.735 | 297.446 | 0.856 |
| | 1 | 2 | 182.403 | 303.188 | 0.849 |
| | 1 | 3 | 178.704 | 300.948 | 0.843 |
| | 1 | 4 | 175.490 | 295.415 | 0.850 |
| 3 | 0 | 1 | 203.762 | 338.190 | 0.854 |
| | 0 | 2 | 233.423 | 375.512 | 0.812 |
| | 0 | 3 | 209.042 | 351.111 | 0.779 |
| | 0 | 4 | 178.290 | 305.830 | 0.842 |
| | 1 | 1 | 160.204 | 274.975 | 0.877 |
| | 1 | 2 | **148.465** | **255.714** | **0.881** |
| | 1 | 3 | 151.524 | 261.359 | 0.877 |
| | 1 | 4 | 190.125 | 327.298 | 0.810 |

Therefore, looking at the results obtained, it can be concluded that the model that better forecasts the PV production is obtained by adding three neurons in the hidden layer and setting 1-time delay step in the input and 2 in the feedback. The training and validation processes of all modelled NARX structures have been analysed to corroborate that there is no overfitting by analysing the MSE obtained from the training and validation data.

The selected model characteristics are described in Table 3.5.

***Table 3.5****. Hyperparameter values of the proposed NARX model for PV production forecasting.*

| **Hyperparameters of NARX** | |
|---|---|
| **Hidden layers** | nº of hidden layers = 1 |
| | number of neurons = 3 |
| **Delay vectors** | Input = 1 |
| | Feedback = 2 |
| **Activation function** | Hidden layer = Hyperbolic tangent |

| | |
|---|---|
| | Output layer = Linear function |
| **Training parameters** | Learning algorithm: Levenberg-Marquardt |

Regarding FFNN, few hyperparameters can be adjusted: (a) the number of neurons in hidden layer, and (b) the activation functions. As stated in Table 3.6, the hidden layer of FFNN is comprised by 5 neurons. As for the NARX, the training and validation process has been analysed to ensure that the network does not suffer from overfitting.

***Table 3.6**. Results of tests for FFNN hyper-parameter adjustment.*

| **Nº of Neurons** | **MAE** | **RMSE** | **$R^2$** |
|---|---|---|---|
| 2 | 143.60 | 253.23 | 0.8849 |
| 4 | 131.62 | 237.86 | 0.8917 |
| 5 | **130.07** | **235.69** | **0.8931** |
| 6 | 132.53 | 239.13 | 0.8911 |
| 8 | 131.75 | 238.03 | 0.8923 |
| 10 | 131.91 | 238.61 | 0.8910 |
| 15 | 132.04 | 241.99 | 0.8872 |
| 20 | 133.02 | 243.59 | 0.8853 |

Finally, the SVR model has been designed by adjusting the hyperparameters by means of a Bayesian optimisation algorithm. Table 3.7 gathers the values corresponding to the hyperparameters $C$, ε and $\gamma$ defined in section 2.4.2 of Chapter 2.

***Table 3.7**. Results of SVR hyper-parameter tuning based on Bayesian optimisation.*

| $C$ | $\varepsilon$ | $\gamma$ |
|---|---|---|
| 166 | 0.002 | 0.003 |

#### 3.4.3.4 Second phase

Regarding input combination, the analysis carried out in the first phase has been used as a reference, selecting once again only solar irradiance as input for all models.

### a. Time Window Selection

The analysis that has been done in the first phase regarding TW selection has been extended in this second phase. Together with using 10 days of TW, 15 days have also been employed. 15 days were selected due to the better results obtained.

Taking into account that the sampling time in the second phase is of one hour, 360 training data points have been introduced, 70% of which have been used to train the model and 30% for validation.

### b. Model hyperparameters adjustment

The hyperparameters of NARX that need to be tuned are stated in first phase. In this case too, a single hidden layer has been kept. Table 3.8 shows the values of each hyperparameter that have been combined in order to choose the NARX model.

***Table 3.8**. Simulation planning for NARX model design in second phase.*

| | | ***Model structure*** | | ***Model hyperparameteres*** | | |
|---|---|---|---|---|---|---|
| | ***Training characteristics*** | ***Input combination*** | ***Time Window (TW)*** | ***Activation function*** | ***neurons*** | ***input and feedback delays*** |
| ***NARX*** | Learning algorithm: *Levenberg-Marquardt* | Solar irradiance (W) | 15 days | Hidden = {linear, tansig}<br>Output = {linear, tansig} | [2, 4, 5, 6, 7, 8, 10, 15] | [2, 4, 6, 8, 10] |
| | Error = MSE | | | Hidden = {linear, tansig}<br>Output = {linear, tansig} | [2, 4, 5, 6, 7, 8, 10, 15] | [2, 4, 6, 8, 10] |
| | Daily NARX training = 3 times | | | Hidden = { linear, tansig}<br>Output = { linear, tansig} | [2, 4, 5, 6, 7, 8, 10, 15] | [2, 4, 6, 8, 10] |
| | | | | Hidden = { linear, tansig}<br>Output = { linear, tansig} | [2, 4, 5, 6, 7, 8, 10, 15] | [2, 4, 6, 8, 10] |

As for the activation functions, there is the same problem of using the sigmoid function, since this function destabilises the output during the night when its value is null. Therefore, tansig function has been applied in hidden layer and better results have been seen when applying linear function in output layer. Table 3.9 shows the value of the hyperparameters of the NARX, when it has been

trained with data from the three meteorological agencies both for predicting August and November PV generation.

***Table 3.9.*** *Structure and hyperparameters values for proposed NARX model for each meteorological agencies and seasons.*

| ***NARX*** | | | | | | | |
|---|---|---|---|---|---|---|---|
| ***Structure & Hyperparameters*** | | | | | | | |
| ***Independent input*** | | Solar irradiance (W) | | | | | |
| ***Time Window*** | | 15 days | | | | | |
| ***Activation Function*** | | Hidden layer = Hyperbolic tangent | | | | | |
| | | Output layer = Linear | | | | | |
| ***Weather Service*** | | ***MF*** | | ***MG*** | | ***ECMWF*** | |
| ***Season*** | | ***November*** | ***August*** | ***November*** | ***August*** | ***November*** | ***August*** |
| ***Number of neurons*** | | 4 | 5 | 4 | 2 | 10 | 10 |
| ***Delays*** | ***Input*** | 3 | 5 | 3 | 5 | 3 | 5 |
| | ***Feedback*** | 5 | 5 | 5 | 5 | 5 | 5 |

Regarding FFNN, the best model characteristics for each data source are gathered in Table 3.10. A single hidden layer has been selected and to determine the number of neurons, the behaviour of the models have been compared by considering from 2 to 15 neurons.

***Table 3.10****. Structure and hyperparameter values for proposed FFNN model for each meteorological agencies and seasons.*

| ***FFNN*** | | | | | | | |
|---|---|---|---|---|---|---|---|
| ***Structure & Hyperparameters*** | | | | | | | |
| ***Independent input*** | | Solar irradiance (W) + Hour vector | | | | | |
| ***Time Window*** | | 15 days | | | | | |
| ***Activation Function*** | | Hidden layer = Sigmoid | | | | | |
| | | Output layer = Lineal | | | | | |
| ***Weather Service*** | | ***MF*** | | ***MG*** | | ***ECMWF*** | |
| ***Season*** | | ***November*** | ***August*** | ***November*** | ***August*** | ***November*** | ***August*** |
| ***Number of neurons*** | | 4 | 6 | 8 | 4 | 10 | 7 |

Finally, SVR has been considered following the same designing procedure as in the first phase. Table 3.11 summarizes the structure and design of selected SVR model.

***Table 3.11**. Structure and hyperparameter values for proposed SVR model for each meteorological agencies and seasons.*

| ***SVR*** | | | | | | |
|---|---|---|---|---|---|---|
| ***Structure & Hyperparameters*** | | | | | | |
| ***Independent input*** | Solar irradiance (W) + Hour vector | | | | | |
| ***Time Window*** | 15 days | | | | | |
| ***Weather Service*** | ***MF*** | | ***MG*** | | ***ECMWF*** | |
| ***Season*** | ***November*** | ***August*** | ***November*** | ***August*** | ***November*** | ***August*** |
| $C$ | 64 | 64 | 2 | 64 | 64 | 64 |
| $\varepsilon$ | 4 | 0.1 | 64 | 4 | 4 | 4 |
| $\gamma$ | 0.25 | 0.5 | 2 | 0.5 | 0.125 | 2 |

## 3.5 RESULTS AND DISCUSSION

### 3.5.1 First phase

This subsection presents the results obtained after performing one-day-ahead forecasting of PV generation by three ML models and one AnM using historical measured data obtained from MF for training.

To begin with, Table 3.12 shows the average of error metrics of each model. It can be observed that all the proposed models predict the month of July 2021 with an $R^2$ above 0.88. Analysing the results in terms of $R^2$, the SVR stands out from the other models with an $R^2$ of 0.934.

***Table 3.12**. Error metrics obtained for the prediction of PV generation during the month of July.*

| Model | MAE | RMSE | $R^2$ |
|---|---|---|---|
| **NARX** | 155.93 | 267.51 | 0.886 |
| **FFNN** | 125.66 | 231.20 | 0.896 |
| **SVR** | 141.81 | 252.46 | **0.934** |
| **AnM** | 234.46 | 406.51 | 0.895 |

Figure 3.13 shows the response of the NARX model of a single week taken from prediction results of the month of July. NARX predicts particularly well the cloudy days, represented in this graph by the production of 22nd and 23rd of July. Figure C.6, Figure C.7 and Figure C.8 in Annex C show the forecasting curves of FFNN, SVR and AnM models respectively in comparison of expected production during the same July week.

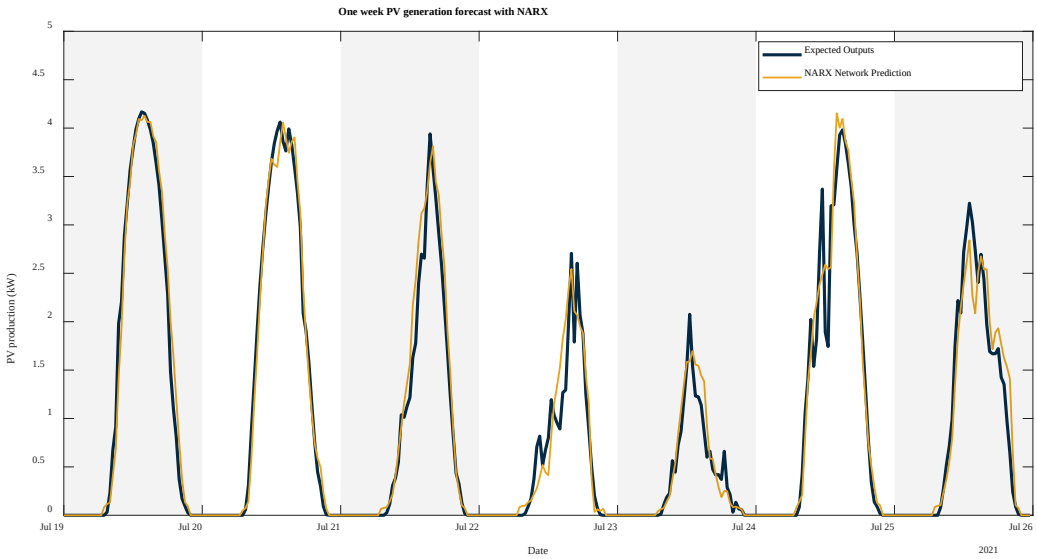


***Figure 3.13**. Forecast of PV generation for a week of July with NARX model.*

Table 3.13 shows the $R^2$ values of the predictions performed by the four models on sunny and on cloudy days. It can be concluded that it is the SVR, which again outperforms the rest of the models on both sunny and cloudy days. Moreover, while on sunny days, where the production is closer to a perfect bell shape, the $R^2$ obtained is around 0.95, on cloudy days the $R^2$ drops to 0.8.

***Table 3.13.** Results of the four models for five sunny days and five cloudy days.*

| **Type of day** | **Date** | **$R^2$** | | | |
|---|---|---|---|---|---|
| | | **FFNN** | **NARX** | **SVR** | **AnM** |
| Sunny days | 05/07/2021 | **0.963** | 0.943 | 0.962 | 0.897 |
| | 09/07/2021 | 0.980 | 0.927 | **0.968** | 0.881 |
| | 10/07/2021 | **0.980** | 0.971 | 0.978 | 0.915 |
| | 19/07/2021 | 0.981 | 0.973 | **0.982** | 0.894 |
| | 26/07/2021 | 0.971 | 0.953 | **0.977** | 0.906 |
| Cloudy days | 06/07/2021 | 0.780 | 0.779 | **0.871** | 0.758 |
| | 07/07/2021 | 0.676 | 0.670 | **0.813** | 0.726 |
| | 08/07/2021 | 0.662 | 0.670 | **0.802** | 0.728 |
| | 13/07/2021 | 0.824 | 0.839 | **0.902** | 0.834 |
| | 06/07/2021 | 0.780 | 0.779 | **0.871** | 0.758 |

### 3.5.2 Second phase

Figure 3.14 and Figure 3.15 show the $R^2$ of the predictions made by each model in August and November months. The two horizontal lines that can be seen in each bar chart represent the $R^2$ value obtained by benchmark models, i.e. the persistence and random models.

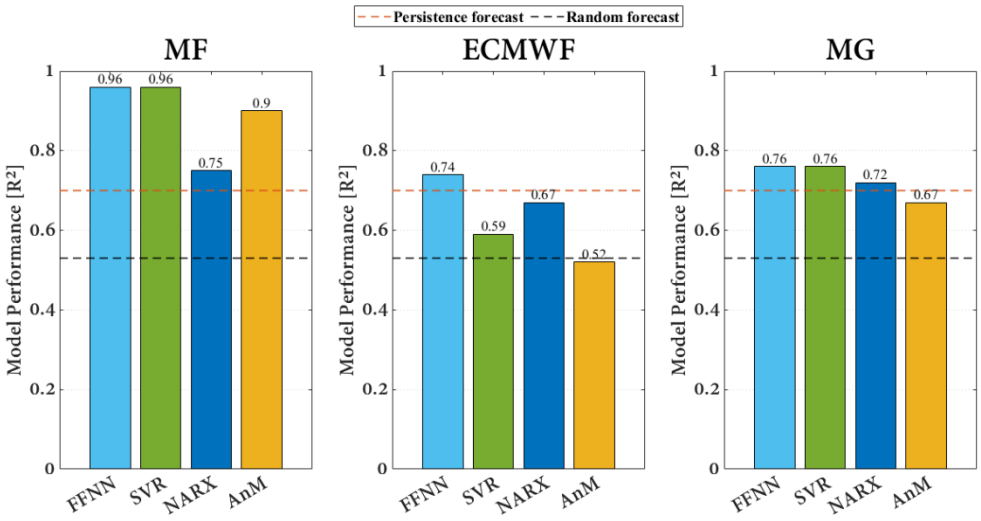


***Figure 3.14**. $R^2$ results for all proposed models and three different meteorological data sources, for November.*

Starting by looking at how the November month is predicted, several conclusions can be drawn. A notable difference can be seen in the results of all models when trained with MF irradiance data and when trained with the predicted MG and ECMWF irradiance data. All four models are able to overcome the $R^2$ of 0.70 of the persistence model when using measured MF data. In contrast, when using predicted data from the two aforementioned agencies, the models present more problems to surpass the persistence, especially when using irradiance data from ECMWF, with which only the FFNN is able to improve the $R^2$ of 0.7 of the persistence.

As for the AnM, it is able to predict very accurately (with a $R^2$ of 0.9) when modelled with measured MF irradiance data. This contrasts with the results obtained by the AnM when using predicted data, since in these cases it fails to outperform the persistence model.

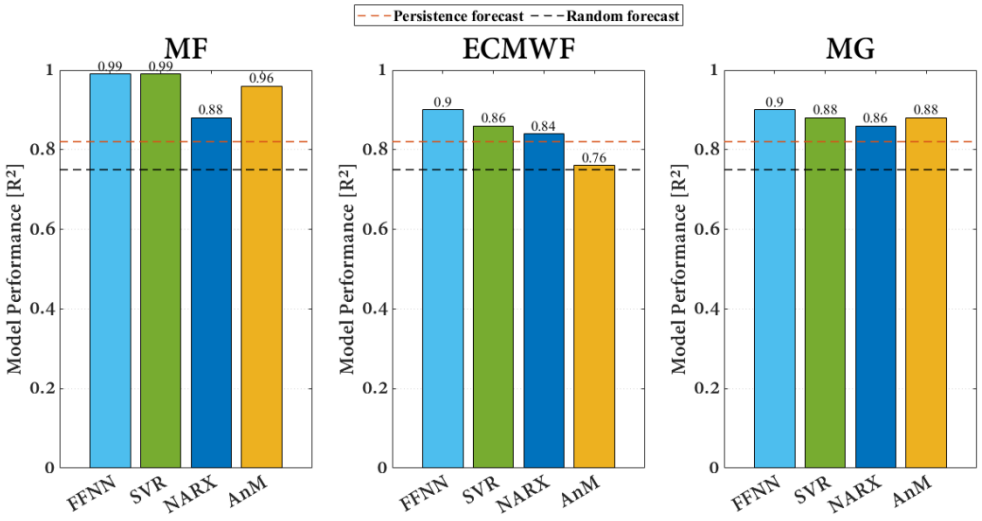


***Figure 3.15**. $R^2$ results for all proposed models and three different meteorological data sources, for August.*

As for the August month, compared with the November results, there is a noticeable improvement in the $R^2$ values of all models. This is because in August the production curves are much closer to a perfect bell shape due to also bell-shaped irradiance curves (see Figure 3.9 and Figure 3.10).

Once again, the models predict more accurately when trained with irradiance data from MF than with predicted solar irradiance data. Anyway, ML models trained with predicted data (MG and ECMWF) have proven to be able to outperform the persistence model, which obtains a $R^2$ of 0.82.

As for the AnM, in the case of August, a difference in its response can also be observed when modelled with measured MF irradiance data and predicted data from both meteorological agencies. Although it surpasses the persistence model in the case of MG, it does not manage to outperform it with ECMWF data, and even narrowly improves random model accuracy.

With the $R^2$ values grouped by model type in Table 3.14, it is possible to conclude that the FFNN is the best model to forecast PV production during the November month. It is followed by SVR and NARX. The SVR obtains a very good prediction result when it is trained with measured irradiance, but it predicts worse than the NARX model when trained with predicted irradiance.

***Table 3.14**. Error metric values of all models for November.*

| | | November | | |
|---|---|---|---|---|
| | | **MAE** | **r** | **$R^2$** |
| **Persistence model** | | 245.32 | 0.82 | 0.70 |
| **Random model** | | 309.04 | 0.72 | 0.53 |
| **FFNN** | **MF** | 59.98 | 0.981 | 0.96 |
| | **ECMWF** | 171.03 | 0.85 | 0.74 |

| | | | | |
|---|---|---|---|---|
| | **MG** | 212.29 | 0.87 | 0.76 |
| **SVR** | **MF** | 55.41 | 0.962 | 0.96 |
| | **ECMWF** | 168.27 | 0.74 | 0.59 |
| | **MG** | 196.73 | 0.70 | 0.76 |
| **NARX** | **MF** | 176.60 | 0.86 | 0.75 |
| | **ECMWF** | 186.80 | 0.81 | 0.67 |
| | **MG** | 224.55 | 0.84 | 0.72 |
| **AnM** | **MF** | 233.80 | 0.95 | 0.90 |
| | **ECMWF** | 243.04 | 0.67 | 0.52 |
| | **MG** | 263.44 | 0.81 | 0.67 |

In August as seen in Table 3.15, the best predictive model is still FFNN followed by SVR, which predicts somewhat worse than FFNN when trained with predicted irradiance. Although the AnM predicts more accurately than NARX in the case of using measured irradiance data, NARX improves the AnM when using predicted irradiance data, instead on summer trained with data from MG.

***Table 3.15**. Error metric values of all models for August.*

| | | **August** | | |
|---|---|---|---|---|
| | | **MAE** | **r** | **$R^2$** |
| **Persistence model** | | 353.03 | 0.90 | 0.82 |
| **Random model** | | 422.12 | 0.86 | 0.75 |
| **FFNN** | **MF** | 77.49 | 0.994 | 0.99 |
| | **ECMWF** | 219.65 | 0.95 | 0.90 |
| | **MG** | 308.13 | 0.95 | 0.90 |
| **SVR** | **MF** | 62.13 | 0.985 | 0.99 |
| | **ECMWF** | 234.10 | 0.92 | 0.86 |
| | **MG** | 299.50 | 0.73 | 0.88 |
| **NARX** | **MF** | 272.52 | 0.93 | 0.88 |
| | **ECMWF** | 302.71 | 0.91 | 0.84 |
| | **MG** | 394.43 | 0.92 | 0.86 |
| **AnM** | **MF** | 207.61 | 0.98 | 0.96 |
| | **ECMWF** | 338.24 | 0.86 | 0.76 |
| | **MG** | 295.95 | 0.93 | 0.88 |

Finally, Figure 3.16 and Figure 3.17 have been added to show more graphically the responses of the NARX model predicting PV production in November and August.

The greater the variability, the greater the difficulty for NARX to follow the measured production curve. Comparing the NARX curve trained with MG and ECMWF data, it is concluded that it follows the real production curve better when trained with MG data. It can be seen that with the ECMWF data, the model predicts the production, in general, significantly below the expected values, except the high peak that predicts the 24$^{th}$ of November. This might be related to the conservative solar irradiance predictions made by ECMWF agency shown in Figure 3.10.

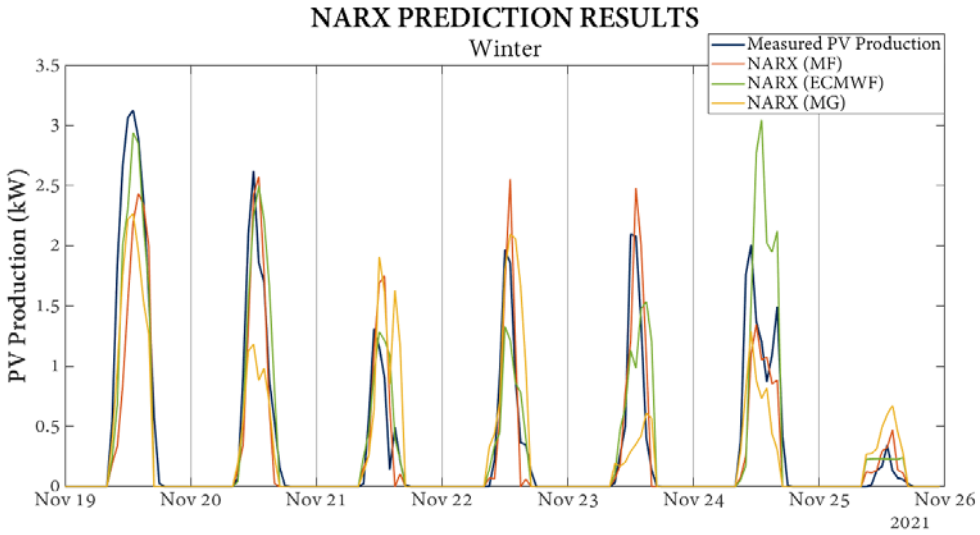


***Figure 3.16**. NARX model prediction results in November when training with different data sources.*

The increase in the $R^2$ values obtained in August (see Table 3.15), translates into improved tracking of all the NARX models to the expected production curve as can be seen in Figure 3.17.

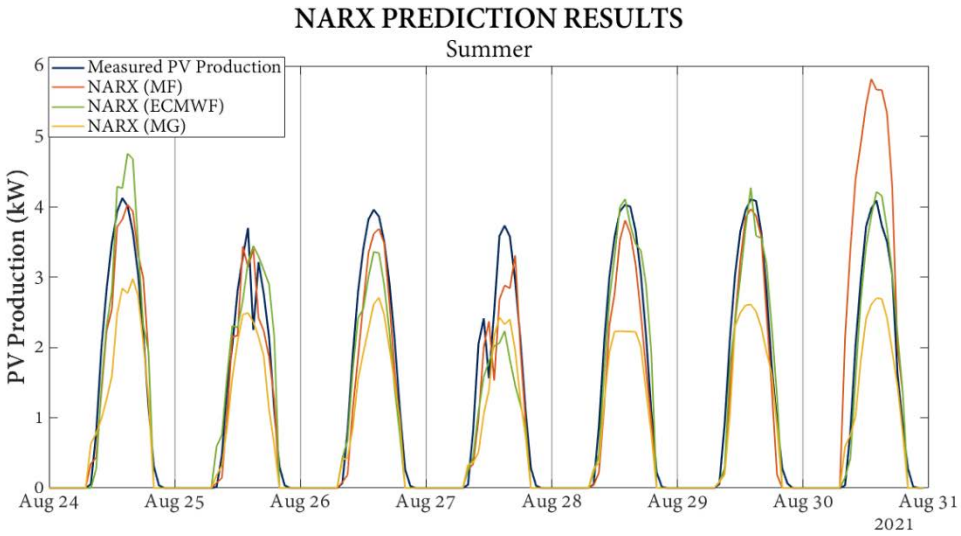


***Figure 3.17**. NARX model prediction results in August when training with different data sources.*

It can be seen that there is not so much difference between the tracking of the model trained with MF data and that of the models trained with predicted MG and ECMWF irradiance data. Anyway,

it should be noted that NARX model sometimes predicts with errors that might not have a clear explanation.

## 3.6 CONCLUSIONS

This third chapter introduces the design, development and analysis of a NARX-type NN model to predict the PV energy generated at ESTIA 1 in order to use it in the optimisation-based EMS described in Chapter 5.

The ML based NARX, FFNN and SVR models together with the AnM proposed in the first phase have been trained with measured solar irradiance data obtained from MF. The results show that for the prediction of July 2021 the NARX is able to predict with a $R^2$ of 0.886, 5.12% worse than the SVR, which is the one that best predicts the month with an average $R^2$ of 0.934. The SVR also outperforms the FFNN and the AnM, predicting 4.07% and 4.18% better respectively.

Regardless of the model used, it has been found that sunny days are predicted more accurately than cloudy days. This is related to the irregular shape that solar irradiance acquires on cloudy days, which makes higher the variability of the PV production curve and forecasting becomes harder.

In a second phase the analysis has been extended to see how the ML models and the AnM perform day-ahead production forecasting instead of using measured solar irradiance data as input, using predicted irradiance data from MG and ECMWF. This second approach is compulsory for the real operation of the EMS.

FFNN has been the model that forecasts with the highest accuracy, which surpasses the rest of the models in almost all the cases. Anyway, even in November or August, NARX has managed to follow the PV production curve with high accuracy. Of particular note is the case of NARX trained with predicted ECMWF data. The ECMWF solar irradiance data, especially in November, shows great variability and the NARX model is able to outperform the SVR and the AnM in both August and November with a $R^2$ of 0.84 and 0.67 respectively.

The AnM presents a significant difference in accuracy when using measured and predicted irradiance data. In the case of November, the $R^2$ difference obtained when using measured irradiance and predicted irradiance data from MG and ECMWF is 42.22% and 25.56% respectively. Being compared with ML models, the last ones are able to predict with higher accuracy when they are trained with predicted data. This shows that to some extent ML models are able to compensate the errors of solar irradiance predictions.

It has also been found that the proposed models perform better when trained with MG irradiance data. In the case of November, on average, the models based on MG data predict with a $R^2$ of 0.72 while those based on ECMWF irradiance data predict with a $R^2$ of 0.63. In August, models trained

with MG irradiance data predict on average with a $R^2$ of 0.88 and those trained with ECMWF irradiance data with a $R^2$ of 0.84.

Furthermore, it can also be concluded that in August all ML models outperform persistence and random models without great difficulty. In November, all the proposed models exceed random model but in case of SVR and NARX models trained with predicted irradiance data from ECMWF, are not able to outperform the persistence model.

In this work it has been shown that with a small data set it is feasible to propose ML models to forecast in short-term PV production. The results show that the NARX model can perform short-term forecast with high accuracy even when it is trained with a small data set of predicted solar irradiance data.

# *CHAPTER 4*

# *BUILDING THERMAL MODEL*

The fourth chapter is dedicated to the design of the thermal model for the building under analysis. This chapter aims to model HVAC system and its associated building thermal capacity.

It begins with an overview of the most relevant studies conducted to date in this field, narrowing down to those that model a building under conditions similar to the ones determined in the case study analysed. This leads to a presentation of the established objectives and the contributions of this chapter. The case study has been then presented and the methodology employed to develop the modelling of the building's thermal behaviour is introduced, followed by the presentation of the results. The chapter ends with a section discussing the conclusions drawn.

## 4.1 PROBLEM STATEMENT

There is no denying the importance of the need to reduce global energy consumption. This is evidenced by laws and directives promoted by international institutions, more or less persistently implemented by states, in order to potentially reverse the environmental issue we face.

Given the large share that buildings play in global consumption, building sector holds substantial potential for energy savings and load shifting, crucial for mitigating high demand peaks.

To achieve these objectives and effectively reduce building consumption it is imperative to design tools and methods for enhancing building electrical efficiency [186], [187]. However, this task can prove challenging without a comprehensive understanding of consumption patterns across different building types.

Numerous factors influence a building's energy performance, including occupant behaviour, occupancy levels, lighting systems, weather conditions, and HVAC system [188]. Among these loads, the HVAC system stands out as having the most significant impact on total energy consumption, typically constituting around half of a building's total energy usage [189]. Moreover, employing advanced strategies for the HVAC control can facilitate the integration of RES [190].

Given these considerations, energy management assumes fundamental importance. Building energy management is often facilitated by an EMS, which it has proved to be a very interesting tool for SC and similar applications.

EMSs use to operate by managing the FLs of buildings. HVAC systems and the associated building thermal capacity are identified as one of the most interesting FL for energy savings [191]. Consequently, the literature frequently explores the development of EMSs with HVAC use optimisation as a central focus [192], [193], [194], [195]. To optimise this FL, it is necessary to model both HVAC system and the associated thermal capacity of the building. Therefore, it is imperative to review different models applied for modelling both.

An initial classification distinguishes between static and dynamic models. Static models, characterised by their ability to describe thermal behaviour exclusively in steady-state conditions, lack the capacity to represent transient stages. On the contrary, dynamic models incorporate the evolution of thermal loads, calculating heat transfer between various building elements. The literature commonly features dynamic modelling approaches, often employing equivalent electrical circuits to represent thermal dynamics.

A second classification based on modelling approach, differentiates models into three types: (a) white-box or physical models, (b) grey-box, and (c) black-box or data-driven models. Figure 2.3 of Chapter 2 depicts the mentioned classification.

White-box models have traditionally dominated building modelling [196]. These highly detailed, high-order models rely on physical equations and building material parameters. However, their complex nature and demand for comprehensive understanding of environmental phenomena render them unsuitable for applications such as MPC [197].

Grey-box models, in contrast, mix a physical model with data-driven models. These simplified models, requiring less complexity than white-box models during design, are better suited for control applications. Moreover, they often require less data than black-box models, as they can extrapolate system behaviour beyond the training data's operational range. The resistor-capacitor (RC) thermal network, based on an equivalent electrical circuit, is an example of grey-box modelling in the thermal analysis of buildings [198], [199].

Black-box or data-driven models require historical data for model identification. The spreading of data availability has increased interest in data-driven models among researchers. Notably, ANNs and in general, ML models have gained prominence over traditional physical models [95]. However, challenges persist in real-world applications, including data accessibility issues, monitoring limitations, and incomplete data sets. While SA models are characterised by simplicity and low computational overhead, their performance may vary depending on the system's complexity [200]. AR models hold particular significance on modelling purposes. They incorporate lagged terms of the same variable, thus allowing the dynamics of the system to be taken into account. Further details on AR models are available in Annex B.

### 4.1.1 Building thermal capacity model

The building's thermal capacity, associated with its HVAC system, constitutes a critical element for modelling. The operation of the air conditioning system is linked to the thermal capacity of the building and both constitute a FL in which the EMS can act [201]. Consequently, the creation of a thermal model of the building serves an important purpose: it effectively describes the thermal performance of the building, i.e. the indoor temperature variation, facilitating the assessment of the effects of energy improvement measures on the building. By assessing the impact of such measures on the building's thermal behaviour, optimal energy-efficient options can be identified [202]. In essence, the thermal model, among other things, serves to forecast the energy requirements of the building.

For many years, physical models, particularly white-box models, have been extensively employed for modelling indoor temperature ($T_{in}$). Despite their dependence on detailed structural

parameters, advancements in software technologies have simplified the modelling process. Notably, the EnergyPlus software utilising plugins such as OpenStudio SketchUp exemplifies this trend [196]. By incorporating specific building characteristics, these models can accurately follow $T_{in}$ evolution and corresponding energy consumption. In the case of [99], building thermal model is built in EnergyPlus with the target of generating temperature data to train a data driven HVAC system model.

Likewise, RC models are also highly appropriate for thermally characterizing a building. Sometimes due to the large number of structural elements that make up a building, the creation of a RC thermal network can also become a difficult task. In [203] a methodology is proposed that consists of first creating a complex RC structure based on physical principles and iteratively eliminating non-identifiable parameters in order to create a structure simple enough to be able to follow the $T_{in}$ with even better results than with more complex structures. A complex structure of the RC model includes many parameters to reflect the detailed thermal interactions between the different building components. There are also works where not only a RC model is used, but this is complemented or derived from other types of models. This is the case of the model proposed in [204], where it is initially proposed a relatively simple RC model in order to provide physical interpretability to the parameters and convert this RC model into an autoregressive model. The main advantage that the designed model offers in addition to being computationally light is that it can be scalable and therefore adapt to modelling various buildings.

Leaving aside physical models and grey-box models, numerous papers have been find that propose NNs and other ML models to see how a building thermally behaves. When it comes to SA based models, the most used for this case are AR models. It is the example in [205] where a building capacity is thermally modelled using several independent variables such as occupancy, lighting, relative humidity, etc. to see how they affect in $T_{in}$. In this case, an ARMAX model combined with Normalised Mutual Information (NMI) is used, which allows obtaining the exact variables that influence the $T_{in}$, serving as a guide for the ARMAX. Likewise, it compares the mentioned model with an ARX model, concluding that the model that combines the NMI with the ARMAX is the one that operates best. Another interesting example is the one proposed in [206], where the energy flexibility of an institutional building wants to be quantified. For this purpose, an ARX model is used to model the thermal behaviour of the mentioned building taking into account the optimal operating points of a geothermal heat pump that operates powered by a PV system. Thanks to the strategy proposed to take advantage of the flexibility, a 40% reduction in demand at peak hour is obtained during morning hours and a 30% reduction during the afternoon.

The Box Jenkins method is usually applied to models such as ARIMA or ARIMAX. As the work presented in [201] that aims to propose an ARMA and ARIMAX models to thermally characterize a building. To do this, ARMA and ARIMAX (with Box-Jenkins method) models are designed, obtaining significantly better results than those of previous works using models such as ARX. In [207], different stochastic algorithms such as Box-Jenkins, ARX, ARMAX and output error (OE) models are proposed to identify the thermal behaviour of an office of a commercial building. The BJ model outperforms the rest of the proposed models which, according to the authors, its noise management is more adequate than that of other algorithms.

Box-Jenkins method is applied to linear time series based models. It is therefore essential to initially analyse whether the system to be modelled can contain nonlinearities.

Regarding ANNs, one of the examples can be seen in [208], where a backpropagation NN (BPNN) with only three layers is used to model both $T_{in}$ and relative humidity in function of $T_{in}, T_{ext}$ and relative humidity. It is concluded that the BPNN model obtains very good results when following both $T_{in}$ and relative humidity curves. The authors of [209] present a simple NN where only certain meteorological variables and previous $T_{in}$ values are used as inputs to the model, leaving aside occupancy or the HVAC system consumption. Even so, it is able to follow $T_{in}$ curve with a RMSE of 0.85ºC.

It must be taken into account that ANNs, and in general black-box models, require large amounts of data so that the model can learn, if feasible, all possible cases. This might be particularly important since these models can present generalization problems when introducing completely new data, that is, data that they have not been trained on. In addition, since black-box models are purely data-driven, they are not guaranteed to follow the underlying physics, so the interpretability of their operation is practically impossible. That is why studies can find like [210], in which despite betting on NNs compared to the classic RC model, proposes a new ANN architecture based on physics, managing to achieve a MAE 40% lower than a classic RC model.

Studying the literature, it has been observed that black-box models present a series of advantages that make this type of models more flexible and more adaptable to controllers such as MPCs. This is verified in [211] where a physical model designed using Termolog software and a black-box modelling approach based on RF are compared. It is seen that in addition to the fact that the latter's response is more accurate, the white-box hardly offers the possibility of improving the performance of MPC. Is in [212] where an ANN-based MPC system model is also used to model the variation of $T_{in}$. In this case the ANN is fed with data provided by a physical model based on a simulation software, so the model integrated in the MPC could be considered as a grey box model. The MPC that optimises with a prediction horizon of 24h and with the objective of

reducing the electricity consumption of the building, manages to reduce the consumption for cooling and heating by 23.74% and 39.02%, respectively, compared to an On/Off control strategy.

### 4.1.2 HVAC model

Despite having seen numerous works focused on analysing thermal capacity of buildings, particular emphasis can be seen in literature on modelling HVAC systems. Modelling these systems facilitates an optimal use of them, a crucial aspect for enhancing building's electrical efficiency due to their substantial energy consumption. Similar to thermal capacity modelling approaches for buildings, various types of models are employed to model HVAC systems.

Physical models, such as the one introduced in [213] where authors opt for highly detailed physical HVAC models, accounting for dynamic regulation characteristics under three operation modes: regulation of the temperature of the cold source, regulation of the final fan and integrated coordinated regulation. Their findings highlight the substantial potential to control of HVAC systems, particularly through integrated control methods.

Despite the prevalence of studies employing physical principles to model HVAC systems, there is a rising trend towards utilising black-box models, particularly ML and DL techniques. Common ML and DL techniques include recurrent neural networks (RNNs) or deep neural networks such as LSTM.

For instance, [214] utilises three different LSTM-based RNN models to represent HVAC system consumption, achieving an nRMSE of 0.13. Notably, these models perform even better with a one-hour horizon (nRMSE of 0.052) than with 24 hour horizon. Additionally, [215] presents three different ML models to represent district-level heating energy consumption, concluding that the autoregressive RNN (ARNN) outperforms other models with an $R^2$ of 0.9899.

The increasing adoption of diverse ML techniques to model HVAC systems is largely due to their ability to capture the nonlinear behaviour exhibited by these systems. It is also important to note that software tools like EnergyPlus may become inefficient, as they often require users to input system characteristics and values from datasheets. These data may differ significantly from real-world conditions due to factors like system degradation and reduction in the coefficient of performance (COP) of heat pumps.

Finally, grey-box models are also widely used in literature for modelling HVAC system. As demonstrated in [216], the combination of EnergyPlus software and LSTM model can serve for HVAC system modelling. Similarly, [217] integrates thermal building modelling using an RC model with HVAC system modelling employing a hybrid ML model, exhibiting successful application in buildings with nRMSE below 10%. Although hybrid models have proven to be a

very interesting approach to modelling building thermal capacity and HVAC system, they require deep knowledge to carry out complex process of designing, as they combine two or more types of models.

### 4.1.3 Conclusions

Given the wide range of modelling techniques used in the literature for both building thermal behaviour and HVAC systems, it becomes imperative to evaluate different models to determine which one is best suited to the case study under analysis.

The most common types of models to be found in the literature are ML-type models, among which mainly SA and ANN models dominate. RC thermal network type models can also be found, but not so many of them are then applied in a MPC.

Also notable is the lack of examples in the literature of modelling with small datasets. In most cases, especially in the case of ANNs, models trained on data sets of years are proposed, which contrasts with the inability in many cases to make large data sets available.

Finally, it is noteworthy that many of the papers are committed to designing linear models, since it is true that these models can be integrated, for example, in an MPC so that the computational cost is not so high. However, linear models are not able to represent nonlinear systems such as HVAC systems.

## 4.2 OBJECTIVES & CONTRIBUTIONS

The main target of this chapter has been to build the control model of the MPC. For that, the FL of the building has been modelled, i.e. the HVAC system associated with the thermal capacity of ESTIA 2 building. A linear model has been adopted aiming the reduction of the computational cost of the MPC. The outputs of the linear models are the internal temperature and the heat pump consumption.

With regard to secondary objectives, three main ones can be highlighted.

- Since the system to be modelled contains nonlinearities, a NARX type NN model has been proposed to see if it is able to capture these nonlinearities.
- It has been attempted to analyse how the training performed with small data set affects the response of the NARX model.
- The NARX model can be daily linearised at the most convenient operating point (OP). Therefore, the aim has been to analyse whether linearised NARX models are able to improve the response of a linear model such as Box-Jenkins (BJ).

Regarding the contributions of this chapter, some noteworthy points merit mention.

- In contrast to the majority of papers in the literature that propose models trained with large data sets, a NARX model and a Box-Jenkins linear model build with a small data set have been designed.
- The models have been trained and validated not with data taken from simulation, but with data obtained from excitation tests conducted in a real building, enhancing the practical applicability of the proposal.

## 4.3 CASE STUDY

### 4.3.1 Main features of the HVAC system

In the subsequent section, an analysis of the air conditioning system of the case study has been undertaken.

The HVAC system comprises 10 DAIKIN brand heat pumps, each equipped with two compressors. Comprehensive details regarding the key attributes of these heat pumps are referenced in the Table C.6 of Annex C.

The outdoor units are linked to a network of 73 indoor units (see Figure 4.1) which include ventilation systems and thermostats. Each outdoor unit interfaces with between 5 and 8 indoor units. Among the indoor units, 60 are master units that receive $T_{sp}$ and 13 are slave units.

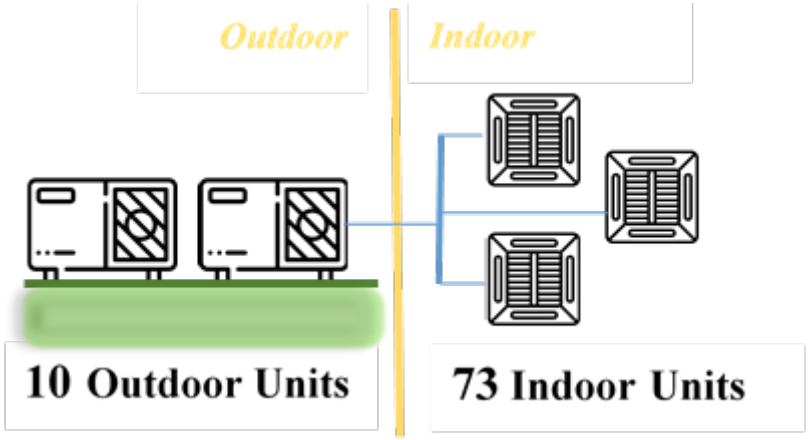


***Figure 4.1.*** *Simplified diagram with the elements that make up the HVAC system.*

The heat pump or outdoor unit to be chosen for modelling is referred to as Group 16 (GR16), REYQ10M7W1B model. This group consists of two compressors. The characteristics of both compressors can be seen in Table 4.1.

***Table 4.1****. Technical characteristics of the heat pump compressors model REYQ10M7W1B.*

| Compressors | | Technical characteristics | | | |
|---|---|---|---|---|---|
| | | **Speed (rpm)** | **Engine power output (kW)** | **Starting method** | **Crankcase heater (W)** |
| 1 | **Inverter** | 1,900~6,480 | 2.2 | Direct online | 33 |
| 2 | **ON-OFF** | 2,900 | 4.5 | Direct online | 33 |

Table 4.2 provides a breakdown of the indoor units linked to outdoor GR16, alongside their respective locations across floors and rooms.

***Table 4.2**. Internal elements connected to GR 16 and their location in the building.*

| External group | Indoor unit | Floor | Room/Office |
|---|---|---|---|
| **GR16** | L2.302 | Ground floor | ESTIA Recherche office |
| | L2.304 | Ground floor | Platform |
| | L2.303 | Ground floor | Platform |
| | L2.305 | First floor | office |
| | L2.306 | First floor | office |
| | L2.307 | First floor | office |

The excitation tests that have been descripted in next section have been carried out in a specific area of ESTIA 2 building named *Platform*. The reason behind selecting the *Platform* to perform the excitation tests is because it is a large space in which thermal excitation can be performed. The aim was first to model this space in a simple way and then to model the entire building, a rather more complex model. Although the aim was to excite the building as a whole, there has not been time to extend the study within the framework of the Thesis. The indoor units located in *Platform* are connected to GR16. That is why this heat pump has been selected for modelling.

From this it can be understood that the control model developed in this chapter represents the thermal behaviour of the *Platform* area and the GR16 heat pump. Nevertheless, in order to test the correct functioning of the EMS optimisation introduced in Chapter 5, the model has been considered to represent the thermal behaviour of the whole building and the HVAC system.

When modelling an existing building constructed years ago, it is common to find a lack of modern monitoring systems that can provide huge amount of historical data. In the case of ESTIA 2, comprehensive data on temperature (internal, set point, etc.) and heat pump consumption is limited because the old monitoring system did not have the functionality to store historical building data. In addition, there have been registration problems with temperature sensors and with the operation of some of the heat pumps of the building.

Furthermore, the decision has been made to model the HVAC system in heating mode. This is due to the available data obtained from excitation tests being sourced from a winter period (between March and April 2023) and the prevailing climate conditions in the area, where the HVAC system predominantly operates in heating mode.

### 4.3.2 Used data analysis

An initial analysis of quality and quantity of available data is essential, as these data require pre-processing to be suitable for the building thermal capacity model and the HVAC model.

On the one hand, meteorological data has been obtained from OpenWeather. Various data points such as $T_{ext}$, humidity, wind speed, and wind direction have been downloaded, all at a frequency of 10 minutes (see Table C.7 of Annex C). Among these parameters, particular attention has been paid to $T_{ext}$ data. $T_{ext}$ plays a significant role in $T_{in}$ variation, thus it has been considered a primary input for the building's thermal modelling.

On the other hand, data from the excitation tests are available. As can be seen in Table C.8 of Annex C there are records of both $T_{in}$ and $T_{sp}$, as well as of the electricity consumption data of the heat pump (accumulated energy).

In Figure 4.2, Figure 4.3, and Figure 4.4, the data from the three data sets is plotted after outlier removal and fixing the same sampling time.


***Figure 4.2.*** *Pre-processed data of Training data set.*

The data set chosen for training is referred to as the *Training data set* (Figure 4.2). This data set not only reflects a wide range of $T_{ext}$, but also contains significant consumption peaks and variations. It consists of 145 data points recorded every 20 minutes during the weekend from March 24$^{th}$ to March 26$^{th}$ of 2023.

The validation of the proposed models has been conducted with two data sets corresponding to two consecutive weekends named *Test 1 data set* and *Test 2 data set.*

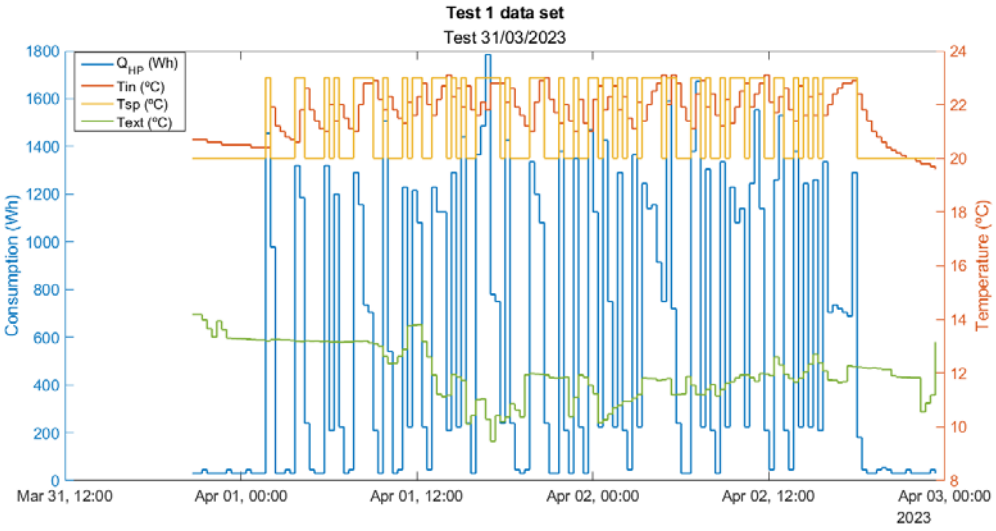


***Figure 4.3**. Pre-processed data of Test 1 data set.*

On the one hand, the *Test 1 data set* (Figure 4.3) corresponds to data acquired during the weekend from March 31st to April 2nd. It contains 153 data points. The $T_{ext}$ in this case covers a considerably smaller range, in concrete from 9ºC to 14ºC.

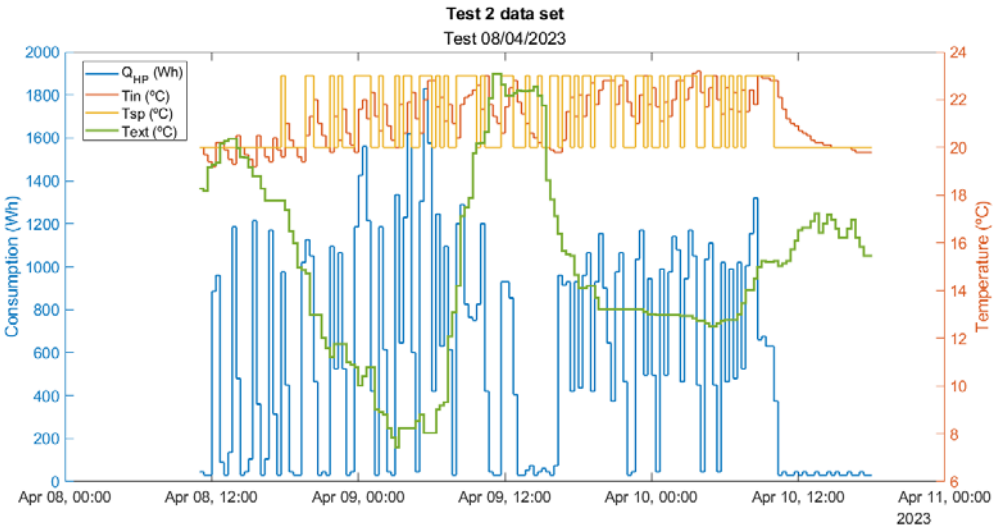


***Figure 4.4.** Pre-processed data of Test 2 data set*

On the other hand, the models are validated with the *Test 2 data set* (Figure 4.4). This data set, which contains 166 data points, has a significantly wider range in terms of $T_{ext}$.

Table 4.3 gathers the characteristics of the three data sets used for training and testing the models after the data has been pre-processed.

***Table 4.3**. Data sets obtained from the excitation tests and pre-processed in order to train and validate models.*

| | Data sets | Considered variables | Sampling time | Data points |
|---|---|---|---|---|
| Training data set | | $T_{ext}$, $T_{in}$, $T_{sp}$, $Q_{hp}$ | 20 min | 145 |
| Validation | Test 1 data set | $T_{ext}$, $T_{in}$, $T_{sp}$, $Q_{hp}$ | 20 min | 153 |
| | Test 2 data set | $T_{ext}$, $T_{in}$, $T_{sp}$, $Q_{hp}$ | 20 min | 166 |

The different lengths of the data sets are related to the conditions under which the tests have been conducted. Sometimes the tests have been able to last a few hours longer.

Anomalous behaviour can be identified halfway through *Test 2 data set* (around 13:00 on April 9th). During this period, despite $T_{sp}$ reaching 23ºC, $T_{in}$ continues to decrease to 19.5ºC because there is no heat provided. This is because the outdoor unit registers a high $T_{ext}$ and the compressor turns off because it understands that heat is not needed inside the *Platform*.

As mentioned earlier, the HVAC system operates in heating mode, with the $T_{sp}$ changing between 20°C and 23°C. As shown in Figure 4.2, Figure 4.3 and Figure 4.4, increasing $T_{sp}$ to 23°C results in a peak of $Q_{hp}$, followed after a sampling time by an increase in $T_{in}$.

The presence of system hysteresis must be also taken into account. The indoor units are affected by a hysteresis related to the indoor temperature. This hysteresis has been modelled and takes on a value of $\Delta T_{hyst} = \pm 0.5$ºC. First, the indoor unit, depending on the heat stored in the heat-carrying liquid, will try to reach the $T_{sp}$. If there is not enough heat stored, the outdoor unit depending on the heat-carrying liquid temperature turns on the compressor.

## 4.4 METHODOLOGY

### 4.4.1 Methodology description

Being the HVAC system and the associated thermal capacity of the ESTIA 2 building FLs in which the EMS will act, both have been modelled.

The first equation, named ***Equation 1***, represents the thermal capacity of the building. It defines the variation of the building $T_{in}$ as a function of one or several inputs. In addition to including these inputs, this equation also incorporates a recurrent term taken into account previous values of $T_{in}$. The recurrent term is necessary to take into consideration the dynamics of the system.

The second equation named ***Equation 2*** represents the HVAC system and it involves determining the heat pump consumption ($Q_{hp}$) through inputs of the model.

Both equations are recursive. The parameters of the equations have been derived through identification or training, which is conducted using excitation tests data. The models need to be updated daily.

Two techniques have been proposed to model *Equation 1* and *Equation 2*: a NARX NN and a model based on Box-Jenkins method, known both for their simplicity and accuracy. The methodology followed for model construction, validation and comparison is depicted in Figure 4.5.

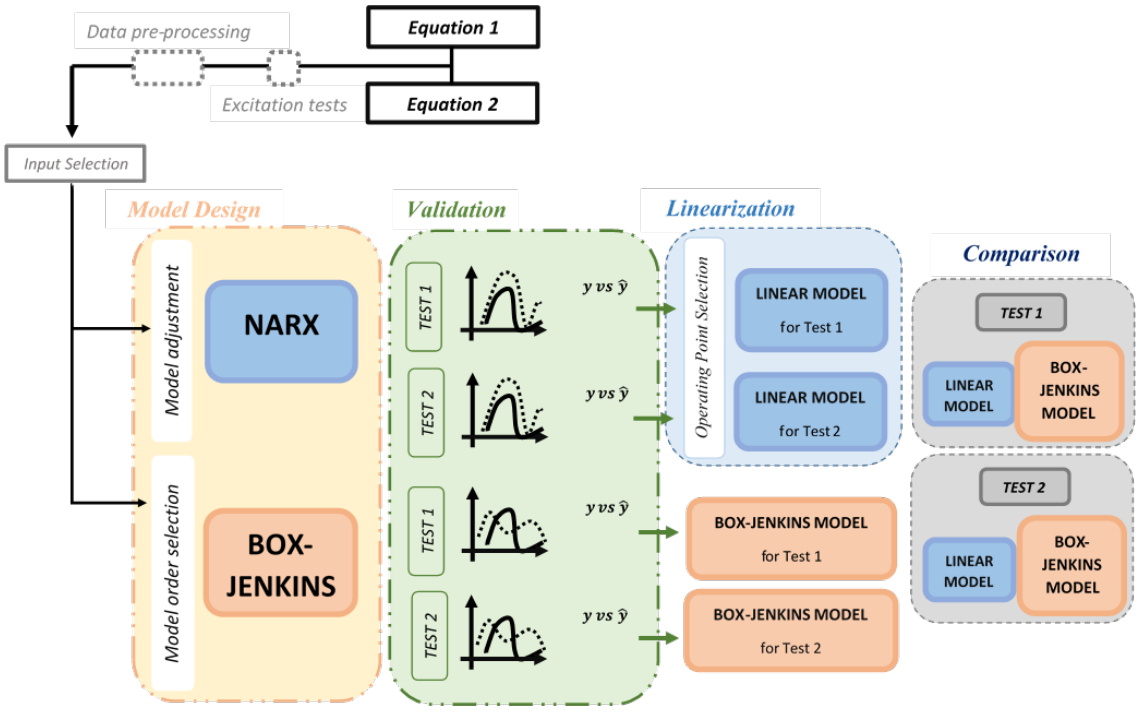


***Figure 4.5****. Methodology followed in the construction of the thermal model.*

First, excitation tests have been carried out to identify or train the NARX NN and Box-Jenkins. After obtaining the data, various processing techniques have been applied to the data in order to meet the requirements of each type of model.

Then, the selection of inputs has been carried out, i.e. the selection of the variables that explain the output, in this case $T_{in}$ and $Q_{hp}$. This selection has been made by observation, analysing initially available data showed in Figure C.9 of Annex C and seeing which variables affect $T_{in}$ and $Q_{hp}$.

$T_{ext}$ and $Q_{hp}$ have been the variables selected to describe the behaviour of $T_{in}$ (*Equation 1*) and $T_{sp}$, $T_{ext}$ and the system hysteresis ($Hyst$) the ones to describe the heat pump consumption (*Equation 2*).

#### 4.4.1.1 NARX neural network

First, a NARX model has been considered for the modelling of *Equation 1* and *Equation 2*. A NN-based model has been selected because in this case the same conditions exist as when designing predictive models of consumption and PV production:

- Little data available for model training.
- Need for a simple model with low computational cost.

NARX model has been designed searching values for the hyperparameters. The hyperparameters have been selected following the same criterion as in Chapter 2 and Chapter 3. In this case, the NARX has been trained with data from a weekend, meaning with *Training data set*. As the NNs randomly initialise the values of the weights each time they are trained, the weekend prediction has been performed three consecutive times and each time $fitting$ and $R^2$ has been calculated. The process is repeated for each combination of hyperparameter values, i.e. for each model constructed. The model with the highest average $fitting$ and $R^2$ has been selected.

The NARX model is capable of capturing nonlinearities, and can be linearised at the desired OPs to represent well the dynamic behaviour of the system. Figure 4.6 describes followed approach in order to linearise NARX models.

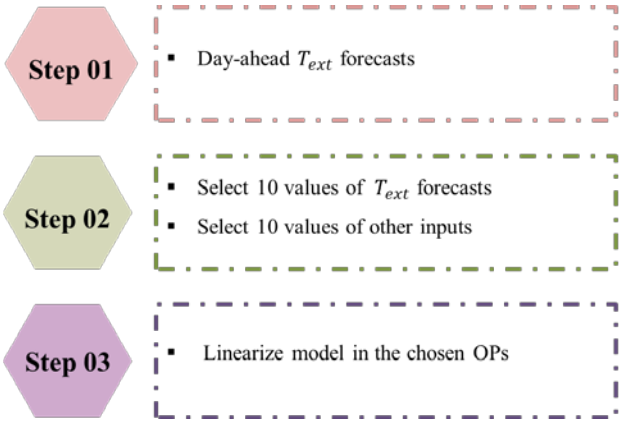


***Figure 4.6.*** *Steps to get daily linearised NARX model.*

For *Equation 1*, two variables have been considered as inputs: $T_{ext}$ and $Q_{hp}$. The values of $T_{ext}$ selected as OPs have been determined according to next day predictions of $T_{ext}$. The $Q_{hp}$ will always be the same and is determined in the range between 0W and the maximum consumption of the heat pump. That said, each day 10 values of $T_{ext}$ and $Q_{hp}$ have been selected and the NARX linearisation has been performed on 100 OPs. 100 OPs have been chosen to analyse the operation of the NARX at each of these OPs.

For *Equation 2* the process is repeated this time considering $T_{ext}$, $T_{sp}$ and $Hyst$ as inputs. The 10 selected values of day-ahead $T_{ext}$ prediction data and 10 values of $T_{sp}$ have been combined to obtain 100 OPs where the NARX has been linearised. As said, in addition to $T_{sp}$ and $T_{ext}$, $Hyst$ has been used as input. Being a binary input, NARX has been linearised in both cases, when it acquires the value 0 and 1. Therefore, in total 200 linear models have been defined.

Among all the linearised models, the models with the best $fitting$ for *Equation 1* and *Equation 2* have been selected.

That said, in case of a real-time application, the problem arises that in the absence of day-ahead values of $T_{in}$ and $Q_{hp}$, the $fitting$ of NARX linear models cannot be calculated (see Equation (4.3)). Therefore, in cases of real-time operation, the NARX model will be linearised at the OP corresponding to the average value of $Q_{hp}$ and day-ahead average value of $T_{ext}$.

The methodology used in this work serves to see if a NARX model trained on small data set is feasible to build a thermal model of a building and can outperform the operation of a linear model such as the Box Jenkins.

#### 4.4.1.2 Box Jenkin method (BJ)

The Box-Jenkins method can be applied using "System Identification Toolbox" of MATLAB. This approach primarily focuses on the identification, estimation, and diagnosis of ARIMA or

other type of statistical model, which are capable of capturing patterns, variations and trends in time series data.

The general equation of an ARIMA model would be expressed as shows Equation (4.1):

$$y(t) = \sum_{i=l}^{nu} \frac{B_i(q)}{F_i(q)} x_i(t - n_{k_i}) + \frac{C(q)}{D(q)} \varepsilon(t), \tag{4.1}$$

where $y$ is the system output, $x_i$ are each of the inputs that describe the output, $n_u$ is the number of inputs, $n_{k_i}$ is the input delay in units of samples, $\varepsilon$ represents the error and $q$ represent the delay operator.

The polynomials to be estimated would be defined as shows Equation (4.2):

$$\begin{aligned} B(q) &= b_0 + b_1 q^{-1} + \cdots + b_{n_b} q^{-nb+1}, \\ C(q) &= 1 + c_0 q^{-1} + \cdots + c_{nc} q^{-nc}, \\ D(q) &= 1 + d_0 q^{-1} + \cdots + d_{nd} q^{-nd}, \\ F(q) &= 1 + f_0 q^{-1} + \cdots + f_{nf} q^{-nf}, \end{aligned} \tag{4.2}$$

where, $n_b$, $n_c$, $n_d$, and $n_f$ define the order of the mentioned polynomials and that need to be defined in the model design process.

The Box-Jenkins method provides numerous advantages. It offers high flexibility to adapt to different types of time series data, which may have various types of trends, nonlinear patterns, etc. The final step of the method, which consists of diagnosing the model residuals, allows for the identification of deficiencies in the model, thereby improving the accuracy of its response.

Box-Jenkins method requires a slightly different data pre-processing compared to NARX model. The mean values of each data set (training and validation) have been subtracted from the corresponding data of the data set. Subtraction of the mean allows to obtain data sets with a mean of 0, which enables comparisons between different data sets. Additionally, the model does not require data normalisation.

The orders of the polynomials of Equation (4.2) have been defined. The model orders have been determined based on the results obtained in the validation stage. The orders have been increased, evaluating whether increasing the orders and, consequently, its complexity, enhances the improvement response of the model.

### 4.4.2 Evaluation Metrics

The choice of evaluation metrics depends on the specific scope of the problem, as well as the type of data employed and the desired outcome. Considering that the objective is to analyse the response of $T_{in}$ (*Equation 1*) and of $Q_{hp}$ (*Equation 2*), two metrics have been selected.

Firstly, the $R^2$ has been used as an evaluation metric (see Equation (2.2)). Thanks to this metric, it is possible to quantify how well the response of a model is adjusted to the real curve.

Secondly, $fitting$ which measures the goodness of fit between the model's response and the measurement data (in percentage) has been calculated (see Equation (4.3)).

$$fitting = \left(1 - \frac{||y_j - \hat{y_j}||}{||y_j - mean(y_j)||}\right) x100[\%] \tag{4.3}$$

where $y_j$ is the validation data output and $\hat{y_j}$ is the output of model.

### 4.4.3 Application of methodology

As mentioned before the inputs of each model have been selected observing Figure C.9 of Annex C and analysing which variables affect $T_{in}$ and $Q_{hp}$ . Equation (4.4) and Equation (4.5) represent in general terms, the structure of both models.

$$T_{in}(t) = f\left(q^{-n}T_{in}(t), q^{-n}T_{ext}(t), q^{-n}Q_{hp}(t)\right) \tag{4.4}$$

$$Q_{hp}(t) = f\left(q^{-n}Q_{hp}(\mathrm{t}), q^{-n}T_{sp}(t), q^{-n}T_{ext}(t), q^{-n}Hyst(t)\right) \tag{4.5}$$

being $q^{-n}$ the n-sample delay operator.

Equation (4.4) represents $T_{in}(t)$ as a function of its previous values, $q^{-n}T_{in}(t)$ and the current and previous values of the following variables: external temperature, $T_{ext}(t)$ and the heat pump consumption $Q_{hp}(t)$.

Equation (4.5) represents the energy consumed by the heat pumps ($Q_{hp}(t)$), from the previous consumption values, $q^{-n}Q_{hp}(t)$, the set point temperature, $T_{sp}(t)$, and the external temperature, $T_{ext}(t)$. Additionally, a term called $Hyst(t)$ has been included.

#### 4.4.3.1 Excitation tests

Excitation tests are necessary to identify most of the frequencies of the system, i.e. to identify the values of the model parameters. The tests have been designed to excite the area *Platform* marked in Figure 4.7 and the associated external group (GR16).

Within this thermal zone, designated units L2.303 and L2.304 operate, with the former serving as the master unit and the latter as the slave. There is a delay of 10 seconds between a $T_{sp}$ change is sent and the indoor unit receives it.

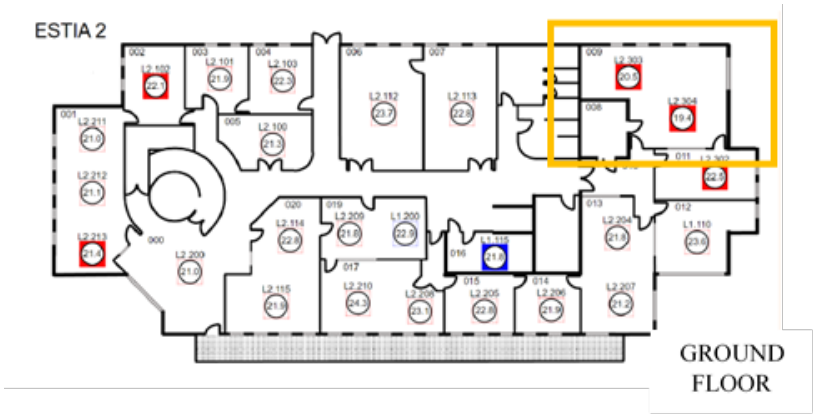


***Figure 4.7**. Ground floor of ESTIA 2 with the area called Platform framed*

Conducting thermal excitation tests in an occupied building presents challenges because these tests involve adjusting $T_{sp}$, potentially affecting occupants' thermal comfort. Users should also be prevented from disturbing the tests. Consequently, tests have been scheduled for weekends when the space is unoccupied, imposing a time constraint of approximately 60 hours.

Test design incorporates as input pseudorandom binary sequence signal (PRBS). PRBS is a binary sequence in which its rectangular pulses can be modulated in width. They are called pseudo-random because even if they are characterize by the random variation of the pulses, in large time horizons they have a periodic behaviour [218].

The PRBS sequence's maximum length is determined by $2^N - 1$. Moreover, to correctly identify the steady-state gain of a dynamic model, the maximum pulse duration ($t_{im}$) must be determined, which needs to be greater than the rise time ($t_R$). In the analysed system $t_R$ takes the value of 2 hours (see Figure 4.8).

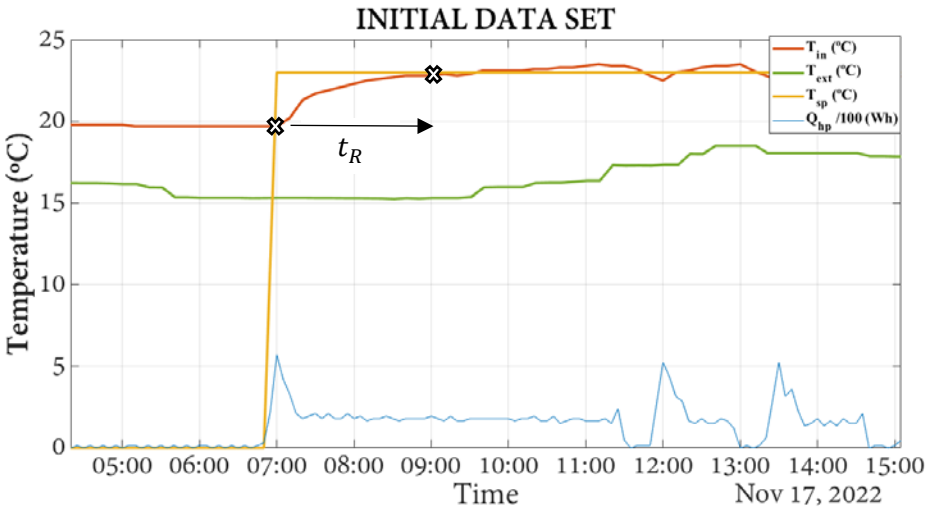


***Figure 4.8**. A zoom from Figure C.9 to see the rise time of the system.*

Being the maximum duration of the pulse $N * T_s$, the condition represented in Equation (4.6) must be fulfilled.

$$t_{im} = N * T_s > t_R \tag{4.6}$$

where $N$ is the number of cells in the shift register and the sampling period is $T_s$.

The need to carry out excitation tests during weekends, constraints the test duration ($L$) to 60h.

$$2^{N-1}T_s < L \tag{4.7}$$

In order to fulfil the condition described by Equation (4.6) and the one specified in Equation (4.7) a sampling time ($T_s$) of 20 minutes and $N = 7$ has been chosen for the PRBS.

Figure 4.9 shows the PRBS signal of length $2^7 - 1 = 127$ pulses that represents almost 44h. This is the PRBS signal used for the tests that have been conducted in the area *Platform*.

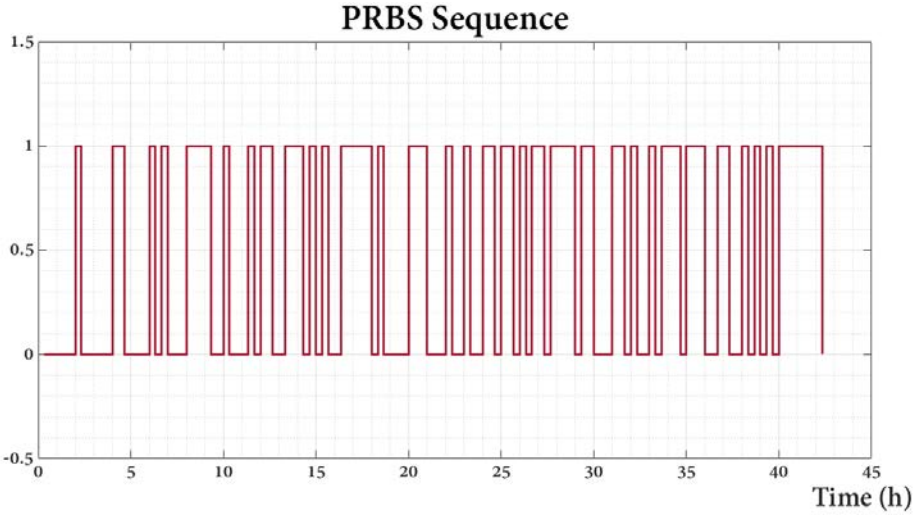


***Figure 4.9**. PRBS sequence used in the excitation tests carried out in ESTIA 2.*

#### 4.4.3.2 Data pre-processing

A series of steps have been followed to pre-process each of the data sets. Initially, outliers have been observed, especially in the $T_{ext}$ data. These visually identifiable outliers have been fixed using linear interpolation. The next step has been to identify both data repetitions and missing data. Regarding the former, it has been found that the daylight saving time change occurred during one of the weekends when the building excitation test was conducted (26/03/2023 02:00am), resulting in repeated data points that have been removed. As for missing data, each instance had to be identified and restored using linear interpolation. Most of the missing data belonged to $T_{ext}$ and involved gaps of no more than two sampling periods, i.e., 20 minutes. Since $T_{ext}$ is not highly variable, linear interpolation proved to be an efficient solution.

Additionally, the sampling time of all recorded variables was not the same. $T_{ext}$ has been recorded every 10 minutes, while $Q_{hp}$ every 5 minutes. Similarly, the sampling time for $T_{in}$ and $T_{sp}$ has been 20 minutes in all three tests conducted. As a sampling time of 20 minutes has been settled for the PRBS, the sampling time of $T_{ext}$, $Q_{hp}$ and $T_{sp}$ has been adjusted by calculating the mean every 20 minutes.

Finally, but only for the data used for the NARX, normalisation has been performed. Normalisation has been carried out to map the data to the range [0, 1], thus avoiding the disproportionate impact of any parameter used as input on the final results due to its large magnitude values. Table 4.4 show the ranges that have been used for normalizing $T_{ext}$ and $Q_{hp}$.

***Table 4.4***. *Normalisation ranges for all the measured variables in excitation tests.*

| Normalisation | Test 1 data set | Test 2 data set |
|---|---|---|
| | [min, max] | [min, max] |
| $T_{ext}$ | [-10, 40] (ºC) | [-10, 40] (ºC) |
| $Q_{hp}$ | [30, 2010] (Wh) | [30, 2010] (Wh) |

Box-Jenkins method does not require data normalisation, so normalisation step has been skipped.

#### 4.4.3.3 Equation 1: ESTIA 2 thermal capacity model

##### a. NARX neural network

Regarding NARX design, the adjusted hyperparameters have been (a) the number of neurons in the hidden layer, (b) the activation function of the hidden and output layers, and (c) the input and

feedback delays. It is also possible to add hidden layers, although in this case a single layer has been kept.

Starting with the selection of the activation function for both layers, it has been clearly shown that the hyperbolic tangent (*tansig*) is the one that best traces the output. The number of neurons that compose the hidden layer is 4 and a delay of 2 for both the input and the feedback has been applied.

Table 4.5 shows the characteristics of the designed model in more detail.

***Table 4.5.*** *Hyperparameter values of the proposed NARX model for Equation 1.*

| ***NARX hyperparameters Equation 1*** | |
|---|---|
| **Hidden layers** | nº of hidden layers = 1 |
| | number of neurons = 4 |
| **Delay vectors** | Input = 2 |
| | Feedback = 2 |
| **Activation fcn** | Hidden layer = Hyperbolic tangent |
| | Output layer = Hyperbolic tangent |
| **Training parameters** | Learning algorithm: *Levenberg-Marquardt* |

NARX has been trained with *Training data set* and validated with the other two data sets: *Test 1 data set* and *Test 2 data set*.

## b. Linearisation of the NARX model (lmNARX)

The NARX model has been built in Simulink and by means of "Model Lineariser", performing a linear analysis of the NARX. The linear analysis has consisted on linearizing NARX at the selected OPs and observing how accurately each of the lmNARX are able to follow the measured $T_{in}$ curve in case of both validation data sets: *Test 1 data set* (see Figure 4.10) and *Test 2 data set* (see Figure 4.11).

The 3D plots (Figure 4.10 and Figure 4.11) show the $fitting$ values for 100-lmNARX models. The values of both figures are gathered in Table C.9 and Table C.10 of Annex C respectively.

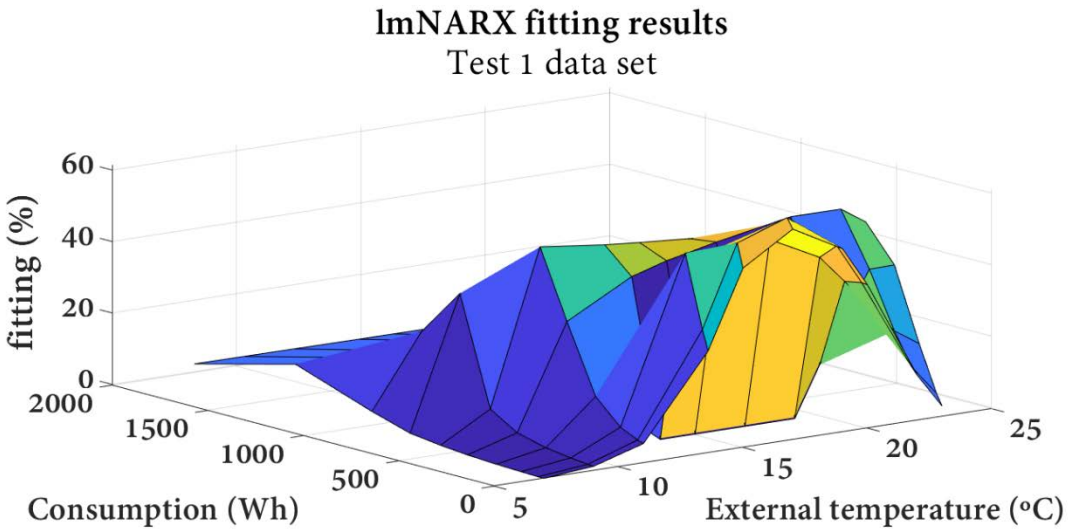


***Figure 4.10***. *$fitting$ values of lmNARX response plotted in 3D for Test 1 data set.*

Figure 4.10 shows that the highest $fitting$ values are around 15ºC-20ºC of $T_{ext}$ and between 0Wh-500Wh of $Q_{hp}$. The OP selected to perform the linearisation has been: $T_{ext} = 17ºC$ and $Q_{hp} = 30Wh$. The lmNARX obtained linearizing in the mentioned OP for the case of *Test 1 data set* is defined by Equation (4.8).

$$T_{in}(t) = \frac{(0.4317q^{-1} - 0.2192q^{-2})T_{ext}(t) + (0.1494\,q^{-1} - 0.0285q^{-2})\,Q_{hp}(t)}{1 - 0.4865q^{-1} - 0.1568\,q^{-2}} \quad (4.8)$$

As Figure 4.11 shows, the ranges where best $fitting$ values have been obtained in *Test 2 data set* are the range between 15ºC and 20ºC of $T_{ext}$ and $Q_{hp}$ ranging from 0Wh to 500Wh. The selected OP in this case has been $T_{ext} = 19ºC$ and $Q_{hp} = 400Wh$.

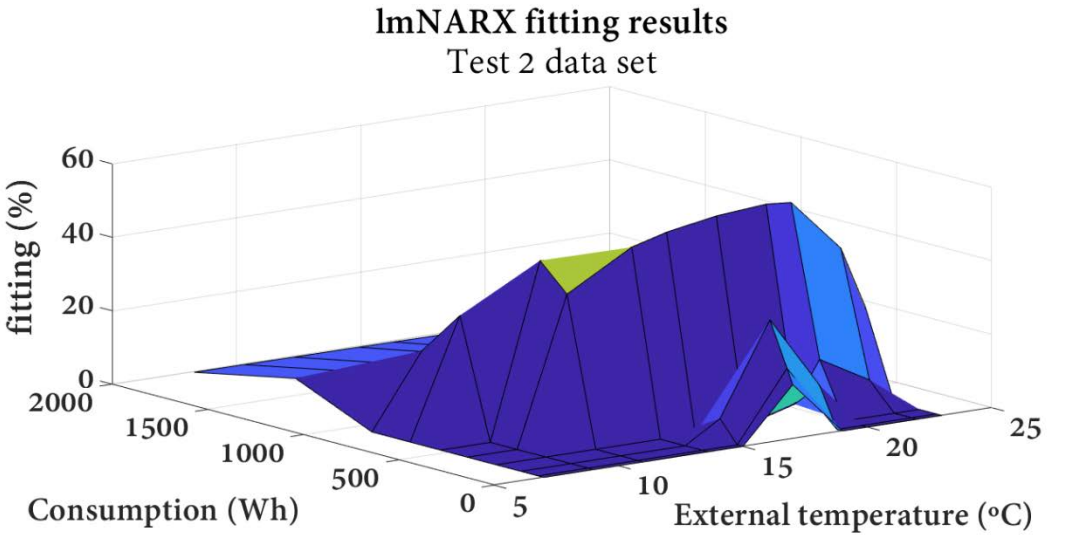


***Figure 4.11***. *$fitting$* values of lmNARX response plotted in 3D for Test 2 data set.

The best lmNARX selected for the case of *Test 2 data set* is defined by Equation (4.9).

$$T_{in}(t) = \frac{\left(-0.006252q^{-1} + 0.01284q^{-2}\right)T_{ext}(t) + \left(0.1994q^{-1} - 0.0482q^{-2}\right)Q_{hp}(t)}{1 - 0.5713q^{-1} - 0.086q^{-2}} \quad (4.9)$$

### c. Box-Jenkins (BJ)

The design of the model has started by establishing the orders of the polynomials in the model. The orders have been set to 4. The result is not improved by increasing the orders and, with lower orders of 2 or 3, the results worsen. The criterion for determining the orders of the model is to obtain the model that best fits the real $T_{in}$ curve, i.e. the aim is to maximise the $fitting$ metric.

As provided by the MATLAB "System Identification Toolbox", optimisation features have been added to the model. The initial conditions of the model have been set to zero for the parameter estimation stage. In the same way, a zero-order hold (*zoh*) has been set. This optimisation feature keeps the input signal constant between samples during data acquisition.

The accuracy of the model has been evaluated using *compare* function from "System Identification Toolbox", which uses as evaluation metric $fitting$ defined by Equation (4.3).

The model obtained is the one defined by both transfer functions of Equation (4.10).

$$T_{in}(t) = \frac{0.05794q^{-1} - 0.156q^{-2} + 0.1856q^{-3} - 0.08122q^{-4}}{1 - 1.795q^{-1} + 1.473q^{-2} - 0.4206q^{-3} - 0.1843q^{-4}} T_{ext}(t)$$

$$T_{in}(t) = \frac{0.001041q^{-1} + 0.0008034q^{-2} - 6.941e-05q^{-3} - 0.0006418q^{-4}}{1 + 0.2832q^{-1} - 0.5892q^{-2} - 0.7004q^{-3} + 0.2398q^{-4}} Q_{hp}(t) \quad (4.10)$$

#### 4.4.3.4 Equation 2: HVAC system model

Some aspects must be taken into consideration in the design of HVAC system model. The operation of HVAC system not only depends on the variations of $T_{in}$ and $T_{ext}$, but also on the temperature of the system's heat-carrying liquid (R-410A), which does not change in the same way as $T_{in}$. In addition, the change in coefficient of performance (COP) due to humidity and $T_{ext}$ introduces nonlinear trends to the system.

It is also important to note that, as mentioned above, the modelled heat pump contains two type of compressors. These are an inverter driven compressor (PI controller) with an output power of

2.2kW and a second On/Off compressor with an output power of 4.5kW (see Table 4.1). The problem is that the operating criteria for both is unknown. This means that it is not known when the PI-controlled compressor is used and when the On/Off compressor is activated. Therefore, it is essential to use models that can capture nonlinearities and unknown a priori elements of the system operation. All this makes NARX an interesting option in order to be able to capture these behaviours efficiently.

### a. NARX neural network

Having already defined the inputs, the hyperparameters of the model have been adjusted. As in the case of *Equation 1*, the hyperparameters to be tuned are (a) the number of neurons in the hidden layer (b) the delays introduced in the input and feedback and (c) the activation functions of both layers: hidden and output layers. In this case too, a single hidden layer has been maintained.

As for *Equation 1*, the criterion to select the hyperparameter values has been to search the maximum $fitting$ and $R^2$ values.

Starting with the latter, the hyperbolic tangent (*tansig*) has been established as the activation function for both layers. The hidden layer is composed of 8 neurons. As for the delays, 2 delays for the inputs and 4 for the feedback have been chosen.

The characteristics of the designed NARX model are given in Table 4.6.

***Table 4.6.*** *Hyperparameter values of the proposed NARX model for Equation 2.*

| ***NARX hyperparameters Equation 1*** | |
|---|---|
| **Hidden layers** | nº of hidden layers = 1 |
| | number of neurons = 8 |
| **Delay vectors** | Input = 2 |
| | Feedback = 4 |
| **Activation fcn** | Hidden layer = Hyperbolic tangent |
| | Output layer = Hyperbolic tangent |
| **Training parameters** | Learning algorithm: *Levenberg-Marquardt* |

### b. Linearised model of NARX (lmNARX)

In order to linearise NARX model, the process that has been followed is explained in section 4.4.1.1. As explained in the mentioned section, 100 linear models of the NARX have been obtained when $Hyst$ is 0 and another 100 linear models when $Hyst$ acquires a value of 1.

The 3D plots (Figure 4.12 and Figure 4.13) aggregates the $fitting$ values for each of the 100-lmNARX models when the hysteresis is 0 and when it is 1 in case of *Test 1 data set* respectively. The $fitting$ values of both figures are gathered in Table C.11 and Table C.12 of Annex C respectively.

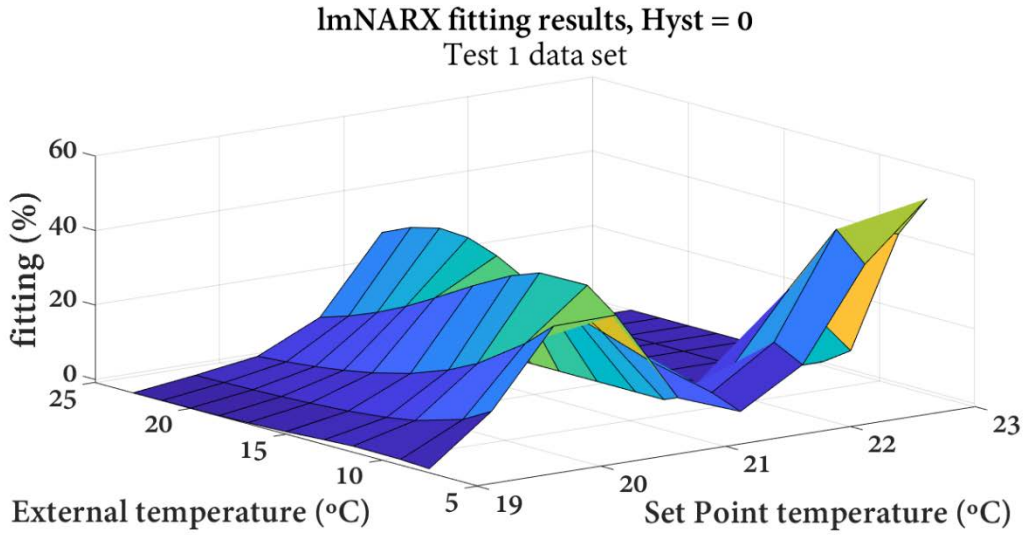


***Figure 4.12***. *$fitting$ values of lmNARX response plotted in 3D for Test 1 data set when Hyst = 0.*

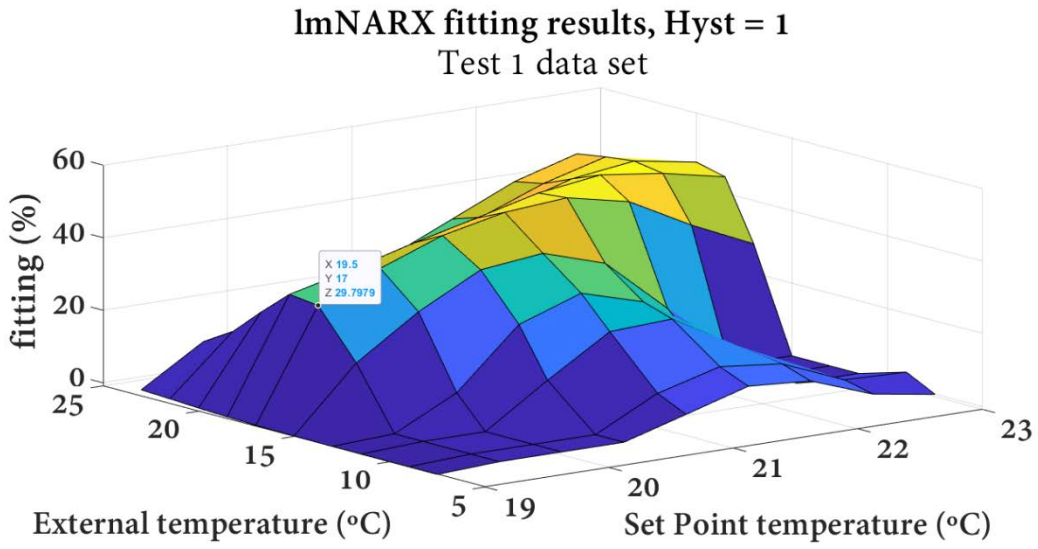


***Figure 4.13***. *$fitting$ values of lmNARX response plotted in 3D for Test 1 data set when Hyst = 1.*

The model with the highest $fitting$ value has been linearised in the OP: $T_{ext} = 7.5ºC, T_{sp} = 23ºC \; and \; Hyst = 0$ and is defined by the transfer function described in Equation (4.11).

$$Q_{hp}(t) = \frac{0.4421q^{-1} - 0.2581q^{-2}}{1 - 0.1247q^{-1} - 0.002997q^{-2} - 0.02852q^{-3} - 0.1636q^{-4}} T_{ext}(t)$$

$$Q_{hp}(t) = \frac{0.09989q^{-1} + 2.807q^{-2}}{1 - 0.1247q^{-1} - 0.002997q^{-2} - 0.02852q^{-3} - 0.1636q^{-4}} T_{sp}(t) \qquad (4.11)$$

$$Q_{hp}(t) = \frac{0.4033q^{-1} - 0.6493q^{-2}}{1 - 0.1247q^{-1} - 0.002997q^{-2} - 0.02852q^{-3} - 0.1636q^{-4}} Hyst(t)$$

For the case of *Test 2 data set*, Figure 4.14 and Figure 4.15 show the $fitting$ values obtained for the lmNARX when maintaining the hysteresis value at 0 and 1 respectively. In the same way, the $fitting$ values of both figures have been given by Table C.13 and Table C.14 of Annex C.

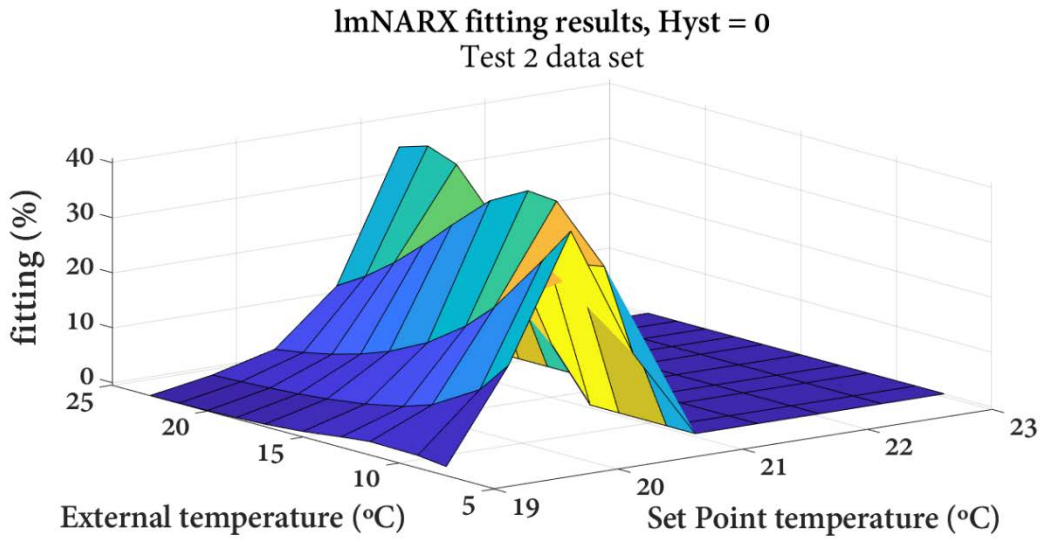


***Figure 4.14***. *$fitting$ values of lmNARX response plotted in 3D for Test 2 data set when Hyst = 0.*

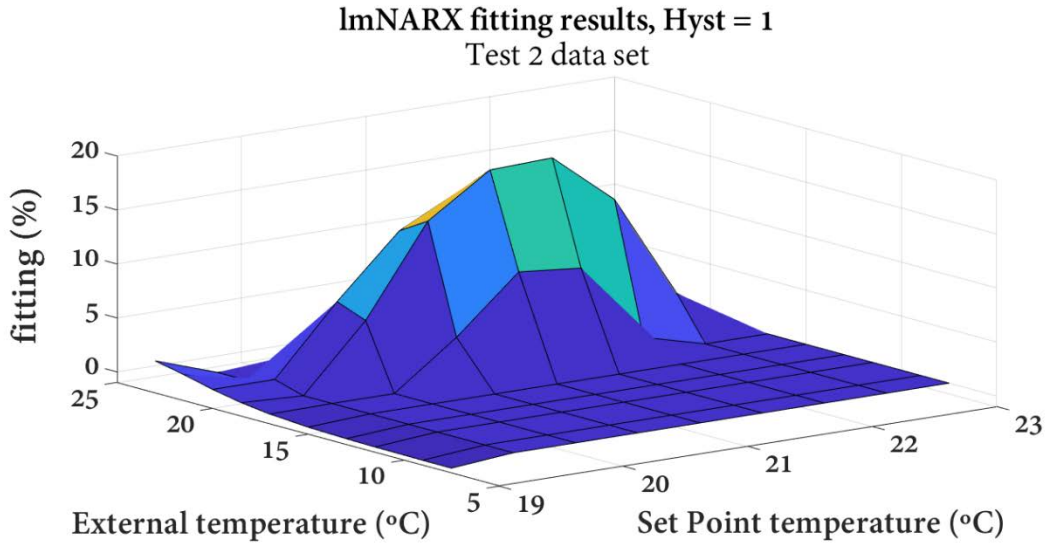


***Figure 4.15.*** *$fitting$ values of lmNARX response plotted in 3D for Test 2 data set when Hyst = 1.*

In the case of Figure 4.15, the $fitting$ values of a vast majority of models is zero, meaning that those linear models are unable to follow the curve of $Q_{hp}$ properly. In this case, the lmNARX that achieves the best $fitting$ is linearised at $T_{ext} = 13ºC, T_{sp} = 20.5ºC$ and $Hyst = 0$.

The best lmNARX selected for the case of *Test 2 data set* is defined by Equation (4.12).ñ

$$Q_{hp}(t) = \frac{0.1203q^{-1} - 0.1811q^{-2}}{1 - 0.01652q^{-1} + 0.0382q^{-2} + 0.01565q^{-3} + 0.0274q^{-4}} T_{ext}(t)$$

$$Q_{hp}(t) = \frac{0.3255q^{-1} + 0.6951q^{-2}}{1 - 0.01652q^{-1} + 0.0382q^{-2} + 0.01565q^{-3} + 0.0274q^{-4}} T_{sp}(t) \quad (4.12)$$

$$Q_{hp}(t) = \frac{0.2238q^{-1} + 0.02216q^{-2}}{1 - 0.01652q^{-1} + 0.0382q^{-2} + 0.01565q^{-3} + 0.0274q^{-4}} Hyst(t)$$

### c. Box-Jenkins (BJ)

For *Equation 2*, the orders of the model have also been set to 4. No improvement has been achieved increasing or decreasing the orders values. The same criterion as in *Equation 1* has been followed for the selection of the model orders.

As for the treatment of the initial conditions of the model during parameter estimation, as in the case of *Equation 1*, initial conditions to zero and option zero-order hold (*zoh*) have been set for defining the constant behaviour of the model between input samples. The model obtained based on Box-Jenkins method is described by the transfer functions defined in Equation (4.13).

$$Q_{hp}(t) = \frac{-6.052q^{-1} + 17.18q^{-2} - 10.13q^{-3} - 1.907q^{-4}}{1 - 0.3391q^{-1} - 1.49q^{-2} - 0.3411q^{-3} + 0.5789q^{-4}} T_{ext}(t)$$

$$Q_{hp}(t) = \frac{41.29q^{-1} - 97.06q^{-2} + 89.37q^{-3} - 30.98q^{-4}}{1 - 1.776q^{-1} + 1.37q^{-2} - 0.3187q^{-3} + 0.02363q^{-4}} T_{sp}(t) \quad (4.13)$$

$$Q_{hp}(t) = \frac{470.4q^{-1} - 708.5q^{-2} + 575.7q^{-3} - 70.88q^{-4}}{1 - 1.749q^{-1} + 1.724q^{-2} - 0.6512q^{-3} + 0.1892q^{-4}} Hyst(t)$$

## 4.5 RESULTS AND DISCUSSION

This section presents the results obtained from the models introduced in the previous section. In this sense, it is considered important to analyse, above all, two aspects of the results: the validity of the proposed models and, the comparison between the performance of Box-Jenkins and the selected lmNARX. This analysis is carried out for both *Equation 1* and *Equation 2*.

### 4.5.1 Equation 1: ESTIA 2 thermal capacity model

The NARX has been first evaluated by plotting its response and calculating the evaluation metrics. Afterwards, the chosen lmNARX and Box-Jenkins outputs have been compared to the measured $T_{in}$ of both *Test 1 data set* and *Test 2 data set*.

#### 4.5.1.1 NARX neural network

As it can be seen in Figure 4.16, NARX model seems to be able to track accurately the rapid variations of $T_{in}$. Taking into account the variable trend of the curve, we consider a $R^2$ of 0.93 to be a good result.

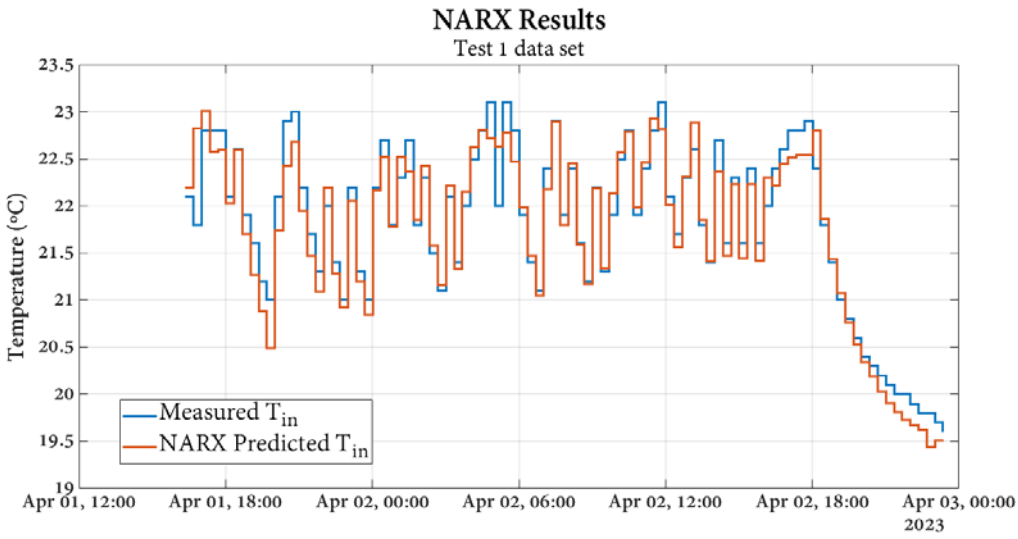


***Figure 4.16.*** *NARX model response of $T_{in}$ for Test 1 data set.*

***Table 4.7****. Fitting and $R^2$ values NARX model response* of *$T_{in}$ for Test 1 data set.*

| **Test 1 data set** | ***fitting (%)*** | **$R^2$** |
|---|---|---|
| **NARX model** | 73.81 | 0.93 |

As it can be seen in Figure 4.17, $T_{in}$ suffers an unexpected drop during the afternoon of April 9th (see section 4.3.2). Although NARX does not reach the recorded minimum of the unexpected drop, it is able to represent and follow it.

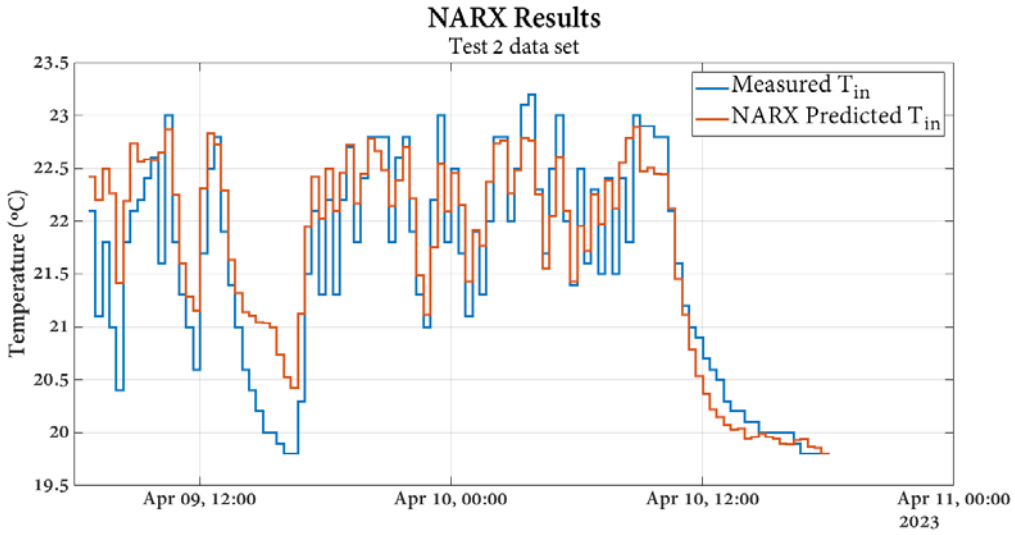


***Figure 4.17**. NARX model response of $T_{in}$ for Test 2 data set.*

***Table 4.8.** Fitting and $R^2$ values of lmNARX and Box-Jenkins responses of $T_{in}$ for Test 1 data set.*

| **Test 2 data set** | ***fitting (%)*** | **$R^2$** |
|---|---|---|
| **NARX model** | 57.07 | 0.81 |

To conclude, NARX model represents the behaviour of $T_{in}$ of *Test 1 data set* considerably better than $T_{in}$ of *Test 2 data set* (73.81% vs 57.07%). This may be by the fact that *Test 2 data set* contains $T_{ext}$ values that are outside the range of the temperatures used to train NARX model (see Figure 4.2). In contrast, in *Test 1 data set* the range of $T_{ext}$ is much smaller, between 9ºC and 14ºC approximately.

### 4.5.1.2 Comparison between lmNARX and BJ

The response of the selected lmNARX (Equation (4.8)-(4.9)) and Box-Jenkins (Equation (4.10)) have been compared with the measured $T_{in}$ for both cases: *Test 1 data set* (see Figure 4.18) and *Test 2 data set* (see Figure 4.19).

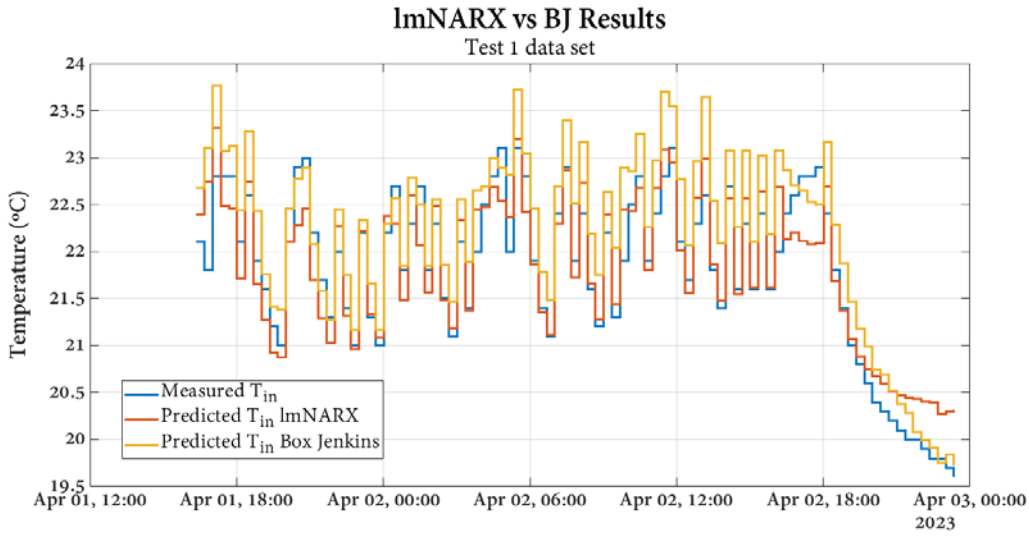


***Figure 4.18**. Comparison of lmNARX and BJ responses* of $T_{in}$ *for Test 1 data set.*

***Table 4.9.** Fitting and $R^2$ values of lmNARX and BJ responses* of $T_{in}$ *for Test 1 data set.*

| **Test 1 data set** | ***fitting (%)*** | **$R^2$** |
|---|---|---|
| **lmNARX** | 61.47 | 0.85 |
| **Box-Jenkins model** | 52.15 | 0.77 |

lmNARX responds with somewhat sharper peaks than BJ. Both models show the ability to follow the rapid variability of the internal temperature. $fitting$ and $R^2$ values of Table 4.9 give a more clear idea of how lmNARX is able to represent $T_{in}$ curve with almost 9% better fitting (see Table 4.9).

Observing the curves in Figure 4.19, it is possible to appreciate a convulsive initial phase where none of the models manages to represent the initial temperature of 22ºC. Both models start from a higher initial temperature than the measured temperature. This lag requires a stabilisation time of approximately 4 hours before the curve can be tracked again.

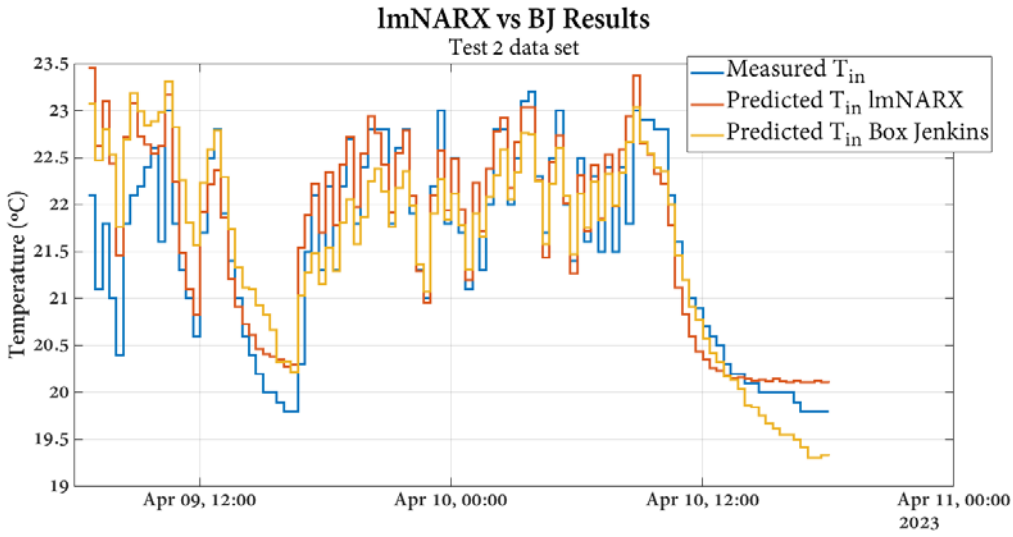


***Figure 4.19.*** *Comparison of lmNARX and Box-Jenkins responses of $T_{in}$ for Test 2 data set.*

***Table 4.10.*** *Fitting and $R^2$ values of lmNARX and Box-Jenkins responses of $T_{in}$ for Test 1 data set.*

| Test 2 data set | *fitting (%)* | $R^2$ |
|---|---|---|
| **lmNARX** | 56.23 | 0.81 |
| **Box-Jenkins model** | 57.25 | 0.82 |

It can be concluded by comparing the evaluation metrics that BJ, with a very narrow margin of less than 2% $fitting$, is able to represent $T_{in}$ curve of the *Test 2 data set* more accurately than $T_{in}$ curve of the *Test 1 data set*. Anyway, both models are able to represent it with a $R^2$ of at least 0.81 (see Table 4.10).

### 4.5.2 Equation 2: HVAC system model

#### 4.5.2.1 NARX neural network

It is important to note that the HVAC system exhibits a high level of variability. As can be seen in Figure 4.20, NARX model has been clearly capable of capturing them. However, NARX model fails to reduce consumption during the afternoon of April 2nd (marked with a yellow square in Figure 4.20), during which consumption remains more or less constant below 700Wh. Despite this fact in conjunction with the fact that there are times when the output does not reach the consumption peaks, the NARX is able to represent $Q_{hp}$ curve with an $R^2$ of 0.83 (see Table 4.11).

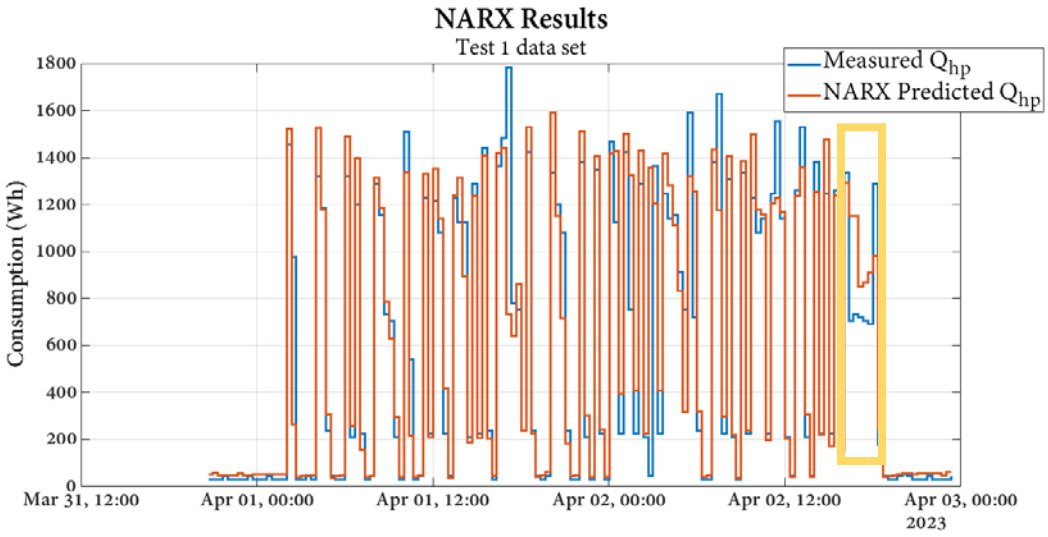


***Figure 4.20***. *NARX model response of $Q_{hp}$ for Test 1 data set.*

***Table 4.11***. *Fitting and $R^2$ values of NARX model response* of $Q_{hp}$ *for Test 1 data set.*

| **Test 1 data set** | ***fitting (%)*** | **$R^2$** |
|---|---|---|
| **NARX model** | 58.47 | 0.83 |

Regarding Figure 4.21, the measured consumption does not have an initial period where its value is zero. This is because, even though $T_{sp}$ is maintained at 20ºC in this initial period, $T_{in}$ is below 20ºC, causing the HVAC system to turn on and hence the peaks of around 1.2kW can be observed. A slight mismatch can be observed in the output related to the first two consumption peaks, where NARX follows the curve with a slight delay, especially during the first peak. This delay of the model output with respect to the measured consumption in the first hours of the test greatly reduces the fit, which is more than 14% lower than in the case of the *Test 1 data set* (see Table 4.12).

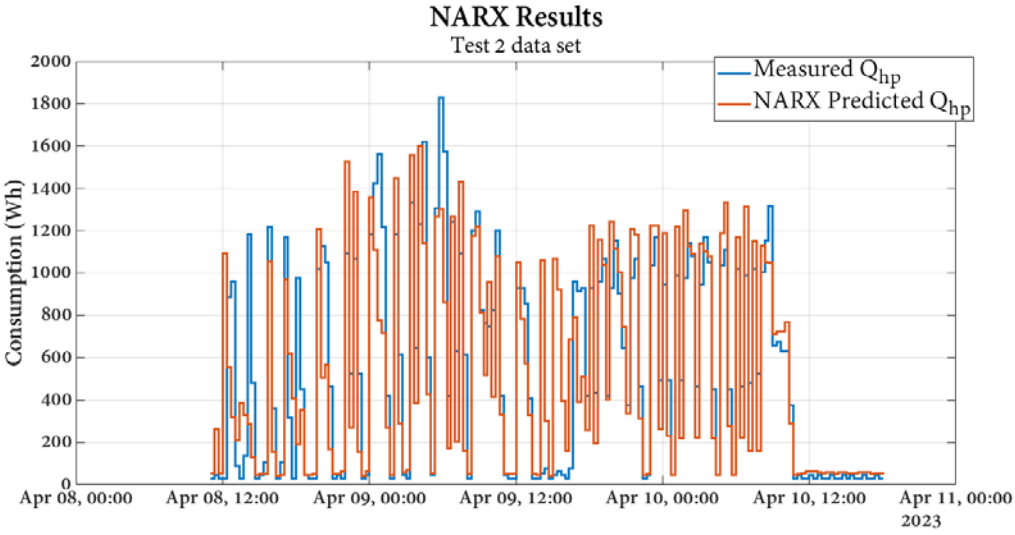


***Figure 4.21**. NARX model response of $Q_{hp}$ for Test 2 data set.*

***Table 4.12**. Fitting and $R^2$ values of NARX model response of $Q_{hp}$ for Test 2 data set.*

| **Test 2 data set** | ***fitting (%)*** | **$R^2$** |
|---|---|---|
| **NARX model** | 44.32 | 0.69 |

### 4.5.2.2 Comparison between lmNARX and BJ

Next step has been to analyse how best lmNARX (Equation (4.11)-(4.12)) and Box-Jenkins (Equation (4.13)) are able to represent the measured $Q_{hp}$ curve of the *Test 1 data set* and *Test 2 data set*.

Several observations can be made by simply looking at Figure 4.22. Both models satisfactorily capture the high variability of the consumption curve. However, the response of the Box-Jenkins model deserves highlighting, as it gives negative consumption values in the early hours of the test where the $Q_{hp}$ is nearly zero. Despite this, is the BJ the one that most accurately represents the $Q_{hp}$ curve with a $fitting$ of 61.39% (see Table 4.13).

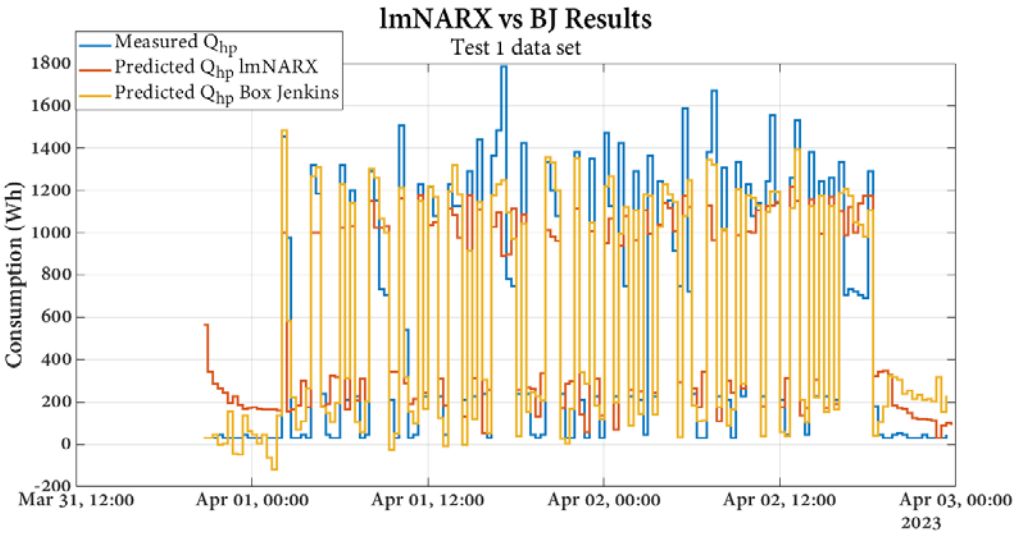


***Figure 4.22**. Comparison of lmNARX and Box-Jenkins responses of $Q_{hp}$ for Test 1 data set.*

***Table 4.13**. Fitting and $R^2$ values of lmNARX and Box-Jenkins responses of $Q_{hp}$ for Test 1 data set.*

| **Test 1 data set** | ***fitting (%)*** | **$R^2$** |
|---|---|---|
| **lmNARX** | 51.59 | 0.77 |
| **Box-Jenkins model** | 61.39 | 0.85 |

Regarding Figure 4.23 and numerical results gathered in Table **4.14**, in general terms, significantly worse results have been obtained when tracking $Q_{hp}$ curve of *Test 2 data set*.

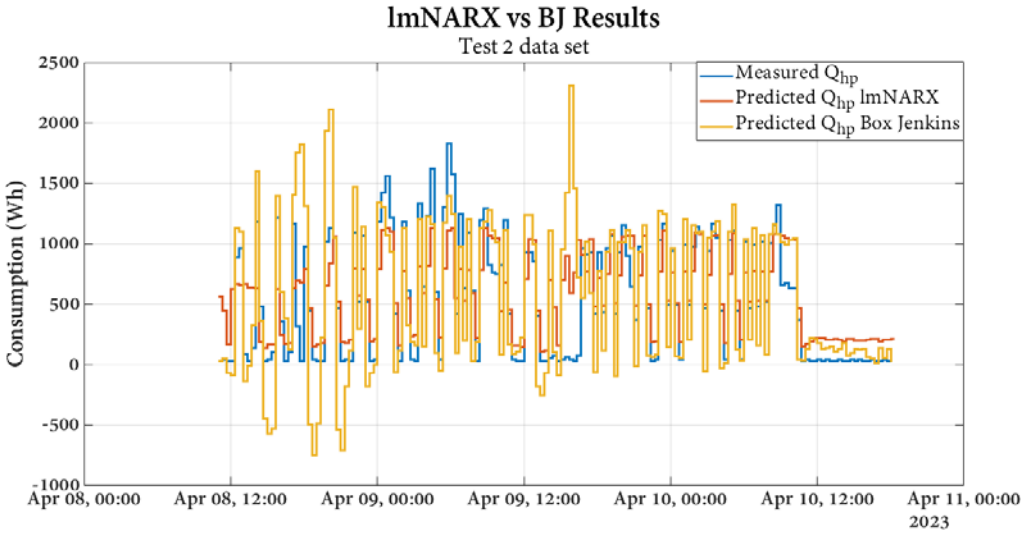


***Figure 4.23.** Comparison of lmNARX and Box-Jenkins responses of $Q_{hp}$ for Test 2 data set.*

***Table 4.14**. Fitting and $R^2$ values of lmNARX and Box-Jenkins responses of $Q_{hp}$ for Test 2 data set.*

| **Test 1 data set** | ***fitting (%)*** | **$R^2$** |
|---|---|---|
| **lmNARX** | 20.79 | 0.65 |
| **Box-Jenkins model** | 8.73 | 0.18 |

Both models exhibit a chaotic response at the beginning of the validation, deviating significantly from the consumption curve. Box-Jenkins also makes the mistake of representing negative consumption values, which is clearly a major factor contributing to the low $fitting$ value achieved (8.73%).

## 4.6 CONCLUSIONS AND FUTURE WORKS

The aim of this fourth chapter has been to model the HVAC system and the thermal capacity of the building so that both models can be used as a control model in the MPC developed in Chapter 5. The outputs of the model have been the consumption of the modelled heat pump and the $T_{in}$ of the modelled area. The control model is a linear model that is updated daily. Linear models can reduce the computational cost of the MPC, which is one of the objectives of the proposed MPC approach.

Due to the nonlinear characteristics of the system to be modelled, a NARX model has been chosen. The NARX captures the nonlinearities while being able to be linearised at convenient OPs, thus capturing the dynamic trend of the system. However, conditions have not made it possible to perform excitation tests during longer periods than concrete weekends. Therefore it has been impossible to obtain large amounts of data to train the model. Training the NARX model with little data set has meant that the results obtained are not as good as they could be. Despite this, the NARX trained with little data manages to represent $T_{in}$ and $Q_{hp}$ with a $R^2$ of 0.93 and 0.81 respectively in the case of *Test 1 data set* and with an $R^2$ of 0.81 and 0.69 for $T_{in}$ and $Q_{hp}$ in the case of *Test 2 data set*.

The linearisation of the NARX has been performed on 100 OPs to model the thermal capacity of the building and on 200 OPs to model the HVAC system. The objective has been to analyse how the NARX operates at these OPs and to select the linear model that best represents $T_{in}$ and $Q_{hp}$ curves. The lmNARX used to model the thermal capacity of the building has been able to represent the $T_{in}$ curve of *Test 1 data set* with a $R^2$ of 0.85 and with a $R^2$ of 0.81 the $T_{in}$ curve of *Test 2 data set*. The response of lmNARX when modelling the HVAC system has been somewhat lower, representing with a $R^2$ of 0.77 the $Q_{hp}$ curve of *Test 1 data set* and with 0.65 the $Q_{hp}$ curve of *Test 2 data set*. Taking into account the limited data for training the NARX model and the high variability of the curves to be represented, we believe that the results are acceptable. However, it would be interesting to conduct more tests to obtain more data used to train the NARX model so that it can learn from more scenarios.

The model based on Box-Jenkins method has proven to be suitable for building thermal modelling; however, the inability to capture nonlinearities might lead to errors in the representation especially of HVAC system consumption.

Only the *Platform* area has been modelled in this study, a large space in the ESTIA 2 building. The idea of modelling this space was to start with something simple to model and then extend the model to the whole building. It was also an accessible space where the tests could be carried out.

However, there was not enough time to be able to extend the field of study and model the building as a whole. Nevertheless, the modelling of the *Platform* has allowed the proposed methodology to be validated. One of the possible future works could be to perform tests in the rest of the ESTIA 2 building in order to model thermally the entire building. Moreover, considering the problems with testing, as well as the various problems we have experienced with the operation of sensors and with the heat pumps themselves, it would be interesting to choose a new building and apply the methodology developed in this chapter.

Finally, it is worth mentioning the possible improvements in the design process of the NARX model, since the adjustment of the hyperparameters could be optimised through the use of genetic algorithms (GAs).

# *CHAPTER 5*

# *OPTIMISATION PROBLEM OF THE EMS*

---

In this fifth chapter, the optimisation task of the EMS is presented. This chapter synthesizes and builds upon the work presented in the preceding chapters.

The chapter opens with expanding the literature review on optimisation-based EMS started in subsection 1.2.2 of Chapter 1. Subsequently, the main and related secondary objectives are presented. Following this, the methodology employed and the case study that served as the application context are introduced. The results are discussed and the main conclusions are drawn.

# 5.1 INTRODUCTION

Model Predictive Control (MPC) is a widely used control strategy, renowned for its ability to handle multi-variable systems with constraints. The MPC make use of a dynamic control model to predict the future behaviour of a system over a finite prediction horizon [219]. Based on these predictions, an optimisation problem is solved at each time step to compute the control signals that minimise a predefined cost function, while ensuring that all constraints are respected.

### 5.1.1 State of the art

In Chapter 1, a comprehensive review of the literature on MPC applications in various energy-related scenarios has been presented. Several key studies have been discussed, highlighting the versatility of MPC when applied to contexts such as Smart Grids, ECs, and SC frameworks. These studies demonstrate the growing interest in optimising energy management in decentralised systems, particularly where coordination among multiple actors or consumers is required, as is the case with CSC scenarios.

Additionally, Chapter 1 examines a range of MPC strategies proposed in the literature that pursue diverse optimisation goals. Among these, particular emphasis is placed on approaches that aim to minimise operational costs [75], maximise the use of RES [77] and enhance the SCR [82].

There are several papers proposing EMS applied to Microgrid schemes, which aim to encourage self-consumption. In [220], they develop a two-level hierarchical MPC applied to a Microgrid composed by a single building with battery systems and PV generation. The improved EMS they propose is powered by a module to identify the real-time parameters of the battery model, which increases the SCR by 4% compared to a simple RB-EMS. Authors of [221] also introduce a hierarchical MPC that includes EVs and a PV installation and aims to maximise SCR. The proposal has proven to be able to increase the SCR by 7% over a case of uncontrolled strategy.

In the specific case of SC scenarios, EMS usually aim to encourage self-consumption as much as possible, since, as highlighted in Chapter 1, one of the great advantages offered by SC schemes is that if a high SCR is reached, the associated consumers can save on their electricity bills. This is the example of [222], which proposes a MPC that aims to optimise the use of electric water heaters (EWHs) by taking advantage of unused PV generation to increase the economic benefit and SCR within a CSC framework. It proposes several control strategies and finally compares them with the performance of a RB-EMS, which fails to outperform any of the proposed strategies. Also [223] introduces a proposal that includes BESS and PV installation managed by

a MPC type EMS that aims the maximisation of SCR and the minimisation of battery degradation. The MPC is able to achieve a SCR of 99.5% and a reduction of 6% of battery degradation.

One subset of MPC that has gained considerable attention **is prediction-based MPCs**. In Chapter 1 examples of predictive model-based EMS approaches have been included, demonstrating how these methods incorporate future predictions into the control strategy to achieve superior performance [78], [79]. In particular, in [77] the authors compare three MPC-based strategies involving PV panels, controllable and uncontrollable loads and BESS. Two of the strategies include forecasts and it is concluded that EMS based on predictions outperform the third one, which does not include predictions. This type of MPC leverage prediction models to improve its performance by offering more accurate estimates of future system states [77].

When the EMS aims to maximise the SCR, it becomes important to have predictions of energy production and the energy to be consumed. When it comes to PV production forecasts, in [224] PV production and electricity market price forecasts are used for the EMS to adjust PV generation to compensate for power fluctuations. In fact, two actions are also defined when the production forecasts fall below or exceed the actual production. On the one hand, electricity is bought from the grid or discharged from the ESS in case the predictions have not reached the actual value and, on the other hand, the battery is charged when it is over-predicted. The prediction errors of both production and consumption depend to a large range of factors as the weather or the occupancy level and behaviour of the users of a building. This can lead to prediction errors which, as demonstrated in [225], influence the decision-making process of an EMS. In [223], it is proved how the uncertainties of forecasts (consumption and PV production) can lead to deterioration of the EMS performance. The results show that the EMS without forecasts achieves a SCR of 99.5% while including forecasts the SCR reduces to 96.5%. Therefore, it is important to properly select predictive models that are able to reduce prediction errors as much as possible.

The forecasting of energy consumption of buildings and PV production are often performed by nonlinear predictive models, which are able to capture the nonlinearities that the system might have. To model these nonlinear systems, ML models and more specifically neural networks have gained relevance. The problem lies in the fact that some NNs need to be trained with large data sets and have complex structures, i.e. several layers composed of many neurons. These complex models entail a higher computational cost.

Nevertheless, **NN**s can enhance the operation of an optimisation-based EMS because they can substantially improve its performance. This is evidenced by [80] where the authors implement in a building an EMS based on NN models that forecast the building consumption, weather conditions and building's comfort specifications aiming minimization of energy consumption and

ensuring occupants comfort. The MPC is implemented in simulation using EnergyPlus software and its performance is compared with a second MPC that does not include predictions as inputs. They conclude that the MPC fed with forecasts outperforms the conventional MPC. In any case, the characteristics of the model that feeds predictions to the MPC must be in accordance with the performance requirements of the MPC. If it is necessary to design a MPC with low processing time or generally low computational cost, complex NNs may not be the most appropriate.

MPCs make use of a **control model**, which can be either a linear model or a nonlinear model. In [226] a MPC and a NARX type NN are combined. The combination is approached in two different ways; by a nonlinear MPC (NMPC), and by a MPC using a local linearisation strategy. The first one has as a control model a NARX that represents the operation of an EV and forces to perform a nonlinear optimisation. In the second approach, the NARX is linearised in real-time and a quadratic problem is solved. The results show that the NMPC delivers superior results but it is computationally demanding compared with the local linearisation approach. Anyway, it is also conclude that the introduction of simple NARX models lead to a reduction in the computational time, making them more suitable for real-time applications.

When an EMS is implemented in a building, the control model usually represents the **thermal behaviour of the building**. The building thermal model is intended to represent the thermal dynamics of the building and it can be very useful for the control of indoor temperature variation and/or heat related with the HVAC system. Thus, in [227] MPC using a RC thermal network type model is proposed to represent the thermal dynamics of the building. The MPC aims at minimizing energy consumption and cost. The designed MPC is compared with an On/Off control and with a PID controller, concluding that it is the MPC that outperforms the rest. However, physical models or even grey-box models such as the RC thermal network, being in general high order models they might hinder the MPC performance. High-order models may not be the most appropriate in cases where a MPC with a low computational cost needs to be designed.

The utilization of nonlinear models as control models might also hinder the MPC performance requiring more complex solvers. However, this type of models are the most appropriate ones to capture the nonlinearities that a system like HVAC can contain. Nevertheless, in the case of wanting the MPC to use a simpler control model in order to avoid complex solvers, the linearisation of the nonlinear model can be performed. One of the most common approach for linearisation is local linearisation, where a linear model around a specific OP approximates the nonlinear system. This method is effective for small deviations from the OP, but loses accuracy as the system moves further away from it. Although there are other linearisation techniques for nonlinear systems such as input-output linearisation or linear parameter varying (LPV) [228], local linearisation offers the advantages of being easy to implement and to ensure stability over

small operating ranges. It is this latter characteristic that may be appropriate for implementation in real-time control applications, in which the system may operate around a certain operating point.

There is also the possibility to enhance performance choosing a suitable **MPC strategy** for the application. A widely used one in literature is the mixed integer programming (MIP) [229], and more specifically, mix-integer linear programming (MILP). MILP is an extension of linear programming (LP) that allows to define variables to be both integer and continuous. This feature makes it conducive to solving more realistic problems, especially when the decisions to be made by the MPC involve discrete variables such as binary decisions. MILP is applied when the cost function that needs to be optimised is a linear function, as well as the constraints that the problem include. MILP has proven to be effective with handling constraints and optimizing [230]. In the case of working with a nonlinear cost function or nonlinear constraints, it will be dealing with nonlinear programming (NLP). This is the case where, for example, in an EMS applied to a building, the thermal dynamics of the building or the behaviour of the air conditioning system are represented with nonlinear equations that comprise the control model of the MPC. There is also the possibility of having to solve a nonlinear problem but working with variables that are both integer and continuous. In this case we would be dealing with mix-integer nonlinear programming (MINLP). In order to know which type of strategy fits the optimisation problem to be solved, it is necessary to analyse the models and the cost function to see if they are linear or nonlinear, as well as, if it is necessary to declare any integer variable. However, it is also necessary to analyse the computational requirements of each type of problem defined, since, especially the nonlinear ones can be very computationally demanding.

### 5.1.2 Conclusions

There is a wide variety of optimisation-based EMS in the scientific literature used to encourage self-consumption by maximizing SCR. Several papers have also shown that EMS that include predictions outperform EMS that do not include them. That is why proposals that introduce prediction-based EMS are increasingly growing. ML models and in particular NNs have proven to be feasible solutions to feed MPCs with predictions.

Furthermore, as mentioned before, there are NMPCs, which use a nonlinear control model and therefore perform nonlinear optimisation. However, as several analysed papers point out, this type of optimisation is more computationally demanding. In order to reduce computational cost, some authors use linear models as the control model of the MPC, but in this case, the MPC performance can be low when the controlled system is very nonlinear. Regarding physical and RC thermal network models, there are often high order models, which might increase the computational cost

of the MPC. Therefore, a good solution could be to design a nonlinear model to capture the nonlinear dynamics of the system and to linearise it regularly at the OP of interest. Thus, a new linear control model can be considered each time the MPC operates, ensuring lower computational cost and taking into account the dynamical behaviour of the system in the corresponding OP.

## 5.2 OBJECTIVES

After reviewing the existing literature on studies related to optimisation problems of MPCs, a set of concrete objectives have been established for this research. The purpose is to explore and justify each of these objectives in this chapter, with a focus on demonstrating their relevance and applicability within the context of EMS applied to SC.

The main objective of this chapter has been to undertake and evaluate the optimisation problem of the proposed EMS. As shown in Figure 1.5 of Chapter 1, the optimisation development phase brings together the work done in Chapter 2, Chapters 3 and Chapters 4. The MPC has as inputs the day-ahead predictions of energy consumption (without the consumption associated to the HVAC system) and PV production both developed in Chapter 2 and Chapter 3 respectively. In conjunction, it uses the HVAC system and the associated building thermal model developed and presented in Chapter 4 as the MPCs control model.

In order to evaluate whether the optimisation module is operating correctly, several aspects have been analysed, which can be defined as secondary objectives.

- The EMS aims to maximise the SCR; therefore, the analysis of the correct performance of the optimisation problem has been conducted to see if its application leads to an increase in the SCR.
- Together with the maximisation of SCR, the EMS must ensure thermal comfort of occupants of the building ESTIA 2, and consequently, certain internal temperature limits are established. It is therefore necessary to check whether the optimisation respects the thermal comfort zone at all times.
- The EMS controls the heating related to the HVAC system by optimally generating the set point temperature. Therefore, the last objective is to analyse the correct operation of the optimisation module by checking the effect of its output, the set point temperature.

By pursuing these goals, the study aims to contribute to the development of an EMS that optimise the performance of HVAC systems in a building.

## 5.3 METHODOLOGY

The MPC has been developed under the approach of being suitable for a real time implementation and which it does not have a high computational cost.

As depicted in Figure 1.5 of Chapter 1, the MPC makes use of day-ahead predictions of energy consumption (without the effect of the HVAC system) and PV production. The predictive models have been designed so that, when trained with little data and with a simple structure, they can feed the MPC with accurate predictions. In addition, a linear model has been applied as the control model used by the MPC, more specifically the thermal behaviour of the building and the associated HVAC model. Thanks to the model, it is able to represent the thermal dynamics of the building and thus to control the needed heat produce by the HVAC by means of the set point temperature. The main objective of the MPC is ultimately to maximise the SCR while ensuring the thermal comfort of the building. As the thermal model has been developed in the heating operation of the heat pump, the optimisation has also been conducted in the same case. This means that in this Thesis, the cooling case is not studied. .

### 5.3.1 Prediction horizon and sampling time

The MPC has a prediction horizon of one day, i.e. it provides the set point temperature for the next 24 hours. Regarding the sampling time used, the SCR is calculated in France every half hour. This said, due to the restrictions mentioned in Chapter 4 regarding the excitation test characteristics, the thermal model has been built with a sampling time of 20 minutes and therefore, the optimisation has been performed every 20 minutes. Furthermore, the predictive models built at Chapter 2 and Chapter 3 forecast with a sampling time of one hour. This decision was taken because, at first, the models were intended to be applicable to Spain, where the SCR is calculated on an hourly basis. In addition, the meteorological data used as inputs to the predictive models are available with a sampling time of one hour. Therefore, in order to integrate the consumption and PV production forecasts in the optimisation module, the sampling period of both has been changed to 20 minutes by interpolation. After all, the Thesis has been a process where certain things have been redefined over time. The lack of time has meant that certain improvements could not be made, among others, the adjustment of the sampling time of the predictions.

### 5.3.2 Optimisation problem

The MPC developed in this Thesis is a strategy based on the optimisation of a cost function and makes use of a control model and predictions of consumption and PV production to provide as control signal the set point temperature.

In this study, the EMS uses as control model a linear model that represents the HVAC system and the associated thermal capacity of the building. The model is represented with Equation (4.8) and Equation (4.11) of Chapter 4.

Once the model developed and the prediction horizon set, it has been necessary to define:

(a) The cost function $J$ of the problem that need to be optimised.
(b) The constraints that the problem need to satisfy.

The cost function represented in Equation (5.1) has been defined where all the terms are energy related terms (kWh). In this way, the function sums in each sampling time $k$ the absolute value of the difference between all the three energy terms.

$$min_{Q_{hp}} J = min_{Q_{hp}} \sum_{k=1}^{n} \left| Q_{pv}(k) - Q_{cons}(k) - Q_{hp}(k) \right| \tag{5.1}$$

where $Q_{pv}(k)$ is the predicted PV energy in kWh in each sampling time $k$ and $Q_{cons}$ is the predicted building energy consumption without HVAC system consumption in kWh at each sampling time $k$. $Q_{hp}(k)$ is the energy consumption of the HVAC system in kWh at each $k$ and $n$ represents the total number of samples.

The aim is to minimize $J$ and thus ensure that the EMS keeps the consumption curve of the building following the production curve for as long as possible. Thus, ensuring to maximise the SCR as much as possible. The constraints that have been defined are related to the thermal comfort zone.

### 5.3.3 Thermal comfort representation

The EMS needs to ensure that the indoor temperature is maintained inside specified ranges. Aiming to define these ranges Dear and Brager model has been used as reference [85]. Dear and Brager model was developed as a basis for the standards of the American Society of Heating, Refrigerating and Air-Conditioning Engineers (ASHRAE).

The authors define a comfort temperature ($T_{comf}$) as the ideal temperature to be maintained in the building. Therefore, they propose the $T_{comf}$ calculation in function of the previous day average external temperature, named $T_{ext,mean}$, as shown in Equation (5.1)

$$T_{comf} = 0.31 * T_{ext,mean} + 17.8 \quad (5.2)$$

Dear and Brager model proposed (see Figure 5.1) a temperature range corresponding to a thermal acceptability of 90% and 80%. These acceptability margins are defined around the comfort indoor temperature.

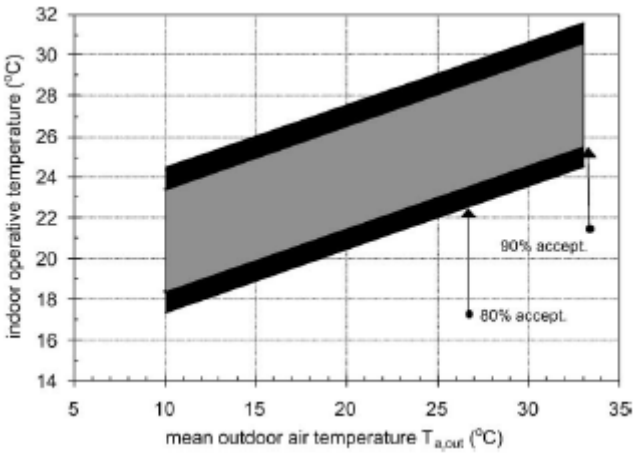


***Figure 5.1.****Proposed adaptive comfort standard (ACS) for ASHRAE Standard 55 [231].*

Therefore, a minimum and maximum indoor temperature have been defined for both 80% and 90% of acceptance. For that, the mean external temperature ($T_{ext,mean}$) of the previous day that needs to be optimised has been calculated.

Taking the calculated $T_{comf}$ as a reference, the internal temperature limits have been established taking into consideration 90% and 80% of acceptability.

$$T_{in,\min 90\%} \leq T_{comf} \leq T_{in,\max 90\%} \quad (5.3)$$

$$T_{in,\min 80\%} \leq T_{comf} \leq T_{in,\max 80\%} \quad (5.4)$$

The 90% of acceptance temperature range has been considered as the first constraint to meet during the work hours take from 08am to 06pm. Due to the low external temperatures that usually are registered in the early hours, it has been decided to apply as a second constraint the 80% acceptance temperature range from 06.40am to 08am. The aim is to preheat in order to do not have a high consumption peak to reach the minimum temperature of $T_{in,\min 90\%}$ needed at 08am.

### 5.3.4 Programming of the optimisation problem

The optimisation problem has been defined and solved in Python using *pyomo* environment. After defining the cost function and the constraints and knowing which variables need to be declared, it can be concluded that, by using linear models and a linear cost function, a simple linear programming (LP) problem has to be solved. The heat pump model includes a priori the hysteresis term that must acquire an integer value, specifically a value of 0 or 1. By declaring the internal temperature, the set point temperature or the heat pump consumption as continuous variables, a MILP problem has arisen. The selection of the employed solver has been made accordingly. Given the inability of the *glpk* solver to find a solution to the optimisation problem, it was decided to use the *ipopt* solver. The *glpk* solver is designed to solve LP problems but can present difficulties when optimising problems with continuous or numerically complex variables. The *ipopt* solver is designed to solve nonlinear problems, but it is nevertheless capable of optimising linear problems and can provide advantages in the face of certain numerical instabilities.

## 5.4 CASE STUDY

Before validating the performance of the EMS by verifying the increase of the SCR after the implementation of the optimisation, the case study selected to perform such validation is first presented.

The selected day has been the 21st of April 2023, Friday, a day of low temperatures during the night and early hours of the day that require turning on the heating in the building. The external temperature data is predicted data obtained from Meteo Galicia and is plotted in Figure 5.2.

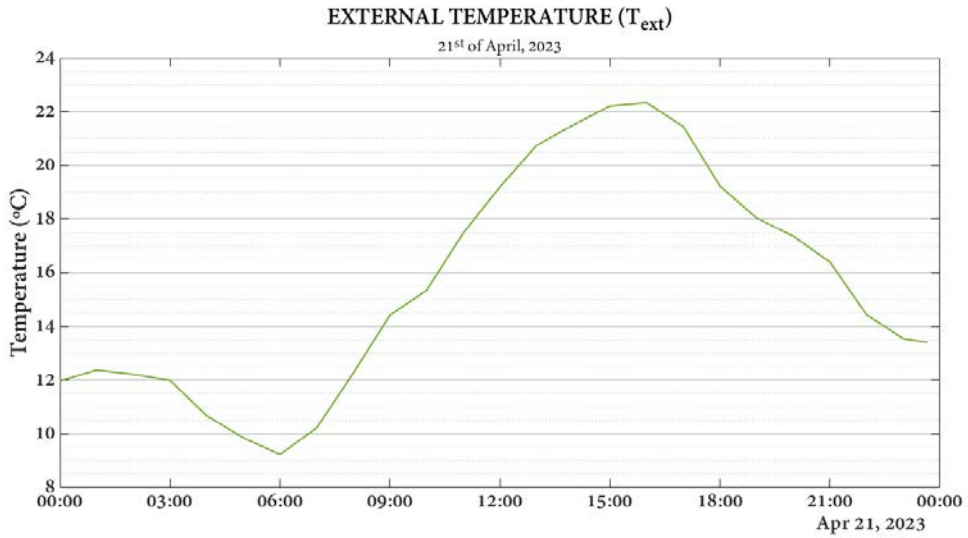


***Figure 5.2.*** *External temperature of 21st of April 2023.*

The temperature data have been predicted with a sampling time of one hour needing to use linear interpolation to set the 20 minutes of sampling time required by the optimisation, as explained in section 1.3.

The PV production curve and building consumption curve without taking into considerations the consumption of the HVAC system of 21st of Abril are plotted in Figure 5.3. The forecasting has been done in both cases with a sampling time of one hour, therefore, linear interpolation has been applied to fix the sampling time of 20 minutes. Moreover, a third curve has been included in order to see the difference of the total consumption and the one without heat pump consumption.

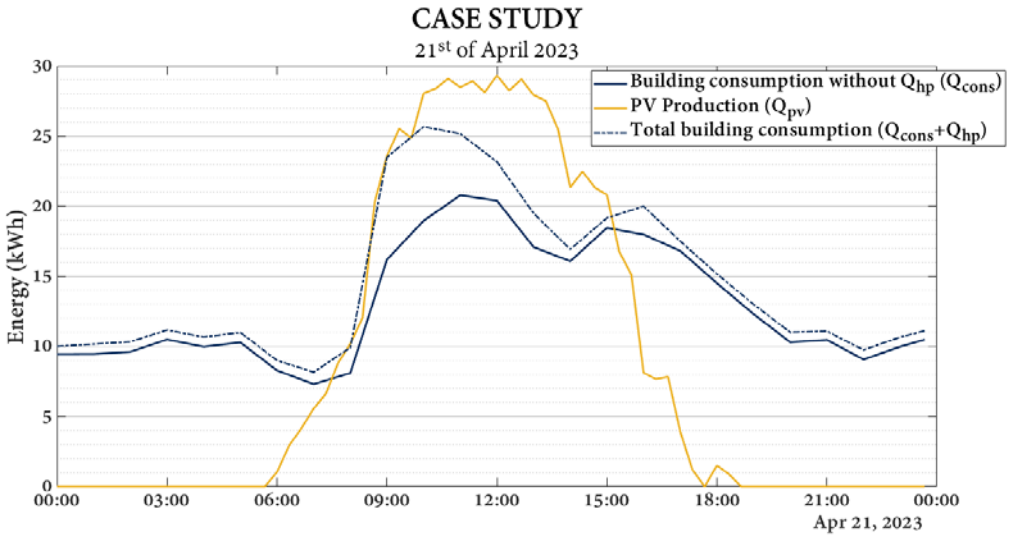


***Figure 5.3**. Consumption and PV production curves of 21st of April 2023.*

In addition, as described in section 1.3 of Chapter 1, an expansion of the PV power plant is planned within the EKATE project framework, which will be implemented in the short term. Thus, the total PV power will increase from 5.6 kWp to 117.17kWp. It has therefore been decided to multiply the PV production by a gain ($G_{PV}$) of 20 in order to emulate this case (see calculations in section 1.3).

Furthermore, since PV production and consumption of the building have been predicted in terms of average power, both the consumption and PV production curves have been transformed into energy terms.

Finally, the thermal model has been initially designed to represent the thermal dynamic of a zone of the building named *Platform*. However, as already mentioned in Chapter 4, the model has been considered in the optimisation as the one that represents the thermal dynamics of the whole building.

Having defined the case study, the temperature constraints that need to be included in the optimisation problem have been fixed. As explained before, the temperature constraints have been set to ensure the thermal comfort zone defined by Dear and Brager model proposal. Therefore, the previous day mean external temperature has been calculated (see Figure 5.4).

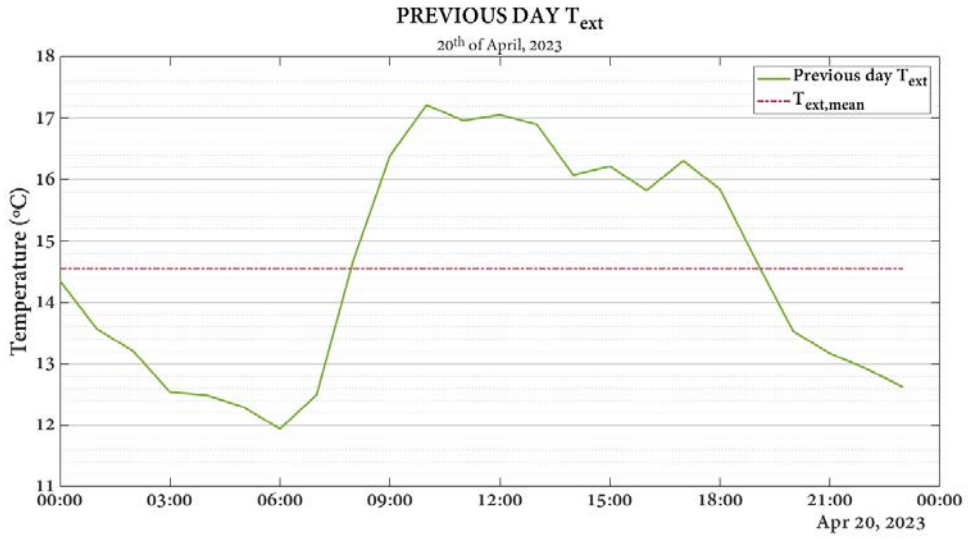


***Figure 5.4**. The external temperature of 20th of April 2023.*

Being the external mean temperature of 20th of April $T_{ext,mean} = 14.5ºC$, the ideal indoor temperature for 21st of April is $T_{comf} = 22.3ºC$. Therefore, the minimum and maximum indoor temperatures have been limited into 90% and 80% of acceptance (see (5.5) and (5.6)).

$$19.8ºC \leq T_{comf} \leq 24.8ºC \quad (5.5)$$

$$18.8ºC \leq T_{comf} \leq 25.8ºC \quad (5.6)$$

## 5.5 RESULTS AND DISCUSSION

The results have been shown according to the objectives set out in section 5.2. Therefore, first consumption curves of 21st of April without applying optimisation have been plotted (see Figure 5.5) aiming to see if an increase in SCR has been achieved when optimisation is carried out.

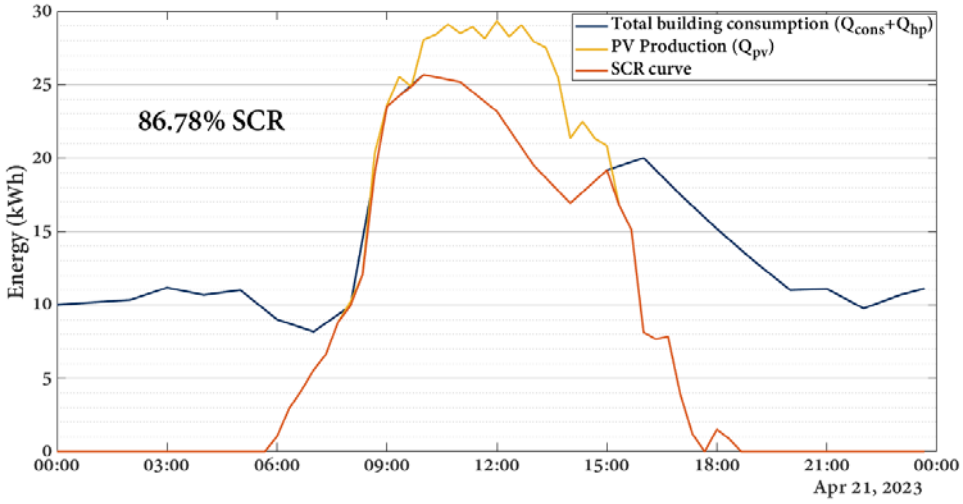


***Figure 5.5**. Energy curves and SCR of 21st of April without optimisation.*

Figure 5.5 shows the PV production curve and the consumption of the building, which includes the heat pump consumption. A third curve has been introduced which represents the self-consumed energy every 20 minutes. A SCR of 86.78% is achieved on the chosen day without optimisation being applied. When no optimisation is applied, the indoor temperatures that were registered during work hours can be seen in Figure 5.6.

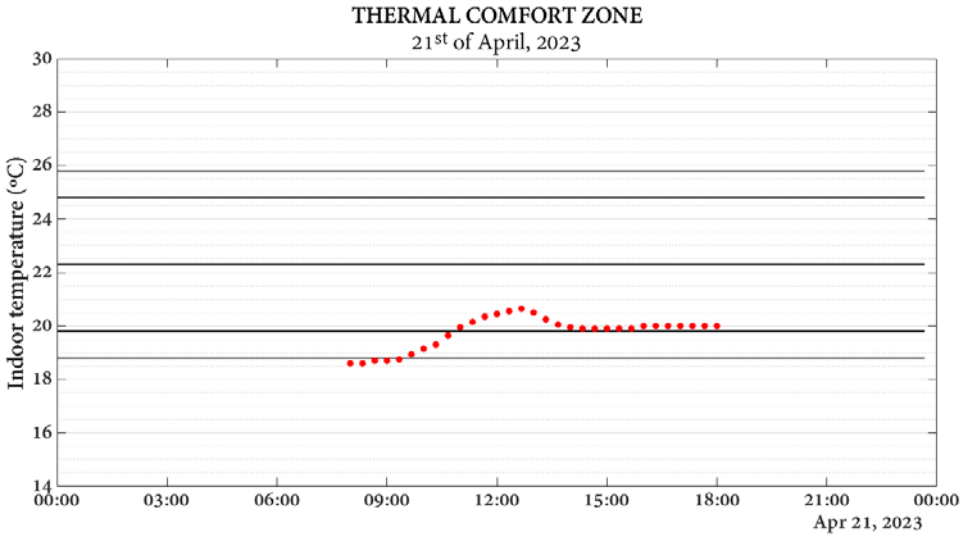


***Figure 5.6**. Indoor temperatures when optimisation isn't applied.*

Although most of the recorded temperatures are within the 90% range of acceptability, in the early hours of the day, which are usually critical due to low temperatures, the comfort temperature is not respected and remains below 19ºC until 09:40am.

Figure 5.7 shows the consumption curves that have been obtained after applying optimisation.

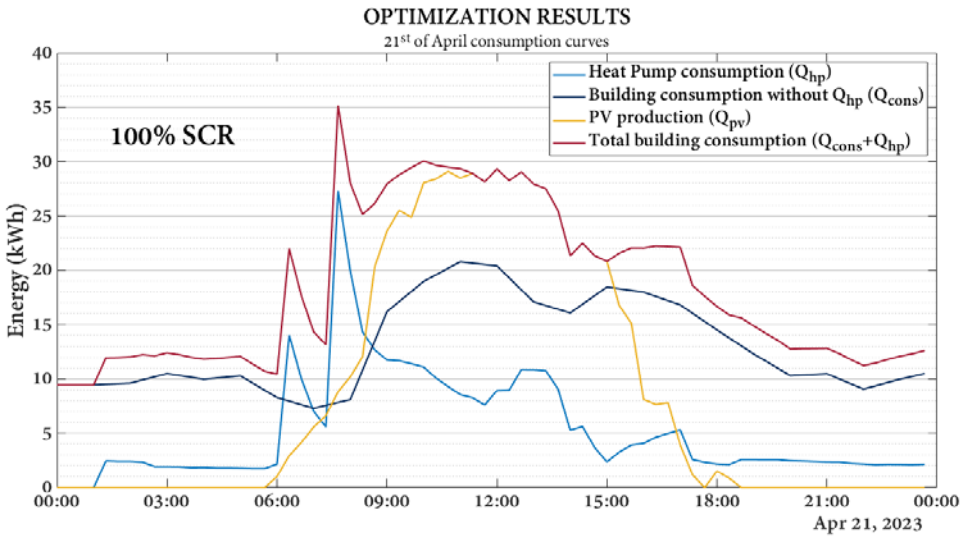


***Figure 5.7**. Energy curves of the case study optimised.*

The PV production curve is drown in yellow while the building consumption curve is in dark blue. The light blue is the consumption of the heat pump and finally the garnet curve represents the sum of building and heat pump consumptions.

As said in section 1.3, the control model has been built with a sampling time of 20 minutes due to the excitation test characteristics. Therefore, the optimisation has been done with the same sampling time and that is why all quantities represented in Figure 5.7 are values of energy produced or consumed every 20 minutes.

On the one hand, there are two consumption peaks of the heat pump at 06:20am and 07:40am specifically. These peaks represent the consumption that the heat pump needs to provide to meet the minimum temperature restrictions set as constraints. It is understood that the consumption peaks that can be seen in the graph do not strictly represent reality. The thermal model obtained in Chapter 4 based on the excitation tests carried out in the *Platform* area of the building has been used. The models representing the thermal behaviour of a single zone of the building and a single heat pump (GR16) have been used as the representative models for the building as a whole and for the 10 heat pumps. Therefore, the optimisation problem tries to use the whole HVAC system to reach the minimum temperature included as a constraint. This increases the consumption considerably, which would not be the case in reality. This is clearly a limit to the modelling.

Nevertheless, it has been proven that the optimisation problem is able to achieve the main objective: to leverage the PV generation surplus to turn on the heat pump consumption making the consumption curve follow the production curve. Thus, it can be seen that from 11:20am to 03:00pm, it is able to use all the excess PV energy for supplying the heat pump consumption. During the first and last hours of the range where $Q_{pv} > Q_{cons}$, the total consumption curve (garnet curve) is not able to follow the PV generation curve. This is due to the higher consumption that the heat pump needs to provide to respect the thermal comfort zone constraint.

Figure 5.8 shows the indoor temperature obtained during the day when applying the optimisation. The indoor temperature values represented by red markers in the figure are the temperatures given by the optimisation problem during the hours that thermal comfort zone must be respected, that is from 08:00am to 06:00pm.

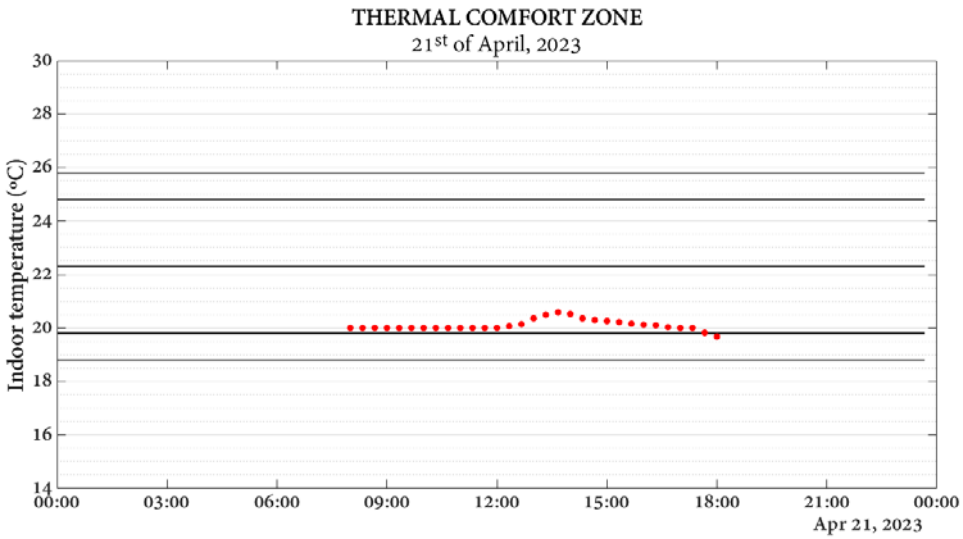


***Figure 5.8**. Indoor temperature values when optimisation is applied.*

It can be seen that in addition to the fact that the optimisation has managed to increase the SCR by 13.22%, it respects the internal temperature restrictions that have been established to ensure at all times the thermal comfort of the occupants of ESTA 2 building.

## 5.6 CONCLUSIONS AND FUTURE WORK

The objective of the work presented in this chapter has been to develop the optimisation module of the proposed Energy Management System designed to control the HVAC system of the building by adjusting the set point temperature. The approach has aimed to maximise the SCR while ensuring occupant thermal comfort and minimising MPC computational cost.

In order to evaluate the performance of the optimisation, the SCR obtained before and after the application of the optimisation has been compared. Without the application of the optimisation, a SCR of 86.78% has been obtained, while the optimisation achieves 100% SCR i.e. in the case study analysed, everything that is produced is consumed. Therefore, the optimisation leads to an increase of 13.22% in SCR. The optimisation also meets the temperature restrictions established to ensure the thermal comfort of the occupants, maintaining the indoor temperature in the comfort range of 90% of acceptability practically at all times during the hours the building is occupied.

There are several problems with the thermal model developed in Chapter 4 and used in the MPC. As it was not possible to perform the thermal excitation tests on the whole building, the thermal dynamics of the building could not have been modelled and the 10 heat pumps neither. Therefore, it has been assumed that the models of the *Platform* area and the GR16 heat pump represent the whole building and the HVAC system. This has led to inconsistencies of the operation of the HVAC system, as the optimisation gives outliers that could not occur in a real situation, such as the consumption peaks at 06:20am and 07:40am. In addition, it is worth mentioning that the excitation tests could only be carried out in a period of low temperatures, so the modelling has been only carried out for the heating mode, leaving aside the modelling in cool mode. In addition to only being able to test during low temperature periods, the tests have only been carried out on weekends, a very short period of time, which has limited significantly the availability of data for modelling.

The objective of optimising the set point temperature has not been achieved. This makes it necessary to revise and improve the thermal model because the used model might not be the good one. On the one hand, it seems that there is some unidentified problem in the HVAC system model because the model is not able to correctly represent the relationship between consumption and set point temperature. This may be due to not having considered the indoor temperature in the HVAC system model directly by means for example of the difference between set point and indoor temperature. Moreover, it has been shown that the HVAC system does not operate in a narrow operating range, but that the operating point at which it works is constantly changing. This means that the linearised model at one operating point used as a control model may not represent the dynamics of the system properly.

As future work it deserves special attention to improve the thermal modelling of the building to obtain better optimisation results. This will require the possibility to obtain more and better data from thermal excitation tests. It could be interesting to carry out the tests in another building, which would allow the possibility to optimise a more centralised HVAC system and to test the whole building and not only one area. In this case, multi-zone optimisation could be performed in order to optimise the temperature regarding, for example, the orientation and isolation of different zones of the building. In addition, the tests could also be carried out in times of high temperatures in order to be able to model in cold mode. The building in which this methodology can be applied should also have quality, reliable data and ensure to some extent that there are no problems with sensors or the operation of air conditioning or other systems.

Furthermore, the optimisation should also be applied in more days in order to be able to generalise the correct performance of the proposed optimisation problem.

Finally, considering that the SCR in France is calculated every 30 minutes, it would be convenient to perform the optimisation every 30 minutes and therefore thermally model the building with a 30-minute sampling time. The possibility of being able to perform further tests in another building could provide the chance to make such a change.

# *CHAPTER 6*

# *GENERAL CONCLUSIONS & FUTURE LINES*

---

This chapter outlines the key conclusions of the Thesis, highlighting its principal contributions and proposing potential directions for future research on the subject.

## 6.1 GENERAL CONCLUSIONS

The main objective of this Thesis has been to develop an intelligent EMS implemented in a single building and based on forecasting models. The EMS is designed to meet the energy demand of ESTIA 2 building by utilising the PV energy generated in the frame of SC, with the goal of maximising the SCR and ensuring occupants thermal comfort.

The aim in Chapter 1 has been to set out the general objectives of the Thesis by providing a context to frame these objectives. Based on this, the EMS proposal is presented from which the tasks and stages necessary to complete its design are derived.

The main objective of Chapter 2 has been to predict the hourly electricity consumption for the next 24 hours for the ESTIA 2 building using a NARX type neural network daily trained on small data sets. Circumstances have forced to design models that use little data for training, having to train the model with a small data set of 21 previous days. Training with little data and a simply structured NARX model allows the possibility of training the models on a daily basis and obtaining MAPE results of less than 14%. This allows, in addition to predicting with a low computational cost, to take into account substantial changes that may occur in the consumption pattern, such as the integration of high consumption elements (heavy machinery, building extension...). The LSTM, unlike the NARX, has a complex structure and is more suitable for cases where it is important to learn long-term data dependencies. In this case, as it does not have a large data set and has to use a reduced time window, the NARX has more potential. In addition, when predicting time series, the recurrent term of the NARX has a great advantage compared to models that do not include it, and this has been proven by the substantial improvement of the SVR predictions when introducing a time vector as input. Only in this way has been SVR able to outperform the accuracy with which NARX predicts.

With regard to the prediction of PV production developed in Chapter 3, emphasis has been placed on specifying the various models that have been used in the literature to predict PV production. The focus has been on those models that can best deal with the problems that the intermittent nature of solar irradiance can generate in the PV production curve. Therefore, ML models and an analytical model have been developed to make day-ahead hourly PV production forecasts using measured and predicted solar irradiance data from different meteorological agencies. Firstly, it has been found that by introducing only solar irradiance as input, the best prediction results are achieved. In addition, the comparison of the operation of ML models with the analytical model has led to the conclusion that ML models are able to compensate to a certain extent for errors in the solar irradiance prediction data. Although the ML models show larger errors in their results

when trained with predicted data instead of measured irradiance data, the difference is not as noticeable as that of the analytical model, which predicts 42.22% worse with predicted data.

After having designed the predictive models, the development of the thermal model of ESTIA 2 building where the EMS is to be applied, has been introduced in Chapter 4. This model is the control model of the MPC, a dynamic model that the MPC uses to predict the future behaviour of the system and thus to maximise the SCR. Regarding the first objective defined, it can be stated that the NARX model has been able to model capturing the nonlinearities of the thermal behaviour of the building and the HVAC system. Proof of this is the accuracy of the NARX responses of $T_{in}$ and $Q_{hp}$: a $R^2$ of 0.93 and 0.81 in case of $T_{in}$ of *Test 1 data set* and *Test 2 data set* respectively have been achieved. In case of $Q_{hp}$. $R^2$ of 0.83 and 0.69 of *Test 1 data set* and *Test 2 data set* respectively have been obtained.

However, there have been problems in carrying out excitation tests on the entire ESTIA 2 building. This has meant that the designed model only represents the thermal dynamics and operation of a single area (*Platform*) and a single heat pump (GR16). The *Platform* area, together with being a large space, was the area in which we were able to perform the excitation tests. Furthermore, we wanted to start with a simple model and then move on and extent to a model of the whole building, which was a much more complex model. However, in the context of this Thesis there has not been time to carry out the extension. Therefore, the thermal model of the *Platform* has been used as if it represented the thermal dynamics of the building as a whole and the 10 heat pumps that make up the HVAC system.

Moreover, the excitation tests have only been possible to perform at weekends. The lack of sufficient data has meant that the training of the NARX model has had to be done with very small data sets. Since NARX is not trained with many data, if it is sometimes linearised at operating points not covered by the training, can present inaccuracy problems. This may be the reason why in some cases the linear NARX models do not improve the accuracy of the proposed Box-Jenkins linear model.

Finally, the sampling time of 20 minutes forces the optimisation to be carried out every 20 minutes, which does not fit in with the SCR calculation that must be carried out in France every 30 minutes. This also contrasts with the sampling time of the predictive models, which predict every hour. Although the aim was to establish a consistent sampling time in all the phases of the Thesis, the accessibility of the data and the circumstances surrounding the case study did not make it possible.

Chapter 5 integrates the work done in previous chapters to conform the optimisation of the EMS that has had the task of controlling the HVAC system by means of the set point temperature in

order to increase the SCR as much as possible. Thus, a comparison of a case study is introduced where the SCR is calculated with and without the application of the optimisation. It is concluded that the MPC-based EMS increases the SCR up to 100% while ensuring the thermal comfort of the occupants at all times.

In spite of this, not all the expected objectives have been achieved, as the MPC does not manage to optimise the set point temperature due to an unidentified inconsistency in the HVAC system model. Two possible errors have been identified, which might cause the model to be not right and need to be revised. On the one hand, the heat pump model does not include the indoor temperature variable in the way we believe it should. The difference between the indoor temperature and the set point temperature is not taken into account to determine the consumption that the heat pump should provide. On the other hand, it has been seen that the heat pump model does not keep operating at a small operating range, but its operation range is wider. This means that by linearising the model to a single OP, the model is not able to describe the dynamics of the system at all times.

## 6.2 FUTURE LINES

Having reviewed the conclusions drawn chapter by chapter, i.e. considering each part of the EMS, the following section defines the research lines that can be developed in the future.

- As for the data pre-processing process carried out before the design of the predictive models, methods such as Principal Component Analysis (PCA) could be applied. This mathematical technique helps to reduce the complexity of the data, reducing its dimensionality and helping to obtain key information from these data. These features could make the selection of inputs and the time window of the predictive model perhaps more effective [157].
- Prediction models have been designed through error trials to reduce as much as possible the selected error metric. This may mean that the values selected for the hyperparameters might not be optimal, as we may be in a local minimum. In the future, techniques for the optimisation of the hyperparameters such as genetic algorithms could be applied.
- HVAC system can be modelled using Spectral Decomposition. This technique could help to decompose the used data in different frequencies helping to adjust better each model to each frequency. By working with separate models for different frequencies, the overall accuracy of the model can be improved, because it focuses better on representing different signal behaviours [232].
- There has not been time to extend the study to cases of e.g. slightly higher temperatures or more irregular PV production days. However, in order to be able to generalize the results of the optimisation problem, it should be applied in more than one day.
- Taking into account that the control model must represent a nonlinear systems such as the HVAC system, a nonlinear optimisation could be carried out and the results could be compared with those obtained following the methodology introduced in the Thesis.

The problem with data accessibility has been a transversal issue throughout this Thesis process. After having validated the methodology, contributions could be extended by choosing a new case study where the availability of data is wider. In this sense, we have started collaborating with ULMA Packaging, a company located in Oñati (Gipuzkoa), in order to use some of their buildings equipped with PV panels as possible case studies. ULMA is made up of five buildings with PV production facilities in some of them and heat pumps that the EMS could use as FLs. In addition, this company has more detailed data stored for each of the consumption elements of ULMA's buildings, as well as indoor and outdoor temperature data. Furthermore, real occupancy data is available, which has been proved to be an interesting input for models to forecast building energy consumption. Thus:

- EMS could have models predicting consumption and production trained with more and better quality data that can further improve its operation. In addition, together with having available real occupancy data of the buildings, meteorological predicted data from Meteo Galicia could be obtained with a resolution of 4km.
- As the set point temperature data is also available, the building thermal model could be built with a NARX model trained with extensive data sets and thus be able to represent a wider range of scenarios. In addition, the modelling of the HVAC system could be simpler because the operation of the system is simpler and more centralised than the analysed case in this Thesis: in ESTIA 2 building the heat pumps were connected to a network of 73 indoor units located throughout the building and the indoor units in each office could be started independently obtaining chaotic and decentralised performance of the HVAC system.
- By having data from not just one building but from the five that comprise ULMA, the self-consumption could be extended to a framework of collective self-consumption, where the PV production generated could meet the consumption of several buildings of the company.

Finally, the work done in this Thesis could be extended by increasing the scope of the MPC. In this work the MPC has sought to maximise the SCR, however, economic criteria could be added to this objective. It could be interesting to calculate the economic benefit that could come with increasing the SCR, since economic savings are also an important factor to be taken into account for the possible participants in SC or in the case of CSC.

# *BIBLIOGRAPHY*

[1] European Parliament and Council of the European Union, 'Directive (EU) 2018/2001 of 11 December 2018 on the promotion of the use of energy from renewable sources (recast).' Official Journal of the European Union, Dec. 21, 2018. Accessed: May 25, 2024. [Online]. Available: https://eur-lex.europa.eu/legal-content/ES/TXT/?uri=CELEX%3A32018L2001

[2] European Parliament and Council of the European Union, 'Directive (EU) 2023/2413 of 18 October 2023 amending Directive (EU) 2018/2001, Regulation (EU) 2018/1999 and Directive 98/70/EC as regards the promotion of energy from renewable sources, and repealing Council Directive (EU) 2015/652.' Official Journal of the European Union, Oct. 31, 2023. Accessed: May 24, 2024. [Online]. Available: https://eur-lex.europa.eu/eli/dir/2023/2413/oj

[3] F. Perez, 'Control of AC/DC Microgrids with Renewables in the Context of Smart Grids: Including Ancillary Services and Electric Mobility', Automatic, Université Paris-Saclay; Universidade federal de Itajuba, Brasil, 2020. Accessed: May 24, 2024. [Online]. Available: https://tel.archives-ouvertes.fr/tel-03050337

[4] M. Stephant, D. Abbes, K. Hassam-Ouari, A. Labrunie, and B. Robyns, 'Distributed optimisation of energy profiles to improve photovoltaic self-consumption on a local energy community', *Simulation Modelling Practice and Theory*, vol. 108, p. 102242, Apr. 2021, doi: 10.1016/j.simpat.2020.102242.

[5] R. H. Lasseter, 'MicroGrids', in *2002 IEEE Power Engineering Society Winter Meeting. Conference Proceedings (Cat. No.02CH37309)*, New York, NY, USA: IEEE, 2002, pp. 305–308. doi: 10.1109/PESW.2002.985003.

[6] J. Yan, F. Wang, H. Wang, J. Tian, and F. Zhuo, 'Coordinated Control Strategy of Multiple DC Microgrids Containing Large-scale PV Systems', in *2021 IEEE 1st International Power Electronics and Application Symposium (PEAS)*, Shanghai, China: IEEE, Nov. 2021, pp. 1–6. doi: 10.1109/PEAS53589.2021.9628441.

[7] M. Rousselot, and F. Pinto Da Rocha, 'Energy efficiency trends in buildings in the EU', *Odysse*, p. 4, Jun. 2021.

[8] M. Economidou, V. Todeschi, P. Bertoldi, D. D'Agostino, P. Zangheri, and L. Castellazzi, 'Review of 50 years of EU energy efficiency policies for buildings', *Energy and Buildings*, vol. 225, p. 110322, Oct. 2020, doi: 10.1016/j.enbuild.2020.110322.

[9] Ministerio para la Transición Ecológica y el Reto Demográfico, 'Cambio climático. Mitigación: políticas y medidas. Residencial, comercial e institucional.', Ministerio para la Transición Ecológica y el Reto Demográfico, gubernamental. Accessed: Apr. 13, 2024. [Online]. Available: https://www.miteco.gob.es/es/cambio-climatico/temas/mitigacion-politicas-y-medidas/edificacion.html

[10] U. Bariss, A. Dandens, and D. Blumberga, 'Smart meters as enablers for feedback information induced energy efficiency and demand response: Case analysis in Latvia', in *2015 IEEE 5th International Conference on Power Engineering, Energy and Electrical Drives (POWERENG)*, Riga, Latvia: IEEE, May 2015, pp. 69–73. doi: 10.1109/PowerEng.2015.7266297.

[11] European Parliament and Council of the European Union, 'Directive 2006/32/EC of 5 April 2006 on energy end-use efficiency and energy services and repealing Council Directive 93/76/EEC'. Official Journal of the European Union, Apr. 27, 2006. Accessed: May 24, 2024. [Online]. Available: https://eur-lex.europa.eu/legal-content/EN/TXT/?uri=celex%3A32006L0032

[12] European Parliament and Council of the European Union, 'Directive 2012/27/EU of 25 October 2012 on energy efficiency, amending Directives 2009/125/EC and 2010/30/EU and repealing Directives 2004/8/EC and 2006/32/EC'. Official Journal of the European Union, Nov. 14, 2012. Accessed: Jul. 07, 2024. [Online]. Available: https://eur-lex.europa.eu/eli/dir/2012/27/oj

[13] European Parliament and Council of the European Union, 'Directive (EU) 2023/1791 of 13 September 2023 on energy efficiency and amending Regulation (EU) 2023/955 (recast).' Official Journal of the European Union, Sep. 20, 2023. Accessed: May 24, 2024. [Online]. Available: https://eur-lex.europa.eu/eli/dir/2023/1791/oj

[14] 'En vigor la nueva Directiva Europea de eficiencia energética', Certificado de Eficiencia Energética. Accessed: May 22, 2024. [Online]. Available: https://certificadodeeficienciaenergetica.com/blog/vigor-nueva-directiva-europea-eficiencia-energetica/#Certificado_de_eficiencia_energetica_documento_clave

[15] Endesa Fundación, 'Smart Buildings y domótica'. Accessed: May 22, 2024. [Online]. Available: https://www.fundacionendesa.org/es/educacion/endesa-educa/recursos/smart-building-casa-domotica

[16] European Commision, 'Overview Article - Smart buildings and smart technologies in Europe: state of play and perspectives', Dec. 07, 2023. Accessed: Jul. 07, 2024. [Online]. Available: https://build-up.ec.europa.eu/en/resources-and-tools/articles/overview-article-smart-buildings-and-smart-technologies-europe-state#:~:text=EU%20policies%20related%20to%20smart,system%2C%20and%20thus%20save%20energy.

[17] European Parliament and Council of the European Union, 'Directive 2010/31/EU of 19 May 2010 on the energy performance of buildings (recast)'. Official Journal of the European Union, Jun. 18, 2010. Accessed: May 28, 2024. [Online]. Available: https://eur-lex.europa.eu/eli/dir/2010/31/oj

[18] European Commision, 'Commission sets out actions to digitalise the energy sector to improve efficiency and renewables integration'. Accessed: May 22, 2024. [Online]. Available: https://ec.europa.eu/commission/presscorner/detail/en/ip_22_6228

[19] UKGBC, 'Net Zero Carbon Buildings Framework'. Accessed: May 22, 2024. [Online]. Available: https://ukgbc.org/resources/net-zero-carbon-buildings-framework/

[20] International Energy Agency (IEA), 'Net Zero by 2050. A Roadmap for the Global Energy Sector', IEA, May 2021. Accessed: Jul. 07, 2024. [Online]. Available: https://www.iea.org/reports/net-zero-by-2050

[21] Interreg Europe, 'Renewable energy self-consumption', Interreg Europe, Sep. 2020. Accessed: May 22, 2024. [Online]. Available: https://www.interregeurope.eu/sites/default/files/inline/Energy_self-consumption__Policy_brief_final.pdf

[22] A. Al-Sorour, M. Fazeli, M. Monfared, A. Fahmy, J. R. Searle, and R. P. Lewis, 'Enhancing PV Self-Consumption Within an Energy Community Using MILP-Based P2P Trading', *IEEE Access*, vol. 10, pp. 93760–93772, 2022, doi: 10.1109/ACCESS.2022.3202649.

[23] EDF, 'Collective self-consumption: share your electricity locally', The solar self-consumption. Accessed: May 24, 2024. [Online]. Available: https://www.edf.fr/en/the-edf-group/supporting-our-clients-on-a-daily-basis/the-solar-self-consumption/collective-self-consumption-producing-and-consuming-renewable-energy-locally

[24] Crusol Energías Renovables, 'Collective self-consumption in Spain. Explanation and practical example'. Accessed: May 22, 2024. [Online]. Available: https://www.crusol.com/collective-self-consumption-in-spain-explanation-and-practical-example/

[25] D. Frieden, J. Roberts, and A. F. Gubina, 'Overview of emerging regulatory frameworks on collective self-consumption and energy communities in Europe', *Int. Conf. Eur. Energy Mark. EEM*, 2019, doi: 10.1109/EEM.2019.8916222.

[26] Jefatura del Estado, 'Real Decreto-ley 15/2018, de 5 de octubre, de medidas urgentes para la transición energética y la protección de los consumidores.' Boletín Oficial del Estado (BOE), Oct. 06, 2018. Accessed: Jul. 06, 2024. [Online]. Available: https://www.boe.es/buscar/pdf/2018/BOE-A-2018-13593-consolidado.pdf

[27] Ministerio para la Transición Ecológica y el Reto Demográfico, 'Orden TED/1247/2021, de 15 de noviembre, por la que se modifica, para la implementación de coeficientes de reparto variables en autoconsumo colectivo, el anexo I del Real Decreto 244/2019, de 5 de abril, por el que se regulan las condiciones administrativas, técnicas y económicas del autoconsumo de energía eléctrica.' Boletín Oficial del Estado (BOE), Nov. 16, 2021. Accessed: May 29, 2024. [Online]. Available: https://www.boe.es/buscar/doc.php?id=BOE-A-2021-18706

[28] Instituto para la Diversificación y Ahorro de la Energía (IDAE), 'Guia de Autoconsumo Colectivo', IDAE, Madrid, Spain, 1, 2023. Accessed: Jul. 07, 2024. [Online]. Available: https://www.idae.es/publicaciones/guia-de-autoconsumo-colectivo

[29] Enedis, 'enedis.fr'. Accessed: May 24, 2024. [Online]. Available: https://www.enedis.fr/

[30] Enogrid, 'Les webinaires sur l'autoconsommation collective en replay', Enogrid. Accessed: May 24, 2024. [Online]. Available: https://enogrid.com/replay-webinaires-autoconsommation-collective/

[31] Enogrid, 'Les clés de réparition en autoconsommation collective'. Accessed: May 24, 2024. [Online]. Available: https://app.livestorm.co/enogrid/les-cles-de-repartition-en-autoconsommation-collective/live?s=80966cdb-bd51-4c23-aba1-1dca3cc848f6#/chat

[32] R. Trevisan, S. Ruffini, E. Ghiani, O. Caboni, and R. Papa, 'Optimal Sizing of PV and Storage in Collective Self-Consumption Groups in Condominiums', in *2023 International Conference on Future Energy Solutions (FES)*, Vaasa, Finland: IEEE, Jun. 2023, pp. 1–6. doi: 10.1109/FES57669.2023.10182815.

[33] M. Gržanić and T. Capuder, 'Is dynamic energy sharing really necessary? The case study of collective renewable self-consumers in Croatia', in *2023 IEEE PES Conference on Innovative Smart Grid Technologies - Middle East (ISGT Middle East)*, Abu Dhabi, United Arab Emirates: IEEE, Mar. 2023, pp. 1–5. doi: 10.1109/ISGTMiddleEast56437.2023.10078631.

[34] N. Goitia-Zabaleta, A. Milo, H. Gaztanaga, and E. Fernandez, 'Full P2P-based Residential Energy Community vs Collective Self-Consumption in Spanish scenario: Participants sizing analysis', in *2022 18th International Conference on the European Energy Market (EEM)*, Ljubljana, Slovenia: IEEE, Sep. 2022, pp. 1–6. doi: 10.1109/EEM54602.2022.9921076.

[35] M. S. Simoiu, I. Fagarasan, S. Ploix, V. Calofir, and S. S. Iliescu, 'Towards Energy Communities: A Multi-Agent Case Study', in *2022 IEEE International Conference on Automation, Quality and Testing, Robotics (AQTR)*, Cluj-Napoca, Romania: IEEE, May 2022, pp. 1–6. doi: 10.1109/AQTR55203.2022.9802060.

[36] D. Menniti, N. Sorrentino, A. Pinnarelli, S. Mendicino, P. Vizza, and G. Polizzi, 'A blockchain based incentive mechanism for increasing collective self-consumption in a nonsumer community', in *2020 17th International Conference on the European Energy Market (EEM)*, Stockholm, Sweden: IEEE, Sep. 2020, pp. 1–6. doi: 10.1109/EEM49802.2020.9221899.

[37] F. Padovani, M. Topel, and B. Laumert, 'Case Study of Shared Solar Applications in a Swedish Energy Community', in *2023 IEEE PES Innovative Smart Grid Technologies Europe (ISGT EUROPE)*, Grenoble, France: IEEE, Oct. 2023, pp. 1–5. doi: 10.1109/ISGTEUROPE56780.2023.10408317.

[38] R. Tjandra *et al.*, 'Optimal sizing of Battery Energy Storage Systems for self-consumption in Urban Micro-grids', in *2022 IEEE PES Innovative Smart Grid Technologies - Asia (ISGT Asia)*, Singapore, Singapore: IEEE, Nov. 2022, pp. 404–408. doi: 10.1109/ISGTAsia54193.2022.10003603.

[39] A. J. Gil Mena, V. F. Nasimba Medina, A. Bouakkaz, and S. Haddad, 'Analysis and optimisation of collective self-consumption in residential buildings in Spain', *Energy and Buildings*, vol. 283, p. 112812, Mar. 2023, doi: 10.1016/j.enbuild.2023.112812.

[40] A. Jager-Waldau *et al.*, 'Self-consumption of electricity produced with photovoltaic systems in apartment buildings - Update of the situation in various IEA PVPS countries', in *2020 47th IEEE Photovoltaic Specialists Conference (PVSC)*, Calgary, AB, Canada: IEEE, Jun. 2020, pp. 0938–0950. doi: 10.1109/PVSC45281.2020.9300442.

[41] M. Molina-Solana, M. Ros, M. D. Ruiz, J. Gómez-Romero, and M. J. Martin-Bautista, 'Data science for building energy management: A review', *Renewable and Sustainable Energy Reviews*, vol. 70, pp. 598–609, Apr. 2017, doi: 10.1016/j.rser.2016.11.132.

[42] A. M. Al-Ghaili, H. Kasim, N. M. Al-Hada, B. N. Jorgensen, M. Othman, and J. Wang, 'Energy Management Systems and Strategies in Buildings Sector: A Scoping Review', *IEEE Access*, vol. 9, pp. 63790–63813, 2021, doi: 10.1109/ACCESS.2021.3075485.

[43] K. Mason and S. Grijalva, 'A review of reinforcement learning for autonomous building energy management', *Computers & Electrical Engineering*, vol. 78, pp. 300–312, Sep. 2019, doi: 10.1016/j.compeleceng.2019.07.019.

[44] S. Aman, Y. Simmhan, and V. K. Prasanna, 'Improving Energy Use Forecast for Campus Micro-grids Using Indirect Indicators', in *2011 IEEE 11th International Conference on Data Mining Workshops*, Vancouver, BC, Canada: IEEE, Dec. 2011, pp. 389–397. doi: 10.1109/ICDMW.2011.95.

[45] S. M. Tercan, A. Demirci, E. Gokalp, and U. Cali, 'Maximizing self-consumption rates and power quality towards two-stage evaluation for solar energy and shared energy storage empowered microgrids', *Journal of Energy Storage*, vol. 51, p. 104561, Jul. 2022, doi: 10.1016/j.est.2022.104561.

[46] K. Ettalbi, H. Elabd, M. Ouassaid, and M. Maaroufi, 'A comparative study of energy management systems for PV self-consumption', in *2016 International Renewable and Sustainable Energy Conference (IRSEC)*, Marrakech: IEEE, Nov. 2016, pp. 1086–1091. doi: 10.1109/IRSEC.2016.7983966.

[47] A. Baniasadi, D. Habibi, W. Al-Saedi, and M. A. S. Masoum, 'PV Self-Consumption Enhancement with Optimal Residential Thermal Energy Management', in *2019 9th International Conference on Power and Energy Systems (ICPES)*, Perth, Australia: IEEE, Dec. 2019, pp. 1–6. doi: 10.1109/ICPES47639.2019.9105462.

[48] D. van der Meer, G. R. Chandra Mouli, G. Morales-Espana Mouli, L. R. Elizondo, and P. Bauer, 'Energy Management System With PV Power Forecast to Optimally Charge EVs at the Workplace', *IEEE Trans. Ind. Inf.*, vol. 14, no. 1, pp. 311–320, Jan. 2018, doi: 10.1109/TII.2016.2634624.

[49] J. Salpakari, T. Rasku, J. Lindgren, and P. D. Lund, 'Flexibility of electric vehicles and space heating in net zero energy houses: an optimal control model with

thermal dynamics and battery degradation', *Applied Energy*, vol. 190, pp. 800–812, 2017, doi: 10.1016/j.apenergy.2017.01.005.

[50] D. Gudmunds, E. Nyholm, M. Taljegard, and M. Odenberger, 'Self-consumption and self-sufficiency for household solar producers when introducing an electric vehicle', *Renewable Energy*, vol. 148, pp. 1200–1215, Apr. 2020, doi: 10.1016/j.renene.2019.10.030.

[51] J. Aguilar, A. Garces-Jimenez, M. D. R-Moreno, and R. García, 'A systematic literature review on the use of artificial intelligence in energy self-management in smart buildings', *Renewable and Sustainable Energy Reviews*, vol. 151, p. 111530, Nov. 2021, doi: 10.1016/j.rser.2021.111530.

[52] G. Halhoul Merabet *et al.*, 'Intelligent building control systems for thermal comfort and energy-efficiency: A systematic review of artificial intelligence-assisted techniques', *Renewable and Sustainable Energy Reviews*, vol. 144, p. 110969, Jul. 2021, doi: 10.1016/j.rser.2021.110969.

[53] T. Farkas *et al.*, 'Assessing the Electrical Energy Consumption for Designing and Developing an Energy Management System in an Educational Building in Romania', in *2023 58th International Universities Power Engineering Conference (UPEC)*, Dublin, Ireland: IEEE, Aug. 2023, pp. 1–6. doi: 10.1109/UPEC57427.2023.10294433.

[54] Q. Jiang, J. Chen, J. Hou, and Y. Liu, 'Research on building energy management in HVAC control system for university library', *Energy Procedia*, vol. 152, pp. 1164–1169, Oct. 2018, doi: 10.1016/j.egypro.2018.09.152.

[55] J. Kang, Y. Guo, and J. Liu, 'Rule-based Energy Management Strategies for a Fuel Cell-Battery Hybrid Locomotive', presented at the IEEE 4th Conference on Energy Internet and Energy System Integration (EI2), 2020. doi: 10.1109/EI250167.2020.9346652.

[56] S. Zhou, Z. Chen, D. Huang, and T. Lin, 'Model Prediction and Rule Based Energy Management Strategy for a Plug-in Hybrid Electric Vehicle With Hybrid Energy Storage System', *IEEE Transactions on Power Electronics*, vol. 36, no. 5, 2020.

[57] B. Ravanbach, P. Klement, B. Hanke, K. von Maydell, J. Helms, and L. Granja, 'Automatic topology identification of weak low voltage networks and load management strategies for micro-mobility applications', in *2020 Fifteenth International Conference on Ecological Vehicles and Renewable Energies (EVER)*, Monte-Carlo, Monaco: IEEE, Sep. 2020, pp. 1–11. doi: 10.1109/EVER48776.2020.9243050.

[58] M. Jafari and Z. Malekjamshidi, 'Optimal energy management of a residential-based hybrid renewable energy system using rule-based real-time control and 2D dynamic programming optimisation method', *Renewable Energy*, vol. 146, pp. 254–266, 2020, doi: https://doi.org/10.1016/j.renene.2019.06.123.

[59] S. Ouédraogo, G. A. Faggianelli, G. Notton, J. L. Duchaud, and C. Voyant, 'Impact of electricity tariffs and energy management strategies on PV/Battery microgrid

performances', *Renewable Energy*, vol. 199, pp. 816–825, 2022, doi: 10.1016/j.renene.2022.09.042.

[60] J. Torres-Moreno, A. Gimenez-Fernandez, M. Perez-Garcia, and F. Rodriguez, 'Energy Management Strategy for Micro-Grids with PV-Battery Systems and Electric Vehicles', *Energies*, vol. 11, no. 3, p. 522, Feb. 2018, doi: 10.3390/en11030522.

[61] A. B. El-Fawair, K. M. Al-Aubidy, and M. A. Al-Khawaldeh, 'Energy Management in Microgrids with Renewable Energy Sources and Energy Storage System', in *2023 20th International Multi-Conference on Systems, Signals & Devices (SSD)*, Mahdia, Tunisia: IEEE, Feb. 2023, pp. 801–806. doi: 10.1109/SSD58187.2023.10411198.

[62] I. Aranzabal *et al.*, 'Optimal Management of an Energy Community with PV and Battery-Energy-Storage Systems', *Energies*, vol. 16, no. 2, p. 789, Jan. 2023, doi: 10.3390/en16020789.

[63] Z. Luo *et al.*, 'Demand Flexibility of Residential Buildings: Definitions, Flexible Loads, and Quantification Methods', *Engineering*, vol. 16, pp. 123–140, Sep. 2022, doi: 10.1016/j.eng.2022.01.010.

[64] D. Yan, T. Li, C. Ma, L. L. Lai, and K. Fung TSANG, 'Cost Effective Energy Management of Home Energy System with Photovoltaic-Battery and Electric Vehicle', in *IECON 2020 The 46th Annual Conference of the IEEE Industrial Electronics Society*, Singapore, Singapore: IEEE, Oct. 2020, pp. 3611–3616. doi: 10.1109/IECON43393.2020.9255317.

[65] A. Chabaud, J. Eynard, and S. Grieu, 'A rule-based strategy to the predictive management of a grid-connected residential building in southern France', *Sustainable Cities and Society*, vol. 30, pp. 18–36, Apr. 2017, doi: 10.1016/j.scs.2016.12.016.

[66] A. Sorour, M. Fazeli, M. Monfared, A. A. Fahmy, J. R. Searle, and R. P. Lewis, 'Forecast-Based Energy Management for Domestic PV-Battery Systems: A U.K. Case Study', *IEEE*, vol. 9, pp. 58953–58965, Apr. 2021, doi: 10.1109/ACCESS.2021.3072961.

[67] A. D. Mustika, R. Rigo-Mariani, V. Debusschere, and A. Pachurka, 'A two-stage management strategy for the optimal operation and billing in an energy community with collective self-consumption', *Applied Energy*, vol. 310, p. 118484, Mar. 2022, doi: 10.1016/j.apenergy.2021.118484.

[68] G. Mor *et al.*, 'Operation and energy flexibility evaluation of direct load controlled buildings equipped with heat pumps', *Energy & Buildings*, vol. 253, p. 111484, 2021, doi: https://doi.org/10.1016/j.enbuild.2021.111484.

[69] M. Wani, A. Swain, and A. Ukil, 'Control Strategies for Energy Optimisation of HVAC Systems in Small Office Buildings using EnergyPlus ™', in *2019 IEEE Innovative Smart Grid Technologies - Asia (ISGT Asia)*, Chengdu, China: IEEE, May 2019, pp. 2698–2703. doi: 10.1109/ISGT-Asia.2019.8880806.

[70] C. D. Korkas, S. Baldi, I. Michailidis, and E. B. Kosmatopoulos, 'Multi-objective control strategy for energy management of grid-connected heterogeneous

microgrids', in *2015 American Control Conference (ACC)*, Chicago, IL, USA: IEEE, Jul. 2015, pp. 5515–5520. doi: 10.1109/ACC.2015.7172202.

[71] S. Chakraborty, G. Modi, and B. Singh, 'A Cost Optimised-Reliable-Resilient-Realtime- Rule-Based Energy Management Scheme for a SPV-BES-Based Microgrid for Smart Building Applications', *IEEE Trans. Smart Grid*, vol. 14, no. 4, pp. 2572–2581, Jul. 2023, doi: 10.1109/TSG.2022.3232283.

[72] A. Sorour, M. Fazeli, M. Monfared, A. Fahmy, J. Searle, and R. Lewis, 'Enhancing Self-consumption of PV-battery Systems Using a Predictive Rule-based Energy Management', in *2021 IEEE PES Innovative Smart Grid Technologies Europe (ISGT Europe)*, Espoo, Finland: IEEE, Oct. 2021, pp. 1–6. doi: 10.1109/ISGTEurope52324.2021.9640051.

[73] A. Herath, S. Kodituwakku, D. Dasanayake, P. Binduhewa, J. Ekanayake, and K. Samarakoon, 'Comparison of Optimisation- and Rule-Based EMS for Domestic PV-Battery Installation with Time-Varying Local SoC Limits', *Electrical and Computer Engineering*, vol. 2019, p. 14, 2019, doi: https://doi.org/10.1155/2019/8162475.

[74] J. B. Rawlings, D. Q. Mayne, and M. Diehl, *Model predictive control: theory, computation, and design*, 2nd edition. Madison, Wisconsin: Nob Hill Publishing, 2017.

[75] T. Mbungu, R. Naidoo, R. Bansal, and M. Bipath, 'Smart SISO-MPC based energy management system for commercial buildings: Technology trends', in *2016 Future Technologies Conference (FTC)*, San Francisco, CA, USA: IEEE, Dec. 2016, pp. 750–753. doi: 10.1109/FTC.2016.7821688.

[76] M. Elkazaz, M. Sumner, and D. Thomas, 'A Hierarchical Centralized Community Energy Management System Using a Model Predictive Controller', in *2020 International Conference on Smart Grids and Energy Systems (SGES)*, Perth, Australia: IEEE, Nov. 2020, pp. 801–806. doi: 10.1109/SGES51519.2020.00148.

[77] Z. Chen, Y. Zhang, and T. Zhang, 'An intelligent control approach to home energy management under forecast uncertainties', in *2015 IEEE 5th International Conference on Power Engineering, Energy and Electrical Drives (POWERENG)*, Riga, Latvia: IEEE, May 2015, pp. 657–662. doi: 10.1109/PowerEng.2015.7266395.

[78] J. Ospina *et al.*, 'Sampling-Based Model Predictive Control of PV-Integrated Energy Storage System Considering Power Generation Forecast and Real-Time Price', *IEEE Power Energy Technol. Syst. J.*, vol. 6, no. 4, pp. 195–207, Dec. 2019, doi: 10.1109/JPETS.2019.2935703.

[79] D. Watari *et al.*, 'Thermal Comfort Aware Online Energy Management Framework for a Smart Residential Building', in *2021 Design, Automation & Test in Europe Conference & Exhibition (DATE)*, Grenoble, France: IEEE, Feb. 2021, pp. 535–538. doi: 10.23919/DATE51398.2021.9473922.

[80] R. Eini and S. Abdelwahed, 'A Neural Network-based Model Predictive Control Approach for Buildings Comfort Management', in *2020 IEEE International Smart*

*Cities Conference (ISC2)*, Piscataway, NJ, USA: IEEE, Sep. 2020, pp. 1–7. doi: 10.1109/ISC251055.2020.9239051.

[81] U. R. Nair, M. Sandelic, A. Sangwongwanich, T. Dragicevic, R. Costa-Castello, and F. Blaabjerg, 'Grid Congestion Mitigation and Battery Degradation Minimisation Using Model Predictive Control in PV-Based Microgrid', *IEEE Trans. Energy Convers.*, vol. 36, no. 2, pp. 1500–1509, Jun. 2021, doi: 10.1109/TEC.2020.3032534.

[82] P. Scarabaggio, R. Carli, J. Jantzen, and M. Dotoli, 'Stochastic Model Predictive Control of Community Energy Storage under High Renewable Penetration', in *2021 29th Mediterranean Conference on Control and Automation (MED)*, PUGLIA, Italy: IEEE, Jun. 2021, pp. 973–978. doi: 10.1109/MED51440.2021.9480353.

[83] Interreg, 'Interreg POCTEFA (Spain – France – Andorra)', Interreg POCTEFA. Accessed: Oct. 31, 2022. [Online]. Available: https://interreg.eu/programme/interreg-spain-france-andorra/

[84] T. Rawat, J. Singh, and S. Sharma, 'Performance Analysis of 400 kWp Rooftop Solar Plant at Swami Keshvanand Institute of Technology, Management & Gramothan, Jaipur using PVsyst', in *2023 International Conference on Power, Instrumentation, Energy and Control (PIECON)*, Aligarh, India: IEEE, Feb. 2023, pp. 1–6. doi: 10.1109/PIECON56912.2023.10085828.

[85] R. J. de Dear and G. S. Brager, 'Thermal comfort in naturally ventilated buildings: revisions to ASHRAE Standard 55', *Energy and Buildings*, vol. 34, no. 6, pp. 549–561, Jul. 2002, doi: 10.1016/S0378-7788(02)00005-1.

[86] Y. Sun, F. Haghighat, and B. C. M. Fung, 'A review of the-state-of-the-art in data-driven approaches for building energy prediction', *Energy and Buildings*, vol. 221, p. 110022, Aug. 2020, doi: 10.1016/j.enbuild.2020.110022.

[87] European Commission, 'Energy Performance of Buildings Directive', European Commission. Accessed: Jul. 03, 2024. [Online]. Available: https://energy.ec.europa.eu/topics/energy-efficiency/energy-efficient-buildings/energy-performance-buildings-directive_en

[88] Ministère de la transition écologique et de la cohésion territoriale, 'Chiffres clés de l'énergie', Ministère de la transition écologique et de la cohésion territoriale, governmental Édition 2023, 2023. Accessed: Jul. 04, 2024. [Online]. Available: https://www.statistiques.developpement-durable.gouv.fr/edition-numerique/chiffres-cles-energie-2023/8-consommation-finale-denergiepar-secteur-et

[89] J. Buitrago and S. Asfour, 'Short-term forecasting of electric loads using nonlinear autoregressive artificial neural networks with exogenous vector inputs', *Energies*, vol. 10, pp. 1-24, 2017, doi: 10.3390/en10010040.

[90] F. M. Bianchi, E. Maiorino, M. C. Kampffmeyer, A. Rizzi, and R. Jenssen, 'An overview and comparative analysis of Recurrent Neural Networks for Short Term Load Forecasting', *Springer International Publishing*, pp. 1–41, 2018, doi: 10.1007/978-3-319-70338-1.

[91] R. J. Hyndman, *Forecasting with exponential smoothing: the state space approach*. in Springer series in statistics. Berlin Heidelberg: Springer, 2008.

[92] P. Singh and P. Dwivedi, 'Integration of new evolutionary approach with artificial neural network for solving short term load forecast problem', *Applied Energy*, vol. 217, pp. 537–549, May 2018, doi: 10.1016/j.apenergy.2018.02.131.

[93] A. Azeem, I. Ismail, S. M. Jameel, and V. R. Harindran, 'Electrical Load Forecasting Models for Different Generation Modalities: A Review', *IEEE Access*, vol. 9, pp. 142239–142263, 2021, doi: 10.1109/ACCESS.2021.3120731.

[94] Y.-H. Hsiao, 'Household Electricity Demand Forecast Based on Context Information and User Daily Schedule Analysis From Meter Data', *IEEE Trans. Ind. Inf.*, vol. 11, no. 1, pp. 33–43, Feb. 2015, doi: 10.1109/TII.2014.2363584.

[95] M. Bourdeau, X. Q. Zhai, E. Nefzaoui, X. Guo, and P. Chatellier, 'Modeling and forecasting building energy consumption: A review of data-driven techniques', *Sustainable Cities and Society*, vol. 48, p. 101533, 2019, doi: 10.1016/j.scs.2019.101533.

[96] C. Aparicio-Fernández, J.-L. Vivancos, P. Cosar-Jorda, and R. A. Buswell, 'Energy Modelling and Calibration of Building Simulations: A Case Study of a Domestic Building with Natural Ventilation', *Energies*, vol. 12, no. 17, p. 3360, Aug. 2019, doi: 10.3390/en12173360.

[97] R. San Jose, J. L. Perez, L. Perez, and R. M. Gonzalez-Barras, 'Sensitivity Analysis of Building Energy Demand for Downscaled Climate Scenarios', in *2018 International Conference on Computational Science and Computational Intelligence (CSCI)*, Las Vegas, NV, USA: IEEE, Dec. 2018, pp. 513–518. doi: 10.1109/CSCI46756.2018.00105.

[98] M. Khalil, A. S. McGough, Z. Pourmirza, M. Pazhoohesh, and S. Walker, 'Machine Learning, Deep Learning and Statistical Analysis for forecasting building energy consumption — A systematic review', *Engineering Applications of Artificial Intelligence*, no. 115, p. 105287, 2022, doi: https://doi.org/10.1016/j.engappai.2022.105287.

[99] S. A. Vaghefi, M. A. Jafari, J. Zhu, J. Brouwer, and Y. Lu, 'A Hybrid Physics-Based and Data Driven Approach to Optimal Control of Building Cooling/Heating Systems', *IEEE Trans. Automat. Sci. Eng.*, vol. 13, no. 2, pp. 600–610, Apr. 2016, doi: 10.1109/TASE.2014.2356337.

[100] K. Santosh, S. Ghosh, and N. Das, *Deep Learning Models for Medical Imaging*, 1st ed. Academic Press, 2021. Accessed: Jul. 03, 2024. [Online]. Available: https://doi.org/10.1016/C2020-0-00344-0

[101] K. R. Dalal, 'Analysing the Role of Supervised and Unsupervised Machine Learning in IoT', in *2020 International Conference on Electronics and Sustainable Communication Systems (ICESC)*, Coimbatore, India: IEEE, Jul. 2020, pp. 75–79. doi: 10.1109/ICESC48915.2020.9155761.

[102] R. P. França, A. C. Borges Monteiro, R. Arthur, and Y. Iano, 'An overview of deep learning in big data, image, and signal processing in the modern digital age', in

*Trends in Deep Learning Methodologies*, Elsevier, 2021, pp. 63–87. doi: 10.1016/B978-0-12-822226-3.00003-9.

[103] R. Ahmed, V. Sreeram, Y. Mishra, and M. D. Arif, 'A review and evaluation of the state-of-the-art in PV solar power forecasting: Techniques and optimisation', *Renewable and Sustainable Energy Reviews*, vol. 124, 2020, doi: https://doi.org/10.1016/j.rser.2020.109792.

[104] T. Jakasa, I. Androcec, and P. Sprcic, 'Electricity price forecasting — ARIMA model approach', in *2011 8th International Conference on the European Energy Market (EEM)*, Zagreb, Croatia: IEEE, May 2011, pp. 222–225. doi: 10.1109/EEM.2011.5953012.

[105] H. Chitsaz, H. Shaker, H. Zareipour, D. Wood, and N. Amjady, 'Short-term electricity load forecasting of buildings in microgrids', *Energy and Buildings*, vol. 99, pp. 50–60, Jul. 2015, doi: 10.1016/j.enbuild.2015.04.011.

[106] K. D, K. D, and D. K, 'Efficient load forecasting in Educational Laboratory facilites: an ARIMA and k-means approach', in *2023 International Conference on Energy, Materials and Communication Engineering (ICEMCE)*, Madurai, India: IEEE, Dec. 2023, pp. 1–6. doi: 10.1109/ICEMCE57940.2023.10434120.

[107] R. Olu-Ajayi, H. Alaka, H. Owolabi, L. Akanbi, and S. Ganiyu, 'Data-Driven Tools for Building Energy Consumption Prediction: A Review', *Energies*, vol. 16, no. 6, p. 2574, Mar. 2023, doi: 10.3390/en16062574.

[108] G. Romeo, 'Data analysis for business and economics', in *Elements of Numerical Mathematical Economics with Excel*, Elsevier, 2020, pp. 695–761. doi: 10.1016/B978-0-12-817648-1.00013-X.

[109] D. Liu, Q. Yang, and F. Yang, 'Forecasting Energy Consumption of Office Building by Time Series Analysis Methods based on Machine Learning Algorithm', in *2019 6th International Conference on Information Science and Control Engineering (ICISCE)*, Shanghai, China: IEEE, Dec. 2019, pp. 297–301. doi: 10.1109/ICISCE48695.2019.00066.

[110] D. Zhao, M. Zhong, X. Zhang, and X. Su, 'Energy consumption predicting model of VRV (Variable refrigerant volume) system in office buildings based on data mining', *Energy*, vol. 102, pp. 660–668, May 2016, doi: 10.1016/j.energy.2016.02.134.

[111] L. Alhmoud and Q. Nawafleh, 'Short-Term Load Forecasting for Jordan Power System Based on NARX-ELMAN Neural Network and ARMA Model', *IEEE Canadian Journal of Electrical and Computer Engineering*, vol. 44, no. 3, pp. 356–363, 2021, doi: 10.1109/ICJECE.2021.3076124.

[112] M. Wasesa, A. R. Tiara, M. A. Afrianto, F. I. Ramadhan, I. N. Haq, and J. Pradipta, 'SARIMA and Artificial Neural Network Models for Forecasting Electricity Consumption of a Microgrid Based Educational Building', in *2020 IEEE International Conference on Industrial Engineering and Engineering Management (IEEM)*, Singapore, Singapore: IEEE, Dec. 2020, pp. 210–214. doi: 10.1109/IEEM45057.2020.9309943.

[113] Y. Yang, J. Che, C. Deng, and L. Li, 'Sequential grid approach based support vector regression for short-term electric load forecasting', *Applied Energy*, vol. 238, pp. 1010–1021, Mar. 2019, doi: 10.1016/j.apenergy.2019.01.127.

[114] M. Q. Raza, M. Nadarajah, D. Q. Hung, and Z. Baharudin, 'An intelligent hybrid short-term load forecasting model for smart power grids', *Sustainable Cities and Society*, vol. 31, pp. 264–275, May 2017, doi: 10.1016/j.scs.2016.12.006.

[115] D.-M. Petroșanu, 'Designing, Developing and Validating a Forecasting Method for the Month Ahead Hourly Electricity Consumption in the Case of Medium Industrial Consumers', *Processes*, vol. 7, no. 5, p. 310, May 2019, doi: 10.3390/pr7050310.

[116] H. Dagdougui, F. Bagheri, H. Le, and L. Dessaint, 'Neural network model for short-term and very-short-term load forecasting in district buildings', *Energy and Buildings*, vol. 203, p. 109408, Nov. 2019, doi: 10.1016/j.enbuild.2019.109408.

[117] W. Kong, Z. Y. Dong, D. J. Hill, F. Luo, and Y. Xu, 'Short-Term Residential Load Forecasting Based on Resident Behaviour Learning', *IEEE Trans. Power Syst.*, vol. 33, no. 1, pp. 1087–1088, Jan. 2018, doi: 10.1109/TPWRS.2017.2688178.

[118] Z. Khan, T. Hussain, A. Ullah, S. Rho, M. Lee, and S. Baik, 'Towards Efficient Electricity Forecasting in Residential and Commercial Buildings: A Novel Hybrid CNN with a LSTM-AE based Framework', *Sensors*, vol. 20, no. 5, p. 1399, Mar. 2020, doi: 10.3390/s20051399.

[119] S.-J. Baek and S.-G. Yoon, 'Short-Term Load Forecasting for Campus Building with Small-Scale Loads by Types Using Artificial Neural Network', in *2019 IEEE Power & Energy Society Innovative Smart Grid Technologies Conference (ISGT)*, Washington, DC, USA: IEEE, Feb. 2019, pp. 1–5. doi: 10.1109/ISGT.2019.8791674.

[120] A. Alammar and W. Jabi, 'Predicting Cooling Energy Demands of Adaptive Facades Using Artificial Neural Network', in *2022 Annual Modeling and Simulation Conference (ANNSIM)*, San Diego, CA, USA: IEEE, Jul. 2022, pp. 656–669. doi: 10.23919/ANNSIM55834.2022.9859413.

[121] N. M. Nawi, W. H. Atomi, and M. Z. Rehman, 'The Effect of Data Pre-processing on Optimised Training of Artificial Neural Networks', *Procedia Technology*, vol. 11, pp. 32–39, 2013, doi: 10.1016/j.protcy.2013.12.159.

[122] G. Kumaravel, S. Kirthiga, G. Vijaya, K. H. A. S. Al Jassasi, S. K. M. AL-Hinai, and A. K. A. Al Ghafreya, 'A Novel Solar PV Generation Forecasting Model for Standalone Power System Using Artificial Neural Network Controller', in *2024 1st International Conference on Trends in Engineering Systems and Technologies (ICTEST)*, Kochi, India: IEEE, Apr. 2024, pp. 1–6. doi: 10.1109/ICTEST60614.2024.10576140.

[123] A. Klein, S. Falkner, S. Bartels, P. Hennig, and F. Hutter, 'Fast bayesian optimisation of machine learning hyperparameters on large datasets', presented at the 20th International Conference on Artificial Intelligence and Statistics, Ft. Lauderdale, FL, USA, 2017. doi: 10.48550/arXiv.1605.07079.

[124] International Energy Agency, 'Global electricity demand set to rise strongly this year and next, reflecting its expanding role in energy systems around the world', IEA 50. Accessed: Jul. 22, 2024. [Online]. Available: https://www.iea.org/news/global-electricity-demand-set-to-rise-strongly-this-year-and-next-reflecting-its-expanding-role-in-energy-systems-around-the-world

[125] Ministerio para la Transición Ecológica y el Reto Demográfico, 'Informe de inventario nacional de gases de efecto invernadero', Ministerio para la Transición Ecológica y el Reto Demográfico, Madrid, Spain, governmental, 2024. Accessed: Jul. 22, 2024. [Online]. Available: https://www.miteco.gob.es/content/dam/miteco/es/calidad-y-evaluacion-ambiental/temas/sistema-espanol-de-inventario-sei-/es-nir-edicion-2024.pdf

[126] U. K. Das *et al.*, 'Forecasting of photovoltaic power generation and model optimisation: A review', *Renewable and Sustainable Energy Reviews*, vol. 81, pp. 912–928, Jan. 2018, doi: 10.1016/j.rser.2017.08.017.

[127] Z. Xin-gang and Z. You, 'Technological progress and industrial performance: A case study of solar photovoltaic industry', *Renewable and Sustainable Energy Reviews*, vol. 81, pp. 929–936, Jan. 2018, doi: 10.1016/j.rser.2017.08.038.

[128] International Renewable Energy Agency (IRENA), 'Renewable Capacity Statistics 2024', IRENA, 2024. [Online]. Available: https://www.irena.org/Publications/2024/Jul/Renewable-energy-statistics-2024

[129] M. Virginia Olano and E. Wesoff, 'Chart: Solar installations set to break global, US records in 2023', Canary Media. [Online]. Available: https://www.canarymedia.com/articles/solar/chart-solar-installations-set-to-break-global-us-records-in-2023

[130] L. M. Halabi, S. Mekhilef, L. Olatomiwa, and J. Hazelton, 'Performance analysis of hybrid PV/diesel/battery system using HOMER: A case study Sabah, Malaysia', *Energy Conversion and Management*, vol. 144, pp. 322–339, Jul. 2017, doi: 10.1016/j.enconman.2017.04.070.

[131] European Commission. Joint Research Centre., *Renewable energy production and potential in EU rural areas.* LU: Publications Office, 2024. Accessed: Jul. 22, 2024. [Online]. Available: https://data.europa.eu/doi/10.2760/458970

[132] A. Al-Othman *et al.*, 'Artificial intelligence and numerical models in hybrid renewable energy systems with fuel cells: Advances and prospects', *Energy Conversion and Management*, vol. 253, p. 115154, Feb. 2022, doi: 10.1016/j.enconman.2021.115154.

[133] F. Wang *et al.*, 'A minutely solar irradiance forecasting method based on real-time sky image-irradiance mapping model', *Energy Conversion and Management*, vol. 220, p. 113075, Sep. 2020, doi: 10.1016/j.enconman.2020.113075.

[134] D. Medved', M. Kolcun, J. Kiraly, O. Shavolkin, and I. Shvedchykova, 'Utilization of Battery Storage System in the Production of Electricity from a Photovoltaic Power Plant', in *2022 22nd International Scientific Conference on Electric Power*

*Engineering (EPE)*, Kouty nad Desnou, Czech Republic: IEEE, Jun. 2022, pp. 1–5. doi: 10.1109/EPE54603.2022.9814137.

[135] K. Başaran, F. Bozyiğit, P. Siano, P. Yıldırım Taşer, and D. Kılınç, 'Systematic literature review of photovoltaic output power forecasting', *IET Renewable Power Generation*, vol. 14, no. 19, pp. 3961–3973, Dec. 2020, doi: 10.1049/iet-rpg.2020.0351.

[136] A. Mellit, A. Massi Pavan, E. Ogliari, S. Leva, and V. Lughi, 'Advanced Methods for Photovoltaic Output Power Forecasting: A Review', *Applied Sciences*, vol. 10, no. 2, p. 487, Jan. 2020, doi: 10.3390/app10020487.

[137] A. Dolara, F. Grimaccia, S. Leva, M. Mussetta, and E. Ogliari, 'A Physical Hybrid Artificial Neural Network for Short Term Forecasting of PV Plant Power Output', *Energies*, vol. 8, no. 2, pp. 1138–1153, Feb. 2015, doi: 10.3390/en8021138.

[138] N. Rahimi *et al.*, 'A Comprehensive Review on Ensemble Solar Power Forecasting Algorithms', *J. Electr. Eng. Technol.*, vol. 18, no. 2, pp. 719–733, Mar. 2023, doi: 10.1007/s42835-023-01378-2.

[139] U. Das *et al.*, 'SVR-Based Model to Forecast PV Power Generation under Different Weather Conditions', *Energies*, vol. 10, no. 7, p. 876, Jun. 2017, doi: 10.3390/en10070876.

[140] K. Barhmi, C. Heynen, S. Golroodbari, and W. van Sark, 'A Review of Solar Forecasting Techniques and the Role of Artificial Intelligence', *Solar*, vol. 4, no. 1, pp. 99–135, Feb. 2024, doi: 10.3390/solar4010005.

[141] S. Sobri, S. Koohi-Kamali, and N. Abd. Rahim, 'Solar photovoltaic generation forecasting methods: A review', *Energy Conversion and Management*, vol. 156, pp. 459–497, Jan. 2018, doi: 10.1016/j.enconman.2017.11.019.

[142] M. Caldas and R. Alonso-Suárez, 'Very short-term solar irradiance forecast using all-sky imaging and real-time irradiance measurements', *Renewable Energy*, vol. 143, pp. 1643–1658, Dec. 2019, doi: 10.1016/j.renene.2019.05.069.

[143] M. J. Espinosa-Gavira, A. Agüera-Pérez, J.-C. Palomares-Salas, J.-J. González-de-la-Rosa, J.-M. Sierra-Fernández, and O. Florencias-Oliveros, 'Cloud motion estimation from small-scale irradiance sensor networks: General analysis and proposal of a new method', *Solar Energy*, vol. 202, pp. 276–293, May 2020, doi: 10.1016/j.solener.2020.03.081.

[144] S. Tiwari, R. Sabzehgar, and M. Rasouli, 'Short Term Solar Irradiance Forecast Using Numerical Weather Prediction (NWP) with Gradient Boost Regression', in *2018 9th IEEE International Symposium on Power Electronics for Distributed Generation Systems (PEDG)*, Charlotte, NC: IEEE, Jun. 2018, pp. 1–8. doi: 10.1109/PEDG.2018.8447751.

[145] S. Theocharides, V. Venizelou, G. Makrides, and G. E. Georghiou, 'Day-ahead Forecasting of Solar Power Output from Photovoltaic Systems Utilising Gradient Boosting Machines', in *2018 IEEE 7th World Conference on Photovoltaic Energy Conversion (WCPEC) (A Joint Conference of 45th IEEE PVSC, 28th PVSEC & 34th EU*

*PVSEC)*, Waikoloa Village, HI: IEEE, Jun. 2018, pp. 2371–2375. doi: 10.1109/PVSC.2018.8547375.

[146] Z. Boussaada, O. Curea, A. Remaci, H. Camblong, and N. Mrabet Bellaaj, 'A Nonlinear Autoregressive Exogenous (NARX) Neural Network Model for the Prediction of the Daily Direct Solar Radiation', *Energies*, vol. 11, p. 620, 2018, doi: 10.3390/en11030620.

[147] W. M. Nkounga *et al.*, 'Short-term Multi Horizons Forecasting of Solar Irradiation Based on Artificial Neural Network with Meteorological Data: Application in the North-west of Senegal', in *2021 Sixteenth International Conference on Ecological Vehicles and Renewable Energies (EVER)*, Monte-Carlo, Monaco: IEEE, May 2021, pp. 1–8. doi: 10.1109/EVER52347.2021.9456600.

[148] M. D. Patel, S. Shah, S. Sinha, R. K. Gupta, S. K. Bharti, and V. P. Singh, 'Solar Irradiation Forecasting - Comparative Analysis of Various Methods', in *2021 IEEE International Conference on Technology, Research, and Innovation for Betterment of Society (TRIBES)*, Raipur, India: IEEE, Dec. 2021, pp. 1–9. doi: 10.1109/TRIBES52498.2021.9751626.

[149] K. Gairaa, M. Guermoui, M. Zaiani, S. Boualit, and S. Benkaciali, 'Contribution of CEEMDAN Decomposition in Enhancing the Forecast of Short-Term Global Solar Irradiation', in *2023 14th International Renewable Energy Congress (IREC)*, Sousse, Tunisia: IEEE, Dec. 2023, pp. 1–5. doi: 10.1109/IREC59750.2023.10389195.

[150] R. De Leone, M. Pietrini, and A. Giovannelli, 'Photovoltaic energy production forecast using support vector regression', *Neural Comput & Applic*, vol. 26, no. 8, pp. 1955–1962, Nov. 2015, doi: 10.1007/s00521-015-1842-y.

[151] A. Dolara, S. Leva, and G. Manzolini, 'Comparison of different physical models for PV power output prediction', *Solar Energy*, vol. 119, pp. 83–99, Sep. 2015, doi: 10.1016/j.solener.2015.06.017.

[152] R. Muhammad Ehsan, S. P. Simon, and P. R. Venkateswaran, 'Day-ahead forecasting of solar photovoltaic output power using multilayer perceptron', *Neural Comput & Applic*, vol. 28, no. 12, pp. 3981–3992, Dec. 2017, doi: 10.1007/s00521-016-2310-z.

[153] M. Hossain, S. Mekhilef, M. Danesh, L. Olatomiwa, and S. Shamshirband, 'Application of extreme learning machine for short term output power forecasting of three grid-connected PV systems', *Journal of Cleaner Production*, vol. 167, pp. 395–405, Nov. 2017, doi: 10.1016/j.jclepro.2017.08.081.

[154] J. Son, Y. Park, J. Lee, and H. Kim, 'Sensorless PV Power Forecasting in Grid-Connected Buildings through Deep Learning', *Sensors*, vol. 18, no. 8, p. 2529, Aug. 2018, doi: 10.3390/s18082529.

[155] J. Huang and M. Perry, 'A semi-empirical approach using gradient boosting and k -nearest neighbors regression for GEFCom2014 probabilistic solar power forecasting', *International Journal of Forecasting*, vol. 32, no. 3, pp. 1081–1086, Jul. 2016, doi: 10.1016/j.ijforecast.2015.11.002.

[156] G.-Q. Lin, L.-L. Li, M.-L. Tseng, H.-M. Liu, D.-D. Yuan, and R. R. Tan, 'An improved moth-flame optimisation algorithm for support vector machine prediction of photovoltaic power generation', *Journal of Cleaner Production*, vol. 253, p. 119966, Apr. 2020, doi: 10.1016/j.jclepro.2020.119966.

[157] K. Kuźniar and M. Zając, 'Some methods of pre-processing input data for neural networks', *Computer Assisted Methods in Engineering and Science*, vol. 22, pp. 141–151, 2015.

[158] J. P. S. Catalao, H. M. I. Pousinho, and V. M. F. Mendes, 'Hybrid Wavelet-PSO-ANFIS Approach for Short-Term Electricity Prices Forecasting', *IEEE Trans. Power Syst.*, vol. 26, no. 1, pp. 137–144, Feb. 2011, doi: 10.1109/TPWRS.2010.2049385.

[159] R. Costa, A. Costa, O. Vilela, and T. Ing Ren, 'Vector Representation and Machine Learning for Short-Term Photovoltaic Power Prediction', in *2023 IEEE International Conference on Systems, Man, and Cybernetics (SMC)*, Honolulu, Oahu, HI, USA: IEEE, Oct. 2023, pp. 1241–1246. doi: 10.1109/SMC53992.2023.10394456.

[160] M. Kolarik, R. Burget, and K. Riha, 'Comparing Normalisation Methods for Limited Batch Size Segmentation Neural Networks', in *2020 43rd International Conference on Telecommunications and Signal Processing (TSP)*, Jul. 2020, pp. 677–680. doi: 10.1109/TSP49548.2020.9163397.

[161] K. J. Iheanetu, 'Solar Photovoltaic Power Forecasting: A Review', *Sustainability*, vol. 14, no. 24, p. 17005, Dec. 2022, doi: 10.3390/su142417005.

[162] T. Ahmad and N. Zhou, 'Ensemble Methods for Probabilistic Solar Power Forecasting: A Comparative Study', in *2023 IEEE Power & Energy Society General Meeting (PESGM)*, Orlando, FL, USA: IEEE, Jul. 2023, pp. 1–5. doi: 10.1109/PESGM52003.2023.10253133.

[163] Y. Xie, C. Li, M. Li, F. Liu, and M. Taukenova, 'An overview of deterministic and probabilistic forecasting methods of wind energy', *iScience*, vol. 26, no. 1, p. 105804, Jan. 2023, doi: 10.1016/j.isci.2022.105804.

[164] H. S. Jang, K. Y. Bae, H.-S. Park, and D. K. Sung, 'Solar Power Prediction Based on Satellite Images and Support Vector Machine', *IEEE Trans. Sustain. Energy*, vol. 7, no. 3, pp. 1255–1263, Jul. 2016, doi: 10.1109/TSTE.2016.2535466.

[165] M. N. Akhter, S. Mekhilef, H. Mokhlis, and N. Mohamed Shah, 'Review on forecasting of photovoltaic power generation based on machine learning and metaheuristic techniques', *IET Renewable Power Generation*, vol. 13, no. 7, pp. 1009–1023, May 2019, doi: 10.1049/iet-rpg.2018.5649.

[166] M. J. Mayer and G. Gróf, 'Extensive comparison of physical models for photovoltaic power forecasting', *Applied Energy*, vol. 283, p. 116239, Feb. 2021, doi: 10.1016/j.apenergy.2020.116239.

[167] W. F. Holmgren, A. T. Lorenzo, M. Leuthold, C. K. Kim, A. D. Cronin, and E. A. Betterton, 'An operational, real-time forecasting system for 250 MW of PV power using NWP, satellite, and DG production data', in *2014 IEEE 40th Photovoltaic*

*Specialist Conference (PVSC)*, Denver, CO, USA: IEEE, Jun. 2014, pp. 0080–0084. doi: 10.1109/PVSC.2014.6925222.

[168] M. Paulescu, E. Paulescu, and V. Badescu, 'Nowcasting solar irradiance for effective solar power plants operation and smart grid management', in *Predictive Modelling for Energy Management and Power Systems Engineering*, Elsevier, 2021, pp. 249–270. doi: 10.1016/B978-0-12-817772-3.00009-4.

[169] R. Perez, S. Kivalov, J. Schlemmer, K. Hemker, D. Renné, and T. E. Hoff, 'Validation of short and medium term operational solar radiation forecasts in the US', *Solar Energy*, vol. 84, no. 12, pp. 2161–2172, Dec. 2010, doi: 10.1016/j.solener.2010.08.014.

[170] Luosongzeren, 'Research on Power Prediction Model of Solar Photovoltaic System Based on ARIMA Time Series', in *2023 IEEE International Conference on Image Processing and Computer Applications (ICIPCA)*, Changchun, China: IEEE, Aug. 2023, pp. 954–957. doi: 10.1109/ICIPCA59209.2023.10257925.

[171] G. Box, G. Jenkins, G. Reinsel, and G. Ljung, *Time Series Analysis: Forecasting and Control*, 5th ed. NJ, USA: Wiley, 2015.

[172] E. G. Kardakos, M. C. Alexiadis, S. I. Vagropoulos, C. K. Simoglou, P. N. Biskas, and A. G. Bakirtzis, 'Application of time series and artificial neural network models in short-term forecasting of PV power generation', in *2013 48th International Universities' Power Engineering Conference (UPEC)*, Dublin: IEEE, Sep. 2013, pp. 1–6. doi: 10.1109/UPEC.2013.6714975.

[173] R. Nguyen, Y. Yang, A. Tohmeh, and H.-G. Yeh, 'Predicting PV Power Generation using SVM Regression', in *2021 IEEE Green Energy and Smart Systems Conference (IGESSC)*, Long Beach, CA, USA: IEEE, Nov. 2021, pp. 1–5. doi: 10.1109/IGESSC53124.2021.9618677.

[174] B. Wolff, J. Kühnert, E. Lorenz, O. Kramer, and D. Heinemann, 'Comparing support vector regression for PV power forecasting to a physical modeling approach using measurement, numerical weather prediction, and cloud motion data', *Solar Energy*, vol. 135, pp. 197–208, Oct. 2016, doi: 10.1016/j.solener.2016.05.051.

[175] S. Cebollada, L. Payá, M. Flores, A. Peidró, and O. Reinoso, 'A state-of-the-art review on mobile robotics tasks using artificial intelligence and visual data', *Expert Systems with Applications*, vol. 167, p. 114195, Apr. 2021, doi: 10.1016/j.eswa.2020.114195.

[176] K. binti Hanifulkhair, A. Priyadi, V. Lystianingrum, and R. Delfianti, 'One Day Ahead Prediction of PV Power Plant for Energy Management System Using Neural Network', in *2020 International Seminar on Intelligent Technology and Its Applications (ISITIA)*, Surabaya, Indonesia: IEEE, Jul. 2020, pp. 107–112. doi: 10.1109/ISITIA49792.2020.9163783.

[177] R. K. Mandal and P. Kale, 'Development of a Decision-Based Neural Network for a Day-Ahead Prediction of Solar PV Plant Power Output', in *2018 4th International Conference on Computational Intelligence & Communication Technology (CICT)*, Ghaziabad: IEEE, Feb. 2018, pp. 1–6. doi: 10.1109/CIACT.2018.8480396.

[178] A. Singhal, G. Raina, D. Meena, C. K. S. Chaudhary, and S. Sinha, 'A comparative analysis of ANN based time series models for predicting PV output', in *2022 IEEE International Conference on Power Electronics, Drives and Energy Systems (PEDES)*, Jaipur, India: IEEE, Dec. 2022, pp. 1–6. doi: 10.1109/PEDES56012.2022.10080149.

[179] R. Al-Rawashdeh, M. Alsarayreh, and A. Al-Odienat, 'Solar Photovoltaic Forecasting Using ANN Network for Central and Southern Regions of Jordan', in *2023 IEEE Jordan International Joint Conference on Electrical Engineering and Information Technology (JEEIT)*, Amman, Jordan: IEEE, May 2023, pp. 50–57. doi: 10.1109/JEEIT58638.2023.10185900.

[180] K. Singh and M. Rizwan, 'AI based Approach for Solar PV Power Prediction with Varying Dust Accumulation Levels', in *2023 International Conference on Recent Advances in Electrical, Electronics & Digital Healthcare Technologies (REEDCON)*, New Delhi, India: IEEE, May 2023, pp. 19–24. doi: 10.1109/REEDCON57544.2023.10150800.

[181] S. Dhingra, G. Gruosso, and G. S. Gajani, 'Modelling Ageing and Power Production of Solar PV Using Machine Learning Techniques', in *2023 International Conference on Electrical, Computer and Energy Technologies (ICECET)*, Cape Town, South Africa: IEEE, Nov. 2023, pp. 1–6. doi: 10.1109/ICECET58911.2023.10389351.

[182] S. Mawande, R. Kulkarni, S. Kakade, and R. Sadakale, 'Estimation of Solar PV Plant Output using LSTM-CNN Algorithm', in *2023 International Conference on Digital Applications, Transformation & Economy (ICDATE)*, Miri, Sarawak, Malaysia: IEEE, Jul. 2023, pp. 231–235. doi: 10.1109/ICDATE58146.2023.10248868.

[183] Q. Li, Y. Xu, B. S. H. Chew, H. Ding, and G. Zhao, 'An Integrated Missing-Data Tolerant Model for Probabilistic PV Power Generation Forecasting', *IEEE Trans. Power Syst.*, vol. 37, no. 6, pp. 4447–4459, Nov. 2022, doi: 10.1109/TPWRS.2022.3146982.

[184] G. Etxegarai, I. Zapirain, H. Camblong, J. Ugartemendia, J. Hernandez, and O. Curea, 'Photovoltaic Energy Production Forecasting in a Short Term Horizon: Comparison between Analytical and Machine Learning Models', *Applied Sciences*, vol. 12, no. 23, p. 12171, Nov. 2022, doi: 10.3390/app122312171.

[185] G. Etxegarai Azkarategi, I. Zapirain Zuazo, H. Camblong Ruiz, J. Hernandez, J. J. Ugartemendia, and O. Curea, 'Photovoltaic power forecast for the next 24 hours with an analytical model and a FFNN model', in *2022 IEEE International Conference on Electrical Sciences and Technologies in Maghreb (CISTEM)*, Tunis, Tunisia: IEEE, Oct. 2022, pp. 1–6. doi: 10.1109/CISTEM55808.2022.10044029.

[186] C. Fan, J. Wang, W. Gang, and S. Li, 'Assessment of deep recurrent neural network-based strategies for short-term building energy predictions', *Applied Energy*, vol. 236, pp. 700–710, Feb. 2019, doi: 10.1016/j.apenergy.2018.12.004.

[187] C. Fan, Y. Sun, K. Shan, F. Xiao, and J. Wang, 'Discovering gradual patterns in building operations for improving building energy efficiency', *Applied Energy*, vol. 224, pp. 116–123, Aug. 2018, doi: 10.1016/j.apenergy.2018.04.118.

[188] J.-S. Chou and N.-T. Ngo, 'Time series analytics using sliding window metaheuristic optimisation-based machine learning system for identifying building energy consumption patterns', *Applied Energy*, vol. 177, pp. 751–770, Sep. 2016, doi: 10.1016/j.apenergy.2016.05.074.

[189] IEA, 'Building Energy Performance Metrics', IEA, París, 2015. [Online]. Available: https://www.iea.org/reports/building-energy-performance-metrics

[190] F. M. Vieira, P. S. Moura, and A. T. de Almeida, 'Energy storage system for self-consumption of photovoltaic energy in residential zero energy buildings', *Renewable Energy*, vol. 103, pp. 308–320, Apr. 2017, doi: 10.1016/j.renene.2016.11.048.

[191] D. Gyalistras *et al.*, 'Analysis of Energy Savings Potentials for Integrated Room Automation', presented at the 10th REHVA World Congress Clima 2010 - Sustainable Energy Use in Buildings, Antalya, Turkey, May 2010.

[192] W. Belazi, S. E. Ouldboukhitine, A. Chateauneuf, and A. Bouchair, 'Thermal modeling of the occupied multi-zone buildings taking into account the uncertainties of occupant behavior', *Case Studies in Thermal Engineering*, vol. 33, p. 101978, 2022, doi: https://doi.org/10.1016/j.csite.2022.101978.

[193] T. A. Nguyen and M. Aiello, 'Energy intelligent buildings based on user activity: A survey', *Energy and Buildings*, vol. 56, pp. 244–257, Jan. 2013, doi: 10.1016/j.enbuild.2012.09.005.

[194] S. Promchaiwattana and D. Banjerdpongchai, 'Design of Supervisory Model Predictive Control for Building HVAC System Subject to Time-Varying Operating Points', in *2022 22nd International Conference on Control, Automation and Systems (ICCAS)*, Jeju, Korea, Republic of: IEEE, Nov. 2022, pp. 1404–1409. doi: 10.23919/ICCAS55662.2022.10003843.

[195] A. David, M. Alamir, and C. L. Pape-Gardeux, 'Data-driven modelling for HVAC energy flexibility optimisation', in *2022 IEEE PES Innovative Smart Grid Technologies Conference Europe (ISGT-Europe)*, Novi Sad, Serbia: IEEE, Oct. 2022, pp. 1–5. doi: 10.1109/ISGT-Europe54678.2022.9960426.

[196] A. Bagnasco, S. Massucco, M. Saviozzi, F. Silvestro, and A. Vinci, 'Design and Validation of a Detailed Building Thermal Model Considering Occupancy and Temperature Sensors', in *2018 IEEE 4th International Forum on Research and Technology for Society and Industry (RTSI)*, Palermo: IEEE, Sep. 2018, pp. 1–6. doi: 10.1109/RTSI.2018.8548424.

[197] M. J. Ellis, 'Machine Learning Enhanced Grey-Box Modeling for Building Thermal Modeling', in *2021 American Control Conference (ACC)*, New Orleans, LA, USA: IEEE, May 2021, pp. 3927–3932. doi: 10.23919/ACC50511.2021.9482715.

[198] W. Wang, Q. Zhou, C. Pan, and F. Cao, 'Energy-efficient operation of a complete Chiller-air handing unit system via model predictive control', *Applied Thermal Engineering*, vol. 201, p. 117809, Jan. 2022, doi: 10.1016/j.applthermaleng.2021.117809.

[199] J. Drgoňa *et al.*, 'All you need to know about model predictive control for buildings', *Annual Reviews in Control*, vol. 50, pp. 190–232, 2020, doi: 10.1016/j.arcontrol.2020.09.001.

[200] H. Zhao and F. Magoulès, 'A review on the prediction of building energy consumption', *Renewable and Sustainable Energy Reviews*, vol. 16, no. 6, pp. 3586–3592, Aug. 2012, doi: 10.1016/j.rser.2012.02.049.

[201] K. Pandey and B. Basu, 'Mathematical modeling for short term indoor room temperature forecasting using Box-Jenkins models: An Indian evidence', *JM2*, vol. 15, no. 3, pp. 1105–1136, Feb. 2020, doi: 10.1108/JM2-08-2019-0182.

[202] J. Terés-Zubiaga, C. Escudero, C. García-Gafaro, and J. M. Sala, 'Methodology for evaluating the energy renovation effects on the thermal performance of social housing buildings: Monitoring study and grey box model development', *Energy and Buildings*, vol. 102, pp. 390–405, Sep. 2015, doi: 10.1016/j.enbuild.2015.06.010.

[203] Z. Wang, Y. Chen, and Y. Li, 'Development of RC model for thermal dynamic analysis of buildings through model structure simplification', *Energy and Buildings*, vol. 195, pp. 51–67, Jul. 2019, doi: 10.1016/j.enbuild.2019.04.042.

[204] J. Palmer Real *et al.*, 'Characterisation of thermal energy dynamics of residential buildings with scarce data', *Energy & Buildings*, vol. 230, 2021, doi: https://doi.org/10.1016/j.enbuild.2020.110530 0.

[205] Z. Jiang *et al.*, 'Data-driven Thermal Model Inference with ARMAX, in Smart Environments, based on Normalised Mutual Information', in *2018 Annual American Control Conference (ACC)*, Milwaukee, WI, USA: IEEE, Jun. 2018, pp. 4634–4639. doi: 10.23919/ACC.2018.8431085.

[206] F. Amara, V. Dermardiros, and A. K. Athienitis, 'Energy Flexibility for an Institutional Building with Integrated Solar System: Case Study Analysis', in *2019 IEEE Electrical Power and Energy Conference (EPEC)*, Montreal, QC, Canada: IEEE, Oct. 2019, pp. 1–6. doi: 10.1109/EPEC47565.2019.9074815.

[207] G. Mustafaraj, J. Chen, and G. Lowry, 'Development of room temperature and relative humidity linear parametric models for an open office using BMS data', *Energy and Buildings*, vol. 42, no. 3, pp. 348–356, Mar. 2010, doi: 10.1016/j.enbuild.2009.10.001.

[208] X. Shi, W. Lu, Y. Zhao, and P. Qin, 'Prediction of Indoor Temperature and Relative Humidity Based on Cloud Database by Using an Improved BP Neural Network in Chongqing', *IEEE Access*, vol. 6, pp. 30559–30566, 2018, doi: 10.1109/ACCESS.2018.2844299.

[209] D. Palaić, I. Matetić, S. Ljubic, I. Štajduhar, and I. Wolf, 'Data-driven Model for Indoor Temperature Prediction in HVAC-Supported Buildings', in *2023 3rd International Conference on Electrical, Computer, Communications and Mechatronics Engineering (ICECCME)*, Tenerife, Canary Islands, Spain: IEEE, Jul. 2023, pp. 1–6. doi: 10.1109/ICECCME57830.2023.10252601.

[210] L. Di Natale, B. Svetozarevic, P. Heer, and C. N. Jones, 'Physically Consistent Neural Networks for building thermal modeling: Theory and analysis', *Applied Energy*, vol. 325, p. 119806, Nov. 2022, doi: 10.1016/j.apenergy.2022.119806.

[211] Y. Maccarana, A. Panza, G. Maroni, L. Sarto, M. F. Carta, and S. Reggiani, 'Comparison of model-based and data-driven approaches for modeling energy and comfort management systems, with a case study', in *2019 IEEE International Conference on Environment and Electrical Engineering and 2019 IEEE Industrial and Commercial Power Systems Europe (EEEIC / I&CPS Europe)*, Genova, Italy: IEEE, Jun. 2019, pp. 1–6. doi: 10.1109/EEEIC.2019.8783703.

[212] A. Agouzoul, E. Simeu, and M. Tabaa, 'Enhancement of Building Energy Consumption Using a Digital Twin based Neural Network Model Predictive Control', in *2023 International Conference on Control, Automation and Diagnosis (ICCAD)*, Rome, Italy: IEEE, May 2023, pp. 1–6. doi: 10.1109/ICCAD57653.2023.10152308.

[213] J. Li *et al.*, 'Refined Modelling Approach of HVACs in Commercial Buildings', in *2021 IEEE Sustainable Power and Energy Conference (iSPEC)*, Nanjing, China: IEEE, Dec. 2021, pp. 2208–2212. doi: 10.1109/iSPEC53008.2021.9736121.

[214] R. Sendra-Arranz and A. Gutiérrez, 'A long short-term memory artificial neural network to predict daily HVAC consumption in buildings', *Energy and Buildings*, vol. 216, p. 109952, Jun. 2020, doi: 10.1016/j.enbuild.2020.109952.

[215] E. Khaoula, B. Amine, and B. Mostafa, 'Forecasting diurnal Heating Energy Consumption of HVAC system using ANN, RNN, ARNN', in *2023 14th International Conference on Intelligent Systems: Theories and Applications (SITA)*, Casablanca, Morocco: IEEE, Nov. 2023, pp. 1–6. doi: 10.1109/SITA60746.2023.10373744.

[216] K. Zingre, S. Srinivasan, and M. Marzband, 'Cooling load estimation using machine learning techniques'.

[217] R. E. Alden, E. S. Jones, S. B. Poore, H. Gong, A. Al Hadi, and D. M. Ionel, 'Digital Twin for HVAC Load and Energy Storage based on a Hybrid ML Model with CTA-2045 Controls Capability', in *2022 IEEE Energy Conversion Congress and Exposition (ECCE)*, Detroit, MI, USA: IEEE, Oct. 2022, pp. 1–5. doi: 10.1109/ECCE50734.2022.9948141.

[218] I. D. Landau and G. Zito, *Digital Control Systems. Design, Identification and implementation.* Springer, 2006. Accessed: Feb. 07, 2024. [Online]. Available: http://rgdoi.net/10.13140/RG.2.2.19321.49764

[219] M. Schwenzer, M. Ay, T. Bergs, and D. Abel, 'Review on model predictive control: an engineering perspective', *Int J Adv Manuf Technol*, vol. 117, no. 5–6, pp. 1327–1349, Nov. 2021, doi: 10.1007/s00170-021-07682-3.

[220] D. Y. Yamashita, I. Vechiu, and J.-P. Gaubert, 'Real-time Parameters Identification of Lithium-ion Batteries Model to Improve the Hierarchical Model Predictive Control of Building MicroGrids', in *2020 22nd European Conference on Power*

*Electronics and Applications (EPE'20 ECCE Europe)*, Lyon, France: IEEE, Sep. 2020, pp. 1–10. doi: 10.23919/EPE20ECCEEurope43536.2020.9215878.

[221] D. Y. Yamashita, I. Vechiu, J.-P. Gaubert, and S. Jupin, 'Hierarchical Model Predictive Control to Coordinate a Vehicle-to-Grid System Coupled to Building Microgrids', *IEEE Trans. on Ind. Applicat.*, vol. 59, no. 1, pp. 169–179, Jan. 2023, doi: 10.1109/TIA.2022.3215978.

[222] O. Laguili, J. Eynard, and S. Grieu, 'Energy Efficiency Improvement Through MPC-Based Management of EWHs in Collective Dwellings', in *2024 9th International Conference on Smart and Sustainable Technologies (SpliTech)*, Bol and Split, Croatia: IEEE, Jun. 2024, pp. 1–6. doi: 10.23919/SpliTech61897.2024.10612569.

[223] U. R. Nair, M. Sandelic, A. Sangwongwanich, T. Dragicevic, R. Costa-Castello, and F. Blaabjerg, 'An Analysis of Multi Objective Energy Scheduling in PV-BESS System Under Prediction Uncertainty', *IEEE Trans. Energy Convers.*, vol. 36, no. 3, pp. 2276–2286, Sep. 2021, doi: 10.1109/TEC.2021.3055453.

[224] M. Amini, S. Esmaeili, M. Sayadlou, A. Khorsandi, and S. H. Hosseinian, 'A Real Time MPC-Based Strategy for PV Plant with Battery Energy Storage', in *2022 30th International Conference on Electrical Engineering (ICEE)*, Tehran, Iran, Islamic Republic of: IEEE, May 2022, pp. 946–950. doi: 10.1109/ICEE55646.2022.9827118.

[225] M. A. K. S. Boralessa, S. Hovden, A. V. U. A. Wickramarathna, and K. T. M. U. Hemapala, 'Effect of Renewable Energy Forecasting Error on Model Predictive Control Based Microgrid Energy Management System', in *2022 IEEE IAS Global Conference on Emerging Technologies (GlobConET)*, Arad, Romania: IEEE, May 2022, pp. 959–962. doi: 10.1109/GlobConET53749.2022.9872520.

[226] A. Hassan, S. Ruiz-Moreno, J. R. D. Frejo, J. M. Maestre, and E. F. Camacho, 'Neural-Network Based MPC for Enhanced Lateral Stability in Electric Vehicles', *IEEE Access*, vol. 12, pp. 23265–23278, 2024, doi: 10.1109/ACCESS.2024.3362236.

[227] S. Abobakr, M. Alosta, M. A. Abdelkefi, A. E. Kaouachi, and L. Sboui, 'MPC-Based Efficient Energy Control and Cost Estimation of HVAC in Buildings', in *2023 IEEE Third International Conference on Signal, Control and Communication (SCC)*, Hammamet, Tunisia: IEEE, Dec. 2023, pp. 1–5. doi: 10.1109/SCC59637.2023.10527780.

[228] A. Elkamel, A. Morsi, M. Darwish, H. S. Abbas, and M. H. Amin, 'Model Predictive Control of Linear Parameter-Varying Systems Using Gaussian Processes', in *2022 26th International Conference on System Theory, Control and Computing (ICSTCC)*, Sinaia, Romania: IEEE, Oct. 2022, pp. 452–457. doi: 10.1109/ICSTCC55426.2022.9931885.

[229] A. Pajares, F. J. Vivas, X. Blasco, J. M. Herrero, F. Segura, and J. M. Andújar, 'Methodology for energy management strategies design based on predictive control techniques for smart grids', *Applied Energy*, vol. 351, p. 121809, Dec. 2023, doi: 10.1016/j.apenergy.2023.121809.

[230] D. Masti, T. Pippia, A. Bemporad, and B. D. Schutter, 'Learning Approximate Semi-Explicit Hybrid MPC with an Application to Microgrids', *IFAC-PapersOnLine*, vol. 53, no. 2, pp. 5207–5212, 2020, doi: 10.1016/j.ifacol.2020.12.1192.

[231] P. Bakmohammadi and E. Noorzai, 'Optimisation of the design of the primary school classrooms in terms of energy and daylight performance considering occupants' thermal and visual comfort', *Energy Reports*, vol. 6, pp. 1590–1607, Nov. 2020, doi: 10.1016/j.egyr.2020.06.008.

[232] X. Yang, G. Zhou, Z. Ren, Y. Qiao, and J. Yi, 'High-precision air conditioning load forecasting model based on improved sparrow search algorithm', *Journal of Building Engineering*, vol. 92, p. 109809, Sep. 2024, doi: 10.1016/j.jobe.2024.109809.

# *ANNEXES*

# ANNEX A

## RECURRENT NEURAL NETWORKS

RNNs have been widely used for forecasting purposes, particularly for predictions in the energy sector [1], [2], [3]. Various types of RNNs have been used to predict resource demand in a power distribution network. Therefore, numerous works can be found where some type of RNN is used to predict the electricity consumption of one or several consumption points associated with the power grid [4], [5]. They have also been used to predict the production of PV installations [6, 7] to foresee the state of charge of electric vehicle batteries [8], [9] or of battery systems (BSS) associated with a MG [10], [11].

RNNs are nowadays one of the most frequently used ANNs and are characterised by their capability to process several nonlinear dynamic systems, creating complex representations from input to output sequences.

RNNs have the characteristic of handling very well the properties that time series present. These properties include the saturation effect, the exponential effect, or the nonlinear interactions that may exist between different variables [12].

Figure A.1 shows a diagram of a simple RNN, where the input, $x$, hidden, $h$, and output, $y$, represent the nodes in the layer. Similarly, $W^i$, $W^h$ y $W^o$ represent the weight matrices located in each layer. Finally, $z^{-1}$ is the unit delay operator, and the polygon represents the nonlinear function, known as the activation function, applied by the neurons.

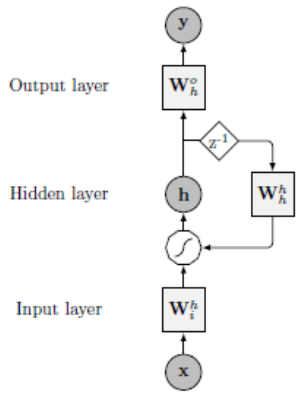


***Figure A.1**. Simple RNN arquitecture.*

RNNs, regardless of their type, have the characteristic of possessing a recurrent term, another aspect that makes them suitable for cases where dealing with time series is required. As mentioned, RNNs, given their well-known universal approximation property, seemingly have the

capability to model any type of dynamic system, but the training phase becomes particularly important for this.

Proper training of a model involves estimating the model's hyperparameters in such a way that, through certain inputs, a target variable can be estimated accurately. However, various methodologies can be employed for this training, often depending on the structure of the NN. In the absence of a standardised methodology for training RNNs, in most cases, the adjustment of weights and biases is performed using Gradient Descent (GD).

GD is one of the most commonly used optimisation algorithms for adjusting the weights and biases of NNs, together with the backpropagation algorithm. The latter seeks to minimise a cost function by propagating the calculated gradients of the error with respect to each of the network's weights backwards.

The cost function can be generally expressed in Equation (A.1) [12]:

$$L_k = E(x, y^*; W_k) + R_\lambda(W_k) \tag{A.1}$$

In this equation, $W_k$ represents the set of weights and biases of the NN, with $x$ being the inputs introduced to the model and $y^*$ the desired output, all recorded in epoch $k$ of the optimisation process.

$E$ is the function that evaluates the prediction error of the NN:

$$E = MSE(y, y^*) = \frac{1}{|x|}\sum(y - y^*)^2 \tag{A.2}$$

In Equation (A.2) the regularisation term ($R_\lambda$) is added, which depends on the value of the set of weights and biases of the model and is used to improve the generalisation capability of the model.

The training is conducted following these steps: first, the values of the weights and biases of the model are randomly initialised. Subsequently, the partial derivative of the cost function with respect to each of the weights is calculated, i.e., the gradient is calculated, or in other words, the slope of the cost function is determined.

$$Gradient = \frac{\partial E}{\partial W_k} \tag{A.3}$$

Using the backpropagation method, this gradient calculation is propagated backwards to adjust the values of the weights. The weight values will be updated so that they move in the direction of the descending slope, i.e., in the direction opposite to the gradient. This process is repeated iteratively until the cost function is minimised as much as possible.

However, in addition to determining whether the new weight value should increase or decrease to minimise the cost function, it is also necessary to determine by how much the value should be increased or decreased. This amount is determined by Equation (A.4) [13].

$$W_{k+1} = W_k + \eta \frac{\partial L_k}{\partial W_k}, \tag{A.4}$$

It can be seen that η, the learning rate, determines how much the weight values should increase. Therefore, η, will be another hyperparameter to tune in many types of RNNs.

As mentioned previously, during the backpropagation algorithm, the gradients are propagated backwards through the network layers. Due to the calculations that must be performed during gradient propagation, various problems can arise depending on the value of the gradient. The most well-known and reviewed in the literature are the Vanishing Gradient and Exploding Gradient problems [14].

The Vanishing Gradient problem occurs when gradients acquire very small values and propagate through several layers. The use of the logistic sigmoid activation function makes this problem more likely to occur, as the derivatives of this function take on values much smaller than 1, causing the gradients of the weights in the network layers to be very low. The low value of the gradients means that during the backpropagation algorithm, the layers receive very little significant information, which not only hinders the learning process but also slows down convergence.

In contrast, the Exploding Gradient problem arises when the gradient increases exponentially. This occurs when the gradient takes on values greater than 1 and propagates backwards through the different layers of the network. This can lead to unstable training and numerical issues.

Although the Vanishing Gradient problem is strongly related to the logistic sigmoid activation function, both problems can have different causes.

Other common problems in NN are underfitting and overfitting. A model suffers from underfitting when it lacks the general capacity to learn the problem, resulting in poor performance during both training and when new data is introduced. Underfitting can be addressed by increasing the model's capacity to fit functions that can map the model's input to its output. Increasing the model's capacity means enhancing its structure, for instance, by adding more layers to the network and/or more neurons to these layers.

Overfitting, on the other hand, presents itself as a generalisation problem that the model may have. This means the model learns too well, too much in detail, during the training phase and lacks the generalisation capacity for new unseen data. When overfitting occurs, we will see that

while the training dataset error decreases significantly with each iteration, the error for unseen data increases with each iteration.

To address this problem, the model's structure can be reduced to lower its complexity. Another possible solution is to limit the values of the weights. This latter method is one of many that fall under regularisation methods, which improve the model's generalisation capability. Another widely used regularisation method is called Early Stopping. It involves monitoring the model's performance during the validation phase and stopping training before performance degrades. According to this method, training stops when the validation error increases for six successive iterations.

It will be important to adapt the type of training, the structure, and the regularisation method according to the type of RNN to be used, which in turn depends on the available data and the complexity of the system we want to represent.

Among the most well-known types of RNNs are, for example, LSTM or GRU networks, both used in time series applications and characterised by their gated architecture. The recurrence in this type of network is guaranteed by the architecture itself, which includes elements like memory cells that allow them to remember past values.

This is not the case for other types of networks, which have a simpler architecture and include a recurrent term through feedback terms. This is the case for NARX networks, widely used in STLF applications, and distinguished by their simplicity and ease of implementation.

## A.1 NARX neural network

NARX neural networks are considered a type of Recurrent Neural Network (RNN) that have been widely used in the literature for time series prediction due to, on the one hand, their easy implementation and, on the other hand, their fast training procedures. As it can be seen in Figure A.2, the prediction of dynamic NNs, such as NARX, is driven by the input-output pairs, as well as, by the previous states of the network, that is to say, by the input and feedback delays.

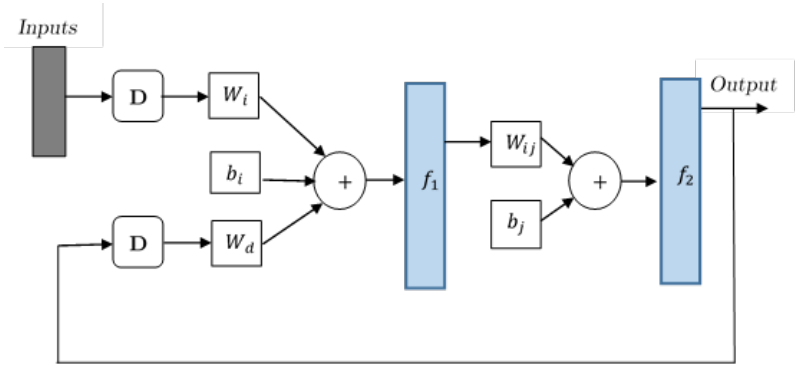


***Figure A.2.*** *General NARX diagram used for forecasting purposes in operational mode.*

where $W_i$ and $W_{ij}$ are the weight matrix, $b_i$ and $b_j$ are the bias and finally, the D block represents the delays, that is to say the number of time delay steps applied to the input and the feedback (output). Finally, $f_1$ and $f_2$ represents the activation function of each layer.

NARX neural networks can be based on MLP structure, which consist on an input layer, one or more hidden layers and output layer that are connected by adjustable weights. Neurons that compose the hidden and output layer are associated with bias values [15]. The weights and biases are adjusted during the training process of the network.

In each layer, each neuron carries out a scalar multiplication of the input vector $x_j$ and the weight matrix $w_{ij}$. Likewise, the activation function ($\varphi$) is added, obtaining Equation (A.5) in the output of each neuron:

$$y_i = f(\sum_{j=1}^{n} x_j * w_{ij}) \tag{A.5}$$

The design of the NARX is done by adjusting the hyperparameters of the network. Hyperparameters are those variables that determine the structure of the network and the ones that determine how the neural network is trained. Among the hyperparameters that can be adjusted are a) the number of hidden layers, b) the number of neurons in the hidden layer, c) the number of delays of input and feedback, d) the activation function of both the hidden and output layers and, finally, e) the training algorithm.

One of the hyperparameters to adjust in a NARX network is the activation function for the hidden and output layers. The activation functions commonly used in neural networks are three: *the linear (lin)*, the *logistic sigmoid (logsig)*, and the *hyperbolic tangent (tansig)* activation function (see Table A.1).

***Table A.1***. *Activation functions used in neural networks.*

| ***Functions*** | ***Definition*** |
|---|---|
| ***Linear*** | $y = x$ |
| ***Logistic sigmoid (logsig)*** | $y = \frac{1}{1+e^{-x}}$ |
| ***Hyperbolic tangent (tansig)*** | $y = \frac{e^{x}-e^{-x}}{e^{x}+e^{-x}}$ |

Equation (A.6) shows the input-output relationship using a NARX, considering several independent inputs:

$$\widehat{y^{t+1}} = f(x_1^t, x_1^{t-1}, x_1^{t-2}, \dots, x_P^{t-D_{xp}}, y^t, y^{t-1}, y^{t-2}, \dots, y^{t-D_y}) \quad \text{(A.6)}$$

where $y^{t+1}$ is the future value of the target variable, $P$ is the total exogenous inputs, $D_{xp}$ is the delay of each exogenous input $x_p$and $D_y$ is the delay of the targeted values. The input and feedback delays represent one of the hyperparameters to be adjusted.

The number of time delay steps of the output, $D_y$, is the one that gives recurrence to the NARX, in contrast to the structures of other RNNs, in which the recurrence is given by the internal state of the network [12]. Additionally, $f$ is the nonlinear mapping function performed by the MLP. MLP is a powerful structure very appropriate to learn any kind of nonlinear mapping [16].

The NARX operates in two different phases or stages: training stage and prediction stage. In this first phase, NARX structure can be based on a MLP structure, in which the model has input neurons with only outgoing connections, output neurons with only incoming connections, and hidden layer neurons with both [12]. This configuration (see Figure A.***3***) is also commonly referred to as an open-loop configuration or series-parallel architecture. The data used as inputs consist of external and independent inputs as well as historical data of the variable to be predicted. A training algorithm is implemented for adjusting the weights and during training, the data flow forward from input to output, similar to a FFNN.

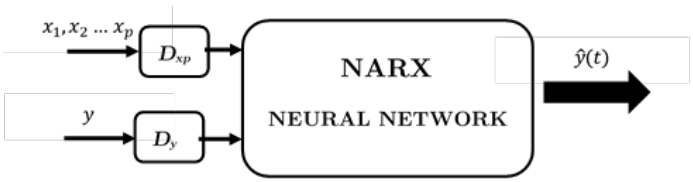


***Figure A.3****. Open- loop or series-parallel arquitecture of a NARX.*

Levenberg-Marquardt (*lm*) is a commonly used training algorithm that adjusts weights and biases by adaptively varying the update of the Gradient Descent (GD) and Gaussian-Newton algorithms [17]. It has become a standard technique for nonlinear least squares problems [18] although it only finds the local minimum, which does not necessarily have to be the global minimum. One of the major advantages is its ability to train a NN between 10 and 100 times faster than the backpropagation gradient descent method. There are also other algorithms in order to train a NN, among others, Bayesian Regularization (*trainbr*) appropriate for noisy or small problems or Scaled Conjugate Gradient (*trainscg*) [19].

On the other hand, we have the prediction stage. After training the model in open-loop, it is understood that the model is now capable of making future predictions of the target variable. This stage is also referred to as the simulation stage or the operational mode of the NN. In this phase, the structure of the network changes from open loop to closed loop, also known as parallel architecture (see Figure A.***4***).

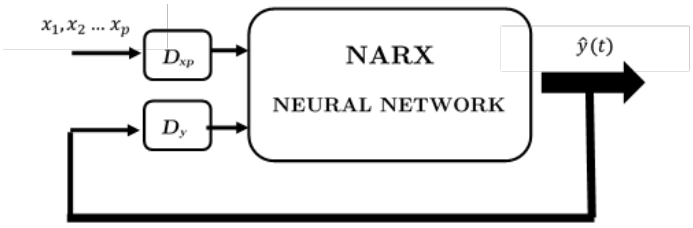


***Figure A.4****. Closed-loop or parallel arquitecture of a NARX.*

Now instead of introducing the historical data of the target variable along with the independent inputs, the network will now be fed back with the variable being predicted. By closing the loop and introducing the predicted values of $y$ as inputs, multi-step ahead predictions can be made, unlike in the training phase in open-loop, where predictions are made one-step ahead.

## A.2 LSTM neural network and SVR

Regarding LSTMs, according to extensive literature, this type of RNN performs well in predicting time sequences and have high capacity to learn from large datasets. Each LSTM layer consists of multiple memory cells that are composed of several "gates" (see Figure A.***5***). These gates serve a specific function: the input gate adds new data, the forget gate removes unnecessary data, the cell state maintains long-term memory, and the output gate transmits data to the next cell [20].

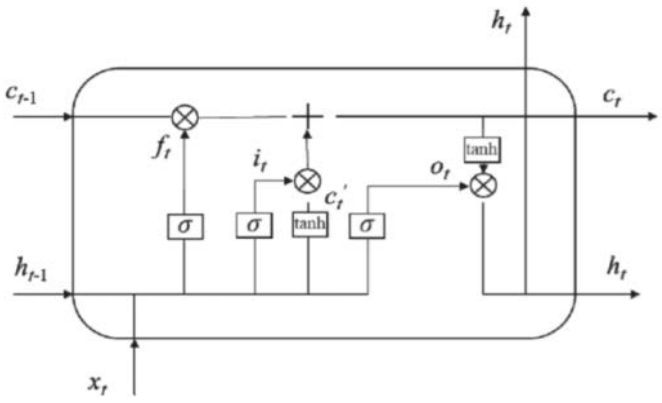


***Figure A.5****. LSTM general diagram.*

The last designed model is a ML model widely used for prediction purposes in the literature: SVR. This model aims to find a function that approximates the relationship between input variables and a continuous target variable while minimizing prediction error. As for

disadvantages, SVRs are highly dependent on hyperparameters, and the selection of parameters determines the model's prediction effectiveness [21].

# ANNEX B

## REGRESSION ANALYSIS

For many years, regression models, both linear and nonlinear, have been employed to predict the internal temperature of buildings. Regression analysis is a technique used to model the relationship between variables. Through regression analysis, we can quantify how a target variable ($y$) changes depending on the value of one or more independent variables ($x$) [22]. The relationship between these variables is described by a function, which includes a term related to the error ($\varepsilon$).

$$y = \beta x + \varepsilon \tag{B.1}$$

This mathematical relationship consist of a finite number of parameters that need to be estimated from data. It is for this reason that regression models are classified as grey-box models.

Among the most common regression models observed in the literature for making predictions are multiple linear regression (MLR) models and nonlinear regression (NLR) models. Both are characterised, unlike simple linear regression models, by taking into account multiple independent variables ($x$) for the estimation of the variable ($y$). This is a fundamental consideration when thermally modelling a building, as the variation in internal temperature is often multifactorial.

Equation (B.2) represents a case of MLR.

$$y = \beta_0 + \beta_1 x_1 + \cdots + \beta_n x_v + \varepsilon, \tag{B.2}$$

where $y$ is the value of the target variable and the term $\beta_n X_v$ represents the effect of the variation of the independent variable $x$ on the variable $y$. $\beta_0$ is the intersection on $y$, that is, the offset or the value of $y$ when the rest of the parameters are 0. The last term $\varepsilon$ represents the error associated with the variation in the estimation of $y$.

Autoregressive Models (AR)

Autoregressive processes are stationary processes, meaning they have constant mean ($\mu$) and variance ($\sigma^2$), thus remaining constant over time. In addition to being stationary, autoregressive processes are stochastic processes, which means that besides having constant mean and variance over time, the value of covariance ($\gamma$) between two periods depends only on the distance or lag and not on the time at which this covariance is calculated. This means that these three statistical values remain unchanged over time, regardless of when they are measured [23].

$$Mean \quad \mu = E(X_k) = E(X_{t+k})$$

$$Variance \quad \sigma^2 = V(X_t) = V(X_{t+k}) \tag{B.3}$$

$$Covariance \quad \gamma_k = E[(X_t - \mu)(X_{t+k} - \mu)]$$

where $\gamma_k$, the autocovariance at lag $k$, is the covariance of the period between the values $X_t$ and $X_{(t+k)}$ which would be separated by a period also $k$.

One of the characteristics of these stochastic processes is the associated white noise, where the values are independently and identically distributed over time with zero mean and equal variance.

$$Mean \quad \mu = 0;$$

$$Variance \quad \sigma^2 = 0; \tag{B.4}$$

$$Covariance \quad \gamma_k = 0;$$

Unlike multiple regression models that predict a target variable by a linear combination of multiple predictors, autoregressive models are based on the combination of past values of a variable. That is, they include autoregressive terms so they predict future values based on past values.

$$Y_t = \phi_0 + \phi_1 Y_{t-1} + \cdots + \phi_p Y_{t-p} + \varepsilon_{t,} \tag{B.5}$$

where $\phi_p$ are constants, the parameters to be identified. ($t$–$p$) represents the lagged term of order $p$, and $\varepsilon_t$ is the white noise with mean, variance, and covariance of 0.

Depending on $p$, the number of lagged terms taken into account to make the prediction determines the order of the model. An autoregressive process AR (1), of order 1, is one in which the current value is based on the immediately preceding value, while an AR (2) process is one in which the current value is based on the two preceding values, and so on.

$$AR\ (1)\ \ Y_t = \phi_0 + \phi_1 Y_{t-1} + \varepsilon_t;$$
$$AR\ (2)\ \ Y_t = \phi_0 + \phi_1 Y_{t-1} + \phi_2 Y_{t-2} + \varepsilon_t \tag{B.6}$$

ARX Model

Autoregressive model with external input (ARX) is a linear representation of a dynamic system, and unlike the AR model, the ARX model includes an external input term. Representing a model in ARX form is the basis of many process dynamics and control analysis methods. The structure of the ARX model is given by the following equation:

$$A(q)y(t) = B(q)x(t - n_k) + \varepsilon(t), \tag{B.7}$$

where $x$, $y$, and $\varepsilon$ are the input, output, and white noise, respectively, and $q$ is the term representing the lag. More specifically, there are two equations:

$$A(q) = 1 + a_1 q^{-1} + \cdots + a_{n_a} q^{-n_a};$$
$$B(q) = b_1 + b_2 q^{-1} + \cdots + b_{n_b} q^{-n_b+1}; \quad \text{(B.8)}$$

where $n_a$ is the number of previous output terms, and $n_b$ is the number of previous input terms used to predict the current output. $n_k$, also known as the dead time, represents the number of input samples that occur before the input affects the output. The coefficient vector $[a_1, a_{n_a}, \ldots, b_1, b_{n_b}]$ represents the weighting applied to the regression terms.

ARMAX Model

An ARMAX (Auto-Regressive Integrated Moving Average with exogenous input) model combines autoregressive (AR) and moving average (MA) models with exogenous variables (X) to model the relationship between a target variable and other independent variables. The MA term, unlike an AR model, which applies total weighting to previous values, considers that the target variable depends linearly on the current value and numerous previous values of a random term [24].

$$A(q)y(t) = B(q)x(t - n_k) + C(q)\varepsilon(t) \quad \text{(B.9)}$$

More specifically,

$$A(q) = 1 + a_1 q^{-1} + \cdots + a_{n_a} q^{-n_a};$$
$$B(q) = b_0 + b_1 q^{-1} + \cdots + b_{n_b} q^{-n_b+1}; \quad \text{(B.10)}$$
$$C(q) = 1 + c_1 q^{-1} + \cdots + c_{n_c} q^{-n_c},$$

where $n_a$ , $n_b y$ $n_c$ represent the order of the ARMAX model.

# ANNEX C

## *SUPPLEMENTARY MATERIAL*

### *C.1 Chapter 2: Supplementary data*

***Table C.2.*** *MAPE results obtained with LSTM model combining different TW and number of neurons.*

| Input combinations | Time Window | Nº Neurons | LSTM MAPE | |
|---|---|---|---|---|
| | | | Winter | Summer |
| Temperature + Occupancy | 7 days | 2 | 23,99 | 16,81 |
| | 7 days | 3 | 24,1 | 17,14 |
| | 7 days | 4 | 24,15 | 16,97 |
| | 7 days | 5 | 23,65 | 17,03 |
| | 7 days | 10 | 23,89 | 16,92 |
| | 7 days | 15 | 24,19 | 17,02 |
| | 7 days | 20 | 24,01 | 17,05 |
| | 7 days | 50 | 24,1 | 17,22 |
| | 14 days | 2 | 23,72 | 14,84 |
| | 14 days | 3 | 23,31 | 14,94 |
| | 14 days | 4 | 23,44 | 15,24 |
| | 14 days | 5 | 23,36 | 15,05 |
| | 14 days | 10 | 22,65 | 14,79 |
| | 14 days | 15 | 22,16 | 15,21 |
| | 14 days | 20 | 22,18 | 14,99 |
| | 14 days | 50 | 23,25 | 15,75 |
| | 21 days | 2 | 19,38 | 14,82 |
| | 21 days | 3 | 19,76 | 14,91 |
| | 21 days | 4 | 19,63 | 14,13 |
| | 21 days | 5 | 20,23 | 14,7 |
| | 21 days | 10 | 19,79 | 14,85 |
| | 21 days | 15 | 18,85 | 14,63 |
| | 21 days | 20 | 19,46 | 14,54 |
| | 21 days | 50 | 20,34 | 15,09 |
| | 28 days | 2 | 21,14 | 13,84 |
| | 28 days | 3 | 20,61 | 13,79 |

| | | | | |
|---|---|---|---|---|
| | 28 days | 4 | 21,02 | 13,73 |
| | 28 days | 5 | 20,96 | 13,65 |
| | 28 days | 10 | 21,03 | 13,73 |
| | 28 days | 15 | 19,99 | 13,67 |
| | 28 days | 20 | 20,64 | 13,6 |
| | 28 days | 50 | 21,07 | 14,03 |

***Table C.3.*** *MAPE results obtained with SVR combining different TW*

| **Input combinations** | **Time Window** | **Winter** | | | **Summer** | | |
|---|---|---|---|---|---|---|---|
| | | **C** | γ | **SVR MAPE** | **C** | γ | **SVR MAPE** |
| **Temperature + Occupancy** | 7 days | 0.040 | 1.1587 | 19.25 | 56.9375 | 0.0029 | 16.14 |
| | 14 days | 0.4945 | 0.7109 | 20.00 | 0.7314 | 1.7969 | 15.29 |
| | 21 days | 14.4654 | 0.0600 | 17.19 | 3.9961 | 2.0133 | 14.24 |
| | 28 days | 3.0190 | 0.0268 | 18.21 | 100 | 0.0090 | 12.95 |

## *C. 2. Chapter 3: Supplementary data*

***Table C.4****. Sunrise and sunset hours during the month of November 2021*

| ***Date*** | ***Sunrise*** | ***Sunset*** |
|---|---|---|
| ***22/10/2021*** | 8:29 | 19:12 |
| ***23/10/2021*** | 8:30 | 19:10 |
| ***24/10/2021*** | 8:31 | 19:09 |
| ***25/10/2021*** | 8:33 | 19:07 |
| ***26/10/2021*** | 8:34 | 19:06 |
| ***27/10/2021*** | 8:35 | 19:04 |
| ***28/10/2021*** | 8:36 | 19:03 |
| ***29/10/2021*** | 8:38 | 19:01 |
| ***30/10/2021*** | 8:39 | 19:00 |
| ***31/10/2021*** | 7:40 | 17:59 |
| ***01/11/2021*** | 7:42 | 17:57 |
| ***02/11/2021*** | 7:43 | 17:56 |
| ***03/11/2021*** | 7:44 | 17:55 |
| ***04/11/2021*** | 7:46 | 17:53 |
| ***05/11/2021*** | 7:47 | 17:52 |

| | | |
|---|---|---|
| ***06/11/2021*** | 7:48 | 17:51 |
| ***07/11/2021*** | 7:49 | 17:50 |
| ***08/11/2021*** | 7:51 | 17:49 |
| ***09/11/2021*** | 7:52 | 17:47 |
| ***10/11/2021*** | 7:53 | 17:46 |
| ***11/11/2021*** | 7:55 | 17:45 |
| ***12/11/2021*** | 7:56 | 17:44 |
| ***13/11/2021*** | 7:57 | 17:43 |
| ***14/11/2021*** | 7:59 | 17:42 |
| ***15/11/2021*** | 8:00 | 17:41 |
| ***16/11/2021*** | 8:01 | 17:40 |
| ***17/11/2021*** | 8:02 | 17:40 |
| ***18/11/2021*** | 8:04 | 17:39 |
| ***19/11/2021*** | 8:05 | 17:38 |
| ***20/11/2021*** | 8:06 | 17:37 |
| ***21/11/2021*** | 8:07 | 17:36 |
| ***22/11/2021*** | 8:09 | 17:36 |
| ***23/11/2021*** | 8:10 | 17:35 |
| ***24/11/2021*** | 8:11 | 17:34 |
| ***25/11/2021*** | 8:12 | 17:34 |
| ***26/11/2021*** | 8:13 | 17:33 |
| ***27/11/2021*** | 8:15 | 17:33 |
| ***28/11/2021*** | 8:16 | 17:32 |
| ***29/11/2021*** | 8:17 | 17:32 |
| ***30/11/2021*** | 8:18 | 17:32 |
| ***01/12/2021*** | 8:19 | 17:31 |
| ***02/12/2021*** | 8:20 | 17:31 |

***Table C.5****. Sunrise and sunset hours during the month of August 2021.*

| ***Date*** | ***Sunrise*** | ***Sunset*** |
|---|---|---|
| ***08/08/2021*** | 7:04 | 21:19 |
| ***09/08/2021*** | 7:05 | 21:18 |
| ***10/08/2021*** | 7:06 | 21:17 |
| ***11/08/2021*** | 7:07 | 21:15 |
| ***12/08/2021*** | 7:08 | 21:14 |
| ***13/08/2021*** | 7:09 | 21:12 |
| ***14/08/2021*** | 7:10 | 21:11 |
| ***15/08/2021*** | 7:11 | 21:09 |
| ***16/08/2021*** | 7:12 | 21:08 |
| ***17/08/2021*** | 7:14 | 21:06 |
| ***18/08/2021*** | 7:15 | 21:05 |
| ***19/08/2021*** | 7:16 | 21:03 |
| ***20/08/2021*** | 7:17 | 21:01 |
| ***21/08/2021*** | 7:18 | 21:00 |

| | | |
|---|---|---|
| ***22/08/2021*** | 7:19 | 20:58 |
| ***23/08/2021*** | 7:20 | 20:57 |
| ***24/08/2021*** | 7:21 | 20:55 |
| ***25/08/2021*** | 7:22 | 20:53 |
| ***26/08/2021*** | 7:24 | 20:52 |
| ***27/08/2021*** | 7:25 | 20:50 |
| ***28/08/2021*** | 7:26 | 20:48 |
| ***29/08/2021*** | 7:27 | 20:46 |
| ***30/08/2021*** | 7:28 | 20:45 |
| ***31/08/2021*** | 7:29 | 20:43 |
| ***01/09/2021*** | 7:30 | 20:41 |
| ***02/09/2021*** | 7:31 | 20:40 |
| ***03/09/2021*** | 7:32 | 20:38 |
| ***04/09/2021*** | 7:34 | 20:36 |
| ***05/09/2021*** | 7:35 | 20:34 |
| ***06/09/2021*** | 7:36 | 20:32 |
| ***07/09/2021*** | 7:37 | 20:31 |
| ***08/09/2021*** | 7:38 | 20:29 |
| ***09/09/2021*** | 7:39 | 20:27 |
| ***10/09/2021*** | 7:40 | 20:25 |
| ***11/09/2021*** | 7:41 | 20:23 |
| ***12/09/2021*** | 7:42 | 20:22 |
| ***13/09/2021*** | 7:44 | 20:20 |
| ***14/09/2021*** | 7:45 | 20:18 |
| ***15/09/2021*** | 7:46 | 20:16 |
| ***16/09/2021*** | 7:47 | 20:14 |
| ***17/09/2021*** | 7:48 | 20:13 |
| ***18/09/2021*** | 7:49 | 20:11 |

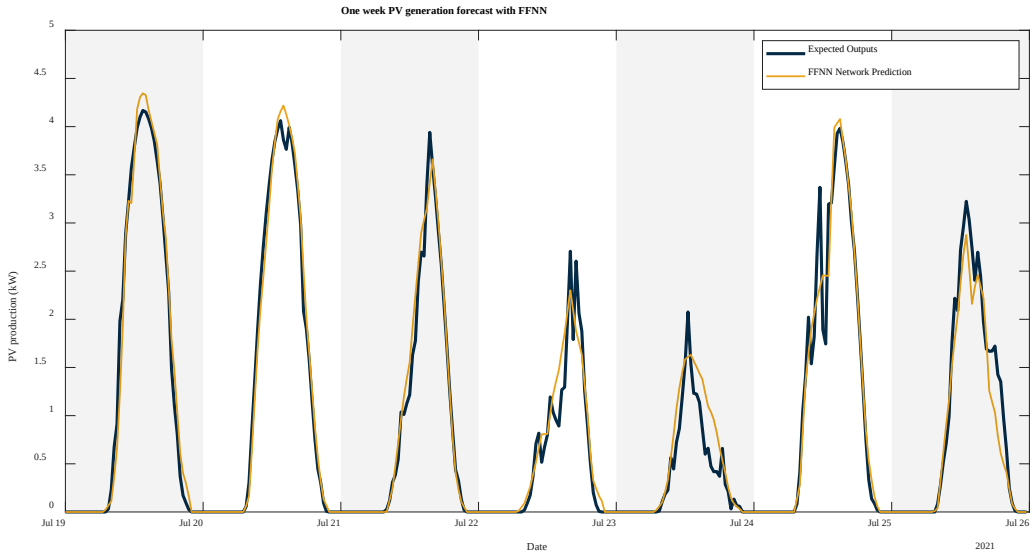


***Figure C.6****. Forecast of PV generation for a week of July with FFNN model.*

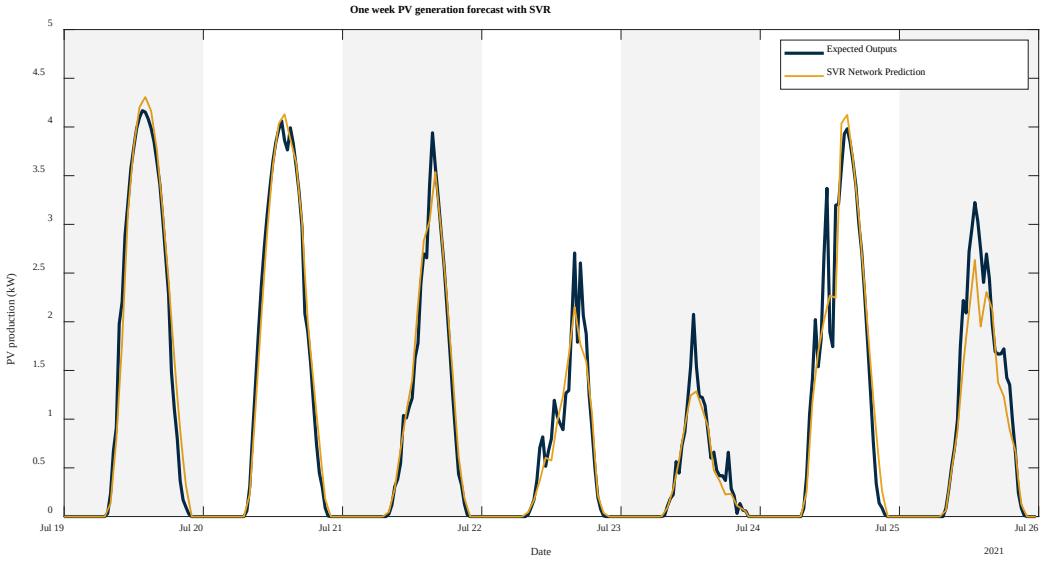


***Figure C.7**. Forecast of PV generation for a week of July with SVR model.*

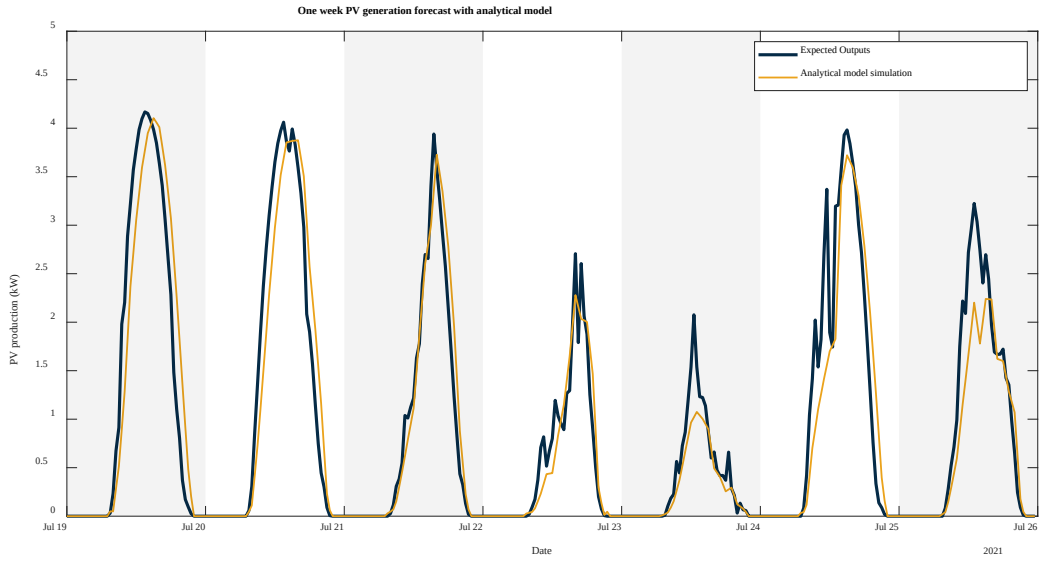


***Figure C.8.** Forecast of PV generation for a week of July with OpenModelica model.*

## *C. 3. Chapter 4: Supplementary data*

***Table C.6****. Technical characteristics of each of the heat pumps that make up the ESTIA 2 building HVAC system.*

| | | Operation Range | | Nominal Capacity (kWh) | | EER & COP | | Power Input (kW) | |
|---|---|---|---|---|---|---|---|---|---|
| **Group** | **Range** | **Cooling (ºCBD)** | **Heating (ºCWB)** | **Cooling** | **Heating** | **Cooling** | **Heating** | **Cooling** | **Heating** |
| 1 | RXYQ5M7W1B | [ -5 ; 43 ] | [ -20 ; 15,5 ] | 14 | 16 | 3,69 | 3,69 | 3,79 | 4,34 |
| 2 | RXYQ8M7W1B | [ -5 ; 43 ] | [ -20 ; 15,5 ] | 22,4 | 25 | 3,21 | 3,63 | 6,97 | 6,89 |
| 3 | RXYQ12M7W1B | [ -5 ; 43 ] | [ -20 ; 15,5 ] | 33,5 | 37,5 | 3,16 | 3,47 | 10,6 | 10,8 |
| 4 | RXYQ8M7W1B | [ -5 ; 43 ] | [ -20 ; 15,5 ] | 22,4 | 25 | 3,21 | 3,63 | 6,97 | 6,89 |
| 5 | RXYQ12M7W1B | [ -5 ; 43 ] | [ -20 ; 15,5 ] | 33,5 | 37,5 | 3,16 | 3,47 | 10,6 | 10,8 |
| 8 | RXYQ5M7W1B | [ -5 ; 43 ] | [ -20 ; 15,5 ] | 14 | 16 | 3,69 | 3,69 | 3,79 | 4,34 |
| 9 | RXYQ5M7W1B | [ -5 ; 43 ] | [ -20 ; 15,5 ] | 14 | 16 | 3,69 | 3,69 | 3,79 | 4,34 |
| 10 | REYQ10M7W1B | [ -5 ; 43 ] | [ -20 ; 15,5 ] | 28 | 31,5 | 3,11 | 3,38 | 9 | 9,31 |
| 11 | REYQ12M7W1B | [ -5 ; 43 ] | [ -20 ; 15,5 ] | 33,5 | 37,5 | 3,16 | 3,47 | 10,6 | 10,8 |
| 16 | REYQ10M7W1B | [ -5 ; 43 ] | [ -20 ; 15,5 ] | 28 | 31,5 | 3,11 | 3,38 | 9 | 9,31 |

***Table C.7.*** *Characteristics of the weather data downloaded from Open Weather.*

| **Data sets time period** | **Measured Parameters** | | **Sampling Time** |
|---|---|---|---|
| 02/05/2022 – 11/04/2023 | Text | External Temperature (ºC) | 10min |
| | p | Pressure (mb) | |
| | rh | Relative humidity (%) | |
| | w | Wind speed (m/s) | |
| | w_dq | Wind direction (0-360º) | |

***Table C.8.*** *Characteristics of the data sets obtained from the excitation tests carried out in the Platform.*

| Data sets | Data sets time period | Measured Parameters | | Sampling Time |
|---|---|---|---|---|
| **Training data set** | 24/03/2023 - 26/03/2023 | $T_{in}$ | Indoor Temperature (ºC) | 20min |
| | | $T_{sp}$ | Set Point Temperature (ºC) | |
| | | $Q_{HP}$ | Consumption data of the Heat Pump (Wh) | 5 min |
| **Test 1 data set** | 31/03/2023 - 02/04/2023 | $T_{in}$ | Indoor Temperature (ºC) | |
| | | $T_{sp}$ | Set Point Temperature | |
| | | $Q_{HP}$ | Consumption data of the Heat Pump (Wh) | 5min |
| **Test 2 data set** | 08/04/2023 - 10/04/2023 | $T_{in}$ | Indoor Temperature (ºC) | 20min |
| | | $T_{sp}$ | Set Point Temperature (ºC) | |
| | | $Q_{HP}$ | Consumption data of the Heat Pump (Wh) | 5min |

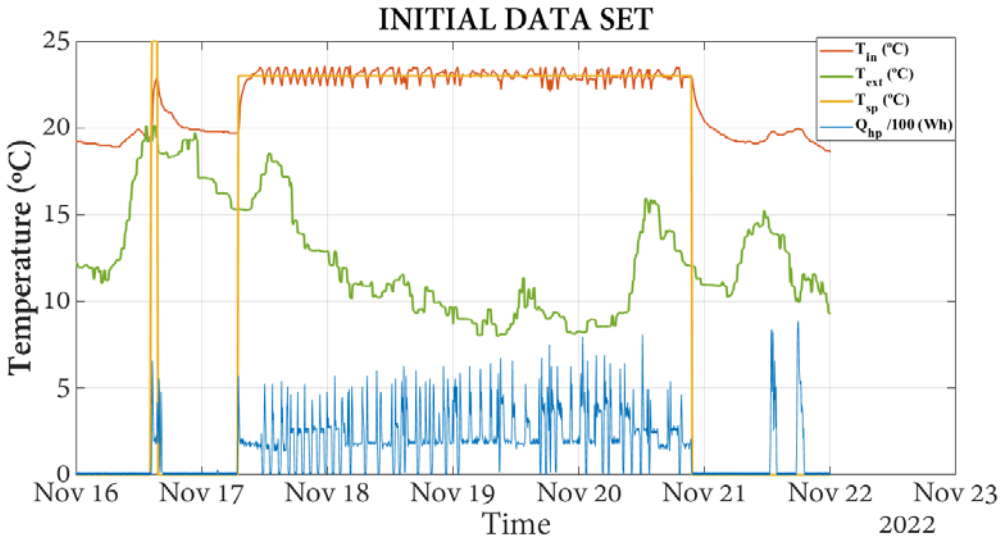


***Figure C.9****. Initial data set used as reference to determine system characteristics*

***Table C.9.*** *Fitting values collected from all lm*NARX response of $T_{in}$ for Test 1 data set.

| | | $Q_{hp}$ (Wh) | | | | | | | | | |
|---|---|---|---|---|---|---|---|---|---|---|---|
| | | **0** | **30** | **120** | **250** | **400** | **541** | **700** | **900** | **1300** | **1830** |
| $T_{ext}$ | **(7** | -0.20 | -0.16 | -0.01 | 0.25 | 0.71 | 1.41 | 2.54 | 5.80 | 13.36 | 5.97 |

| | | | | | | | | | | |
|---|---|---|---|---|---|---|---|---|---|---|
| **9** | 1.03 | 1.17 | 1.67 | 2.70 | 4.76 | 9.39 | 39.50 | 26.06 | 13.11 | 5.90 |
| **11** | 5.20 | 5.77 | 8.09 | 14.84 | 33.72 | 52.59 | 37.95 | 25.39 | 12.90 | 5.83 |
| **13.6** | 28.31 | 33.88 | 53.99 | 0 | 43.44 | 50.35 | 36.63 | 24.73 | 12.65 | 5.74 |
| **15** | 49.95 | 56.60 | 54.06 | 0 | 46.35 | 49.48 | 36.07 | 24.43 | 12.53 | 5.69 |
| **17** | 58.70 | **61.47** | 54.06 | 0 | 49.43 | 48.40 | 35.35 | 24.02 | 12.36 | 5.655 |
| **19** | 51.03 | 51.44 | 46.96 | 0 | 51.99 | 47.34 | 34.65 | 23.64 | 12.25 | 5.81 |
| **20** | 39.89 | 40.05 | 39.13 | 13.93 | 53.29 | 46.67 | 34.26 | 23.45 | 12.26 | 6.16 |
| **22** | 12.42 | 14.37 | 23.12 | 38.54 | 53.22 | 43.87 | 32.99 | 23.09 | 12.78 | 6.96 |
| **23** | 2.66 | 5.91 | 18.50 | 38.65 | 48.59 | 40.83 | 31.69 | 22.81 | 13.07 | 5.87 |

***Table C.10.*** *Fitting values collected from all lm*NARX response of $T_{in}$ for Test 2 data set.

| | | $Q_{hp}$ (Wh) | | | | | | | | | |
|---|---|---|---|---|---|---|---|---|---|---|---|
| | | **0** | **30** | **120** | **250** | **400** | **541** | **700** | **900** | **1300** | **1830** |
| $T_{ext}$ (ºC) | **7** | 0 | 0 | 0 | 0 | 0 | 0 | 0 | 0 | 9.10 | 3.47 |
| | **9** | 0 | 0 | 0 | 0 | 0 | 0 | 32.32 | 19.93 | 8.98 | 3.44 |
| | **11** | 0 | 0 | 0 | 0 | 40.16 | 47.36 | 31.43 | 19.53 | 8.85 | 3.39 |
| | **13.6** | 0 | 0 | 0 | 0 | 50.20 | 45.57 | 30.42 | 19.04 | 8.68 | 3.33 |
| | **15** | 0 | 0 | 5.91 | 0 | 52.81 | 44.70 | 29.93 | 18.78 | 8.58 | 3.29 |
| | **17** | 14.69 | 18.72 | 30.72 | 0 | 55.13 | 43.51 | 29.23 | 18.42 | 8.43 | 3.19 |
| | **19** | 0 | 0 | 10.76 | 3.85 | 56.23 | 42.08 | 28.41 | 17.95 | 8.16 | 2.79 |
| | **20** | 0 | 0 | 0 | 14.96 | 55.64 | 40.87 | 27.74 | 17.53 | 7.81 | 2.10 |
| | **22** | 0 | 0 | 0 | 7.29 | 41.11 | 33.44 | 23.55 | 14.69 | 5.05 | 0 |
| | **23** | 0 | 0 | 0 | 0 | 23.78 | 23.67 | 17.51 | 10.42 | 1.58 | 0 |

***Table C.11.*** *Fitting values collected from all lmNARX response of $Q_{hp}$ for Test 1 data set when Hyst= 0.*

| Hyst = 0 | | $T_{ext}$ (ºC) | | | | | | | | | |
|---|---|---|---|---|---|---|---|---|---|---|---|
| | | 7.5 | 9 | 11.5 | 13 | 15 | 17 | 18.5 | 20 | 21.5 | 23 |
| $T_{sp}$ (ºC) | 7.5 | -0.79 | 0.36 | 13.12 | 33.38 | 33.63 | 8.70 | 2.40 | 12.28 | 36.60 | 51.59 |
| | 19 | -0.73 | 0.78 | 8.83 | 26.55 | 39.57 | 16.62 | 5.42 | 16.25 | 43.9 | 39.98 |
| | 19.5 | -0.52 | 0.88 | 5.07 | 17.71 | 39.40 | 20.96 | 0 | 4.00 | 24.35 | 5.13 |
| | 20 | -0.28 | 0.48 | 3.82 | 13.92 | 36.54 | 23.30 | 0 | 0 | 0 | 0 |
| | 20.5 | 0.23 | -0.12 | 2.76 | 10.18 | 31.05 | 28.14 | 0 | 0 | 0 | 0 |
| | 21 | 0.79 | -0.51 | 2.09 | 7.56 | 24.95 | 33.67 | 0 | 0 | 0 | 0 |
| | 21.5 | 0.95 | -0.66 | 1.75 | 6.14 | 20.67 | 36.44 | 0 | 0 | 0 | 0 |
| | 22 | 0.73 | -0.75 | 1.51 | 5.06 | 16.95 | 36.89 | 0 | 0 | 0 | 0 |
| | **22.5** | 0.27 | -0.80 | 1.34 | 4.25 | 13.87 | 35.00 | 0 | 0 | 0 | 0 |
| | **23** | -0.16 | -0.82 | 1.23 | 3.64 | 11.42 | 31.58 | 0 | 0 | 0 | 0 |

***Table C.12.*** Fitting values collected from all lmNARX response of $Q_{hp}$ for Test 1 data set when Hyst= 1.

| **Hyst = 1** | | $T_{ext}$ **(ºC)** | | | | | | | | | |
|---|---|---|---|---|---|---|---|---|---|---|---|
| | | **7.5** | **9** | **11.5** | **13** | **15** | **17** | **18.5** | **20** | **21.5** | **23** |
| $T_{sp}$ **(ºC)** | **7.5** | -0.41 | 1.25 | 17.84 | 40.47 | 16.38 | 0 | 0 | 0 | 0 | 0 |
| | **19** | -0.33 | 1.87 | 12.03 | 33.63 | 30.78 | 0 | 0 | 0 | 0 | 0 |
| | **19.5** | -0.02 | 2.02 | 6.90 | 22.85 | 40.32 | 0 | 0 | 0 | 0 | 0 |
| | **20** | 0.33 | 1.44 | 5.19 | 17.98 | 40.79 | 0 | 0 | 0 | 0 | 0 |
| | **20.5** | 1.07 | 0.56 | 3.71 | 13.08 | 37.08 | 9.00 | 0 | 0 | 0 | 0 |
| | **21** | 1.89 | -0.01 | 2.77 | 9.61 | 30.74 | 22.16 | 0 | 0 | 0 | 0 |
| | **21.5** | 2.12 | -0.24 | 2.28 | 7.70 | 25.70 | 31.15 | 0 | 0 | 0 | 0 |
| | **22** | 1.80 | -0.36 | 1.92 | 6.25 | 21.10 | 37.16 | 0 | 0 | 0 | 0 |
| | **22.5** | 1.14 | -0.43 | 1.65 | 5.15 | 17.21 | 39.10 | 0 | 0 | 0 | 0 |
| | **23** | 0.50 | -0.47 | 1.45 | 4.31 | 14.06 | 37.50 | 0 | 0 | 0 | 0 |

***Table C.13.*** *Fitting values collected from all lmNARX response of $Q_{hp}$ for Test 2 data set when Hyst= 0.*

| **Hyst = 0** | | $T_{ext}$ (ºC) | | | | | | | | | |
|---|---|---|---|---|---|---|---|---|---|---|---|
| | | **7.5** | **9** | **11.5** | **13** | **15** | **17** | **18.5** | **20** | **21.5** | **23** |
| $T_{sp}$ (ºC) | 0 | -0.41 | 1.25 | 17.84 | 40.47 | 16.38 | 0 | 0 | 0 | 0 | 0 |
| | 19 | -0.33 | 1.87 | 12.03 | 33.63 | 30.78 | 0 | 0 | 0 | 0 | 0 |
| | 19.5 | -0.02 | 2.02 | 6.90 | 22.85 | 40.32 | 0 | 0 | 0 | 0 | 0 |
| | 20 | 0.33 | 1.44 | 5.19 | 17.98 | 40.79 | 0 | 0 | 0 | 0 | 0 |
| | 20.5 | 1.07 | 0.56 | 3.71 | 13.08 | 37.08 | 9.00 | 0 | 0 | 0 | 0 |
| | 21 | 1.89 | -0.01 | 2.77 | 9.61 | 30.74 | 22.16 | 0 | 0 | 0 | 0 |
| | 21.5 | 2.12 | -0.24 | 2.28 | 7.70 | 25.70 | 31.15 | 0 | 0 | 0 | 0 |
| | 22 | 1.80 | -0.36 | 1.92 | 6.25 | 21.10 | 37.16 | 0 | 0 | 0 | 0 |
| | 22.5 | 1.14 | -0.43 | 1.65 | 5.15 | 17.21 | 39.10 | 0 | 0 | 0 | 0 |
| | 23 | 0.50 | -0.47 | 1.45 | 4.31 | 14.06 | 37.50 | 0 | 0 | 0 | 0 |

***Table C.14.*** *Fitting values collected from all lmNARX response of $Q_{hp}$ for Test 2 data set when Hyst= 1.*

| **Hyst = 1** | | $T_{ext}$ (ºC) | | | | | | | | | |
|---|---|---|---|---|---|---|---|---|---|---|---|
| | | **7.5** | **9** | **11.5** | **13** | **15** | **17** | **18.5** | **20** | **21.5** | **23** |
| $T_{sp}$ (ºC) | **0** | -0.51 | -0.50 | 0 | 0 | 0 | 0 | 0 | 0 | 0 | 0 |
| | **19** | -0.51 | -0.49 | 0 | 0 | 0 | 0 | 0 | 0 | 0 | 0 |
| | **19.5** | -0.51 | -0.46 | 0 | 0 | 0 | 0 | 0 | 0 | 0 | 0 |
| | **20** | -0.51 | -0.42 | 0 | 0 | 0 | 0 | 0 | 0 | 0 | 0 |
| | **20.5** | -0.51 | -0.30 | 0 | 0 | 0 | 0 | 0 | 0 | 0 | 0 |
| | **21** | -0.50 | -0.05 | 0 | 0 | 4.28 | 9.42 | 8.86 | 1.52 | 0 | 0 |
| | **21.5** | -0.48 | 0.27 | 0 | 6.05 | 14.33 | 18.15 | 18.34 | 13.57 | 3.95 | 0 |
| | **22** | -0.45 | 0.78 | 0.78 | 7.07 | 12.70 | 15.60 | 15.96 | 11.75 | 0.97 | 0 |
| | **22.5** | -0.40 | 1.42 | 0 | 1.75 | 6.84 | 9.89 | 10.41 | 5.67 | 0 | 0 |

| | | | | | | | | | | |
|---|---|---|---|---|---|---|---|---|---|---|
| **23** | -0.30 | 1.98 | 0 | 0 | 1.52 | 4.90 | 5.35 | -0.97 | 0 | 0 |

## *BIBLIOGRAPHY*

[1] E. Liu, Y. Wang, and Y. Huang, 'Short-term Forecast of Multi-load of Electrical Heating and Cooling in Regional Integrated Energy System Based on Deep LSTM RNN', in *2020 IEEE 4th Conference on Energy Internet and Energy System Integration (EI2)*, Wuhan, China: IEEE, Oct. 2020, pp. 2994–2998. doi: 10.1109/EI250167.2020.9347300.

[2] X. Guo, Q. Zhao, S. Wang, D. Shan, and W. Gong, 'A short-term load forecasting model of LSTM neural network considering demand response', *Complexity*, vol. 2021, p. 7, 2021, doi: https://doi.org/10.1155/2021/5571539.

[3] F. Dewangan and M. Biswal, 'Medium-Term Load Forecasting Using ANN and RNN in Microgrid Integrating Renewable Energy Source', in *2023 2nd International Conference for Innovation in Technology (INOCON)*, Bangalore, India: IEEE, Mar. 2023, pp. 1–5. doi: 10.1109/INOCON57975.2023.10101126.

[4] M. A. Yahya, S. P. Hadi, and L. M. Putranto, 'Short-Term Electric Load Forecasting Using Recurrent Neural Network (Study Case of Load Forecasting in Central Java and Special Region of Yogyakarta)', in *2018 4th International Conference on Science and Technology (ICST)*, Yogyakarta: IEEE, Aug. 2018, pp. 1–6. doi: 10.1109/ICSTC.2018.8528651.

[5] V. Bui, V. H. Nguyen, T. L. Pham, J. Kim, and Y. M. Jang, 'RNN-based Deep Learning for One-hour ahead Load Forecasting', in *2020 International Conference on Artificial Intelligence in Information and Communication (ICAIIC)*, Fukuoka, Japan: IEEE, Feb. 2020, pp. 587–589. doi: 10.1109/ICAIIC48513.2020.9065071.

[6] S. M. Awan, Z. A. Khan, and M. Aslam, 'Solar Generation Forecasting by Recurrent Neural Networks Optimised by Levenberg-Marquardt Algorithm', in *IECON 2018 - 44th Annual Conference of the IEEE Industrial Electronics Society*, Washington, DC: IEEE, Oct. 2018, pp. 276–281. doi: 10.1109/IECON.2018.8591799.

[7] N. Park and H. K. Ahn, 'Multi-Layer RNN-based Short-term Photovoltaic Power Forecasting using IoT Dataset', in *2019 AEIT International Annual Conference (AEIT)*, Florence, Italy: IEEE, Sep. 2019, pp. 1–5. doi: 10.23919/AEIT.2019.8893348.

[8] G. Abbas, M. Nawaz, and F. Kamran, 'Performance Comparison of NARX & RNN-LSTM Neural Networks for LiFePO4 Battery State of Charge Estimation', in *2019 16th International Bhurban Conference on Applied Sciences and Technology (IBCAST)*, Islamabad, Pakistan: IEEE, Jan. 2019, pp. 463–468. doi: 10.1109/IBCAST.2019.8667172.

[9] G. Javid, M. Basset, and D. O. Abdeslam, 'Adaptive Online Gated Recurrent Unit for Lithium-Ion Battery SOC Estimation', in *IECON 2020 The 46th Annual Conference of the IEEE Industrial Electronics Society*, Singapore, Singapore: IEEE, Oct. 2020, pp. 3583–3587. doi: 10.1109/IECON43393.2020.9254506.

[10] G. Capizzi, F. Bonanno, and C. Napoli, 'Recurrent neural network-based control strategy for battery energy storage in generation systems with intermittent

renewable energy sources', in *2011 International Conference on Clean Electrical Power (ICCEP)*, Ischia, Italy: IEEE, Jun. 2011, pp. 336–340. doi: 10.1109/ICCEP.2011.6036300.

[11] R. E. Alden, E. S. Jones, S. B. Poore, H. Gong, A. Al Hadi, and D. M. Ionel, 'Digital Twin for HVAC Load and Energy Storage based on a Hybrid ML Model with CTA-2045 Controls Capability', in *2022 IEEE Energy Conversion Congress and Exposition (ECCE)*, Detroit, MI, USA: IEEE, Oct. 2022, pp. 1–5. doi: 10.1109/ECCE50734.2022.9948141.

[12] F. M. Bianchi, E. Maiorino, M. C. Kampffmeyer, A. Rizzi, and R. Jenssen, 'An overview and comparative analysis of Recurrent Neural Networks for Short Term Load Forecasting', *Springer International Publishing*, pp. 1–41, 2018, doi: 10.1007/978-3-319-70338-1.

[13] C. Pittapally, 'Backpropagation and Gradient Descent', Medium. Accessed: May 21, 2024. [Online]. Available: https://medium.com/@cpittapa/backpropagation-and-gradient-descent-369e33fb7466

[14] K. Sharma, 'Vanishing/Exploding Gradients Problem', Medium. Accessed: May 21, 2024. [Online]. Available: https://medium.com/@kushansharma1/vanishing-exploding-gradients-problem-1901bb2db2b2#:~:text=The%20vanishing%20gradient%20problem%20occurs,gradients%20grow%20exponentially%20during%20backpropagation.

[15] M. Khalil, A. S. McGough, Z. Pourmirza, M. Pazhoohesh, and S. Walker, 'Machine Learning, Deep Learning and Statistical Analysis for forecasting building energy consumption — A systematic review', *Engineering Applications of Artificial Intelligence*, no. 115, p. 105287, 2022, doi: https://doi.org/10.1016/j.engappai.2022.105287.

[16] Z. Boussaada, O. Curea, A. Remaci, H. Camblong, and N. Mrabet Bellaaj, 'A Nonlinear Autoregressive Exogenous (NARX) Neural Network Model for the Prediction of the Daily Direct Solar Radiation', *Energies*, vol. 11, p. 620, 2018, doi: 10.3390/en11030620.

[17] B. Kumaraswamy, 'Neural networks for data classification', in *Artificial Intelligence in Data Mining*, Elsevier, 2021, pp. 109–131. doi: 10.1016/B978-0-12-820601-0.00011-2.

[18] M. I. A. Lourakis, 'A Brief Description of the Levenberg-Marquardt Algorithm Implemened by levmar', [Online]. Available: https://users.ics.forth.gr/~lourakis/levmar/levmar.pdf

[19] M. Hudson Beale, M. T. Hagan, and H. D. Demuth, 'Deep Learning Toolbox Getting Started Guide', Mar. 2022.

[20] I. Zapirain, G. Etxegarai, J. Hernández, Z. Boussaada, N. Aginako, and H. Camblong, 'Short-term electricity consumption forecasting with NARX, LSTM, and SVR for a single building: small data set approach', *Energy Sources, Part A: Recovery,*

*Utilization, and Environmental Effects*, vol. 44, no. 3, pp. 6898–6908, Sep. 2022, doi: 10.1080/15567036.2022.2104410.

[21] G. Etxegarai, I. Zapirain, H. Camblong, J. Ugartemendia, J. Hernandez, and O. Curea, 'Photovoltaic Energy Production Forecasting in a Short Term Horizon: Comparison between Analytical and Machine Learning Models', *Applied Sciences*, vol. 12, no. 23, p. 12171, Nov. 2022, doi: 10.3390/app122312171.

[22] Q.-N. Nguyen, C.-T. Phan, V.-N. Dinh, B.-K. P. Truong, T.-H. T. Dang, and T.-H. Do, 'A Small-Scale Temperature Forecasting System using Time Series Models Applied in Ho Chi Minh City', in *2022 IEEE International Conference on Communication, Networks and Satellite (COMNETSAT)*, Solo, Indonesia: IEEE, Nov. 2022, pp. 229–234. doi: 10.1109/COMNETSAT56033.2022.9994437.

[23] J. Villavicencio, 'Introducción a Series de Tiempo'. Accessed: Feb. 07, 2024. [Online]. Available: http://www.estadisticas.gobierno.pr/iepr/LinkClick.aspx?fileticket=4_BxecUaZmg%3D#:~:text=3.1.%2DProceso%20estoc%C3%A1stico%20estacionario&text=En%20resumen%20si%20una%20serie,son%20invariantes%20respecto%20al%20tiempo.

[24] S. Shukla, R. Ramaprasad, S. Pasari, and S. Sheoran, 'Statistical Analysis and Forecasting of Wind Speed', in *2022 4th International Conference on Energy, Power and Environment (ICEPE)*, Shillong, India: IEEE, Apr. 2022, pp. 1–6. doi: 10.1109/ICEPE55035.2022.9798358.